Dissertation zur Erlangung des Doktorgrades der
Fakultät für Mathematik und Physik der
Albert-Ludwigs-Universität Freiburg im Breisgau

Pure univariate quantum marginals and electronic transport properties of geometrically frustrated systems

Alexandre Miguel de Araújo Lopes

2015

Albert-Ludwigs-Universität Freiburg im Breisgau
Fakultät für Mathematik und Physik

Dekan

Prof. Dr. Dietmar Kröner

Betreuer

Prof. Dr. David Gross

Referent

Prof. Dr. David Gross

Koreferent

Prof. Dr. Gerhard Stock

Tag der mündlichen Prüfung

20.04.2015

Prüfer

Prof. Dr. Alexander Blümen

Prof. Dr. David Gross

Prof. Dr. Tobias Schätz

To my wife Filipa and my son David

Preface

This PhD thesis is the culmination of several years of research done mainly at the Institute of Physics of the University of Freiburg. This thesis is rather unusual in that it is split into two disjoint parts, although both are concerned with physics. The first part was undertaken under the supervision of Junior Professor David Gross with the collaboration of Christian Schilling, Matthias Christandl, James Whitfield and Panagiotis Papanastasios. This part is concerned with the quantum marginal problem for distinguishable particles and Fermions and aims to provide an overview of it while giving some new results on the subject. It uses tools from Quantum Information Theory and Symplectic Geometry in order to tackle the problem. As the second part, it is a continuation of the research I began on my Bachelor and continued to do during my Master's. It was done in close collaboration with the University of Aveiro, my main collaborator being Ricardo Dias, but it also counted with a minor collaboration of Bruno António. This part is concerned, mainly, with the so called AB_2 chains, an example of an itinerant geometrically frustrated system, their electronic properties and transport properties. It uses several tools from Condensed Matter. While this may be an unusual combination, it allowed me to broaden my horizons without losing touch with the area where I came from: Condensed Matter. It also allowed me to learn new subjects while still being quite productive, since I was not forced to learn everything from scratch.

During the course of my research and while writing this thesis there were many ups and downs, and life changing events for me. For instance I got married and became a father. I couldn't have made it without the support of my family, friends and colleagues. As such I would like to thank my supervisor David Gross as without him I wouldn't be here and this thesis wouldn't exist; my collaborators Christian Schilling, to whom I thanks for having read the first part of this manuscript, Matthias Christandl, James Whitfield, Bruno António and in particular Ricardo Dias, my former supervisor, collaborator and friend. Thank you for being always there to chat not only about science but also about life in general and also for reading the second part of this manuscript; my office colleagues and friends for the fun times in the middle of desperate times Richard Küng, Johan Aberg, Rafael Chaves, Christian

Majenz, Kinan Halabi, Robert Stierlen, Pagiotis Papanastasiou; all of my students for their dedication, for their nice reviews of my work and for taking the time to let me teach them and in turn let me learn how to teach; my friends, Lidia del Rio, for without her I wouldn't have met David, and wouldn't have gone to Freiburg, Florian Hermanns for the music and being always next door and keeping in touch after so many years, Telmo Coutinho for being an awesome friend since we were little kids, Astrid de Wijn for the falafel moments and sharing an office with me and thanks to Elisabeth Fraczek for being sane in the middle of so much insanity, for introducing me to board games, and for being such a good friend even if we're far apart and many years have passed; and obviously I would like to thank all of my family, in particular my parents, Vasco Manuel Dias Lopes and Anabela Baptista Campos de Araújo Lopes, my brother Mário Cláudio de Araújo Lopes and my dear and truly awesome wife Filipa Isabel Serra e Silva. Her support proved to be invaluable to maintain my mental health during this time. In case I have forgotten somebody, please excuse me.

Financial acknowledgments

The author would like to acknowledge the financial support of:

- Fundação para a Ciência e a Tecnologia, cofinanced by FSE/POPH, under grant SFRH / BD / 68867 / 2010.

- Excellence Initiative of the German Federal and State Governments (grant ZUK 43).

Contents

Abstract

Quantum many-body systems present a formidable challenge to tackle either analytically or numerically. As such any extra tools we can get to treat such systems are of utmost importance for practical applications. In the first part of this thesis, we address the pure univariate quantum marginal problem, whose full solution has been found recently [1]. Such problem asks for the possible eigenvalues of the one-particle reduced density matrices (1-RDMs) of a globally pure state. It presents a deep insight into the local properties of many-body systems and a possible tool for the simplification of the analysis of such systems. We present a simple solution of the fact that whenever the spectrum of the 1-RDMs of a state, which are one particle objects, is extremal, it leads to significant structural simplifications of the states that can give rise to such 1 RDMs. In order to probe the physical relevance of such simplifications we consider the problem in quantum chemistry. We address as well the marginal problem for Fermions Fock space and characterized the mode and particle marginals. We show that for the particle reduction there are no constraints in Fock space, unlike in the case of a fixed number of particles. We consider also the mode marginals for free Fermions and fully characterize it. Resorting to the Jordan-Wigner transformation the obtained characterization corresponds exactly to the one known for a system of qubits. Finally we examine the computational complexity of deciding from local spectral information whether many-body states are entangled or not. We show that while it is true that few easily obtainable physical measurements may be sufficient to witness many-body entanglement, the classical post processing of the obtained data is, in principle, intractable in the sense that the problem is NP-complete. In the second part of this thesis we study the electronic transport properties of geometrically frustrated systems, with special emphasis on the AB_2 chain. We begin by studying it in the non interacting case and proceed to give an exact solution in the strong coupling limit when considering interacting spinless Fermions. We propose, as well, a method for constructing localized states in non-interacting geometrically frustrated systems which leads to states which are highly localized. We then study the conductance through the AB_2 chain and show that localized states in geometrically frustrated systems lead to rather interesting behavior in the two terminal

electronic conductance through such systems. In particular in the absence of magnetic flux these localized states act as filters of the zero frequency conductance peak (where we refer to the frequency of an incident electron). The addition of magnetic flux changes the behavior of the localized states in the conductance: some still filter the zero frequency peak while others contribute to the appearance of a zero frequency peak, and as such the conductance profile exhibits a zero frequency peak with a dip, which is a distinct fingerprint of the existence of localized states. We finally propose a new method for calculating the conductance through interacting clusters, and shown that it is in agreement with already well known methods. We use it to calculate the conductance through interacting spinless AB_2 chains. We show that the non-interaction conductance profiles persist for small values of the interaction and that some possibly expected conductance peaks are actually experimentally non-accessible due to the flat band of the AB_2 chain.

Part I

Quantum marginals

Acknowledgments

The work contained in this part has been done by the author under the supervision of David Gross. Chapter 3 counted with the support of Christian Schilling. The author thanks him for useful discussions, as well as for writing the first form of the "Fermionic strong degenerate selection rule" for a doubly degenerate spectrum and for coming up with the first example of such rule. Chapter 4 counted with the support of Christian Schilling, Matthias Christandl, James Whitfield, Michael Walter, Stefan Knecht and Markus Reiher. Their contributions are indicated in the text. Chapter 6 counted with the support of Panagiotis Papanastasiou. The author thanks him for useful discussions and for having treated the BISEP-LARGEST-B problem.

Organization

This part is organized as follows. In Chapter 1 we introduce and state the quantum marginal problem. In particular we focus on the univariate pure quantum marginal problem, which will form the basis of this entire part. In Chapter 2 we give some examples of systems for which the univariate pure quantum marginal problem admits a simple solution and introduce some terminology and concepts that will be necessary in the following chapters. In Chapter 3 we give a constructive proof of the fact that whenever the spectra of one-particle reduced density matrices (1-RDMs) is extremal its pre-image is not the entire Hilbert space but a smaller subset, leading to significant simplifications of the corresponding wavefunctions. This fact has been mentioned in the literature but no proof has been given. We not give a simple proof but generalize it to the important case of degenerate 1-RDMs spectra. In Chapter 4 we probe whether or not one can apply the previously mentioned simplification to quantum chemistry in order to improve the speed and accuracy of calculating ground states. We show that arriving at clear conclusions is not simple and plagued by several complications. In Chapter 5 we address the quantum marginal problem in Fermionic Fock space and show that there are no non-trivial constraints on the spectrum of 1-RDMs in Fock space. We also fully characterize the mode reduction in Fock space. In Chapter 6 we prove that deciding whether or not a many-body system is entangled, using localizable entanglement as an entanglement measure, from the spectra of its 1-RDMs alone is computational intractable (in the sense that the general problem is NP-hard) and in Chapter 7 we conclude.

Chapter 1

Introduction

In quantum mechanics, a quantum state is a bounded, linear and unitary trace Hermitian operator ρ on an Hilbert space $\mathcal{H}$. For simplicity we shall restrict our discussion to finite dimensional quantum systems, $\dim \mathcal{H} < \infty$. In such case, this operator is usually known as *density matrix*. In the particular case of a rank 1 density matrix, it can be written as $\rho = |\psi\rangle \langle\psi| , \quad |\psi\rangle \in \mathcal{H}$. In this case, $|\psi\rangle$ is called *state vector*.

An observable A is an hermitian operator $A = A^\dagger$ on $\mathcal{H}$. Hermiticity guarantees that such operator is diagonalizable and that its eigenvalues are real. The importance of this lies in the fact that quantum mechanics axiomatizes that the eigenvalues of such operator are the possible outcomes of experimental measurements performed on the system.

Given the statistical nature of quantum mechanics, it is usual to deal with the expected value of an observable: the average value one would obtain by performing a given measurement on an ensemble of systems all prepared in the same quantum state ρ. Such expected value is given by $\langle A \rangle = \operatorname{tr} \rho A$.

Up to now we have not specified whether the system is composed or not of several particles, modes, or other subsystems. Let us assume that it composed of N subsystems, which induces a tensor product structure on our global Hilbert space: $\mathcal{H} = \otimes_{i=1}^{N} \mathcal{H}_i$. Consider now an operator A_I that acts only non-trivially on a subset $I \subset \{1, \dots N\}$ of our system. Then it is a priori expected that we do not need information about the full state ρ to calculate the expected value of A_I. Hence we search for an operator ρ_I such that:

$$\langle A \rangle = \operatorname{tr} \rho A = \operatorname{tr} \rho_I A_I. \tag{1.1}$$

Such operator, given by $\rho_I = \operatorname{tr}_I^c \rho$, where tr_I^c denotes the trace over all subsystems in the complement of I, is called a *reduced density operator*. The partial trace operator is the quantum analogue of the classical marginalization in the following sense: consider n random variables $\{x_1, \dots x_n\}$ with joint probability distribution $p(x_1, \dots, x_n)$. Let $I \subset \{x_1, \dots x_n\}$.

Then the marginal distribution of I is $p_I = \sum_{I^c} p(x_1, \dots x_n)$. The quantum analogue consists of considering n particles in a state ρ, the analogue of the classical joint probability distribution $p(x_1, \dots, x_n)$, and the partial trace $\rho_I := \mathrm{tr}_{I^c}\, \rho$, the analogue of the classical marginal distribution p_I. Hence ρ_I is also called a *quantum marginal*. We shall from now on use the term quantum marginal and reduced density operator interchangeably. Whenever $|I| = n$, the operator ρ_I is known as an n-RDM of ρ.

We can now ask the following question: given a set of n marginals $\rho_{I_{(i)}}$, where the sets $I_{(i)}$ may or not have empty intersection, are these marginals *compatible* (see Fig. 1.1)? By compatibility we mean that these marginals all come from the same global state by tracing out the appropriate parts

$$\rho_{I_{(i)}} = \mathrm{tr}_{I^c_{(i)}}\, \rho. \tag{1.2}$$

Such problem, of determining the relation between global quantum states and their reductions

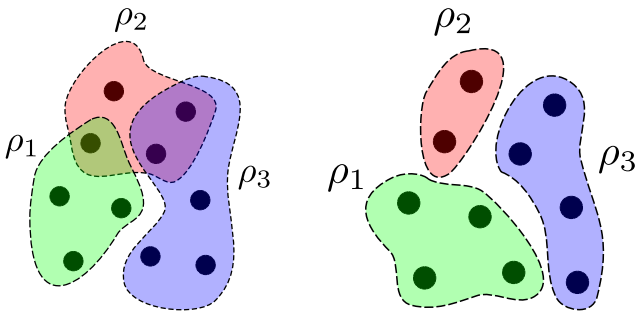

(a) Overlapping set of marginals

(b) Non-overlapping set of marginals

Figure 1.1: A set of quantum marginals can be either overlapping (a) or non-overlapping (b). The overlapping case is in general QMA-Complete but the non-overlapping is potentially computationally tractable.

is known as the *quantum marginal problem*. This problem arose originally in the quantum chemistry community in the 1960s [2], where it is know as the *N-representability problem*. Recently, due to the advent of quantum information theory there has been a resurgence in the problem. This has lead to significant progress. On the one hand tools from (classical and quantum) *computational complexity theory* have been employed to show that the most general version of the problem is probably intractable, even for a quantum computer, for it is QMA-Complete [3–5]. On the other hand it has been discovered that the so-called *univariate quantum marginal problem* exhibits an extremely rich structure which can be completely described, at least in principle [1,6–10]. The hardness results apply only to marginal problems where the given density matrices act on overlapping regions, and it may very well be that the univariate marginal problem is tractable (see Fig. 1.1). Indeed, in a celebrated paper [1], Klyachko has identified the mixed one-body (univariate) marginal problem as the membership problem for a certain *moment polytope*. More concretely, for a system of N particles in a state

ρ, the map

$$\mu : \rho \mapsto \left(\rho_1^{(1)}, \dots \rho_N^{(1)}\right) \tag{1.3}$$

with $\rho_i^{(1)}$ the 1-RDM of the ith particle, is a moment map (see appendix A for a small discussion of symplectic geometry and the moment map).

In the present text we shall only consider the pure univariate marginal problem where one asks if a given set of 1-RDMs (hence univariate) is compatible with a globally pure state. Note that the mixed version of this problem is trivial, for given a set of marginals $\rho_1^{(1)}, \dots \rho_N^{(1)}$ there is *always* a global state from which these marginals can arise, namely $\rho = \rho_1^{(1)} \otimes \rho_N^{(1)}$. In the univariate situation things simplify significantly. To begin with,in this case the set of marginals is necessarily non-overlapping and one needs only to consider the spectra of such 1-RDM as we show in an instant. Solutions to the one-body marginal problem have been applied to the study of several problems. Examples include the qualitative analysis of many-body ground-states [11, 12], entanglement theory [10, 13], and the study of generic states [9].

In principle, Klyachko's work gives rise to an algorithm for constructing the set of compatible density operators. However, the task remains extremely involved and very few closed-formula solutions have been obtained. What is more, there is no formal proof that there are (or not) efficient algorithms for solving this problem. For systems of n-qubits [6], several low-dimensional cases with and without symmetry [1, 14, 15] and some SL-orbits [10, 13], a complete characterization of the polytope has been obtained.

Note that if a set $\{\rho_i^{(1)}\}_i, i = 1, \dots, n$ of one-particle density operators arises as the reductions of a globally pure state, then the same is true for $\{U_i \rho_i^{(1)} U_i^\dagger\}_i$ for any set of local unitaries U_i. One may then use this unitary freedom to assume that all local densities are diagonal with eigenvalues $\lambda^{(i)} = \operatorname{spec} \rho_i$ ordered non-increasingly. Thus, the problem may be phrased solely in terms of spectra: when can a set of vectors $\{\lambda^{(i)}\}$ appear as the eigenvalues of the reductions of a pure quantum state? A compatible set of spectra for n systems of dimension d each may naturally be embedded as $\oplus_{i=1}^n \lambda^{(i)}$ into $\mathbb{R}_+^{dn}$. Due to the fact that the map from a global state to its local reductions is a moment map [1] and due to Kirwan's convexity theorem [16], the set of points λ in $\mathbb{R}_+^{d_n}$ forms a *convex polytope* Δ, which can, e.g., be described as intersection of half-spaces. Assuming that these half-spaces coincide with the facets of this polytope, which we will do from now onwards so we have a minimal description of our polytope, it can be described in terms of the inequalities defining its facets

$$\kappa \cdot \lambda + \kappa_0 \leq 0 \tag{1.4}$$

where κ is a vector normal to the facet F pointing *outwards*, as depicted in Fig. 1.2 and κ_0 and offset, describing the Euclidean distance from the facet to the origin of the coordinate system. We call this polytope *spectral polytope* and such inequality a *spectral inequality*.

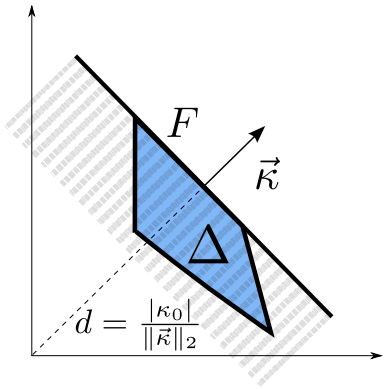

Figure 1.2: A half-space with normal vector κ and offset κ_0 which coincides with a facet F of a convex polytope Δ.

For the case of Fermions in particular it has been known for a long time that the anti-symmetry of the Fermionic wavefunction while implying the Pauli's exclusion principle, is stronger than this principle alone. For a Fermionic system with a well defined number of Fermions, the Pauli's exclusion principle is equivalent to restricting the eigenvalues of the 1-RDM to a value between 0 and 1 (when one normalizes the 1-RDM such that its trace equals the total number of Fermions.). Anti-symmetry, on the other hand, implies extra constraints on these eigenvalues. It has been shown fairly recently by Klyachko [15] that, for a globally pure state, these constrains correspond to a convex polytope on the set of eigenvalues of the 1-RDM.

One of the reasons for the interest in quantum marginals is due to the following elementary problem: given a quantum system described by an Hamiltonian H, the problem of finding the ground state (GS) energy is a variational problem over the set of all states S, i.e.,

$$E_{GS} = \min_{\rho \in S} \operatorname{tr}(\rho H). \tag{1.5}$$

Due to the curse of dimensionality this problem is clearly intractable for large systems (i.e. consisting of a large number of sub-systems). However, given that all physical Hamiltonians are two body Hamiltonians (at least outside the realm of high-energy physics [17]), we can write $H = \sum_i \sum_{j>i} H^{i,j}$. In this case we have

$$E_{GS} = \sum_i \sum_{j>i} \min_{\rho_{i,j}} \operatorname{tr}\left(\rho_{i,j} H^{i,j}\right) \tag{1.6}$$

and obviously one only needs 2-RDMs to calculate the GS energy. We then have to minimize over a considerably smaller subspace of states than the entire Hilbert space, which may lead us to believe we have simplified our problem. We must now require, however, that all the $\rho_{i,j}$ correspond to partial traces of the *same* global system, i.e. that these reductions are *com-*

patible with a global state ρ. Unfortunately in such problem we have, in general, overlapping sets of reduced density matrices and the problem seems to be intractable in its generality. As such, interesting as it may seem, we will not treat it here. Several authors have, however, given considerable attention to this problem, commonly referred to as the 2-representability problem [2, 18, 19]. Semidefinite programming algorithms based on some identified necessary conditions for 2-representability (but not sufficient) show promising results in the calculation of ground states in quantum chemistry [20].

Chapter 2

Representing quantum marginals and some fully characterizable situations

In this chapter we show how to represent the spectral polytope and review some results for fully characterizable settings.

2.0.1 Representing the spectral polytope

Distinguishable particles

Consider an arbitrary pure state of n qudits, with different local dimensions $|\psi\rangle \in \mathcal{H} = \mathbb{C}^{d_1} \otimes \ldots \otimes \mathbb{C}^{d_n}$. Let $\{|x_i\rangle\}_{x_i=1}^{d_i}$ be a basis for the jth qubit subspace and let $\{|\vec{x}\rangle_{x_i=1}^{d_i} = |x_1\rangle \ldots |x_n\rangle\}$ be a basis for $\mathcal{H}$. Then one can write, for a chosen orthonormal basis

$$|\psi\rangle = \sum_{x_1,\ldots x_n} c_{\vec{x}} |\vec{x}\rangle , \tag{2.1}$$

where $\vec{x} = (x_1, x_2, \ldots x_n)$, $x_i = 1, \ldots d_i$. Then, the density matrix corresponding to this state is given by,

$$\rho = \sum_{x_i, x_j'} c_{\vec{x}} \bar{c}_{\vec{x}'} |\vec{x}\rangle \langle \vec{x}'| \tag{2.2}$$

where the bar denotes complex conjugate. From here it is a simple exercise to show that the (k, l) element of the 1-RDM of the ith qudit is given by,

$$\left(\rho_i^{(1)}\right)_{k,l} = \sum_{\vec{x} \neq i} c_{\vec{x}|_{i=k}} \bar{c}_{\vec{x}|_{i=l}} \tag{2.3}$$

where we have used the shorthand notation $\sum_{\vec{x}\neq i} := \sum_{x_1} \ldots \sum_{x_{i-1}} \sum_{x_{i+1}} \ldots \sum_{x_n}$ and where $\vec{x}|_{i=b} = (x_1, \ldots x_{i-1}, b, x_{i+1}, \ldots x_n)$.

For any given $|\psi\rangle$, it is always possible to choose the basis $|\vec{x}\rangle$ such that the 1-RDMs are

diagonal, a choice that will impose conditions on the coefficients $c_{\vec{x}}$. In the particular case of qubits, these conditions are

$$\sum_{\vec{x}\neq i} c_{\vec{x}}|_{i=1}\,\bar{c}_{\vec{x}}|_{i=2} = 0,\ \forall i = 1,\dots n \quad \text{(diagonality)} \tag{2.4}$$

In this chosen basis, the spectra of the ith 1-RDM will be given by

$$\begin{aligned} \operatorname{spec}(\rho_i^{(1)}) &= \left(\lambda_1^{(i)},\dots,\lambda_{d_i}^{(i)}\right) \\ \lambda_j^{(i)} &= \sum_{\vec{x}\neq i} |c_{\vec{x}}|^2_{i=j} = \langle j|\operatorname{tr}_{\setminus i}\rho\,|j\rangle \end{aligned} \tag{2.5}$$

where we use the notation $\operatorname{tr}_{\setminus i}$ to denote the partial trace over all subsystems except the ith one. Note that due to the trace condition, $\operatorname{tr}\rho_i^{(1)} = 1$, the spectrum of the ith 1-RDM is representable by $d_i - 1$ real numbers. Note that due to the trace condition and positive semi-definiteness of density operators one must have $0 \leq \lambda_1^{(i)},\dots\lambda_{d_i}^{(i)} \leq 1$. Then, taking into consideration all the 1-RDMs, their spectra give rise to a polytope of admissible spectra in $\mathbb{R}_+^m$, $m = \sum_i^n d_i - n$. For qubits, one can choose $\nu_j := \lambda_1^j - \lambda_2^j$ to represent the spectra and it is a simple exercise to see that, in this case, product states map to the vertices of an hypercube of side 1, centered at the origin. Specifically, in the case of 3 qubits, which plot is amenable to human comprehension, one has

$$\begin{aligned} |000\rangle &\to (1,1,1) & |001\rangle &\to (1,1,-1) \\ |010\rangle &\to (1,-1,1) & |011\rangle &\to (1,-1,-1) \\ |100\rangle &\to (-1,1,1) & |101\rangle &\to (-1,1,-1) \\ |110\rangle &\to (-1,-1,1) & |111\rangle &\to (-1,-1,-1) \end{aligned} \tag{2.6}$$

We know that the admissible spectra will be inside of this cube, but it won't necessarily be

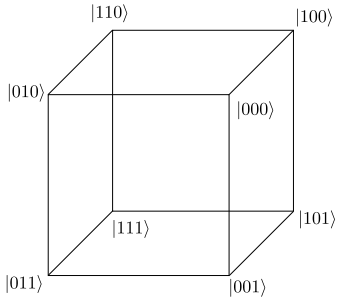

Figure 2.1: The points which the product states map to.

the entire cube. In fact, as we will see shortly the result is more interesting than that. We get a convex polytope if we intersect the image of the moment map (in our case, our partial

trace) with the positive Weyl chamber [1], but not necessarily so if we don't (c.f theorem 55, chapter A). In Fig. 2.2 we plot the entire spectral polytope for 3 qubits for $\nu_i = \lambda_1^{(i)} - \lambda_2^{(i)}$ and its intersection with the positive Weyl chamber, which we choose to be given by $\lambda_j^{(i)} \geq \lambda_{j+1}^{(i)}$, such that for qubits we have, inside the Weyl chamber, $\operatorname{spec} \rho_i^{(1)} = (\lambda_{\max}^{(i)}, \lambda_{\min}^{(i)})$. As can be seen, representing the entire polytope, a star shaped polytope, is not only redundant, but much more complicated, as it is not convex, and hence cannot be represented as intersection of half-spaces. As such whenever we talk about the spectral polytope, we alway refer to its restriction to the above chosen positive Weyl chamber.

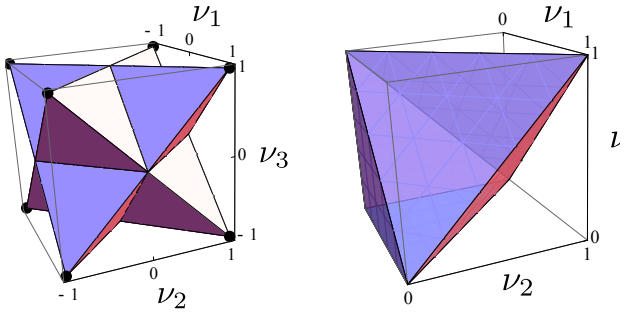

(a) Entire spectral polytope

(b) Restricted to positive Weyl chamber

Figure 2.2: The entire spectral polytope for 3 qubits (a), and its restriction to $\nu_i \geq 0$ (our positive Weyl chamber) (b).

Note also that it is not difficult to see that one can write the *spectral inequality*

$$D = \kappa_0 + \sum_{i=1}^{n} \sum_{j=1}^{d_i} \kappa_{i,j} \lambda_j^{(i)} \leq 0 \tag{2.7}$$

as an expectation value $\langle \hat{D} \rangle_\psi$,

$$\hat{D} = \kappa_0 \mathbb{1} + \sum_{i=1}^{n} \sum_{j=1}^{d_i} \kappa_{i,j} \left[\mathbb{1}^{i-1} \otimes |j\rangle \langle j| \otimes \mathbb{1}^{n-i} \right] \tag{2.8}$$

Fermions

For Fermions things are analogous to case of distinguishable particles, except that there is only one 1-RDM. Let us begin by considering a Hilbert space of N Fermions and a one particle Hilbert space $\mathcal{H}_1$ of dimension d, which we call modes (also known as orbitals in quantum chemistry) $\mathcal{H} = \Lambda^N \mathcal{H}_1 \subset (\mathcal{H}_1)^{\otimes d}$, where $\Lambda^N \mathcal{V}$ denotes the Nth exterior power of the vector

[1] A Weyl chamber is a concept from representation theory, and its definition can be found in any good book on the subject, e.g. [21]. For our discussion, however, it is not important to be acquainted with the definition, but simply to know that "restricting to the positive Weyl chamber" will introduce some constraints on our spectra.

space $\mathcal{V}$ [22]. From now onwards we make the following identification $\mathcal{H}_1 \cong \mathbb{C}^d$. Let $\{|i\rangle_{i=1}\}^d$ be a basis for the single particle space $\mathbb{C}^d$. Then a basis for the product space $\mathcal{H}_1^{\otimes d}$ is given by $\{|i_1\rangle \otimes \ldots \otimes |i_N\rangle\}_{i_1,\ldots i_N=1}^d$. Let us define the *antisymmetrizer*

Definition 1. *Let $\{|i_1\rangle \otimes \ldots \otimes |i_N\rangle\}_{i_1,\ldots i_N=1}^d$ be a basis for $\mathcal{H}$. The antisymmetrizer is a linear operator $\mathcal{A} : H^{\otimes N} \to \Lambda^N(H)$ given by*

$$\mathcal{A}\left(|i_1\rangle \otimes \ldots \otimes |i_N\rangle\right) := \frac{1}{N!} \sum_{\pi \in S_N} \epsilon_\pi \, |\pi(i_1)\rangle \otimes \ldots \otimes |\pi(i_N)\rangle \tag{2.9}$$

where S_N is the symmetric group of dimension $N!$ and ϵ_π is the completely antisymmetric tensor, also called the Levi-Civita symbol, $\epsilon_\pi = \epsilon_{\pi(1),\ldots\pi(p)}$.

Based on the above definition let us also define the wedge product [2]

Definition 2. *The wedge product of $|\psi\rangle \in \Lambda^N\mathcal{V}$, with dimension l and $|\phi\rangle \in \Lambda^M\mathcal{V}$ with dimension m is given by*

$$|\psi\rangle \wedge |\phi\rangle = \mathcal{A}\left(|\psi\rangle \otimes |\phi\rangle\right) \tag{2.10}$$

In particular, a basis for $\mathcal{H}$ is given by $\{|i_1\rangle \wedge \ldots \wedge |i_N\rangle\}_{i=1}^d$. Such states are also called *Slater determinants*. We note that the term Slater determinant appears to be more used whenever one deals with the representation of wavefunctions in a position basis, in particular in Chemistry [23]. We will, however, make use of the term often. An alternative to the wedge product is to make use of second quantization [24]

$$a_{i_1}^\dagger \ldots a_{i_N}^\dagger \, |0\rangle = |i_1\rangle \wedge \ldots \wedge |i_N\rangle \tag{2.11}$$

where $a_i^\dagger$ creates a fermion in the ith mode and $|0\rangle$ is the vacuum. Second quantization makes it very easy to write the 1-RDM $\rho^{(1)}$ of a pure state $|\psi\rangle$ [2],

$$\langle i| \, \rho^{(1)} \, |j\rangle = \langle\psi| \, a_i^\dagger a_j \, |\psi\rangle \tag{2.12}$$

Note that $\operatorname{tr} \rho^{(1)} = N$, with N the number of Fermions, which is the usual normalization in quantum chemistry.

Consider now all possible N particles Slater determinants. Our wavefunction ca be expanded as,

$$|\psi\rangle = \sum c_{i_1,\ldots,i_N} \, |i_1\rangle \wedge \ldots \wedge |i_N\rangle \tag{2.13}$$

Analogous to what we have done for distinguishable particles, we can choose, for a given $|\psi\rangle$, as single particle basis an eigenbasis of the 1-RDM. In the case of Fermions eigenvectors of the 1-RDM are often called *natural orbitals*, while eigenvalues are often called *natural occupation*

[2] It is common to define the wedge product as $|\psi\rangle \wedge |\phi\rangle = \frac{(l+m)}{l!m!}\mathcal{A}\left(|\psi\rangle \otimes |\phi\rangle\right)$ [22]

numbers [23]). This basis induces a basis for the N particle Hilbert space. We call such an expansion of $|\psi\rangle$ an expansion in natural orbitals. In this case,

$$\rho^{(1)} = \sum_{i=1}^{d} \lambda_i |i\rangle \langle i| \tag{2.14}$$

with λ_i the natural occupation numbers. Note that are $m = \binom{N}{d}$ distinct Slater determinants and that each Slater determinant maps to a point in a unit hypercube centered at the origin (but not to all of them since there are only m Slater points against d^N vertices), which we call the Pauli hypercube. Note that the Pauli hypercube is independent of the number of Fermions and only depends on the number of modes. Note also that the trace condition implies that $\sum_i \lambda_i = N$, which defines an hyperplane which intersects the Pauli cube. The moment polytope for the case at hand will further restrict our geometric object.

Identically to what we have done for indistinguishable particles, we impose $\lambda_i \geq \lambda_{i+1}$, such that the only Slater determinant mapping to a point in the positive Weyl chamber is the *ordered Slater state* $|1\rangle \wedge |2\rangle \wedge \ldots \wedge |n\rangle$, written in a basis of natural orbitals of $|\psi\rangle$.

As we have seen Pauli's exclusion principle amounts to $0 \leq \lambda_i \leq 1$, so we call the non-trivial facets (those not coinciding with the boundary of the positive Weyl chamber) *generalized Pauli constraints* or gPCs for short, since they strengthen Pauli's exclusion principle [12].

We often represent spectral inequalities

$$D = \kappa_0 + \sum_{i=1}^{d} \kappa_i \tag{2.15}$$

by $D = \langle \hat{D} \rangle_\psi \leq 0$, as done in [12] where

$$\hat{D} = \kappa_0 \mathbb{1} + \sum_i \kappa_i a_i^\dagger a_i \tag{2.16}$$

in a chosen basis of natural orbitals of $|\psi\rangle$.

2.1 Some fully characterizable settings

2.1.1 Indistinguishable particles

Bipartite systems

In the case of a bipartite system composed of parts A and B with local dimensions d_A and d_B, respectively, the full characterization of the pure univariate marginal problem is trivial due to Schmidt decomposition/ singular value decomposition.

Consider a pure state $|\psi\rangle \in \mathcal{H} = \mathcal{H}_A \otimes \mathcal{H}_B$ and let $\{|u_i\rangle\}_{i=1}^{d_A}$ and $\{|v_i\rangle\}_{i=1}^{d_B}$ be orthonormal

basis for $\mathcal{H}_A$ and $\mathcal{H}_B$, respectively. Then by Schmidt decomposition $|\psi\rangle$ can be written as [25]

$$|\psi\rangle = \sum_{i=1}^{m} c_i \, |u_i\rangle \otimes |v_i\rangle \,, \tag{2.17}$$

where $m = \min(d_A, d_B)$. Assume, without loss of generality that $d_B - d_A = d, d > 0$. Then the 1-RDMs for our system, in the above chosen basis, are trivially

$$\begin{aligned} \rho_1^{(1)} &= \mathrm{diag}(|c_1|^2, \ldots |c_{d_A}|^2) \\ \rho_2^{(1)} &= \mathrm{diag}(|c_1|^2, \ldots |c_{d_A}|^2, 0, \ldots, 0) \end{aligned} \tag{2.18}$$

i.e. the spectra of the two 1-RDMs are identical up to some trailing zeros.

For the particular case of two qubits, $d_A = d_B = 2$. Then $\mathrm{spec}(\rho_A) = \mathrm{spec}(\rho_B) = (\lambda_{\max}, \lambda_{\min})$.

n Qubits

Consider a system of n qubits. Let $\rho_i = \mathrm{tr}_{\setminus i}\, \rho$ and $\mathrm{spec}\, \rho_i = (\lambda_{\min}^{(i)}, \lambda_{\max}^{(i)})$. Since $\lambda_{\min}^{(i)} + \lambda_{\max}^{(i)} = 1$ there is only one parameter describing the spectrum of each reduction. It has been proved by Higuchi and Sudberry [6] that such reduced spectra must satisfy

$$\lambda_{\min}^{(i)} \leq \sum_{j \neq i} \lambda_{\min}^{(j)}, \forall i. \tag{2.19}$$

Conversely, a given spectra corresponds to a globally pure state only if it fulfills these conditions.

One can restate this conditions by using instead the difference of the eigenvalues of the 1-RDMs, $\nu_i := \lambda_{\max}^{(i)} - \lambda_{\min}^{(i)}$, in which case we get

$$\nu_i \geq \sum_{j \neq i} \nu_j - (n-2), \forall i. \tag{2.20}$$

Let us assume, without loss of generality that $\lambda_{\min}^{(i)} \geq \lambda_{\min}^{(i+1)}$, i.e. we simply relabel qubits such that the first one has the largest minimal 1-RDM eigenvalue, the second the second largest and so on. Then the inequalities in (2.19) reduce to the the single inequality (plus ordering),

$$\lambda_{\min}^{(1)} \leq \sum_{i=2}^{n} \lambda_{\min}^{(i)} \tag{2.21}$$

Identically, if we assume $\mu_i \geq \mu_{i+1}$, they reduce to the single non trivial inequality (plus ordering)

$$\nu_n \geq \sum_{j \neq n} \nu_j - (n-2) \,. \tag{2.22}$$

The resulting polytope for 3 qubits, is plotted in Fig 2.3.

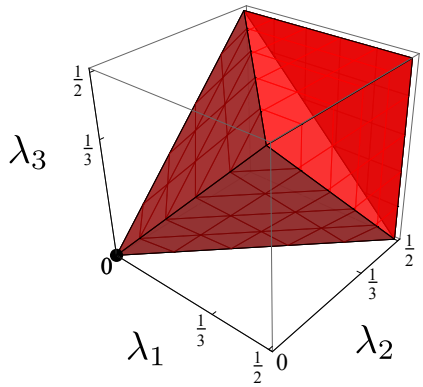

Figure 2.3: Higuchi polytope for 3 qubits for $\lambda_i = \lambda_i^{\min}$. The black dot corresponds to the local spectra of the product state $|0\rangle \otimes |0\rangle \otimes |0\rangle$.

2.1.2 Fermions

2 particles

We consider the case of two Fermions and d modes, $\mathcal{H} = \Lambda^2(\mathbb{C}^d) \subset \mathbb{C}^d \otimes \mathbb{C}^d$. Note that a pure 2 Fermions state can be written as [26]

$$|\psi\rangle = \sum_{i=1}^{d} c_i u_i^\dagger v_i^\dagger |0\rangle , \tag{2.23}$$

where for d even $\{|v_i\rangle , |u_i\rangle\}_{i=1}^{d/2}$ is an orthonormal basis for $\mathbb{C}^d$ and, identically, for d odd $\{|v_i\rangle , |u_i\rangle\}_{i=1}^{(d-1)/2} \cup \{|w\rangle\}$. Let us then make the following correspondence, for d even

$$\begin{aligned} a_{2i-1}^\dagger &= u_i^\dagger \\ a_{2i}^\dagger &= v_i^\dagger \end{aligned} \tag{2.24}$$

for $i = 1, \ldots, d/2$, while for d odd we consider

$$\begin{aligned} a_{2i-1}^\dagger &= u_i^\dagger \\ a_{2i}^\dagger &= v_i^\dagger \\ a_d^\dagger &= w^\dagger \end{aligned} \tag{2.25}$$

In this case, given the definition of 1-RDM, Eq. 2.12, and written the above basis, ρ is diagonal. Its spectra is trivially always doubly degenerate, its eigenvalues being $|c_i|^2$ except for potentially an unpaired eigenvalue equal to 0 whenever d is odd.

Particle-hole duality

One fairly important result is that there is a relationship between the spectral polytopes in $\Lambda^N(\mathbb{C}^d)$ and $\Lambda^{d-N}(\mathbb{C}^d)$.

Lemma 3. *Consider the Hilbert space $\mathcal{H} = \Lambda^N(\mathbb{C}^d)$ and let $D(\lambda)$ define the facets of its spectral polytope. Then the spectral polytope for $\mathcal{H} = \Lambda^{d-N}(\mathbb{C}^d)$ is obtained from the previous spectral polytope via the substitution $\lambda_i \to \lambda_{d-i+1}$.*

This lemma has been proven by Altunbulack [27]. Here we give a self contained proof of this fact based on Hodge duality. To do so let us first define the Hodge start operator

Definition 4 (Hodge star operator)**.** *Let $\{|e_i\rangle\}_{i=1}^d$ be a basis for $\mathbb{C}^d$. Then the Hodge star operator, also known as Hodge dual, is a linear map $\star : \Lambda^N(\mathbb{C}^d) \to \Lambda^{d-N}(\mathbb{C}^d)$ given by*

$$\star\left(|e_{i_1}\rangle \wedge \ldots \wedge |e_{i_N}\rangle = \epsilon_{i_1,\ldots i_N;i_{N+1},\ldots,i_d} \left|e_{i_{N+1}}\right\rangle \wedge \ldots \wedge |e_{i_d}\rangle\right)$$

where $\epsilon_{i_1,\ldots i_N;i_{N+1},\ldots,i_d}$ is the Levi-Civita symbol.

Since the dimension of both spaces is the same and the Hodge dual is injective when restricted to a basis of $\Lambda^N(\mathbb{C}^d)$, it is in fact an *isomorphism*. From the above, if we let $a_i^\dagger$ be the second quantization creation operator related to the basis vector $|e_i\rangle$, the Hodge star operation can be cast into the form

$$\star\left(a_{i_1}^\dagger \wedge \ldots \wedge a_{i_N}^\dagger\right) = \epsilon_{i_1,\ldots i_N;i_{N+1},\ldots,i_d} a_{i_{N+1}}^\dagger \wedge \ldots \wedge a_{i_d}^\dagger \tag{2.26}$$

We define also $\star\langle\psi| := (\star|\psi\rangle)^\dagger$. We are now in position to prove Lemma 3.

Proof. Let $|\psi\rangle \in \mathcal{H} \cong \Lambda^N(\mathbb{C}^d)$. Let $\{a_i^\dagger|0\rangle\}_{i=1}$ be a set of natural orbitals of $|\psi\rangle$. Obviously $|\psi\rangle$ can be expanded in the many-particle basis constructed from this single particle basis,

$$|\psi\rangle = \sum_{i_1,\ldots i_N} c_{i_1,\ldots i_N} a_{i_1}^\dagger \ldots a_{i_N}^\dagger |0\rangle . \tag{2.27}$$

Then the eigenvalues of the 1-RDM are given by, as seen before, $\lambda_i = \sum_{i_1,\ldots i_N, i\in\{i_1,\ldots i_N\}} |c_{i_1,\ldots,i_N}|^2$. Consider now the Hodge dual of $|\psi\rangle$,

$$\star|\psi\rangle = \sum_{i_1,\ldots i_N} |c_{i_1,\ldots,i_N}| \star\left(a_{i_{i_1}}^\dagger \ldots a_{i_N}^\dagger |0\rangle\right) \tag{2.28}$$

and let us calculate the 1-RDM for this state. $\rho' = (\star\langle\psi|)\, a_i^\dagger a_i\, (\star|\psi\rangle)$. It is pretty obvious it

is diagonal in the basis we have chosen, so we only need to consider the diagonal elements

$$\begin{aligned}\lambda_i' &= \sum_{i_1,\ldots i_N, i\notin\{i_1,\ldots i_N\}} |c_{i_1,\ldots,i_N}|^2 \\ &= 1 - \sum_{i_1,\ldots i_N, i\in\{i_1,\ldots i_N\}} |c_{i_1\ldots i_N}|^2 = 1-\lambda_i\end{aligned} \tag{2.29}$$

The important thing to note now is that since the Hodge star is an isomorphism, it will map all possible states of $\mathcal{H}$ into all possible states of $\mathcal{H}'$ and the same with the spectral polytope. Note also that if $\lambda_i \geq \lambda_{i+1}$ then obviously $1-\lambda_i \leq \lambda_{i+1}$ such that then the spectra inequalities of $\mathcal{H}$ can be transformed into those of $\mathcal{H}'$ by $\lambda_i \to 1-\lambda_{d-i+1}$. □

Note that since the one and two fermion situations are trivial and due to the duality stated above, the first non-trivial scenario occurs for 3 Fermions and 6 modes $\mathcal{H} = \Lambda^3\left(\mathbb{C}^6\right)$.

3 Fermions and 6 modes

The case $\mathcal{H} = \Lambda^3\left(\mathbb{C}^6\right)$ is the lowest dimensional non-trivial Fermionic problem and has been treated numerically by Dennis and Borland in 1972 [28]. Although they have failed to prove analytically the necessity and sufficiency of the conditions, their efforts marked a step forward in understanding the quantum marginal problem.

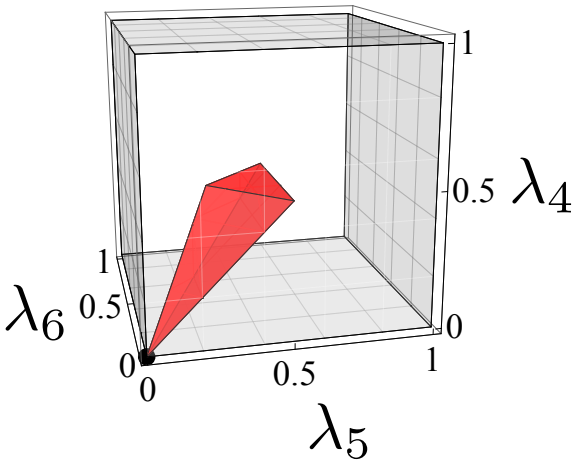

Figure 2.4: Dennis-Borland reduced polytope, along with the reduced Pauli cube. The black point is the local spectrum of the ordered Slater point, which is (1,1,1,0,0,0), corresponding to (0,0,0) in our reduced polytope.

The inequalities defining the moment polytope in this case are given by

$$\begin{aligned}\lambda_1+\lambda_6 = \lambda_2+\lambda_5 = \lambda_3+\lambda_4 = 1 \\ 2-(\lambda_1+\lambda_2+\lambda_4) \geq 0\end{aligned} \tag{2.30}$$

Note that due to the 3 equalities, one can effectively represent the moment polytope in $\mathbb{R}^3$ making the Denis-Borland case the only non-trivial Fermionic case whose moment polytope is plotable. In Fig. 2.4 we show a plot of this reduced polytope, along with a reduced Pauli cube.

Chapter 3

One particle based simplification of a many body wavefunction

As seen in the previous chapters the spectra of the 1-RDMs of a system of particles are subject to a several constraints, which, in the case of Fermions, generalize Pauli's exclusion principle. The set of possible eigenvalues of the 1-RDMs of the system has been identified as a so-called *moment polytope*. It has been mentioned in the literature [11] that states which eigenvalues lie on the boundary of the spectral polytope exhibit a strongly simplified structure, but no proof was given. Here, we derive this statement using only elementary methods, generalizing (and in particular instances strengthening) the theory for the physically important case of degenerate spectra.

3.1 Introduction

It is a long know fact that some particular forms of the 1-RDM(s) lead to a specific form of the wavefunctions that can give rise to such 1-RDMs. As an example, let us consider a Fermionic system with N Fermions and n modes/orbitals if the spectrum of the 1-RDM $\rho^{(1)}$ is $(\underbrace{1,...1}_{n},\underbrace{0,...,0}_{n-N})$ then the associated wavefunction has to be, up to a phase, $|\phi_1\rangle \otimes \ldots \otimes |\phi_n\rangle$ where $|\phi_i\rangle$ is the ith eigenvector of $\rho^{(1)}$. For a system of N distinguishable particles, if all 1-RDMs have spectra $(1, 0, \ldots, 0)$, then the only wavefunction giving rise to such spectra must be given by $\left|\phi_1^1\right\rangle \otimes \phi_1^N$ where $\left|\phi_i^j\right\rangle$ is the ith eigenvector of the jth particle. Both these examples correspond to a vertex on the corresponding spectral polytope. This may raise the question of whether there are further simplifications or not if one lies on one of the facets of the spectral polytope and if so, what simplifications are these. The answer turns out to be affirmative and the simplifications for the case of non-degenerate spectra has been given by Klyachko in [11]. However Klyachko has not given a proof for this simplification, which he

calls "*selection rule*" [1].

Here we prove this fact and generalize it for the case of degenerate 1-RDMs. We also show that while in general degeneracy weakens the "selection rule", in some instances degeneracy leads actually allows one to draw stronger conclusions than the non-degenerate case. An added benefit of our approach is that it does not require knowing the spectral polytope globally, which is a big plus since this polytope seems to be extremely difficult to calculate, in the sense that there is not yet an efficient algorithm to do so (and there may never be one) [29] (Michael Walter, personal communication, 2014).

To that effect we introduce two methods of deriving the "selection rule". In the first method we introduce, which we call *tangent space method* we begin by computing the full tangent space at a given state $|\psi\rangle$. The tangent space which gives us the directions in which we can, infinitesimally, change our state. By calculating the image of the tangent space under the moment map, we readily obtain the directions in which we can move up to first order in spectral space. Since, for a state with extremal local spectra we are not allowed, to first order, to leave the corresponding facet of the spectral polytope, the image of the tangent space under the moment map effectively coincides with our facet. As we prove, the spectra of some particular basis vectors lie in the affine plane generated by our facet and these basis vectors are the ones that are allowed to show up in the expansion of $|\psi\rangle$, effectively proving the "selection rule". The results obtained from this method are valid also in the case of degenerate 1-RDMs. In the second method, which is simpler than the tangent space method, we consider the imaginary time evolution (or mathematically speaking, the flow, hence the name) of a state $|\psi\rangle$ generated by the operator $\hat{D}$ as defined in Chapter 2. The average value of $\hat{D}$ changes due to this evolution, and as we prove it can either decrease or remain constant. The important point that we prove, using perturbation theory, is that it that it remains constant if and only if $|\psi\rangle$ is an eigenstate of $\hat{D}$. This has consequences on the form of $|\psi\rangle$. While this method is very elementary and allows us to prove the selection rule for a non-degenerate case, we cannot extended it to a general degenerate case. However, given it simplicity we were able to use it for proving a stronger statement in the non-degenerate case for some particular situations.

3.2 Tangent space method

Let us consider a system of N particles with Hilbert space $\mathcal{H}$. Our derivation works equally well for a system of distinguishable particles or Fermions.

We shall focus solely on the pure state scenario. Such states correspond to the set $\mathbb{P}(\mathcal{H})$

[1] We note that this terminology is unfortunately, not the best, as a selection rule already a precise meaning in physics and chemistry, being a constraint on quantum transitions, which is certainly not the case here.

of all normalized, rank-one projection operators (assumed Hermitian) on $\mathcal{H}$:

$$\mathbb{P}(\mathcal{H}) = \left\{ |\psi\rangle\langle\psi| \;\middle|\; |\psi\rangle \in \mathcal{H},\, \langle\psi|\psi\rangle = 1 \right\}.$$

which are extremal points of the set of all states and are isomorphic to the projective Hilbert space of $\mathcal{H}$, a smooth manifold [30], which justifies our notation.

Let $\mathcal{L}(\mathcal{H})$ be the set of linear operators on $\mathcal{H}$ and let us consider the set of Hermitian/self-adjoint (not necessarily local) operators $\mathrm{i}\mathfrak{f} = \left\{ H \in \mathcal{L}(\mathcal{H}) |\, H = H^\dagger \right\}$ and the set of traceless local Hermitian operators embedded into $\mathcal{L}(\mathcal{H})$, $\mathrm{i}\mathfrak{g} = \left\{ h = \oplus_i h_i,\, h_i \in \mathcal{L}(\mathcal{H}_i) |\, h_i = h_i^\dagger \wedge \mathrm{tr}\; h_i = 0 \right\}$, $\mathrm{i}\mathfrak{g} \subset \mathrm{i}\mathfrak{f}$, where $\oplus$ denotes the *Kronecker sum*, $A \oplus B := A \otimes \mathbb{1} + \mathbb{1} \otimes B$. In physical terms, the set $\mathrm{i}\mathfrak{f}$ can be thought of as the set of all possible N particle Hamiltonians while $\mathrm{i}\mathfrak{g}$ can be thought of as the set of all (traceless) local 1-particle Hamiltonians acting on n particles. Alternatively, it may prove convenient to swap the word Hamiltonian for observables in the previous sentence. Both of these sets have an associated Lie algebra structure. For a system of n qudits with local dimensions d_i and defining $d = \prod_{i=1}^n d_i$ we have $\mathfrak{f} = \mathfrak{u}(d)$, the Lie algebra of the unitary group $U(d)$, and $\mathfrak{g} = \mathfrak{su}(d_1) \oplus \cdots \oplus \mathfrak{su}(d_n)$, the Lie algebra of $SU(d_1) \otimes \ldots \otimes SU(d_n)$. For a system of N Fermions with single particle space of dimension d, i.e. d orbitals/modes, the Hilbert space is $\Lambda^N(\mathbb{C}^d)$ which will take to be embedded into $\mathcal{H} = \left(\mathbb{C}^d\right)^{\otimes N}$ and we have $\mathfrak{f} = \mathfrak{u}(d^n)$ and $\mathfrak{g} = \mathfrak{su}(d) \oplus \ldots \oplus \mathfrak{su}(d)$. Note that one reason we choose to work with traceless operators is because $\mathfrak{su}$ is a semisimple Lie algebra while $\mathfrak{u}$ is not, which makes $\mathfrak{su}$ more "well-behaved" [31, Chapter 6]. We take as well f^* to denote the vector space dual to the Lie algebra f and connect them via the Hilbert-Schmidt inner product, i.e. for $\langle X, - \rangle := \mathrm{tr}\,[X -] \in \mathfrak{f}^*$ for $X \in \mathfrak{f}$.

In the following discussion we take our manifold $\mathbb{P}(\mathcal{H})$ to be embedded into $\mathrm{i}\mathfrak{f}^*$. This will make the following easier and cleaner.

Let us consider the *linear* map μ that maps Hermitian operators *onto* local, traceless Hermitian operators, $\mu : \mathrm{i}\mathfrak{f}^* \to \mathrm{i}\mathfrak{g}^*$,

$$\mu : H \mapsto \bigoplus_i \left(h_i - \frac{1}{d_i} \mathbb{1}_{d_i} \,\mathrm{tr}\, H \right) \tag{3.1}$$

with

$$h_i = \mathrm{tr}_{\setminus i}\, H \tag{3.2}$$

with $\bigoplus$ represents the Kronecker sum. In the particular case where we restrict the domain of μ to $\mathbb{P}(\mathcal{H})$ [2], μ is a *moment map* (cf. Appendix A). It maps pure states $\rho =: |\psi\rangle\langle\psi|$ onto their local spectra,

$$\mu : \rho \mapsto \bigoplus_i \left(\rho_i^{(1)} - \frac{1}{d_i} \mathbb{1}_{d_i} \,\mathrm{tr}\, \rho \right), \tag{3.3}$$

[2] This restriction is no longer linear since $\mathbb{P}(\mathcal{H})$ is *not* a linear space.

with $\rho_i^{(1)} = \rho^{(1)}$ and $d_i = d$ for Fermions. In other words, μ is just the partial trace operation, where the reduced density matrices are still embedded into our global space of operators (up to setting the trace to zero).

It will prove necessary to prove the following lemma regarding μ

Lemma 5. *The linear map μ is a Hilbert-Schmidt projection operator, i.e. $\mu^2 = \mu$, $\mu = \mu^\dagger$.*

Proof. From the definition of μ it is obvious that $\mu^2 = \mu$. Hence, we need only to prove that μ is self adjoint with respect to the Hilbert-Schmidt inner product, i.e. $(H, \mu(K)) = (\mu(H), K), \forall H, K \in \mathfrak{if}$, where $(H, K) := \operatorname{tr} HK$ is the Hilbert-Schmidt inner product. Let us begin by expanding these operators in a product basis,

$$H = H^{i_1,\ldots,i_n}_{j_1\ldots,j_n} |i_1\rangle \langle j_1| \otimes \ldots \otimes |i_n\rangle \langle j_n| \tag{3.4}$$

where $i_k = \{1, \ldots d_k\}$ and where we have used summation convention. Now,

$$(H, \mu(K)) = \operatorname{tr} H^{i_1,\ldots,i_n}_{j_1\ldots,j_n} |i_1\rangle \langle j_1| \otimes \ldots \otimes |i_n\rangle \langle j_n| \, \mu(K) \tag{3.5}$$

Note that $K_k = \operatorname{tr}_{\setminus k}(K) = K^{i_1,\ldots i_k,\ldots i_n}_{i_1\ldots j_k\ldots i_n} |i_k\rangle \langle j_k|$. Hence we have

$$(H, \mu(K)) = \sum_{k=1}^{n} \operatorname{tr} H^{i_1,\ldots,i_n}_{j_1\ldots,j_n} |i_1\rangle \langle j_1| \otimes \ldots \otimes A_k \otimes \ldots \otimes |i_n\rangle \langle j_n| \tag{3.6}$$

with

$$A_k = \left[K^{i'_1,\ldots i'_k,\ldots i'_n}_{i'_1\ldots j'_k\ldots i'_n} - \frac{1}{d_i} \delta^{i'_k}_{j'_k} \operatorname{tr} H \right] |i_k\rangle \langle j_k|i'_k\rangle \langle j'_k| \tag{3.7}$$

So finally we get

$$\begin{aligned} (H, \mu(K)) &= \sum_{k=1}^{n} H^{i_1,\ldots i_k\ldots,i_n}_{i_1\ldots j_k\ldots i_n} \left[K^{i'_1,\ldots j_k,\ldots i'_n}_{i'_1\ldots i_k\ldots i'_n} - \frac{1}{d_i} \delta^{j_k}_{i_k} \operatorname{tr} H \right] \\ &= \sum_{k=1}^{n} \left[H^{i_1,\ldots i_k\ldots,i_n}_{i_1\ldots j_k\ldots i_n} K^{i'_1,\ldots j_k,\ldots i'_n}_{i'_1\ldots i_k\ldots i'_n} - \frac{\operatorname{tr} H \operatorname{tr} K}{d_i} \right] \end{aligned} \tag{3.8}$$

Since this expression is invariant under $H \leftrightarrow K$, we have $(H, \mu(K)) = (\mu(H), K)$, or $\mu = \mu^\dagger$. □

Also, for reasons that will be clarified in an instant, we will need to know the tangent space at ρ to $\mathbb{P}(\mathcal{H})$, which is given by,

$$\begin{aligned} T_\rho \mathbb{P}(\mathcal{H}) &= \left\{ \partial_t|_0 \left(|\phi(t)\rangle \langle \phi(t)| \right) \;\middle|\; \langle \phi(t)|\phi(t)\rangle = 1, \, |\phi(0)\rangle = |\psi\rangle \right\} \\ &= \left\{ |\partial_t|_0 \phi(t)\rangle \langle \psi| + |\psi\rangle \langle \partial_t|_0 \phi(t)| \;\middle|\; \langle \phi(t)|\phi(t)\rangle = 1, \, |\phi(0)\rangle = |\psi\rangle \right\} \end{aligned} \tag{3.9}$$

Since $\langle \partial_t|_0 \phi(t)|\psi\rangle = 0$, we finally arrive at,

$$T_\rho \mathbb{P}(\mathcal{H}) = \left\{ |\phi\rangle\langle\psi| + |\psi\rangle\langle\phi| \;\middle|\; \langle\phi|\psi\rangle = 0 \right\} \tag{3.10}$$

With respect to a basis containing $|\psi\rangle$ as its first element, the tangent space is

$$T_\rho \mathbb{P}(\mathcal{H}) = \left\{ \begin{pmatrix} 0 & \phi^\dagger \\ \phi & 0 \end{pmatrix} \;\middle|\; \phi \in \mathbb{C}^{d-1} \right\}. \tag{3.11}$$

Fig. 3.1 shows the geometry of our problem. Given the equation above it is not difficult to show that the Hilbert-Schmidt projection $P_\psi : \mathrm{i}\mathfrak{f}^* \to T_\rho \mathbb{P}(\mathcal{H})$ can be written as

$$P_\psi : H \mapsto |\psi\rangle\langle\psi|\,(\mathrm{i}H) + (\mathrm{i}H)^\dagger\,|\psi\rangle\langle\psi| \tag{3.12}$$

Let $\mathrm{Ad}_g : \mathfrak{g} \to \mathfrak{g}\; g \in G$ defined by $\mathrm{Ad}_g X := g^{-1} X g \cdot X \in \mathfrak{g}$ denote the adjoint action of the group G on its Lie algebra $\mathfrak{g}$ and let $\mathrm{ad}_X := \partial_t|_0 \mathrm{Ad}_{\mathrm{e}^{tX}}$, $X \in \mathfrak{g}$ denote its differential, which for matrix Lie algebras (which is what we consider in our discussion) is simply given by the the commutator, $\mathrm{ad}_X Y = [X, Y]$, $X, Y \in \mathfrak{g}$. We let then, $\mathrm{Ad}^*_g : \mathfrak{g}^* \to \mathfrak{g}^*$, given by $\mathrm{Ad}^*_g := (\mathrm{Ad}_g)^*$, denote the *coadjoint* action of the group G on the dual of its Lie algebra g^*. We then have

Observation 6. *For Hermitian H we have*

$$\partial_t|_0 \; \mathrm{Ad}_{\mathrm{e}^{\mathrm{i}tH}} \rho = \mathrm{ad}_{\mathrm{i}H} \rho \cong P_\psi H, \tag{3.13}$$

where we have identified $\mathfrak{g}$ with its dual $\mathfrak{g}^*$ and hence made use of the adjoint action. [3].

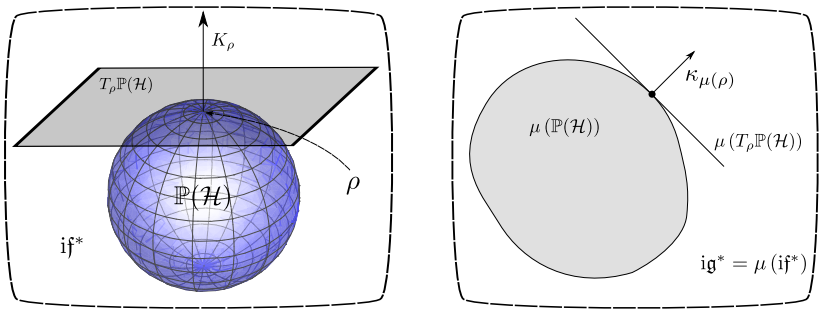

(a) Pre-image of μ (b) Image of μ

Figure 3.1: Our original space and its image under μ.

Let us define $\mathrm{i}\mathfrak{g}_\psi = \{h \in \mathrm{i}\mathfrak{g} |\; \mathrm{ad}_{\mathrm{i}h}\,\rho = 0\}$, in a sense the group of local (albeit traceless) symmetries of ρ, i.e. those observables $h \in \mathfrak{g}$ such that $[h, \rho] = 0$.

[3] To be really precise we should have made use of the coadjoint action, since $\rho \in \mathfrak{g}^*$. We will however simply identify $\mathfrak{g}$ with its dual whenever necessary.

The following lemma will be central to our discussion. It tells us that the infinitesimal changes in the 1-RDMs are given by the annihilator of the local symmetries of ρ.

Lemma 7. *It holds that*

$$\mu\left(T_\rho \mathbb{P}(\mathcal{H})\right) = \mathrm{i}\mathfrak{g}^0_\psi \subset \mathrm{i}\mathfrak{g}^* \tag{3.14}$$

Proof. We begin by considering the embedding $\mathrm{i}\mathfrak{g} \hookrightarrow \mathrm{i}\mathfrak{f}$ and identify our spaces with their duals.

$$\begin{aligned} \mu\left(T_\rho\right) &= \mathrm{range}\left(\mu P_\psi\right) \\ &= \ker\left[\left(P_\psi \mu\right)\right]^\perp \\ &= \left\{h \in \mu(\mathrm{i}\mathfrak{f}^*) | P_\psi h = 0\right\}^\perp \\ &\cong \left\{h \in \mathrm{i}\mathfrak{g} |\, \mathrm{ad}_{\mathrm{i}h}\, \rho = 0\right\}^0 \end{aligned} \tag{3.15}$$

where the complement is to be taken in $\mathrm{i}\mathfrak{g}^*$ and where we made use of the fact that the orthocomplement of the range of a linear transformation is the kernel of the adjoint transformation [32, Chapter II], that μ and P_ψ are both projectors and the projection-flow relation, Eq. (3.13). □

Let $\mathfrak{t}$ be a Cartan subalgebra of $\mathfrak{g}$, which in $\mathrm{i}\mathfrak{g}$ corresponds to a maximally commuting set of local, traceless Hamiltonians, to which we refer to as *maximal toral subalgebra* [4]. In other words, to the diagonal matrices of $\mathrm{i}\mathfrak{g}$, after an appropriate choice of basis. We then denote this set of maximally commuting operators as $\mathrm{i}\mathfrak{t}$.

The following lemma will marks the difference between the case of non-degenerate 1-RDMs and that of degenerate 1-RDMs

Lemma 8. *Let ρ be a state such that $\mu(\rho) \in \mathrm{i}\mathfrak{t}^*$. Then $h \in \mathrm{i}\mathfrak{g}_\psi$ are diagonal except for the blocks corresponding to degenerate subspaces of $\rho_i^{(1)}$. In particular, whenever all the 1-RDMs are non degenerate, $h \in \mathrm{i}\mathfrak{t}$.*

Proof. By definition, $h \in \mathrm{i}\mathfrak{g}_\psi$ means that $\mathrm{ad}_{\mathrm{i}h}\, \rho = 0$ this is equivalent to

$$\mathrm{Ad}_{e^{\mathrm{i}th}}\, \rho = \rho$$

Now, let A, B be two arbitrary linear operators with $A = A_1 \otimes \ldots \otimes A_n$ a product operator. Assume $ABA^{-1} = B$. In this case, given the definition of partial trace, we have the following invariance

$$\mathrm{tr}_{\setminus i}\, ABA^{-1} = A_i \left(\mathrm{tr}_{\setminus i}\, B\right) A_i^{-1} \tag{3.16}$$

[4] This is true because we work only with semisimple Lie algebras here. $\mathfrak{su}(d)$ is semisimple and its complexification, $\mathfrak{sl}(d, \mathbb{C})$ is semisimple as well [31] (Chapter 6), which means that the maximal toral subalgebra and the Cartan subalgebra are actually identical

Now, by the above, linearity and the definition of the moment map, this implies that

$$\mu\left(\mathrm{Ad}_{e^{ith}}\,\rho\right) = \mathrm{Ad}_{e^{ith}}\,\mu\left(\rho\right) \tag{3.17}$$

which in turn, by definition, must equal $\mu(\rho)$. Hence $\mu(\rho)$ is invariant under the coadjoint action of e^{ith}, or relaxing our notation since we are dealing with matrix Lie groups, $[h, \mu(\rho)] = 0$. This in particular means that $\left[h_i, \rho_i^{(1)}\right] = 0$. □

These result implies that whenever $\rho_i^{(1)}$ is non degenerate, h_i is diagonal. Otherwise it will only be block diagonal, each block having the same size as the corresponding degenerate subspace of $\rho_i^{(1)}$. In the particular case where all 1-RDMs are non degenerate, $h \in \mathfrak{it}$.

We are now in position to make a small intermission and explain our line of thought. Note that we can always find a basis in which the 1-RDMS are diagonal, and so they all commute. Hence we take them to live in $\mathfrak{it}$. It will prove fruitful for our derivation to understand the range of the differential of μ at ρ, but since μ is linear this is just the image of the tangent space at ρ under the action of μ, i.e. $\operatorname{range} d_\rho\mu = \mu(T_\rho\mathbb{P}(\mathcal{H}))$, and that is why we have previously calculated the tangent space at ρ. We are interested in preserving our "diagonality" to first order, i.e. we do not want to leave $\mathfrak{it}$. One justification for this is the following: The map $\mu(\rho)\cap\mathfrak{it} \mapsto \left(\operatorname{spec}\rho_1^{(1)}, \dots \rho_N^{(1)}\right)$ is an isomorphism, but it is no longer so if we do not restrict to the maximal toral subalgebra. Therefore talking about $\mu(\rho)\cap\mathfrak{it}$ or talking about the spectral polytope is the same thing. Hence we consider the intersection $\mu(T_{|\psi\rangle\langle\psi|}\mathbb{P}(\mathcal{H}))\cap\mathfrak{it}$. Then from Eq. (3.17), if no 1-RDM is degenerate, it follows that $i\mathfrak{g}_\psi \subset \mathfrak{it}$, i.e. the elements of $\mathfrak{g}_\psi$ are diagonal as well. It is however not necessarily so if there are degeneracies. That means that if there are degeneracies it is not *a priori* obvious how to calculate the intersection of the expression in lemma 7 with $\mathfrak{it}$.

Here, we make the crucial observation that the local symmetries of ρ, $\mathfrak{g}_\psi$ should be used to choose our maximal toral subalgebra, $\mathfrak{it}$, and consequently a local basis. In fact, let $\mathfrak{it}_\psi$ be *any* maximal toral subalgebra of $i\mathfrak{g}_\psi$. Then the following lemma holds

Lemma 9. *The set of commuting operators* $\mathfrak{it}_\psi$ *can be extended to a maximal set of commuting operators* $\mathfrak{it}$ *of* $\mathfrak{ig}$ *such that* $\mu(|\psi\rangle\langle\psi|) \in \mathfrak{it}^*$.

Proof. From lemma 8 we have that $\mu(|\psi\rangle\langle\psi|)$ commutes with $i\mathfrak{g}_\psi$ (again identifying $\mathfrak{ig}$ with its dual). From here it follows that $\{\mu(|\psi\rangle\langle\psi|)\}\cup i\mathfrak{g}_\psi$ is a set of commuting operators. One can then choose $\mathfrak{it}$ such that $\{\mu(|\psi\rangle\langle\psi|)\}\cup i\mathfrak{g}_\psi \subset \mathfrak{it}$. □

The following lemma is fundamental for the case of degenerate 1-RDMs,

Lemma 10. *The annihilator of* $i\mathfrak{g}_\psi$ *intersected with a set of maximally commuting operators of* $\mathfrak{ig}$ *is equal to the annihilator of the set of maximally commuting operators of* $i\mathfrak{g}_\psi$ *intersected*

with the set of maximally commuting operators of $\mathrm{i}\mathfrak{g}$*, i.e.*

$$\mathrm{i}\mathfrak{g}_\psi^0 \cap \mathrm{i}\mathfrak{t} = \mathrm{i}\mathfrak{t}_\psi^0 \cap \mathrm{i}\mathfrak{t} \tag{3.18}$$

We will prove this lemma shortly. To do so let us define just a few more things.

Let $t \in \mathfrak{t}$ and define the particular adjoint action $\mathrm{ad}_t : \mathfrak{g} \to \mathfrak{g}^{\mathbb{C}}$, $\mathrm{ad}_t : X \mapsto [t, X]$, where $\mathfrak{g}^{\mathbb{C}}$ is the complexification of $\mathfrak{g}$ then we have the following

Lemma 11. ad_t *is a self adjoint operator with respect to the Hilbert-Schmidt inner product.*

Proof.

$$\begin{aligned} \mathrm{tr}\left(\mathrm{ad}_t(X)^\dagger Y\right) &= \mathrm{tr}[t, X]^\dagger Y \\ &= -\mathrm{tr}[t, X^\dagger]Y \\ &= \mathrm{tr}\, X^\dagger [t, Y] \\ &= \mathrm{tr}\, X^\dagger \,\mathrm{ad}_t\, Y \end{aligned} \tag{3.19}$$

hence we have $\mathrm{ad}_t^\dagger = \mathrm{ad}_t$ □

We now note that $t \in t_\psi$ is an endomorphism in $g_\psi^{\mathbb{C}}$ and $g^{\mathbb{C}}$. As an Hermitian operator ad_t can be diagonalized over a complex field, which explains why we consider the complexification of $\mathfrak{g}$. Given that, we can then actually decompose $g_\psi^{\mathbb{C}}$ as a vector space, in the following way

$$\mathfrak{g}_\psi^{\mathbb{C}} = \mathfrak{t}_\psi^{\mathbb{C}} \oplus_\alpha r_{\psi,\alpha} \tag{3.20}$$

where $r_{\psi,\alpha}$ are weight spaces of $g_\psi^{\mathbb{C}}$ with respect to ad_t corresponding to eigenvalue α, that is

$$r_{\psi,\alpha} = \{g \in \mathfrak{g}_\psi \mid \mathrm{ad}_t\, g_\psi = \alpha(t) g_\psi,\ \forall t \in \mathfrak{t}_\psi\}. \tag{3.21}$$

From here it follows trivially that (since the orthocomplement of a direct sum is the intersection of orthocomplements)

$$\left(\mathfrak{g}_\psi^{\mathbb{C}}\right)^\perp = \mathfrak{t}_\psi^{\mathbb{C}} \cap \bigcap_\alpha r_{\psi,\alpha}^\perp \tag{3.22}$$

We note that $\mathfrak{t}$ is contained in the joint 0-eigenspace of $\mathrm{ad}_t(g^{\mathbb{C}}), t \in \mathfrak{t}_\psi$ and that $r_{\psi,\alpha}$ is an α eigenspace and so we make the following observation

Observation 12. $\mathfrak{t} \subset r_{\psi,\alpha}^\perp$.

We can now prove Lemma 10.

Proof.

$$\begin{aligned}\left(g_\psi^{\mathbb{C}}\right)^\perp \cap \mathfrak{t} &= \left(\mathfrak{t}_\psi^{\mathbb{C}} \bigcap_\alpha \mathfrak{t}\right) \cap \mathfrak{t} \\ &= \mathfrak{t}_\psi^{\mathbb{C}} \cap \mathfrak{t} \\ &= \mathfrak{t}_\psi \cap \mathfrak{t}\end{aligned} \tag{3.23}$$

we also note that $g_\psi^{\mathbb{C}} \cap \mathfrak{t} = g_\psi$ and $\left(g_\psi^{\mathbb{C}}\right)^\perp \cap \mathfrak{t} = (g_\psi)^\perp \cap \mathfrak{t}$. and from here one has

$$\mathrm{i}\mathfrak{g}_\psi^\perp \cap \mathrm{i}\mathfrak{t} = \mathrm{i}\mathfrak{t}_\psi^\perp \cap \mathrm{i}\mathfrak{t} \tag{3.24}$$

□

Let

$$\mathcal{H}_\lambda = \{|x\rangle \in \mathcal{H} |\, \forall h \in \mathrm{i}\mathfrak{t},\, h\,|x\rangle = \lambda^w(h)\,|x\rangle\} \tag{3.25}$$

be a *weight space* associated with the *weight* $\lambda^w : \mathrm{i}\mathfrak{t} \to \mathbb{C}$ [5]. Let also

$$\mathcal{H} = \bigoplus_{\lambda^w} \mathcal{H}_{\lambda^w} \tag{3.26}$$

be a decomposition of $\mathcal{H}$ into weight spaces. It is worthwhile to note that in this case, and as long as there is no degeneracy, the weight spaces are all one dimensional and hence every weight vector can be labeled by the corresponding weight $|x\rangle =: |\lambda^w\rangle$.

For $|\psi\rangle \in \mathcal{H}$ and the choice of a maximal toral algebra, let $\operatorname{supp}\rho$ be the set of weights λ^w such that $|\psi\rangle$ has non-zero overlap with the associated weight spaces

$$\operatorname{supp}\rho = \{\lambda^w \,|\, P_{\mathcal{H}_\lambda^w}\,|\psi\rangle \neq 0\}.$$

where $P_{\mathcal{H}_{\lambda^w}} = |\lambda^w\rangle\langle\lambda^w|$.

Lemma 13. *It holds that*

$$\begin{aligned}\mu\big(T_{|\psi\rangle\langle\psi|}\mathbb{P}(\mathcal{H})\big) \cap \mathrm{i}\mathfrak{t} = \operatorname{span}\{&\mu(|\lambda_i^w\rangle\langle\lambda_i^w|) - \mu(|\lambda_j^w\rangle\langle\lambda_j^w|)\,| \\ &\lambda_i^w, \lambda_j^w \in \operatorname{supp}\rho\}.\end{aligned}$$

Proof. Let $t \in \mathrm{i}\mathfrak{t}$. Then t can be decomposed as $t = \sum_i \lambda_i^w(h)\,|\lambda^w\rangle\langle\lambda^w|$. On the other hand we can write $|\psi\rangle = \sum_{i|\lambda_i^w \in \operatorname{supp}\rho} c_i\,|\lambda_i^w\rangle$. From here it follows that $[t, |\psi\rangle\langle\psi|] = 0$ if and only if

[5] we use the superscript w to avoid confusion between weights and eigenvalues of 1-RDMs, even though both will be shown to be related

$\lambda_i^w(t) = \lambda_j^w(t)$ for all $\lambda_i^w, \lambda_j^w \in \operatorname{supp}\rho$. Hence

$$\begin{aligned}\mathfrak{it}_\psi &= \{\lambda_i^w - \lambda_j^w \mid \lambda_i^w, \lambda_j^w \in \operatorname{supp}\rho\}^\perp \cap \mathfrak{it} \\ &= \operatorname{span}\{\lambda_i^w - \lambda_j^w \mid \lambda_i^w, \lambda_j^w \in \operatorname{supp}\rho\}^\perp \cap \mathfrak{it}\end{aligned}$$

where we made use of the fact that the intersection of orthocomplements is the linear span of the orthocomplement. Taking the orthocomplement on both sides and using lemma 7 and lemma 10 we arrive at

$$\mu\big(T_{|\psi\rangle\langle\psi|}\mathbb{P}(\mathcal{H})\big) \cap \mathfrak{it} = \operatorname{span}\{\lambda_i^w - \lambda_j^w \mid \lambda_i^w, \lambda_j^w \in \operatorname{supp}\rho\}.$$

Now, since $\lambda^w(t) = \langle\lambda^w| t |\lambda^w\rangle = \operatorname{tr}|\lambda^w\rangle\langle\lambda^w| t$, we use the natural pairing $\lambda^w(-) := \operatorname{tr}[\,|\lambda^w\rangle\langle\lambda^w| -]$. What is more, since t is local and traceless, $\operatorname{tr}[\,|\lambda^w\rangle\langle\lambda^w| -] = \operatorname{tr}[\mu(|\lambda^w\rangle\langle\lambda^w|)-]$ and make the identification. $\lambda^w := \mu[|\lambda^w\rangle\langle\lambda^w|]$. We then get

$$\begin{aligned}\mu\big(T_{|\psi\rangle\langle\psi|}\mathbb{P}(\mathcal{H})\big) \cap \mathfrak{it} = \operatorname{span}\{&\mu(|\lambda_i^w\rangle\langle\lambda_i^w|) - \mu(|\lambda_j^w\rangle\langle\lambda_j^w|) \mid \\ &\lambda_i^w, \lambda_j^w \in \operatorname{supp}\rho\}.\end{aligned}$$

□

This important lemma tells us that the directions in spectral space in which we can move whenever we perturb infinitesimally a state $|\psi\rangle$, are given by the linear span of the differences of the image, under the moment map, of the weight vectors in the support of $|\psi\rangle$. As it stands, it is valid for states which spectra lies either on the boundary or inside of the spectral polytope. Since or objective is to prove the selection rule, valid for states with extremal local spectra, we shall restrict our attention to states $|\psi\rangle$ such that $\mu(|\psi\rangle\langle\psi|) \in F$, with F a facet of the spectral polytope (as described above, talking about the spectra of the 1-RDMs, or $\mu(|\psi\rangle\langle\psi|)$ is the same thing, hence we abuse notation an write $\mu(|\psi\rangle\langle\psi|) \in F$ when what we actually mean is that the spectra of the 1-RDMs lie on a facet.) We then state, finally, the main result of this section

Theorem 14. *Let $\mu(\rho) \in F$, where F is a regular facet (co-dimension 1) of the moment polytope.*

Then we have

$$\operatorname{supp}\rho \subset \operatorname{aff} F \tag{3.27}$$

Proof of Theorem 14. If $\mu(|\psi\rangle\langle\psi|) \in F$, then $\mu(|\psi\rangle\langle\psi|) + \big[\mu(T_{|\psi\rangle\langle\psi|}\mathbb{P}(\mathcal{H})) \cap \mathfrak{it}\big]$ is an hyperplane contained in the affine hull of the facet F, for else we could move outside of the facet (in state space that would imply actually leaving $\mathbb{P}(\mathcal{H})$, i.e. the set of pure states). Then by

lemma 13 it follows that for any $\lambda_i^w \in \operatorname{supp} |\psi\rangle\langle\psi|$, $\mu(|\lambda_i^w\rangle\langle\lambda_i^w|)$ must lie on the hyperplane coinciding with the facet F. □

From here it follows that if $\mu(|\lambda_i^w\rangle\langle\lambda_i^w|)$, $\mu(\left|\lambda_j^w\right\rangle\left\langle\lambda_j^w\right|) \in \operatorname{aff} F$, $\kappa(\mu(|\lambda_i^w\rangle\langle\lambda_i^w|) - \mu(\left|\lambda_j^w\right\rangle\left\langle\lambda_j^w\right|) = 0$. Applying this theorem to a facet F defined by a spectral inequality $D(\cdot)$ we obtain the following physically relevant corollary

Corollary 15 (Selection rule for degenerate 1-RDMs)**.** *Let $|\psi\rangle$ be a state which spectra saturates a spectral inequality $D(\cdot) \leq 0$. Then, expanding $|\psi\rangle = \sum_x c_x |x\rangle$ as in Eq. 2.8 and 2.16, where the basis $|x\rangle$ is taken to be constructed from the eigenbasis of the 1-RDMs, there is a choice of eigenbasis (which is not unique in the degenerate sub-spaces) such that*

$$\hat{D}|\vec{x}\rangle \neq 0 \Rightarrow c_{\vec{x}} = 0 \tag{3.28}$$

3.3 Flow method

We give now an alternative and much shorter derivation of the selection rule based on perturbation theory for the non-degenerate case. We also present a strengthened result for the degenerate case, for specific spectral inequalities.

Let H be a Hermitian operator and $|\psi\rangle$ a state vector. Let us now consider the family of states that arise under the "imaginary time evolution" (in mathematical language, the flow) of $|\psi\rangle$ under H:

$$|\psi(t)\rangle := \frac{e^{tH}|\psi\rangle}{\|e^{tH}|\psi\rangle\|_2}. \tag{3.29}$$

the one has

$$\begin{aligned}
\partial_t|_0 \langle H\rangle_{\psi(t)} &= \partial_t|_0 \operatorname{tr}\left(H\frac{e^{tH}|\psi\rangle\langle\psi|e^{tH^\dagger}}{\operatorname{tr} e^{tH}|\psi\rangle\langle\psi|e^{tH^\dagger}}\right) \\
&= \operatorname{tr} H^2|\psi\rangle\langle\psi| + \operatorname{tr} H|\psi\rangle\langle\psi|H - 2\Big(\operatorname{tr}|\psi\rangle\langle\psi|H\Big)^2 \\
&= \langle 2H^2\rangle_\psi - 2\langle H\rangle_\psi^2 =: 2\ \mathrm{Var}_\psi(H).
\end{aligned} \tag{3.30}$$

Note that the variance is non-negative and vanishes if and only if $|\psi\rangle$ is an eigenvector of H. Thus we conclude that the expectation value of H increases under the action of e^{tH}, unless we act on an eigenvector.

We can now formulate the following theorem

Theorem 16. *Let $|\psi\rangle$ be a state vector whose 1-RDMs are diagonal with non-degenerate and non-increasingly ordered eigenvalues λ, D a spectral inequality and $\hat{D}$ be the diagonal operator*

associated with D as discussed in Chapter 2. Then

$$D(\lambda) = 0 \Leftrightarrow \hat{D}\,|\psi\rangle = 0.$$

Proof. We prove it for Fermions. The case for distinguishable particles follows trivially by using the appropriate definition of $\hat{D}$.

Denote the ith diagonal element of the reduced density as $d_i(t)$. First let us note that while $\langle\hat{D}\rangle_\psi = D(\lambda)$, $\langle\hat{D}\rangle_{\psi(t)} = \kappa_0 + \sum_i \sum_j \kappa_{i,j} d_j^{(i)}(t)$ (an expression valid for distinguishable particles and fermions alike) does not equal, in principle, $D(\lambda(t))$. By first order non-degenerate perturbation theory [33, Chapter II.2], the differential of an eigenvalue equals the differential of the associated main diagonal element, i.e.

$$\partial_t|_0 \lambda_j^{(i)}(t) = \partial_t|_0 d_j^{(i)}(t). \tag{3.31}$$

It follows that

$$\begin{aligned} \partial_t|_0\Big(\kappa_0 + \sum_i \sum_j \kappa_{i,j}\lambda_j^{(i)}(t)\Big) &= \partial_t|_0\Big(\kappa_0 + \sum_i \sum_j \kappa_{i,j} d_j^{(i)}(t)\Big) && (3.32)\\ &= \partial_t|_0 \langle\hat{D}\rangle_\psi = 2\,\mathrm{Var}_\psi(\hat{D}). && (3.33) \end{aligned}$$

Therefore, unless $|\psi\rangle$ is an eigenvector of $\hat{D}$, the flow generated by $\hat{D}$ will increase the value of the inequality for small t. Thus, if $|\psi\rangle$ already attains the maximum, it must be in the kernel of $\hat{D}$. □

From this theorem, we get the following important physical statement as a corollary

Corollary 17 (Non-degenerate selection rule)**.** *Let $|\psi\rangle$ be a state saturating a spectral inequality D. Assume also that the 1-RDMs of $|\psi\rangle$ are non degenerate. Then, expanding $|\psi\rangle = \sum_x c_{\vec{x}}\,|\vec{x}\rangle$ as in Eq. 2.8 and 2.16, where the basis $|\vec{x}\rangle$ is taken to be constructed from the eigenbasis of the 1-RDMs one has*

$$\hat{D}\,|\vec{x}\rangle \neq 0 \Rightarrow c_{\vec{x}} = 0 \tag{3.34}$$

For Fermions, the above presented approach can, in some special situations be generalized to degenerate cases. Consider a Fermionic state $|\psi\rangle$ with 1-RDM spectrum given by λ non-increasingly ordered. For simplicity let us assume that $\rho^{(1)}$ has a single degenerate subspace, V, of dimension m with corresponding eigenvalues $\lambda_l \ldots \lambda_{l+m-1}$, for fixed l. The generalization to an arbitrary number of degenerate subspaces follows trivially from our approach. Let us focus on a given spectral inequality $D(\lambda)$ and assume that the given spectrum saturates it, $D(\lambda) = 0$. Let S_m be the set of permutations that will act of the degenerate eigenvalues, i.e.

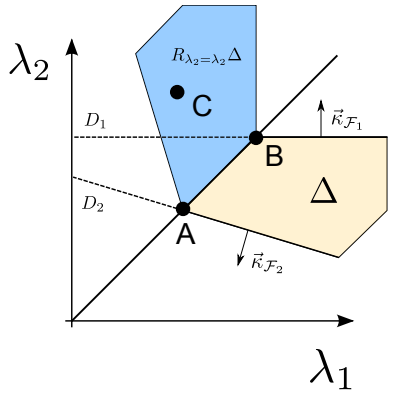

Figure 3.2: Polytope Δ and its reflection along the $\lambda_1 = \lambda_2$ axis $R_{\lambda_1=\lambda_2}\Delta$. Note that $D_2 \leq 0$ is a "valid inequality"not only for the polytope but also for the reflected one. As we will see, point A may then admit a stronger selection rule. The same doesn't happen with point B as for example point C, violates inequality $D_1 \leq 0$.

inside of V. In some cases $D(\pi\lambda'), \forall\pi \in S_m$ and for all non-increasingly ordered spectrum λ', remains a valid inequality (see Fig. 3.2), in the sense that $D(\pi\lambda') < 0$. Let us make the assumption that $D(\pi\lambda') < 0, \forall\pi \in S_i$. We assume as well that there is a decreasingly ordered spectrum λ (hence non-degenerate) such that $D(\lambda) = 0$, These assumption separates the cases where our approach works and where it doesn't. Whenever these assumptions fail, the results form the next section apply. These assumption have implications on the form of the normal vector κ as we will see shortly. First let us prove the following lemma

Lemma 18. *Let $\lambda \in \mathbb{R}^m_+$ be a vector with strictly decreasingly ordered entries. Then* $\max_{\pi\in S_m} \kappa \cdot \pi\lambda = \kappa^{\downarrow} \cdot \lambda$. *Moreover this solution is unique (up to reordering of degenerate components of κ).*

Proof. Let us begin by proving the case $m = 2$. In this case there are only two possibilities: the maximum is attained either for $\kappa_{\max}\lambda_1 + \kappa_{\min}\lambda_2$ or for $\kappa_{\min}\lambda_1 + \kappa_{\max}\lambda_2$. Since by assumption $(\kappa_{\max} - \kappa_{\min})(\lambda_1 - \lambda_2) \geq 0$, it follows that $\kappa \cdot \lambda \leq \kappa^{\downarrow} \cdot \lambda$. For an arbitrary m we can apply the above procedure iteratively. Consider $\kappa_1\lambda_1 + \kappa_2\lambda_2 + \ldots$. This sum can be be increased by swapping κ_1 and $\kappa_1^{\downarrow}$, identically to what we have previously done. It can then be again increased by swapping κ_2 and $\kappa_2^{\downarrow}$, and so on. This procedure achieves the maximum possible value for the inner product and from here it follows that $\kappa_i \geq \kappa_{i+1}$. The uniqueness follows trivially (up to re-ordering of potentially degenerate components of κ). □

We can now see what implications our previous assumptions have on the form of κ,

Lemma 19. *Let S_m be the symmetric group of order m, λ an arbitrary non-increasingly ordered Fermionic 1-RDM spectrum and $D(\lambda) = \kappa_0 + \kappa \cdot \lambda \leq 0$ a spectral inequality. Let $\pi\lambda$ denote the action of $\pi \in S_m$ on m contiguous coordinates of λ, $\lambda_l, \cdots \lambda_{l+m-1}$ for fixed l.*

Assume as well that there is a decreasingly (hence non-degenerate) ordered spectrum λ' such that $D(\lambda) = 0$. Then if $D(\pi\lambda) < 0, \forall \pi \in S_m$ it follows that $k_i \geq k_{i+1}, \quad i = l, \dots l + m - 1$.

Proof. Note that from our definition of spectral inequality, there is a spectrum λ' that saturates our spectral inequality, $D(\lambda') = 0$, where as always, we assume the spectrum to be non-increasingly ordered. Let $V = \{l, \dots, l + m - 1\}$. Then it holds that, for some $\pi \in S_m$

$$\begin{aligned} 0 = D(\lambda') &= \kappa_0 + \sum_{i=1}^{d} \kappa_i \lambda'_i \\ &\leq \kappa_0 + \sum_{i \notin V} \kappa_i \lambda'_i + \sum_{i \in V} \kappa_i^{\downarrow} \lambda'_i = D(\pi\lambda') \leq 0, \end{aligned} \tag{3.35}$$

where $\kappa^{\downarrow}$ denotes a reordering, in non-increasing order, of those components of κ which index is contained in V and where we have used the fact that the maximum of $\kappa \cdot \lambda$ is obtained whenever the components of κ are non-increasingly ordered (Lemma 18). Hence, it follows that $\kappa_i \geq \kappa_{i+1}, \quad i = l, \dots l + m - 1$. □

Theorem 20. *Let $|\psi\rangle$ be a Fermionic state vector whose 1-RDMs are diagonal with non-increasingly ordered eigenvalues, λ and degenerate eigenspaces V_i of dimension m_i, $D(\cdot)$ a spectral inequality which remains valid after disjoint permutation inside the subspaces V_i, and $\hat{D}$ any of the diagonal operator associated with D as discussed in Chapter 2. Assume as well that the spectrum λ saturates D, $D(\lambda) = 0$, and that there's a decreasingly (hence non-degenerate) spectrum λ' such that $D(\lambda') = 0$ Then,*

$$\hat{D} |\psi\rangle = 0, \forall \hat{D} \tag{3.36}$$

Proof. Let to first order, $d_i(t) = d_i + t\bar{d}_i$ denote the perturbed diagonal element of the perturbed 1-RDM and $\lambda(t) = \lambda_i + t\bar{\lambda}$ the perturbed eigenvalues, obtained by application of Eq. 3.29. Then by Schur-Horn's theorem, applied to each degenerate space, we have

$$\bar{d}_{V_i} \prec \bar{\lambda}_{V_i} \tag{3.37}$$

where $\vec{x}_V$ denote the restriction of the vector $\vec{x}$ to the subspace V. It means, geometrically, that $\bar{d}_{V_i}$ is contained in the convex hull of the points obtained by permuting all coordinates of $\bar{\lambda}$. A well known fact in linear programming is that the maximum of an objective function is obtained at a vertex of the feasible region. Combining this with what was just stated above we have that $\kappa_{V_i} \cdot \bar{d}_i \leq \max_{\pi \in S_{m_i}} \kappa_{V_i} \cdot \pi\bar{\lambda}_{V_i}$. But from Lemma 19 we have that $\kappa_i \geq \kappa_{i+1}$, moreover, we know that $\max_{\pi \in S_{m_i}} \kappa_{V_i} \cdot \pi\vec{\bar{\lambda}}_{V_i} = \kappa_{V_i}^{\downarrow} \cdot \bar{\lambda}_{V_i}$ (Lemma 18) and hence we have

$$\kappa_{V_i} \cdot \bar{d}_{V_i} \leq \kappa_{V_i} \cdot \bar{\lambda}_{V_i} \tag{3.38}$$

Note that for the non degenerate subspaces we have $\partial_t|_0\lambda_i(t) = \partial_t|_0 d_i(t)$. Then we have, to first order

$$\begin{aligned} D(\lambda(t)) &= D(\lambda) + t\partial_t|_0 D(\bar{\lambda}) \geq D(\lambda) + t\sum_i \bar{d}_i \\ &= D(\lambda) + 2t\,\mathrm{Var}(\hat{D}_\psi) \end{aligned} \tag{3.39}$$

Since, by assumption $D(\lambda) = 0$, and $D(\lambda(t)) \leq 0$, we have $\mathrm{Var}(\hat{D}_\psi) = 0$ and hence $|\psi\rangle$ must be in the kernel of $\hat{D}$. □

From this theorem we get the following physical statement as a corollary

Corollary 21 (Fermionic strong degenerate selection rule)**.** *Let $|\psi\rangle$ be a Fermionic state saturating a spectral inequality $D(\cdot) \leq 0$ for which there is a decreasingly (hence non-degenerate) spectrum λ' such that $D(\lambda') = 0$. Assume also that the 1-RDM of $|\psi\rangle$ has degenerate subspaces, V_i, of dimensions m_i. Let S_{mi} denote the symmetric group of order m_i which will act exclusively on the ith degenerate subspace and let $D(\lambda)$ be a spectral inequality which remains valid under permutations inside V_i, $D(\pi_1 \times \pi_2 \times \ldots \lambda) < 0, \forall \pi_i \in S_{m_i}$. Then, expanding $|\psi\rangle = \sum_x c_x |\vec{x}\rangle$ as in Eq. 2.16, where the basis $|x\rangle$ is taken to be constructed from an eigenbasis of the 1-RDM one has not only*

$$\hat{D}\,|\vec{x}\rangle \neq 0 \Rightarrow c_{\vec{x}} = 0, \forall\, \hat{D} \tag{3.40}$$

but also that only *Slater determinants for which either all m_i natural orbitals for the subspace V_i show up or none are allowed to have a non-zero coefficient in the expansion above.*

3.4 Some examples

For simplicity let us for a moment focus on the three qubit scenario, $\mathcal{H} = \left(\mathbb{C}^2\right)^{\otimes 3}$. Let $\mathrm{spec}\,\rho^{(i)} = (\lambda_1^{(i)}, \lambda_2^{(i)})$. From now on we make the identification $\lambda^{(i)} = \lambda_2^{(i)}$ For states with ordered local spectra, this is given by $\mathrm{spec}\,\rho^{(i)} = (\lambda_{\max}^{(i)}, \lambda_{\min}^{(i)})$. In this case the spectral inequalities are given by Eq. 2.19. Such polytope can be embedded into $\mathbb{R}^3$. In this specific case the Lie algebra $\mathfrak{g}$ is $\mathfrak{su}(2) \oplus \mathfrak{su}(2) \oplus \mathfrak{su}(2)$. The maximal toral subalgebra of $\mathfrak{g}$, $\mathfrak{t}$ is generated by $\mathrm{i}\sigma_z \oplus \mathrm{i}\sigma_z \oplus \mathrm{i}\sigma_z = \mathrm{i}\sigma_z \otimes \mathbb{1} \otimes \mathbb{1} + \mathbb{1} \otimes \mathrm{i}\sigma_z \otimes \mathbb{1} + \mathbb{1} \otimes \mathbb{1} \otimes \mathbb{1} \otimes \sigma_z$. Then the weight vectors of Eq. 3.25 are given by $|\lambda^\omega\rangle = |x_1, x_2, x_3\rangle$, $x_i = 0, 1$, i.e. product states, and their image under the moment map by $\lambda = (x_1, x_2, x_3)$, $x_i = 0, 1$.

Let us focus on one of the non-trivial facets of the polytope, i.e. one such that the 1-RDMs

are non degenerate. Let us take the facet with affine hull given by

$$\lambda^{(2)} - \lambda^{(1)} - \lambda^{(3)} = 0. \tag{3.41}$$

If we choose a state $\rho = |\psi\rangle\langle\psi|$ such that $\mu(\rho) \in F$ but its 1-RDMs are non-degenerate, by Corollary 15 the support of ρ is contained in $\{(0,0,0),(0,1,1),(1,1,0)\}$. In such case the structure of $|\psi\rangle$ is given by

$$|\psi\rangle = c_{0,0,0}\,|0,0,0\rangle + c_{0,1,1}\,|0,1,1\rangle + c_{1,1,0}\,|1,1,0\rangle \tag{3.42}$$

in the basis of natural orbitals of $\rho_i^{(1)}$.

Let us now choose a state ρ such that $\mu(\rho)$ lies in the intersection between the non-trivial boundary and the positive Weyl chamber (which means that at least one of the 1-RDMS is degenerate), take for example a state whose 1-RDMs are given by

$$\begin{aligned} \rho_1 = \rho_3 &= \begin{pmatrix} 3/4 & 0 \\ 0 & 1/4 \end{pmatrix} \\ \rho_2 &= \begin{pmatrix} 1/2 & 0 \\ 0 & 1/2 \end{pmatrix} \end{aligned} \tag{3.43}$$

Expanding our state as

$$|\psi\rangle = \sum_{i_1,i_2,i_3=0,1} c_{i_1,i_2,i_3}\,|i_1,i_2,i_3\rangle \tag{3.44}$$

where, as before, $|i_j\rangle$ is an eigenvector of the jth 1-RDM, it is easy to verify, that for this specific spectra a valid pre-image of the moment map is given by,

$$\begin{aligned} c_{0,0,0} &= -\frac{\sqrt{3}}{2\sqrt{2}} \\ c_{1,1,0} = c_{0,1,1} &= \frac{\sqrt{3}}{4} \\ c_{1,0,0} = c_{0,0,1} &= \frac{1}{4} \\ c_{0,1,0} &= \frac{\sqrt{2}}{4} \\ c_{1,0,1} = c_{1,1,1} &= 0 \end{aligned} \tag{3.45}$$

which appears to have support on 6 weights, instead of the 3 we would expect when lying on the facet and inside of the positive Weyl chamber (not on the boundary). However, performing

the transformation

$$\begin{aligned} -\frac{\sqrt{3}}{2}\left|0\right\rangle + \frac{1}{2}\left|1\right\rangle &\to \left|0\right\rangle \\ \frac{1}{2}\left|0\right\rangle + \frac{\sqrt{3}}{2}\left|1\right\rangle &\to \left|1\right\rangle \end{aligned} \tag{3.46}$$

on the second qubit, we can bring $|\psi\rangle$ into the form

$$\begin{aligned} c_{0,0,0} &= \frac{1}{\sqrt{2}} \\ c_{0,1,1} &= \frac{1}{2} \\ c_{1,1,0} &= \frac{1}{2} \end{aligned} \tag{3.47}$$

Let us see a similar example for Fermions. Consider the Dennis-Borland scenario $\mathcal{H} = \Lambda^3\left(\mathbb{C}^6\right)$. In this case the spectral polytope is given by

$$\begin{aligned} \lambda_i + \lambda_{7-i} &= 1 \\ D(\lambda) := \lambda_1 + \lambda_2 + \lambda_4 - 2 &\leq 0 \end{aligned} \tag{3.48}$$

plus ordering $\lambda_i \geq \lambda_{i+1}$. Consider now the state

$$\begin{aligned} |\psi\rangle = \Big[&\alpha c_1^\dagger c_4^\dagger c_5^\dagger + \sqrt{|\alpha|^2+|\beta|^2}c_1^\dagger c_2^\dagger c_3^\dagger + \beta c_2^\dagger c_4^\dagger c_6^\dagger + \\ &\mathrm{i}\left(\alpha c_1^\dagger c_3^\dagger c_5^\dagger + \sqrt{|\alpha|^2+|\beta|^2}c_1^\dagger c_2^\dagger c_4^\dagger + \beta c_2^\dagger c_3^\dagger c_6^\dagger\right)\Big]\left|0\right\rangle \end{aligned} \tag{3.49}$$

with $|\alpha|^2 > |\beta|^2$, written in an eigenbasis of its 1-RDM (natural orbitals). In this case the spectrum of the 1-RDM is given by

$$\lambda = \{(2|\alpha|^2+|\beta|^2, |\alpha|^2+2|\beta|^2, |\alpha|^2+|\beta|^2, |\alpha|^2+|\beta|^2, |\alpha|^2, |\beta|^2\}). \tag{3.50}$$

This state lies the intersection of the non-trivial facet, since we have $D(\lambda) = 0$, with the positive Weyl chamber, since we have $\lambda_3 = \lambda_4$.

The support of this state is given by 6 Slater determinants and not the 3 we would expect for the non-degenerate case. However, if we rotate the single particle basis according to

$$\begin{aligned} \frac{1}{\sqrt{2}}\left(c_3^\dagger + \mathrm{i}c_4^\dagger\right) &\to c_3^\dagger \\ \frac{1}{\sqrt{2}}\left(c_3^\dagger - \mathrm{i}c_4^\dagger\right) &\to c_4^\dagger \end{aligned} \tag{3.51}$$

we end up with

$$|\psi\rangle = \left[\alpha c_1^\dagger c_4^\dagger c_5^\dagger + \sqrt{|\alpha|^2+|\beta|^2}c_1^\dagger c_2^\dagger c_3^\dagger + \beta c_2^\dagger c_4^\dagger c_6^\dagger\right]\left|0\right\rangle \tag{3.52}$$

which agrees with Corollary 15: *whenever there is degeneracy of the 1-RDM, there is always a basis in which the selection rule is valid.*

We finally provide an example of the application of Corollary 21, the Fermionic strong selection rule. Let us consider again the Dennis-Borland scenario and the spectrum $\lambda = (1, \frac{2}{3}, \frac{2}{3}, \frac{1}{3}, \frac{1}{3}, 0)$. This spectrum saturates Eq. (3.48). Note that in this case, $\kappa_4 \geq \kappa_5$, plus we can find a valid strictly decreasing spectrum that saturates our inequality, e.g. $\vec{\lambda'} = (0.9, 0.8, 0.7, 0.3, 0.2, 0.1)$. Hence we expect that the results from Corollary 21 apply. In this case the state $|\psi\rangle$ is supported by only eight Slater determinants (see e.g. [34]) which due to $\lambda_6 = 0$ reduces to those four Slater determinants which contain the natural orbital $|1\rangle$, i.e. $c_1^\dagger c_2^\dagger c_3^\dagger|0\rangle$, $c_1^\dagger c_2^\dagger c_4^\dagger|0\rangle$, $c_1^\dagger c_3^\dagger c_5^\dagger|0\rangle$ and $c_1^\dagger c_4^\dagger c_5^\dagger|0\rangle$. Using the geometric picture for Fermionic spectra λ which was explained and used in detail in [35] and the fact that the corresponding 1-RDM is diagonal with respect to$\{|i\rangle\}_{i=1}^6$ it is an elementary exercise to show that the most general form for $|\psi\rangle$ is then given by

$$|\psi\rangle = \frac{1}{\sqrt{3}}\left[\sqrt{2}c_1^\dagger c_2^\dagger c_3^\dagger + e^{i\varphi}c_1^\dagger c_4^\dagger c_5^\dagger\right]|0\rangle \tag{3.53}$$

with some relative phase φ. Indeed, this expansion agree with Corollary 21 since both Slater determinants that show up do contain either both degenerate orbitals $|4\rangle, |5\rangle$ or none of them.

3.5 Flowing in a given direction

While calculating $\mu(\rho)$ is a trivial endeavor, calculating an inverse for it $\mu(\rho)^{-1}$ is not (not to mention it is not unique), and it is the entire difficulty of the pure univariate quantum marginal problem. We present here a lemma that allows us from an arbitrary state $|\psi\rangle$ with spectra λ to flow, up to first order, in any direction, say until we arrive at a spectra λ' with pre-image ρ'. This not only allows us to find a valid solution to $\mu(\rho')^{-1}$ but also to find whether or not λ is "far-away" from the facets of the spectral polytope. This will be made precise in Chapter 4 but we present here our lemma since we feel like its presentation agrees more with the spirit of this chapter.

Lemma 22. *Let*

$$X := (\mu P_\psi)^+,$$

where the $^+$ *denotes the Moore-Penrose pseudo-inverse. Then for every* $\delta \in \operatorname{range}\mu$,

$$\partial_t|_0\, \mu(e^{-\mathrm{i}tX\delta}\psi) = \delta.$$

Proof. We begin by noting that $X = X^\dagger$, since the operation of conjugation and transposition

commutes with the Moore-Penrose inverse [36, Corollary (4.8.5.3)]. Then we can write

$$\begin{aligned}\partial_t|_0\, \mu(e^{-\mathrm{i}tX\delta}\psi) &= \partial_t|_0\, \mu(e^{-\mathrm{i}tX^\dagger\delta}\psi) \\ &= \mu\left((\mathrm{i}X)^\dagger\delta\,|\psi\rangle\langle\psi| + |\psi\rangle\langle\psi|\,\mathrm{i}\delta^\dagger X\right)\end{aligned}$$

Comparing with equation 3.12, one gets

$$\begin{aligned}\mu\left((\mathrm{i}X)^\dagger\delta\,|\psi\rangle\langle\psi| + |\psi\rangle\langle\psi|\,\mathrm{i}\delta^\dagger X\right) &= \mu P_\psi\,(\mu P_\psi)^+\,\delta \\ &= \delta\end{aligned}$$

where we have used the fact that $\delta = \delta^\dagger$ since the range of μ is the set of local Hermitian operators. □

3.6 Conclusions

The general intractability of N particle systems means that any useful information one can get locally is prized. Several works have demonstrated that local information alone can be very useful in characterizing different scenarios. Here we have given a simple proof of the already known fact that the extremality of the spectra of the 1-RDMs significantly reduces the family of pure states that give rise to such spectra. We have also presented a proof of this very simplification in the case of degenerate 1-RDMs and shown that in some particular cases one can draw stronger conclusions than in the non-degenerate case something that, to the best of our knowledge has never been addressed before. This paves the way for simplifying calculations of ground states in physics and chemistry, something we will address in the following chapter.

Chapter 4

Pure univariate marginals and ground states in quantum chemistry

Quantum chemistry concerns itself with the calculating of physical quantities of interest such as energy, polarization, etc., for small quantum systems, usually molecules. Due to the fact that an analytical solution of the Schrödinger equation is only possible for the Hydrogen atom, this leaves us with little choice but to resort to numerical calculations in order to compute these physical quantities of interest for other atoms and molecules. Such calculations usually imply choosing a finite set of basis functions. To obtain good results, a very large basis set might need to be used, which is computationally demanding. In this chapter we probe whether the ground-state wavefunctions of small atomic systems have an extremal spectra of its 1-RDMs. If such fact would prove true, we could then greatly simplify our numerical calculations, for according to the results of the previous chapter only a small number of coefficients of the expansion of the wavefunction in natural orbitals would be non-zero.

4.1 N-representability

In the quantum chemistry community the Fermionic quantum marginal problem is usually known as the *N-representability problem*. Let us begin by considering an atomic system composed of N electrons. In this case our Hilbert space $\mathcal{H} = \mathcal{H}_L \otimes \mathcal{H}_S$ where $\mathcal{H}_L = L^2(\mathbb{R}^3)$, the space of square integrable functions on $\mathbb{R}^3$ is the orbital Hilbert space and $\mathcal{H}_S = \mathbb{C}^2$ is the spin Hilbert space. Since it is numerically impossible to consider an infinitely large Hilbert space, one considers the *truncated* Hilbert space $\mathcal{H} = \Lambda^N\left(\mathbb{C}^d\right)$ of N electrons and d orbitals [1] Very often one is interested in the electronic properties of the ground state of a given atom or molecule. In order to calculate these properties one usually makes use of the so called

[1] These are usually not just spatial orbitals, but rather spin-orbitals, containing the spatial and spin degrees of freedom.

electronic Hamiltonian which is to be defined down below.

As in chapter 1, the density matrix for this Hamiltonian is given by $\rho = |\psi\rangle\langle\psi|$ and the 1-RDM by

$$\rho^{(1)} = \sum_{i,j} \langle\psi| a_i^\dagger a_j |\psi\rangle a_i^\dagger |0\rangle\langle 0| a_j \tag{4.1}$$

where $|0\rangle$ is the vacuum and $a_i^\dagger, a_i$ creation and annihilation operators respectively of a fermion in mode i. We take $\{a_i^\dagger |0\rangle\}_{i=1}^d$ to be a basis for the single particle Hilbert space, which induces a basis for the N-particles Hilbert space in the usual way. We consider as well a very special basis: a basis of eigenvector of $\rho^{(1)}$ which we denote by $\{b_i^\dagger |0\rangle\}$

$$\rho^{(1)} b_i^\dagger |0\rangle = \lambda_i b_i^\dagger |0\rangle \tag{4.2}$$

Such states are called in quantum chemistry *natural orbitals* (with respect to state ρ) and the eigenvalues of $\rho^{(1)}$, λ_i *natural occupation numbers*. One of the reasons such concepts are used in quantum chemistry is because the basis of natural orbitals tends to give very good convergence for some algorithms in quantum chemistry [23, 37]. We use such concepts here because they make the following discussion easier. Note that $0 \leq \lambda_i \leq 1$. Such restriction is simply a restatement of the Pauli's exclusion principle: each mode can have at most one electron.

It must be stated that chemists very often use simply the result from Pauli's exclusion principle to calculate electronic properties of atoms and molecules, i.e. the Hartree-Fock approximation. We expect that a knowledge of generalized Pauli constraints will allow us to improve the results from a simple Hartree Fock calculation, without having to consider the full Hilbert space, which would be unfeasible.

4.2 The electronic Hamiltonian

We let lower case indices refer to electrons while upper case indices to nuclei. Let M_I denote the mass of the Ith nuclei in units of the electron mass and Z_I its charge. Let $r_{i,j}$ denote the distance between the ith and jth electrons, $r_{i,I}$ the distance between the ith electron and the Ith nuclei, and $R_{I,J}$ the distance between the Ith and Jth nuclei. The general Coulomb non-relativistic Hamiltonian, written in position basis, for a system consisting of N electrons and M nuclei is (see Fig. 4.1),

$$\begin{aligned} H = &- \sum_{i=1}^N \frac{1}{2}\nabla_i^2 - \sum_{I=1}^M \frac{1}{2M_I}\nabla_I^2 - \sum_{i=1}^N \sum_{I=1}^M \frac{Z_I}{r_{i,I}} \\ &+ \frac{1}{2}\sum_{i,j=1}^N \frac{1}{r_{i,j}} + \frac{1}{2}\sum_{I,J=1}^M \frac{Z_I Z_J}{R_{I,J}} \end{aligned} \tag{4.3}$$

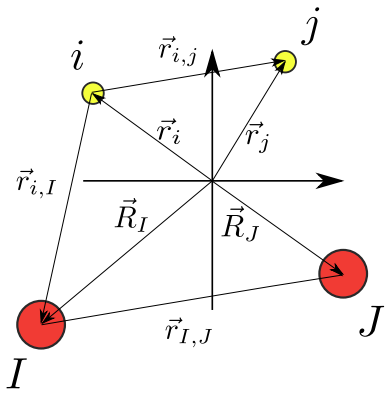

Figure 4.1: Diagram showing the coordinates used. Electrons are depicted as small, yellow circles while nuclei are depicted as large red circles.

Let us now consider the Born-Oppenheimer approximation (for more information check [23], p. 43). In this approximation one considers the fast moving electrons to be moving in a field of static ions. This approximation factorizes the total Hamiltonian into a nuclear an an electronic Hamiltonian. We will only be concerned with the electronic part. The electronic Hamiltonian is given by,

$$H_e = T + C \tag{4.4}$$

where T contains one electron terms and C the two electron Coulomb interaction

$$\begin{aligned} T &= -\frac{1}{2}\sum_{i=1}^{N}\nabla_i^2 - \sum_{i=1}^{N}\sum_{I=1}^{M}\frac{Z_I}{r_{i,I}} \\ V &= \frac{1}{2}\sum_{i,j=1}^{N}\frac{1}{r_{i,j}} \end{aligned} \tag{4.5}$$

A bit on notation. We let $|\psi\rangle = |\phi\rangle \otimes |\sigma\rangle$ where $|\phi\rangle$ is an orbital wavefunction and $|\sigma\rangle = |\uparrow\rangle, |\downarrow\rangle$ denotes the spin. Then we call $|\psi\rangle$ a *spin-orbital* wavefunction. There are several methods for (approximately) diagonalizing the electronic Hamiltonian. Some of these methods such as coupled cluster [23] are non variational, and as such we don't consider them here. The fact that they are non-variational means that the obtained grounds state may in fact be lower than the real one and the obtained spectra of the 1-RDM may have nothing to do with the physical one. By using a variational method we expect that by increasing the basis size, for example, we can increase convergence and get closer to the real wavefunction. Probably the easiest method is the Hartree-Fock method/approximation. The Hartree Fock approximation is a variational problem which consists in minimizing the expected value of the electronic Hamiltonian over a set of Slater determinants (hence the approximation). The

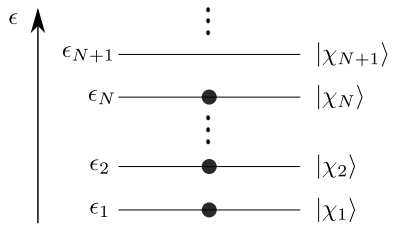

Figure 4.2: Electron levels

ground state energy of the electronic Hamiltonian is given by,

$$E_{GS} = \inf\{\langle\Psi| H |\Psi\rangle \,|\, |\Psi\rangle \in \mathcal{H}, \| |\Psi\rangle \| = 1\} \tag{4.6}$$

where

$$\mathcal{H} = \Lambda^N \left(L^2(\mathbb{R}^3) \otimes \mathbb{C}^2\right) \tag{4.7}$$

with $L^2(\mathbb{R}^3)$ the square integrable functions in $\mathbb{R}^3$, is the full Hilbert space for our problem. On the other hand, the Hartree-Fock energy is given by

$$E_{HF} := \inf\{\langle\Psi| H |\Psi\rangle \,|\, |\Psi\rangle \in SD_N, \| |\Psi\rangle \| = 1\} \tag{4.8}$$

where SD_N is the set of Slater determinants, $SD_N \subseteq \mathcal{H}$. Note that in this case, the ground state wavefunction obtained will be a single Slater determinant, $|\psi_{HF}\rangle = |\psi_1\rangle \wedge \ldots \wedge |\psi_N\rangle$. In this case, the total energy E equals the sum of the energies for each electron plus exchange interactions. By optimizing over all spin-orbitals one can get a set of spin-orbitals with increasing energy, $|\chi_1\rangle, |\chi_2\rangle \ldots$. The Hartree Fock ground state is then $|\psi\rangle = |\chi_1\rangle \wedge \ldots \wedge |\chi_N\rangle$. We then say that orbitals 1 through N are occupied and this can be represented as in Fig. 4.2 which are the usual diagrams one encounters in chemistry.

4.3 Configuration Interaction

The configuration interaction method (CI), which is a post-Hartree Fock method, meaning that it can be used after one has obtained optimized spin-orbitals using the Hartree Fock method, takes into consideration electron electron interactions [23]. Consider a system of N Fermions and let us assume that we have found the optimized Hartree-Fock orbitals $\{|\chi_1\rangle, |\chi_2\rangle \ldots\}$ with corresponding energies $\{\epsilon_1, \ldots \epsilon_2 \ldots\}$, $\epsilon_i \leq \epsilon_{i+1}$. In this case the Hartree-Fock ground state is given by $|\Psi_{HF}\rangle = |\psi_1\rangle \wedge \ldots \wedge |\psi_N\rangle$. Then a basis for $\mathcal{H}$ is given by considering the set of N particle states consisting of the the Hartree-Fock ground state, plus single excitations, obtained by exchanging one of the orbitals comprising the HF ground state by another one, double excitations, and so on. That is $\{|\Psi_{\mathrm{HF}}\rangle, a_i^\dagger a_j |\Psi_{\mathrm{HF}}\rangle, a_i^\dagger a_j^\dagger a_l a_k |\Psi_{\mathrm{HF}}\rangle, \ldots\}$. Whenever one considers only single excitations, and diagonalizes the electronic Hamiltonian

in this space, this is know as CI-S. If one considers instead single and double excitations this is known as CI-SD. Finally whenever one considers all possible excitations this is known as full-CI. In theory, diagonalizing the electronic Hamiltonian using full-CI give us an exact result. In practice, however, one must work with a truncated basis and full-CI gives us an exact result only up to truncation.

4.4 Spectral truncation

The concept of spectral truncation has been first mentioned and used by Klyachko [11] in the analysis of whether a particular ground state of Lithium has or not an extremal value of the eigenvalues of its 1RDM. This has been made precise by Schilling et al. in [12, 34]. The idea is the following:

Lemma 23 (Schilling et al. [12]). *Consider a state $|\psi\rangle \in \Lambda^N\left(\mathcal{H}_d^{(1)}\right)$, where $\mathcal{H}_d^{(1)}$ is the single particle Hilbert space, with local spectrum given by $\lambda = (\lambda_1, \ldots, \lambda_d)$. Let now $\Lambda^{N'}\left(\mathcal{H}_{d'}^{(1)}\right)$ with $N < N', d < d'$ be another Hilbert space. Then there exist states $|\phi\rangle \in \Lambda^{n'}\left(\mathcal{H}_{d'}^{(1)}\right)$ with $N' = N+\delta N$, $d' = d+\delta N+l$, $\delta_N, l \geq 0$ with local spectrum given by $\lambda' = (\underbrace{1, \ldots, 1}_{\delta N}, \lambda_1, \ldots \lambda_d, \underbrace{0 \ldots, 0}_{l})$.*

The importance of this idea steams from the fact that since it is terribly difficult to generate the inequalities defining the spectral polytope for high-dimensional settings [29] (Michael Walter, personal communication, 2014), one may need to resort to lower dimensional settings, where such inequalities are available. It is also important to know the amount of error one makes when using truncation. This is made precise by the following lemma

Lemma 24 (Schilling et al. [12]). *Consider two many-body Fermionic Hilbert spaces, $\Lambda^N\left(H_d^{(1)}\right)$ and $\Lambda^{N'}\left(H_{d'}^{(1)}\right)$ with $N' = N + \delta N$, $d' = d + \delta N + l$, $\delta_N, l \geq 0$. Every generalized Pauli constraint $D'(\cdot) \leq 0$ corresponding to $\Lambda^{N'}\left(H_{d'}^{(1)}\right)$ relevant for the pinning analysis is given by*

$$D'(\lambda') = D(\lambda^{tr}) + \mathcal{O}\left(\lambda_{d'+1-l}\right) + \mathcal{O}\left(1 - \lambda_{\delta_N}\right)$$

where $D(\cdot)$ is a generalized Pauli constraint corresponding to $\Lambda^{N'}\left(H_{d'}^{(1)}\right)$ and $\lambda^{(tr)} := (\lambda_{\delta N+1}, \ldots \lambda_{d'-l})$ a truncated spectrum.

For a good reference on the concept of spectral truncation, as well as examples of its usage, we refer the reader to [34].

4.5 Basis functions

In order to use full-CI and calculate numerically the ground state of the electronic Hamiltonian one needs to introduce a truncated basis for the problem. A great computation effort comes

from calculating the 2-particles integrals coming from Eq. (4.5). These can be simplified by considering certain types of basis functions. We now review some of the common types of basis functions used in quantum chemistry.

4.5.1 Common types of basis functions

Let $\mathbf{r} := x\mathbf{e}_x + y\mathbf{e}_y + z\mathbf{e}_z$, $r := \|\mathbf{r}\| = \sqrt{x^2+y^2+z^2}$. Then we can define the following functions used to model atomic orbitals in quantum chemistry.

Definition 25. *In quantum chemistry a Slater type orbital (STO) is a function given by*

$$s(r,\theta,\phi) := Ar^{n-1}e^{-\zeta r}Y_{l,m}(\theta,\phi) \tag{4.9}$$

where A is a normalization constant, n the principal quantum number of the orbital, ζ the orbital exponent and r, θ, ω the spherical coordinates of the electron with respect to the nucleus. These basis functions have the advantage that they can describe wavefunctions with a cusp at the nucleus, as for example the 1s orbital of Hydrogen [23]. However, the calculation of Coulomb integrals of molecules is not so straightforward when one uses STOs. Therefore, Gaussian basis functions are used instead:

Definition 26. *In quantum chemistry, a Cartesian* primitive Gaussian basis functions *(PGBF) also called a Cartesian Gaussian type orbital (GTO) is a function given by*

$$g_\nu(r,\theta,\psi,\zeta) := A(x-x_0)^k(y-y_0)^m(z-z_0)^n e^{-\zeta(r-r_0)^2} \tag{4.10}$$

where $k+m+n=l$, the orbital angular momentum number of the orbital(e.g. $l=0$ for an S type orbital), while r_0 is the center of the Gaussian and A is simply a normalization constant so that $\|g\|=1$. $\nu=(k,m,n)$.

Definition 27. *A Spherical PGBF is of the form*

$$g_\nu(r,\theta,\phi,\zeta) := AY_{l,m}(\theta,\phi)(r-r_0)^l e^{-\zeta(r-r_0)^2} \tag{4.11}$$

where $Y_{l,m}$ are the spherical harmonics, l is the orbital quantum number and $m=-l,\dots,l$ is the magnetic quantum number. $\nu=(l,m)$.

From the above one can define

Definition 28. *A contracted Gaussian basis function (CGBF) is a linear combination (contraction) of PGBF. It is given by,*

$$G_\nu(r-r_0) := \sum_i c_i g_\nu(r,\theta,\phi,\zeta_i) \tag{4.12}$$

where the c_i are called contraction coefficients and g_ν are PGBFs.

A set of these functions is usually used to provide a basis for the orbital subspace of our problem. CGBF are often used in order to simplify the calculation of the 1 and 2-particle integrals even though they fail to have a cusp at the nucleus. One sacrifices this property in order to simplify the calculations of the integrals and hence be able to use larger basis sets. These are the type of basis functions we have used in the calculations done in this chapter.

4.6 Algorithm for atomic full-CI

We now give a brief account of the full-CI algorithm we have used to calculate the spectra of the 1-RDMs. Our objective is to probe whether the ground state of atomic systems has an 1-RDM with extremal spectrum.

1. Choose a basis for the single particle Hilbert space
2. Calculate the kinetic and Coulomb integrals for the basis functions
3. Orthogonalize the basis
4. Calculate the Hamiltonian matrix in the orthonormalized basis using the rules described in [23] and diagonalize it to obtain the exact ground state and ground state energy in the truncated subspace
5. Calculate the 1-RDM and finally diagonalize it.

We will now describe the algorithm in more detail. Let us consider a system of N Fermions.

1 - Choosing a basis

Choosing a basis is an important step when considering full-CI, for it is basically the only approximation that one makes when solving the electronic Hamiltonian. One can use one of several references and databases containing basis functions optimized for a given atomic element. One example of such database is [38]. Let us consider a single particle orbital basis $\{\phi_i\}_{i=i}^{K}$ of size K. Then the basis for the single particle space is given by $\{|\psi_i\rangle\}_{i=i}^{2K}$ where $|\psi_k\rangle = |\phi_i\rangle \otimes |\sigma_j\rangle$ with $\{|\sigma_j\rangle\}_{j=1}^{2}$ a spin basis.

2 - Kinetic and Coulomb integrals calculations

After choosing the basis one should calculate the 1-particle and 2-particle integrals for the basis functions. Kinetic and Coulomb integrals have some symmetries that can be explored in order to avoid the calculation of repeated integrals. Also, one of the facts to keep in mind is that orbital basis functions used in quantum chemistry tend to be real (and here we assume so), which also simplifies our calculations.

Consider a single particle basis of dimension K For the one particle integrals we have

$$\langle i|\, h\, |j\rangle = \langle j|\, h\, |i\rangle\,. \tag{4.13}$$

where h represents the single-particle interaction for one electron, i.e.,

$$\langle i|\, h\, |j\rangle = \int \mathrm{d}\,\vec{x}_1 \chi_i(\vec{x}_1) \left(-\frac{1}{2}\nabla_1^2 - \sum_{I=1}^{M} \frac{Z_I}{r_{1,I}} \right) \chi_j(\vec{x}_1). \tag{4.14}$$

Then, instead of calculating all matrix elements, one needs only to the matrix elements for $i \leq j$. That means that instead of having to calculate K^2 integrals, one need only to calculate $\frac{K(K+1)}{2}$ integrals.

The two particle integrals

$$(\langle\chi_i| \otimes \langle\chi_j|)\, r_{12}^{-1}\, (|\chi_k\rangle \otimes |\chi_l\rangle) = \int \mathrm{d}\, x_1\, \mathrm{d}\, x_2 \chi_i(x_1)\chi_j(x_2) r_{12}^{-1} \chi_k(x_1)\chi_l(x_2) \tag{4.15}$$

are invariant under the permutations:

$$\begin{aligned} i &\leftrightarrow j \\ k &\leftrightarrow l \\ (i,j) &\leftrightarrow (k,l) \end{aligned} \tag{4.16}$$

i.e., $2^3 = 8$ identical expressions, so one needs only to calculate the matrix elements for $i \leq j, k \leq l, i \leq k, j \leq l$, which reduces the number of integrals from K^4 to $K(K+1)(K(K+1)+2)/8$. Things can be even further simplified for a lot of these integrals are necessarily zero (see [23] for more details). After all these simplifications it remains to calculate the non-zero integrals. The precise way of calculating these integrals depends on the form of the chosen basis functions, and several packages available in the literature for the their calculation. In our case we have decided to use PyQuante [39], which uses Gaussian basis functions, for its simplicity

3 - Basis orthogonalization

Since the single particle orbital basis is, in general, not orthonormal, one should properly orthonormalize this basis. Let us assume that it is normalized but not orthogonal. Then its Gram matrix will be given by $G_{i,j} = \langle\psi_i|\psi_j\rangle$ and $G_{i,i} = 1$. Obviously, $\mathrm{tr}\, G = K$. Via knowledge of this Gram matrix, one can orthogonalize directly the Kinetic and Coulomb operators by using the following result

Theorem 29. *Let $\{|\chi_i\rangle\}_{i=1}^n$ denote an orthonormal basis of a vector space $\mathcal{V}$ obtained by the Gram-Schmidt procedure on a non-orthonormal basis $\{|\sigma\rangle\}_{i=1}^n$ of $\mathcal{V}$. Let $\boldsymbol{A}$ be an operator in*

$\mathcal{V}^{\otimes p}$. *Then the matrix representation of* $\boldsymbol{A}$ *in the orthonormal basis* $A^{(\chi)}$ *is related to that in the non-orthonormal basis* $A^{(\sigma)}$ *by,*

$$A^{(\chi)} = R^{\otimes p} A^{(\sigma)} R^{T^{\otimes p}} \tag{4.17}$$

where $R = L^{-1}$ *with* L *the Cholesky decomposition [40] of the Gram matrix of the non-orthonormal basis.*

Proof. Let $\{|\chi\rangle_{i=1}^{n}\}$ and $\{|\sigma\rangle\}_{i=1}^{n}$ denote an orthonormal and a non-orthonormal basis, respectively, of a vector space $\mathcal{V}$.

Also, let

$$G_{i,j} = \langle \sigma_i | \sigma_j \rangle \tag{4.18}$$

denote the Gram matrix of the non-orthonormal basis [1].

Let L be the invertible mapping from the orthogonal basis to the non-orthogonal basis,

$$|\sigma_i\rangle = L_{ij} \, |\chi_j\rangle \tag{4.19}$$

where L is a lower diagonal matrix. Moreover, we have we have $G = LL^{\dagger}$. In fact, since G is positive definite and L is a lower diagonal matrix, this is just the Cholesky decomposition of G, which in this case, is unique. Consider an arbitrary linear operator A in $\mathcal{V}$. Then the matrix elements of A in the non-orthonormal basis, $A_{i,j}^{(\sigma)}$ are related to those in the orthonormal basis $A_{i,j}^{(\chi)}$ by

$$A^{(\sigma)} = L^{-1} A^{(\chi)} (L^{-1})^T \tag{4.20}$$

The case for higher order tensor follows trivially. □

Hence one can orthonormalize the Kinetic and Coulomb tensors by doing,

$$T' = RTR^T \tag{4.21}$$

and

$$C' = (R \otimes R) \, C_{ij;kl} \left(R^T \otimes R^T \right) \tag{4.22}$$

where $R = \left(\text{Cholesky}(G)^{-1}\right)$ and in this case T' and C' denote the matrix representation of the kinetic and Coulomb operators in the original non-orthonormal basis.

4 - Hamiltonian matrix construction and diagonalization

Now that we have orthonormalized our single particle basis, we can proceed to calculate the full Hamiltonian of the system. Note that a Slater basis constructed from these orthonormal single particle basis functions provide an orthonormal basis for our N particle system of

[1] In Physics it is customary to call this matrix the *overlap matrix*.

Element	Used basis	Calculated energy (Ha)	Literature (Ha)	|error order of magnitude|
Helium	6-31++G**	- 2.887 36	- 2.903 72 [41]	10^{-2}
Lithium	6-31++G**	- 7.431 88	- 7.478 06 [42]	10^{-2}
Beryllium	6-31++G**	-14.616 63	-14.667 35 [43]	10^{-1}

Table 4.1: Calculated energies using full-CI and Gaussian basis functions for several atoms compared against some of the best values in the literature, calculated using different methods.

dimension $\binom{2K}{N}$. Using the rules in [23] for calculating matrix elements of an operator in an orthonormal Slater basis, its very easy to construct our symmetric Hamiltonian matrix. Note that since the majority of our integrals will be zero, the Hamiltonian matrix is expected to be sparse.

All that remains of the Hamiltonian problem is to obtain its lowest eigenvalue and eigenvector using a suitable method like the Lanczos algorithm (which is implemented, for example, in the ARPACK package).

5 - Calculation of the 1-RDM

One should now calculate the reduced density matrix. One way of achieving this is by working with second quantization. In this case, one can use Eq. (2.12) to calculate the matrix elements of the 1-RDM. Given our, now orthonormal, orbitals $\{\chi_i\}_{i=1}^K$ let $\{S_k\}$ denote the N particle basis constructed by forming all possible anti-symmetric products of our orbitals. Let $a_i^\dagger$ be the second quantization creation operator that creates an electron in the ith orbital, i.e.

$$a_i^\dagger |0\rangle = |\chi_i\rangle \tag{4.23}$$

Note that the ground state is already expanded in the N particle basis above, $|\Psi_{GS}\rangle = \sum_{i=1}^L c_i |S_i\rangle$, such that calculating the density matrix elements is now easy. In fact, $a_i a_j^\dagger |S_k\rangle = s_k |S_l\rangle$ where $s_i = \pm 1$. All that remains now is to calculate inner products, which are trivial in the orthonormal N particle basis.

Finally one only needs to suitably diagonalize the density matrix, taking into that it is symmetric.

4.7 Results

First let us note that since Helium only has two electrons, the spectral polytope is in this case trivial (cf. chapter 1). Hence we are interested in studying from the Lithium atom upwards. Using the method above, we have calculated the energy (see table 4.1) and the 1-RDM (see appendix D) for Helium (for benchmark purposes), Lithium and Beryllium using well known basis functions (our program can be obtained at *https://github.com/aalopes/atomicCI*). As can be seen the calculated energy is still very far from some of the best results in the literature

(obtained through different methods) and hence any analysis as to whether these ground states have extremal 1-RDM spectrum or not makes no sense. We could still try, however, to make this analysis, but since the eigenvalues of the 1-RDMs do not decay fast enough, we encounter another problem. Let us look at Lithium, for example. If aim for a truncation error of order 10^{-6} we have to consider 11 eigenvalues, which means we truncate our scenario to $\Lambda^3(\mathbb{C}^{11})$. But for this case, a spectral polytope is not available, and hence we cannot proceed with our analysis. An alternative to our approach would be to use the Hylleraas method. The Hylleraas method is a variational method that allows one to find the ground state energy of low number atomic systems with very high precision. Some of the best results in the literature regarding the ground state of Helium, Lithium and Beryllium appear to have been obtained by the Hylleraas method [41, 43].

Unfortunately Hylleraas method is based on integrals containing the inter particle distance [44, 45], and obtaining the 1-RDM from the minimization procedure seems to be unfeasible by analytical methods. The usage of numerical methods seems also to be not so trivial, at least if one is interested in keeping the high precision of Hylleraas. As such we have decided to stay away from the Hylleraas method for our objective.

In order to help us we have requested the assistance of James D. Whitfield, an expert in quantum chemistry who also works in quantum information. He has used commercial software to calculate the 1-RDM of small atoms using CI methods. The results by him obtained have not been qualitatively different to the ones we have obtained, suffering from the same problems. Our conclusion is that the basis truncation error seems to be a big problem. The kind of basis functions one uses in quantum chemistry are meant to be used for molecules, not for high precision calculations for single atoms.

In order to address our small basis size we have requested the assistance from the group of Prof. Dr. Markus Reiher which focus on the "development of theory and algorithms for the calculation of electronic structures based on the first principles of quantum mechanics". They have not only used full-CI with an incredibly large number of basis sets (in the order of several hundreds) but they have also performed calculations using density matrix renormalization group (DMRG). The results *per se* (which we do not display here, since research is still ongoing) are very good and the calculated energies are very close to the best results in the literature, the absolute error magnitude being of order 1×10^{-4}. Also by adding more and more basis functions one does achieve energy convergence. However the problem is now that since the single particle basis is extremely large, one needs to truncate the 1-RDM spectra to make use of the available inequalities. Given the available results, we realized that no spectral truncation was up to our standards and realized that one needs an alternative method for deciding whether one has or not a state whose 1RDM spectrum is extremal. This may either be by getting the inequalities defining the spectral polytopes for higher dimensional settings (which seems currently to be unfeasible using state of the art algorithms [29] (Michael Walter,

personal communication, 2014) or by finding alternative methods, such as the one we describe in the next section.

Our problem has then shifted from the truncation of the single basis to a mathematical one, of generating the inequalities defining high order spectral polytopes. After we have arrive at the above-mentioned conclusions, Benavides-Riveros et al. [46] have published an article where, using CI, they draw some conclusions on the extremality of the eigenvalues of the 1-RDM of the ground state of the Lithium atom. We find, however, that their results suffer from the same problem as ours, namely lack of precision. More concretely, the energy by them obtained has an error of the same order of magnitude as the one by us obtained.

4.8 Flow algorithm for Fermions

In this section, and based on the ideas exposed in Chapter 2 we develop an algorithm that allows us to witness if a given local spectrum is close to a boundary of the spectral polytope.

We present this content in a less formal but more algorithmical point of view, rendering it, we hope, more suitable for practical implementations.

Assume that we have numerical/experimental data in spectral space, $\lambda \in \mathbb{R}^d$, for a system of N Fermions and d modes and we don't know he compatibility inequalities for the setting at hand. We want to use numerical methods to find whether or not we are Δ close to a face of the moment polytope, where the notion of closeness will be introduced below.

We first write μ, as defined in Eq. 3.1, as a projection operator (that this is possible, has been prove in Lemma 5). For that we need find a basis for the space of traceless, local Hamiltonians. One possible orthogonal basis for this space is given by the $d^2 - 1$ matrices

$$S_x^{ij} = E_{ij} + E_{ji}, \quad i = 1, \dots d, j \geq i \tag{4.24}$$

$$S_y^{ij} = -\mathrm{i}E_{ij} + \mathrm{i}E_{ji}, \quad i = 1, \dots d, j \geq i \tag{4.25}$$

$$S_Z^i = \frac{\sqrt{2}}{\sqrt{i+i^2}} \operatorname{diag}(\underbrace{1, \cdots, 1}_{k}, -i, 0, \dots, 0), \quad i = 1, \dots d-1 \tag{4.26}$$

where $E_{i,j}$ is a matrix with a 1 in the ith row, jth column and zeros for all other elements. Note that all the above matrices are normalized to 2 (in a Hilbert-Schmidt sense). For $d = 2$ the above basis reduce to the well known Pauli matrices.

Note that for our Hilbert space $\mathcal{H} = \Lambda^N(\mathbb{C}^d)$ μ is actually a superoperator. To make this easier to implement, we work not on $\mathcal{H}$ but on $\mathcal{L}(\mathcal{H})$, the space of linear operators of $\mathcal{H}$ where μ can be represented as a matrix. For that effect we vectorize our operators S_j, $j = x, y, z$.

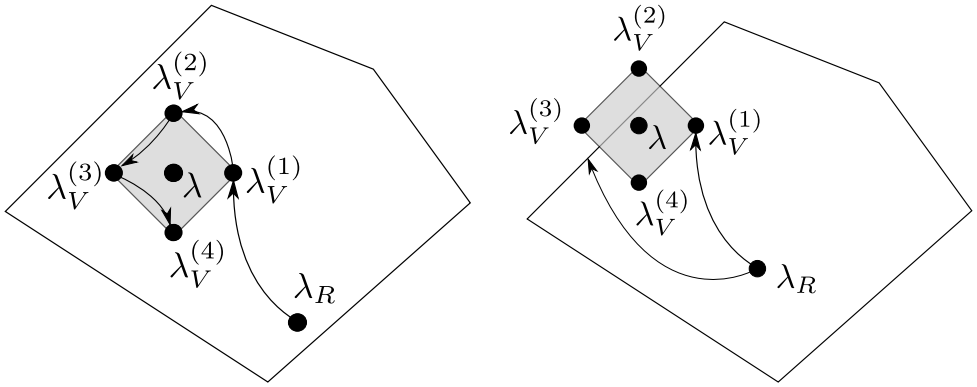

(a) 1-norm ball inside polytope (b) 1-norm ball outside polytope

Figure 4.3: Two possible scenarios when we flow from our randomly generated state to a pre-image of the vertices of a 1-norm ball around our experimental spectrum λ. In (a) the ball is completely inside the spectral polytope and we are able to flow to all vertices. In (b) part of the ball is outside of the polytope and we are unable to reach all vertices (doing so would imply flowing from a pure state to a non-pure one), hitting a facet of the spectral polytope.

By doing that μ can be written as

$$\mu = \frac{1}{2}\left[\sum_{i=1}^{N}\sum_{j=x,y,z}\left|\mathbb{1}^{(i-1)}\otimes S_j\otimes\mathbb{1}^{(n-i)}\right\rangle\left\langle\mathbb{1}^{(i-1)}\otimes S_j\otimes\mathbb{1}^{(n-i)}\right|\right] \tag{4.27}$$

Now, we will want to write μ as an operator on $\mathcal{L}(\Lambda^N\mathbb{C}^d)$ and not on $\mathcal{L}(\mathbb{C}^{nd})$ for else the matrix representation of μ will blow up exponentially. To do so, we make use of the "rules" in [23, Chapter 2].

We now put a 1-norm ball of radius δ around λ which will have $2d$ vertices, $\lambda_V^{(i)}, i = 1,\ldots,2d$. We then choose a pure state at random ψ_R. Such state can be created by choosing its coefficients on a Slater basis according to a uniform distribution and normalizing the final state.

We wish now to make ψ_R flow in such a way that its image (under the moment map, i.e. its local spectra) flows from λ_R to $\lambda_V^{(i)}$. To that effect, consider the flow of ψ_R in the direction of X (see Lemma. 22)

$$\psi_R(t) = e^{\mathrm{i}tX(\rho_R-\rho_V^{(i)})}\psi_R \tag{4.28}$$

with $X = (\mu P_\psi)^+$. For $t\to 0$ we get (where $\leftarrow$ means assignment)

$$\psi_R \leftarrow \psi_R + \mathrm{i}tX\delta\psi_R \tag{4.29}$$

following by re-normalizing ψ_R.

We iterate until we reach (or fail to do so in a given number of iterations), in spectral space,

λ_V, updating $|\psi_R\rangle$ in every iteration according to Eq. (4.29). Note that, for implementation purposes, we have chosen X to be an operator in $\mathcal{L}\left(\Lambda^N(\mathbb{C}^d)\right)$ such that the 1-RDMs $\rho_R - \rho_V^{(i)}$ must be written as vectors in the same space. To do so, we embed $A \in \mathcal{L}\left(\mathbb{C}^d\right)$ into $\mathcal{L}\left(\Lambda^N(\mathbb{C}^d)\right)$ in the following way: we begin by writing $A \to \sum_{i=1}^{N} \mathbb{1}^{(i-1)} \otimes A \otimes \mathbb{1}^{(n-i)}$ and then calculate the matrix elements of A in $\Lambda^N(\mathbb{C}^d)$ in a Slater basis in the same way we have done before and then vectorize this matrix representation. Also note, that the 1-RDM of ψ_R will, in principle, be non diagonal in our basis. In order to subtract both 1-RDMs, one should be careful with the basis, since we want to work on the space of diagonal 1-RDMs, with non-increasingly ordered spectra [2] Let U be a unitary that not only diagonalizes ρ_R but that brings its spectrum into non-increasing order

$$\rho_R^{\text{diag}} = U \rho_R U^\dagger \tag{4.30}$$

Then one should do

$$\rho_R^{\text{diag}} - \rho_V = U^\dagger \left[\rho_R^{\text{diag}} - \text{diag}(\lambda_V)\right] U \tag{4.31}$$

where diag(v) denotes a matrix with the vector v in its main diagonal.

One should repeat the procedure for all $\lambda_V^{(i)}$. Now, if we do reach a λ_V we know that it must be inside the moment polytope (cf. 2). In this case, if we reach all λ_V, our 1-norm ball must be inside the polytope and we know that λ is at least a distance δ away from a facet of the polytope (and for large δ certainly *not* quasi-extremal or "quasi-pinned" [35]).

On the other hand if we don't reach at least one of the λ_V we can't say anything. It may be that the point we could not reach is outside of the polytope or it may be that we are unable to reach the point for some other reason, such as numerical instability, a non full-dimensional tangent space, etc. . In Fig. 4.3 we show two possible scenarios.

Note that even though we have exposed this algorithm for Fermions, it works, with minor modifications, for qudits as well. Unfortunately the above mentioned algorithm, since it relies on the implementation of superoperators, requires matrix with m^4 elements, $m = \dim(\Lambda^N(\mathbb{C}^d)) = \binom{N}{d}$ which makes it impractical for even low dimensional scenarios. As an example, consider $n = 5$, $d = 10$. In this case $m = 252$ and the matrix representation of μ has $\approx 4 \times 10^9$ elements. Assuming that we store these as 32-bits floating-point numbers and taking into consideration that one would need twice the size for complex numbers, we would need $\approx 30GiB$ of RAM just to store μ! [3]

One way of modifying the algorithm is to consider the empirical flow:

$$|\psi_R(t)\rangle = e^{\mathrm{i}t(\rho_R - \rho_V^{(i)})} |\psi_R\rangle \,. \tag{4.32}$$

[2] Corresponding to $\mathfrak{t}^+$, the positive Weyl chamber of the dual of the Lie algebra of the torus, in Eq. (A.27) in Appendix A.

[3] Making no use of sparsity.

In this case one is obviously not flowing in the optimal direction, but we may expect that there will be some overlap with the right direction and that we will, eventually, flow to our desired point. Note as well, that since there are no superoperators, but only operators on $\Lambda^N(\mathbb{C}^d)$, which means matrices as big as $m = 2$ instead of m^4 Unfortunately numerical tests showed that this flow tends to converge to the ordered Slater point. This means it will get very close to most of the experimental points (since Hartree-Fock tends to be a good approximation for many scenarios [47]), but it will not, in general, reach the precision we need to make any sensible statement regarding the extremality of the 1-RDM spectra. The author is still convinced, however, that the ideas here presented may be of use in deciding the extremality of the 1-RDM spectrum for scenarios for which the spectral polytope is not yet known.

4.9 Conclusions

The calculation of physical properties of molecules is of utmost importance for technological applications in diverse areas such as biochemistry, biology, pharmaceutical areas, material engineering, among others. If one could, at least in some instances, simplify the calculation of ground states by knowing that such states have certain simpler structure than an arbitrary state, this would be a terrific advance. Given that, we feel that it is important to know whether ground states of the quantum chemistry Hamiltonian have corresponding 1-RDMs with extremal spectra or not. We have concluded that using Full-CI and the standard basis sets used in quantum chemistry results in truncation errors that are far too high to come up with a conclusive answer. Using larger basis may indeed solve the truncation error issue but it shifts the problem to another one: getting the inequalities defining the spectral polytope for large settings which appears to be, at the moment, unfeasible.

Chapter 5

Quantum marginals in Fock space

In this chapter we consider the univariate quantum marginal problem in Fock space. First we show that two kinds of one particle reductions are possible: particle and mode, and proceed to characterize these two reductions. We show, for example, that for the particle reduction in Fock space, no constraints other than the Pauli's exclusion principle are imposed on the spectrum of the 1-RDM.

5.1 Introduction

When working in Fock space two types of reductions are possible: one can either trace out modes or particles. To the best of our knowledge, two natural questions remain unanswered in Fock space. The first and maybe the more natural asks what are the constraints on the spectra of the 1-RDM when one considers a globally pure state. We prove in the next section that, other than the Pauli constraints, no further constrains arise from anti-symmetry in Fock space. Another question asks, for quasi-free Fermionic states (also know as Gaussian Fermionic states), what is the set of allowed spectra of the single modes correlation (or covariance) matrices. While this problem has been treated for bosons [48] it has, apparently, never been treated for Fermions (perhaps owing to the greater importance of bosons to the quantum optics community). In section III we treat this problem and give a full characterization of the single mode correlation matrices spectra.

5.2 Fock space reductions

In this section we begin by addressing the types of reduction one can have in Fock space.

We begin with the very definition of Fock space.

Definition 30 (Fermionic Fock space)**.** *Let $\mathcal{H}_1$ denote a single particle Hilbert space describing n modes, i.e. $dim\mathcal{H}_1 = n$ We then define the N particle Hilbert space $\mathcal{H}^{(N)}$ as*

$\mathcal{H}^{(N)} := \Lambda^N \mathcal{H}_1$. *Then the Fock space corresponding to n modes,* $\mathcal{F}_n$ *is defined as*

$$\mathcal{F}_n = \oplus_{i=0}^{\infty} \mathcal{H}^{(i)} = \oplus_{i=0}^{n} \mathcal{H}^{(i)}. \tag{5.1}$$

In this picture Fock space is seen as a direct sum of *Fock layers* (a Fock layer is an exterior power $\Lambda^i(\mathcal{H}_1)$))each corresponding to a different, but well defined, number of particles.

To proceed with our discussion we will need to make use of the so called second quantization

Definition 31 (Fermionic algebra)**.** *Let* $a_i^\dagger$ *be a linear operator in Fock space The following relations define a Fermionic algebra*

$$\begin{aligned} \left\{a_i, a_j^\dagger\right\} &= \delta_{i,j} \mathbb{1}_{\mathcal{F}}, \\ \{a_i, a_j\} &= 0 \end{aligned} \tag{5.2}$$

as well as to define the vacuum state

Definition 32 (Vacuum state)**.** *A vacuum state for type a particles is a state* $|0_a\rangle$ *such that*

$$a_i |0_a\rangle = 0 \tag{5.3}$$

where a_i *is the annihilation operator for a type a particle in mode i.*

Since we work exclusively with one type of particles in what follows we write $|0\rangle := |0_a\rangle$.

Consider now an arbitrary state in Fock space $|\psi\rangle \in \mathcal{F}_n = \oplus_{i=1}^{n} \Lambda^i \mathbb{C}^n$. We can then extend the our previous definition of 1-RDM 2.12 to an arbitrary state in Fock space. In this case, and considering the direct sum decomposition of Fock space we can write $|\psi\rangle = \sum_{i=0}^{n} c_i |\psi_i\rangle$, $|\psi_i\rangle \in \Lambda^i \mathbb{C}^n$, where we deal exclusively with normalized states and therefore $\sum_{i=1}^{n} |c_i|^2 = 1$. We then obtain the following relation between the 1RDM of a Fock state and those of the several Fock layers

$$\gamma = \sum_{i=0}^{n} |c_i|^2 \rho^{(1),(i)}. \tag{5.4}$$

where $\rho^{(1),(i)}$ is the 1-RDM of $|\psi_i\rangle$.

In a way analogous to bosons, one can define Fermionic Gaussian states, c.f. [49]. In doing so, one concludes that an n modes Fermionic state ρ is Gaussian if and only if its corresponding correlation matrix M, an $2n \times 2n$ skew-symmetric matrix is given by,

$$M_{i,j} = \frac{\mathrm{i}}{2} \operatorname{tr}\left(\rho \left[c_i, c_j\right]\right). \tag{5.5}$$

By definition the density matrix ρ_j, obtained by tracing out all modes except the jth one is given by the 2×2 principal submatrix of M.

5.3 Free Fermions Fock space particle marginal problem

In this section we treat the case of particle reductions in Fock space.

Let us define the set $\{(b_1, \dots b_n) | b_i = 0, 1, b_i > b_{i+1}\}$ We begin then by stating the trivial lemma regarding states with a Slater determinant-like form in Fock space

Lemma 33. *The spectra of all possible Slater determinants in Fock space $\mathcal{F}_n$ is given by S_n, after re-ordering the eigenvalues in non-increasing order.*

Proof. Consider $|\psi\rangle = c_{i_1}^\dagger c_{i_2}^\dagger \dots c_{i_N}^\dagger |0\rangle \in \mathcal{F}_n$. Then the spectrum of γ is identical to the spectrum of $\rho^{(N)}$ and given by N 1's and $n - N$ 0's. Moreover, if we order the spectrum non-increasingly we obtain $\lambda := \operatorname{spec} \gamma = (\underbrace{1, \dots, 1}_{N}, \underbrace{0, \dots, 0}_{n-N})$. Considering all possible values of $N = 0, \dots n$, $\operatorname{spec} \gamma = S_n$ for Slater determinants. □

As an added result, we note that in an n-mode Fock space there are n different ordered Slater states (an ordered Slater state is one which corresponding 1-RDM is ordered non-increasingly).

We will need the following Lemma regarding our previously defined Fock space 1-RDM

Lemma 34. *Let O be a one-body observable $\rho = |\psi\rangle\langle\psi|$ a state in Fock space and $\gamma = \sum_{i=1}^n i\rho^{(1),(i)}$, where $\rho^{(1),(i)}$ is the 1-RDM of the ith Fock layer. Then*

$$\operatorname{tr}\left[\left(\oplus_{i=1}^n O \otimes \mathbb{1}_{\mathcal{H}_1^{\otimes(i-1)}} + ... + \mathbb{1}_{\mathcal{H}_1^{\otimes(i-1)}} \otimes O\right)\rho\right] = \operatorname{tr}(O\gamma) \tag{5.6}$$

Proof. Since $|\psi\rangle \in \mathcal{F}_n$, it can be written as $|\psi\rangle = \sum_{i=0}^n c_i |\psi_i\rangle$, $|\psi_i\rangle \in \Lambda^i \mathcal{H}_1$. Let us define $O_i := \mathbb{1}_{\mathcal{H}^{\otimes(i-1)}} \otimes O \otimes \mathbb{1}_{\mathcal{H}^{\otimes(n-i-1)}}$ to keep our notation simpler. Then we have

$$\begin{aligned}
\operatorname{tr}\left[(\oplus_{i=1}^n O_i)\rho\right] &= \langle\psi| \oplus_{i=1}^n O_i |\psi\rangle \\
&= \sum_{i=1}^n \sum_{j=1}^n c_i^* c_j \langle\psi_i| \oplus_{i=1}^n O_i |\psi_j\rangle \\
&= \sum_{i=1}^n |c_i|^2 \langle\psi_i| \oplus_{i=1}^n O_i |\psi_i\rangle \\
&= \sum_{i=1}^n |c_i|^2 \operatorname{tr}\left(O\rho^{(1),(i)}\right) \\
&= \operatorname{tr}(O\gamma),
\end{aligned} \tag{5.7}$$

since $\oplus_{i=1}^n O_i$ is block diagonal, each block being contained in a single Fock layer. □

This proves that the definition of the 1-RDM given in Eq (5.4) makes sense.

We will need as well the following lemma, regarding the geometry of the set of local spectra in Fock space

Lemma 35. *The non-increasingly ordered spectra of the 1-RDM γ in Fock space $\mathcal{F}_n$ is a convex polytope.*

Proof. To prove this we follow the discussion of [9]. $\mathcal{F}_n = \oplus_{i=1}^n \Lambda^i \mathcal{H}_1$ with $\mathcal{H}_1$ a single particle Hilbert space. To begin with we consider the embedding $\Lambda^i \mathcal{H}_1 \subset (\mathcal{H}_1)^i$. We let single particle observables act as $\oplus_{i=1}^n O \otimes \mathbb{1}_{\mathcal{H}_1^{\otimes(i-1)}} + ... + \mathbb{1}_{\mathcal{H}_1^{\otimes(i-1)}} \otimes O$. This corresponds to the embedding of Lie algebras induced by the map $U \mapsto \oplus_{i=1}^n U^{\otimes i}$. From Lemma 34, this embedding induces a map $\rho \mapsto \gamma$. It follows that the one-body Fock space marginal for Fermions amounts to determining a moment map and hence the non-increasingly ordered spectra of γ forms a convex polytope.

□

We can then state the following theorem regarding marginal constraints on Fock space.

Theorem 36. *In Fock space there are no constraints on the spectra of the 1RDM other than those imposed by the Pauli's exclusion principle, i.e. for $\rho \in F_n$,*

$$\operatorname{spec} \gamma \in \{(\lambda_1, \ldots, \lambda_n)\} | \lambda_i \geq \lambda_{i+1},\ \lambda_i \in [0,1]\}. \tag{5.8}$$

Proof. We define the Pauli polytope to be the set consisting of the Pauli constraints (occupation numbers must be between 0 and 1),

$$P_n = \{(\lambda_1, \ldots, \lambda_n)\} | \lambda_i \geq \lambda_{i+1}, \lambda_i \in [0,1]\}. \tag{5.9}$$

Let us now consider the set $S_n = \{(b_1, \ldots b_n) \, | b_i = 0, 1, b_i > b_{i+1}\}$. Consider now the convex hull of S_n,

$$\begin{aligned} \operatorname{conv} S_n = \{ & p_0 \, (0, \ldots, 0) + p_1 \, (1, 0, \ldots, 0) \\ & + \ldots + p_n \, (1, \ldots, 1) \, | \sum_{j=0}^{n} p_j = 1\} \\ = \{ & \left(\sum_{j=1}^{n} p_j, \sum_{j=2}^{n} p_j, \ldots p_n \right) | \sum_{j=0}^{n} p_j = 1\}. \end{aligned} \tag{5.10}$$

Consider an arbitrary point $(\lambda_1, \lambda_2, \dots \lambda_n) \in P_n$. Then, defining in Eq. (5.10),

$$\begin{aligned} p_k &= \lambda_k - \lambda_{k+1}, \\ \lambda_0 &:= 1, \\ \lambda_{n+1} &:= 0. \end{aligned} \tag{5.11}$$

one has

$$\sum_{j=k}^{n} p_j = \lambda_k. \tag{5.12}$$

It is easy to check that

$$\sum_{j=0}^{n} p_j = \sum_{j=0}^{n} \lambda_k - \lambda_{k+1} = \lambda_0 - \lambda_{n+1} = 1. \tag{5.13}$$

From here it follows that $\operatorname{conv} S_n = P_n$.

Let F_n be the set of allowed spectra of the 1RDM in Fock space. As stated in Lemma 33, S_n is the spectra of Slater states in Fock space. Hence it must be that $S_n \subset F_n$. Also, since P_n is nothing more than the Pauli exclusion principle, which any Fermions must abide to, it gives us an *outer approximation* to F_n and we must have $F_n \subset P_n$. Given that F_n is convex (Lemma 35) and since we have $\operatorname{conv} S_n = P_n$, and the chain of inclusions $S_n \subset F_n \subset P_n$, we have $F_n = P_n$ and we can readily conclude that Fock space there are no more constraints other than the Pauli's exclusion principle. □

Something that is also interesting to note is that $|S_n| = n+1$ while P_n is a polytope embedded in an n dimensional space. Hence S_n is the set of *extreme* points of P_n and P_n is a *simplex*. Note that it is obvious that the argument above fails for the fixed-particle number scenario, since in that case there is only one ordered Slater state and obviously $\operatorname{conv} S_n \neq P_n$.

A consequence of Theorem 36 is that, unlike for the case of a well defined number of Fermions discussed in Chapter 3, the extremality of the spectrum of the 1-RDM in Fock space has no non-trivial structural implications in the form of the wavefunctions in Fock space.

5.3.1 Gaussian Fermions particle marginal problem

We now review some results on free-Fermions and connected them to the Fock space marginal problem.

Let us define our the single particle Hilbert space to be $\mathcal{H} = \operatorname{span}\left\{a_i^\dagger |0\rangle \dots a_n^\dagger |0\rangle\right\}$. To simplify our notation, we shall drop the vacuum state and make the following identification $\mathcal{H} = \operatorname{span}\left\{a_i^\dagger \dots a_n^\dagger\right\}$. From here it follows that $\mathcal{H}^* = \operatorname{span}\{a_i \dots a_n\}$

Let us group the creation and annihilation operators into a column vector α, which we

will call the Bogoliubov annihilation operator [50]

$$\alpha = \begin{pmatrix} a_1 \\ \vdots \\ a_n \\ a_1^\dagger \\ \vdots \\ a_n^\dagger \end{pmatrix} \tag{5.14}$$

with $\alpha = \mathcal{H}^* \oplus \mathcal{H}$ The Bogoliubov creation operator is defined to be the Hermitian conjugate of the Bogoliubov annihilation operator

$$\alpha^\dagger = \begin{pmatrix} a_1^\dagger & \dots & a_n^\dagger & a_1 & \dots & a_n \end{pmatrix} \tag{5.15}$$

The Fermionic anticommutation relations, Eq. (31), then take the form

$$\begin{aligned} \left\{\alpha_i, \alpha_j^\dagger\right\} &= \delta_{i,j} \mathbb{1}_{\mathcal{F}}, \\ \{\alpha_i, \alpha_j\} &= \delta_{i,j-n} \mathbb{1}_{\mathcal{F}} = s_{i,j} \mathbb{1}_{\mathcal{F}} \end{aligned} \tag{5.16}$$

where $s \in \mathrm{End}\,(\mathcal{H}^* \oplus \mathcal{H})$ has matrix form

$$s = \begin{pmatrix} 0 & I_n \\ I_n & 0 \end{pmatrix} \tag{5.17}$$

and satisfies

$$\begin{aligned} s &= s^{-1}, \\ s^2 &= I_{2n}. \end{aligned} \tag{5.18}$$

Obviously, just like normal Fermionic operators, it follows from Eq. (5.16) that the Bogoliubov operators are nilpotent, $(\alpha_i)^2 = 0$.

We define the unitary Bogoliubov transformation to be given by

$$\beta = T\alpha \tag{5.19}$$

with $T \in \mathrm{End}\,(\mathcal{H}^* \oplus \mathcal{H})$ the $2n \times 2n$ matrix given by

$$T = \begin{pmatrix} U^* & V^* \\ V & U \end{pmatrix} \tag{5.20}$$

where U, V are $n \times n$ matrices. In order to ensure that this transformation is canonical, T

must satisfy [50]

$$TsT^T = s \tag{5.21}$$

Note that seen as a 2×2 block matrix, s swaps columns when it multiplies a 2×2 block matrix from the right, while it swaps lines when it multiplies such a matrix from the left. Then, for a unitary Bogoliubov transformation, one has

$$T^* = sTs \tag{5.22}$$

and Eq. (5.21) can be written as

$$TT^\dagger = \mathbb{1} \tag{5.23}$$

which is equivalent to the perhaps more usual relations [51]

$$UU^\dagger + VV^\dagger = \mathbb{1}, \qquad UV^T + VU^T = 0, \tag{5.24}$$

$$U^\dagger U + VV^* = \mathbb{1}, \qquad U^T V^* + V^\dagger U = 0. \tag{5.25}$$

Note that in Condensed Matter one usually uses a particular Bogoliubov transformation, sometimes called *special* Bogoliubov transformation [50]. See appendix C for more details.

The T matrices form a group, which is easily shown to be isomorphic to the orthogonal group $O(2n)$ as can be seen by considering the following similarity transformation,

$$O = UTU^\dagger \tag{5.26}$$

with

$$U = \frac{1}{\sqrt{2}} \begin{pmatrix} I_n & I_n \\ -\mathrm{i}I_n & \mathrm{i}I_n \end{pmatrix} \tag{5.27}$$

Clearly $U^\dagger = U^{-1}$, hence it is unitary and the above transformation is indeed a similarity transformation and $T \cong O$. Now, $O(2n)$ is a disconnected group composed of two connected components, corresponding to $\det O = \pm 1$. Hence, the Bogoliubov transformation forms also a disconnected group with two connected components. Note now that the Bogoliubov transformation $T \in \mathrm{End}\,(\mathcal{H}^* \oplus \mathcal{H})$ which acts by left multiplication on Bogoliubov creation operators induces a unitary operator on Fock space, $S \in \mathcal{F}_n$, which acts by conjugation on these very same operators,

$$S\alpha_i S^\dagger = (T\alpha)_i \tag{5.28}$$

Let us denote by $O^{(\mathrm{even})}$ the elements of the orthogonal group that are in $SO(2n)$ and by $O^{(\mathrm{odd})}$ the ones in $O(2n) \backslash SO(2n)$, and identically for $T^{(\mathrm{even})}$, $T^{(\mathrm{odd})}$ and $S^{(\mathrm{even})}$, $S^{(\mathrm{odd})}$. Then we can write,

$$O^{(\mathrm{even})} = \mathrm{e}^{\dot{O}} \tag{5.29}$$

where $\dot{O}$ is an element of the Lie algebra of $O(2n)$, $\dot{O} = -\dot{O}^T$. Differentiating Eq. (5.26) one gets

$$\dot{T} = U^\dagger \dot{O} U \tag{5.30}$$

setting $\dot{T} = -\mathrm{i}K$ we have,

$$T = \mathrm{e}^{-\mathrm{i}K} \tag{5.31}$$

with [50]

$$\begin{aligned} K &= K^\dagger \\ K^T &= -sKs \end{aligned} \tag{5.32}$$

We now want to find the S matrices defined above. Consider the ith element of the action of T on α

$$\begin{aligned} (T\alpha)_i &= \left(\mathrm{e}^{-\mathrm{i}K}\alpha\right)_i \\ &= \left(\sum_{l=0}^{\infty} \frac{1}{l!} \left(-\mathrm{i}K\right)^l \alpha\right)_i \end{aligned} \tag{5.33}$$

Consider, for simplicity, the first order term $\mathrm{i}K\alpha$

$$\begin{aligned} -\mathrm{i}K_{i,j}\alpha_j &= \frac{i}{2}\left(-K^T_{j,i}\alpha_j - K_{i,j}\alpha_j\right) \\ &= \frac{i}{2}\left(\left(sKs\right)_{j,i}\alpha_j - K_{k,j}\delta_{i,k}\alpha_j\right) \\ &= \frac{i}{2}\left(K_{k,j}s_{j,i}\alpha^\dagger_k - K_{k,j}\delta_{i,k}\alpha_j\right) \end{aligned} \tag{5.34}$$

where we made use of Eq. (5.32) and the fact that $s_{k,j}\alpha_j = \alpha^\dagger_k$ Now, consider the relation,

$$[\alpha^\dagger_k \alpha_j, \alpha_i] = s_{j,i}\alpha^\dagger_k - \delta_{i,k}\alpha_j \tag{5.35}$$

which is easily deduced, making use of Eq. (5.16). Hence, Eq. (5.34) can be written,

$$\left(-\mathrm{i}K\alpha\right)_i = [1/2\mathrm{i}\alpha^\dagger K\alpha, \alpha_i] \tag{5.36}$$

From here it is a simple exercise to check that

$$(T\alpha)_i = \alpha_i + \left[\frac{1}{2}\mathrm{i}\alpha^\dagger K\alpha, \alpha_i\right] + \left[\frac{1}{2}\mathrm{i}\alpha^\dagger K\alpha, \left[\frac{1}{2}\mathrm{i}\alpha^\dagger K\alpha, \alpha_i\right]\right] + \ldots \tag{5.37}$$

Making use of Hadamard's Lemma

$$e^B A e^{-B} = A + [B, A] + \frac{1}{2}[B, [B, A]] + \ldots \tag{5.38}$$

one readily arrives at

$$S = \mathrm{e}^{1/2\alpha^\dagger K\alpha}. \tag{5.39}$$

Now for O^{odd}, one can write

$$O^{(\mathrm{odd})} = RO^{(\mathrm{even})} \tag{5.40}$$

where R is *any* reflection, det $R = -1$. Consider $T_R = U^\dagger RU$. Then one has

$$T^{(\mathrm{odd})} = T_R e^{-\mathrm{i}K} \tag{5.41}$$

Consider now the particular reflection matrix

$$\begin{aligned} T_R &= \begin{pmatrix} A & B \\ B & A \end{pmatrix}, \\ A &= \begin{pmatrix} 0 & & & \\ & -1 & & \\ & & \ddots & \\ & & & -1 \end{pmatrix}, \\ B &= \begin{pmatrix} 1 & & & \\ & 0 & & \\ & & \ddots & \\ & & & 0 \end{pmatrix} \end{aligned} \tag{5.42}$$

That this is a valid T matrix, is obvious since $T_R T_R^\dagger = \mathbb{1}$. That this is a reflection matrix is easily seen by considering the determinant of partitioned matrices [52, Th. 1]

$$\det T_R = \det\left(A^2 - B^2\right) = -1 \tag{5.43}$$

The action of our particular T_R on α is given by

$$\begin{aligned} \alpha_1 &\to \alpha_{n+1} \\ \alpha_{n+1} &\to \alpha_1 \\ \alpha_j &\to -\alpha_j, \quad j \neq 1, n+1 \end{aligned} \tag{5.44}$$

This action can be mimicked in Fock space by by considering the unitary (and Hermitian) operator $S = \alpha_1 + \alpha_1^\dagger = a_1 + a_1^\dagger$,

$$Sa_iS^\dagger = \begin{cases} a_1^\dagger, & i = 1 \\ -a_i, & i \neq 1 \end{cases} \tag{5.45}$$

Hence we have

$$S^{(\mathrm{odd})} = \mathrm{e}^{1/2\alpha^\dagger K\alpha}\left(\alpha_1 + \alpha_1^\dagger\right) \tag{5.46}$$

Note that independently of K, $S^{(\mathrm{even})}$ contains even powers of creation and annihilation operators, hence the state $S^{(\mathrm{even})}\left|0\right\rangle$ is always a linear combination of states lying in Fock layers with an even number of particles. Likewise, $S^{(\mathrm{odd})}$ creates Fermionic states with an odd particle parity. Note also, that since T and S are related by a continuous transformation, the set of S operators is disconnected with two connected components.

The S operators act on the Fock vacuum to create a set of states, called quasi-free states or Gaussian states, i.e. the states that can be obtained from a Bogoliubov transformation of the vacuum,

$$\rho_{\mathrm{free}} = \left\{\left|\psi\right\rangle\left\langle\psi\right| : \left|\psi\right\rangle = S\left|0\right\rangle, \mathrm{Admissible}\, S\right\} \tag{5.47}$$

At this point, we are interested in obtaining the 1-RDM for the quasi-free states. We begin with the generalized 1-RDM

Definition 37 (Generalized one particle density matrix)**.** *For a globally pure state, $\rho = \left|\psi\right\rangle\left\langle\psi\right|$, the generalized one particle reduced density matrix (generalized 1-RDM) for type α Bogolyubons is defined as*

$$\Gamma_{i,j} = \left\langle\psi\right| \alpha_j^\dagger \alpha_i \left|\psi\right\rangle. \tag{5.48}$$

To cast the generalized 1-RDM into matrix form let us first define the pair tensor, $\kappa^{(a)}$

$$\kappa_{i,j}^{(a)} = \left\langle\psi\right| a_j a_i \left|\psi\right\rangle. \tag{5.49}$$

By definition, $\kappa = -\kappa^T$, i.e., κ is skew-symmetric. In a change of the single particle basis, κ transforms as a $\binom{2}{0}$ tensor, unlike the 1-RDM, which is a $\binom{1}{1}$ tensor.

In matrix form, we can write the generalized 1-RDM as

$$\Gamma^{(\alpha)} = \begin{pmatrix} \gamma^{(\alpha)} & \kappa^{(\alpha)} \\ -(\kappa^{(\alpha)})^* & 1 - (\gamma^{(\alpha)})^* \end{pmatrix}. \tag{5.50}$$

It is easily seen that that Γ is Hermitian, $\Gamma = \Gamma^\dagger$.

In a unitary Bogoliubov transformation (see Eq. (5.19)), we have

$$\Gamma^{(\beta)} = T\Gamma^{(\alpha)}T^\dagger. \tag{5.51}$$

T is unitary, thus $\Gamma^{(\beta)} \cong \Gamma^{(\alpha)}$. Let us now consider the state $\left|\psi\right\rangle$ to be the Fock vacuum of the operators b. It is then fairly obvious that we must have $\gamma^{(\beta)} = \kappa^{(\beta)} = 0$ and therefore

$$\Gamma^{\beta} = \begin{pmatrix} 0 & 0 \\ 0 & I_n \end{pmatrix}. \tag{5.52}$$

We then have that spec $\left(\Gamma^{(\alpha)}\right) = \text{spec}\left(\eta\Gamma^{(\beta)}\right) = \overbrace{0,\cdots 0}^{n}, \overbrace{1,\cdots,1}^{n}$, which is the spectrum of the generalized 1-RDM of a pure Gaussian state.

Let us now see how to relate the spectrum of the generalized 1-RDM to the spectrum of the 1-RDM.

Now, from Eq. (5.51) and Eq. (5.20) it follows that

$$\Gamma^{(\alpha)} = \begin{pmatrix} VV^\dagger & V^\dagger U \\ U^\dagger V & U^\dagger U \end{pmatrix} \tag{5.53}$$

comparing with Eq. (5.50) we arrive at,

$$\begin{aligned} \gamma &= V^\dagger V \\ \kappa &= V^\dagger U \end{aligned} \tag{5.54}$$

Now, note that $\Gamma^{(\alpha)} = \left(\Gamma^{(\alpha)}\right)^2$ which follows from the simple fact that $\Gamma^{(\beta)} = \left(\Gamma^{(\beta)}\right)^2$ trivially and from Eq. (5.51).

One then has

$$\begin{pmatrix} VV^\dagger & V^\dagger U \\ U^\dagger V & U^\dagger U \end{pmatrix} = \begin{pmatrix} VV^\dagger VV^\dagger + V^\dagger UU^\dagger V & VV^\dagger V^\dagger U + V^\dagger UU^\dagger U \\ U^\dagger VVV^\dagger + U^\dagger UU^\dagger V & U^\dagger VV^\dagger V + U^\dagger UU^\dagger U \end{pmatrix} \tag{5.55}$$

And from here, considering Eq. (5.54), it follows that

$$\begin{aligned} \gamma - \gamma^2 &= \kappa\kappa^\dagger \\ \gamma\kappa &= \kappa\gamma^* \end{aligned} \tag{5.56}$$

From here it is a simple exercise to see that eigenvalues of $\gamma^{(\alpha)}$, an arbitrary Gaussian 1-RDM, can only consist of an arbitrary number of 0s and 1s and doubly degenerate values in the interval $(0, 1)$. Since the map from the set of quasi-free states to the spectra of their 1-RDM is continuous, we expect these spectra to be disconnected with two connected components.

5.3.2 Constraints and convexity of the local spectra

Let σ be an arbitrary free fermion state. As we have seen the spectrum of $\sigma^{(1)}$ consists of an arbitrary number of 0's and 1's and doubly degenerate values in the interval $[0, 1]$. Let us define the set $G'_n = (\lambda_1, \ldots, \lambda_n)$ with $\lambda_i \in [0, 1]$ and $\lambda_i \leq \lambda_{i+1}$, to be the (ordered) set of allowed spectra for the one particle reduced density matrix $\sigma^{(1)}$ arising from a free fermion n mode state.

For n even, it is easy to see that one can write G_n as the following union of disjoint sets

$$\begin{aligned} G_n = &\left\{ \left(l_1, l_1, l_2, l_2, \ldots, l_{n/2}, l_{n/2}\right) \,|\, l_i \in [0,1],\, l_i \geq l_{i+1}, \right\} \\ &\sqcup \left\{ \left(1, l_1, l_1, \ldots, l_{n/2-1}, l_{n/2-1}, 0\right) \,|\, l_i \in [0,1],\, l_i \geq l_{i+1} \right\}. \end{aligned} \tag{5.57}$$

Note that the first set above contains all situations where the number of 1's is even (and the number of 0's as well) while the second set contains all situations where the number of 1's is odd (and the number of 0's as well). For n odd is is also easy to see that we can write G_n as the following union of disjoint sets,

$$\begin{aligned} G_n = &\left\{ \left(l_1, l_1, l_2, l_2, \ldots, l_{\frac{n-1}{2}}, l_{\frac{n-1}{2}}, 0\right) \,|\, l_i \in [0,1],\, l_i \geq l_{i+1} \right\} \\ &\sqcup \left\{ \left(1, l_1, l_1, \ldots, l_{\frac{n-1}{2}}, l_{\frac{n-1}{2}}\right) \,|\, l_i \in [0,1],\, l_i \geq l_{i+1} \right\}. \end{aligned} \tag{5.58}$$

Where the first set above contains all situations where the number of 1's is even (and the number of 0's is odd) while the second set contains all situations where the number of 1's is odd (and the number of 0's is even).

From the construction above it is obvious that G_n is disconnected with two connected components as expected (except for the trivial case G_0). Note also that the spectrum of the 1-RDM the vacuum state is trivially $(0, \ldots, 0)$. Hence, for n even, $\left\{ \left(l_1, l_1, l_2, l_2, \ldots, l_{n/2}, l_{n/2}\right) \right\}$ correspond to the spectra of the states that are connected to the vacuum state while for n odd, the equivalent is $\left\{ \left(l_1, l_1, l_2, l_2, \ldots, l_{\frac{n-1}{2}}, l_{\frac{n-1}{2}}, 0\right) \right\}$.

From its disconnectedness it follows that G_n is not convex. One could however expect, based on the convexity results of the moment map, its components to be convex. This is indeed the case, a fact that can be easily seen by using an approach identical to that used in proving theorem 36 (which we don't pursue here since it constitutes a simple exercise).

It is obvious that one has, $S_n \subset G'_n$, with S_n the set of Slater determinants, and thus, from the results of the previous section, the convex hull of the spectra of Gaussian states also generates the entire spectra in Fock space. If Fig. 5.1 we plot the spectra of the 1-RDM for Slatter, Gaussian and arbitrary states in a 2 and 3 modes Fock space.

5.4 Gaussian Fermionic mode marginal problem

In order to describe a Fermionic system consisting of n modes, we consider $2n$ creation/annihilation operators satisfying the canonical anti-commutation relations (CAR)

$$\left\{ a_i, a_j^\dagger \right\} = \delta_{i,j} \mathbb{1} \tag{5.59}$$

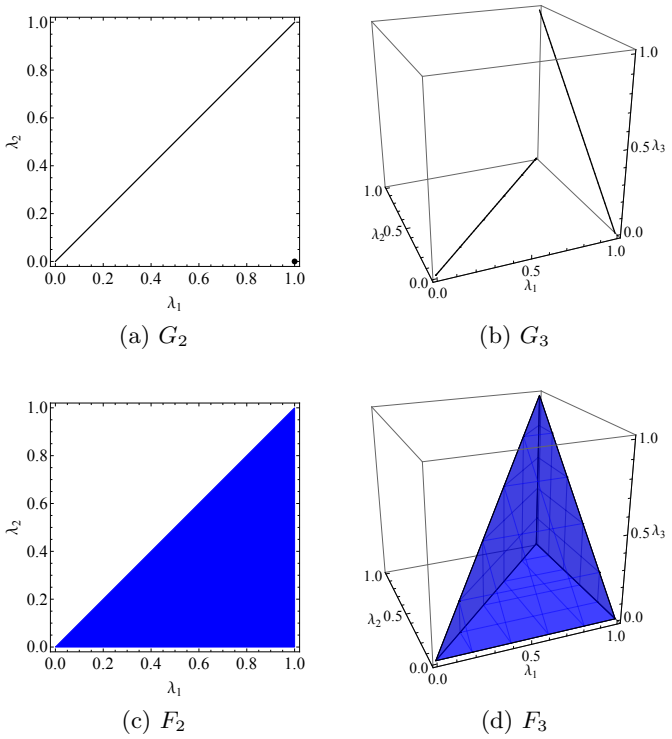

(a) G_2 (b) G_3

(c) F_2 (d) F_3

Figure 5.1: Set of allowed local spectra for 2 and 3 modes. The spectra of ordered Slater states are marked by black dots.

Identical to the way one goes from creation and annihilation operators to coordinate and momentum ones for bosons, we make the following unitary transformation

$$\begin{aligned} c_{2j-1} &= a_j^\dagger + a_j, \\ c_{2j} &= -\mathrm{i}\left(a_j^\dagger - a_j\right). \end{aligned} \tag{5.60}$$

These $2n$ operators correspond to Majorana operators, for they are Hermitian and satisfy the CAR,

$$\{c_i, c_j\} = 2\delta_{i,j}\mathbb{1}. \tag{5.61}$$

In a way analogous to bosons, one can define Fermionic Gaussian states, cf. [49]. In doing so, one concludes that an n modes Fermionic state ρ is Gaussian if and only if its corresponding correlation matrix (or covariance matrix) M, an $2n \times 2n$ skew-symmetric matrix, is given by,

$$M_{i,j} = \frac{\mathrm{i}}{2}\,\mathrm{tr}\left(\rho\,[c_i, c_j]\right). \tag{5.62}$$

Using equation (5.61) this can be cast into the form

$$M_{i,j} = \mathrm{i}\,\mathrm{tr}\left(\rho c_i c_j\right) - \mathrm{i}\delta_{i,j}. \tag{5.63}$$

Being a real skew-symmetric matrix, M can be brought into a block diagonal form under the action $O \in O(2n)$,

$$OMO^T = \oplus_{j=1}^{n} \begin{bmatrix} 0 & \mu_j \\ -\mu_j & 0 \end{bmatrix}. \tag{5.64}$$

By definition the correlation matrix corresponding to the reduced density matrix ρ_j, obtained by tracing out all modes except the jth one is given by the 2×2 principal submatrix of M,

$$N_j = \begin{bmatrix} 0 & -\nu_j \\ \nu_j & 0 \end{bmatrix} = \begin{bmatrix} M_{2j-1,2j-1} & M_{2j-1,2j} \\ M_{2j,2j-1} & M_{2j,2j} \end{bmatrix} \tag{5.65}$$

with $\nu_j = \mathrm{i}\,\mathrm{tr}\,(\rho c_{2j-1} c_{2j})$. Given a correlation matrix M, in order to characterize all its 2×2 principal submatrices we will make use of the following theorem

Theorem 38 (Skew-Symmetric Sing-Thompson [53, 54])**.** *Let $d = (d_1 \dots d_n) \in \mathbb{C}^n$ arranged such that $|d_1| \geq \dots \geq |d_n|$ and let $s = (s_1 \dots s_n) \in \mathbb{R}$ such that $s_1 \geq \dots s_n \geq 0$. Then a $2n \times 2n$ skew symmetric matrix exists with $d_1 \dots d_n$ as its superdiagonal and $s_1, s_1 \dots s_i, s_i \dots s_n, s_n$ as its singular values if and only if*

$$\begin{aligned} \sum_{i=1}^{k} |d_k| &\leq \sum_{i=1}^{k} s_i, \quad k = 1, \dots n, \\ \sum_{i=1}^{n-1} |d_i| - |d_n| &\leq \sum_{i=1}^{n-1} s_i - s_n. \end{aligned} \tag{5.66}$$

In our case, first note that the set of singular values of M is given by $s = (\mu_1, \mu_1, \dots \mu_k, \mu_k, \dots \mu_n, \mu_n)$. Without loss of generality we assume that $\mu_i \geq \mu_{i+1} \geq 0$. Note now that the superdiagonal elements of M are given by $(-\nu_1, \dots - \nu_n)$ We also assume, again without loss of generality, that $\nu_i \geq \nu_{i+1} \geq 0$. Hence, we can then make use of Theorem 38 to fully characterize M,

$$\begin{aligned} \sum_{i=1}^{k} \nu_k &\leq \sum_{i=1}^{k} \mu_i, \quad k = 1, \dots n, \\ \sum_{i=1}^{n-1} \nu_i - \nu_n &\leq \sum_{i=1}^{n-1} \mu_i - \mu_n. \end{aligned} \tag{5.67}$$

Let us now connect these results with the marginal problem for qubits. Note that any Gaussian state can be cast into the form (cf. [49], Eq. (19)),

$$\rho\,(\mu_1, \dots \mu_n) = \frac{1}{2^n} \prod_{j=1}^{n} (I + \mathrm{i}\mu_i c_{2j-1} c_{2j}) \tag{5.68}$$

with pure (Gaussian) states corresponding to $\mu_i = \pm 1$. We can map these pure Gaussian state into a qubit state using a Jordan-Wigner transformation (cf. Appendix E),

$$\rho\left(\mu_1, \ldots \mu_n\right) = \frac{1}{2^n} \otimes_{j=1}^{n} \left(\mathbb{1} - \mu_i Z_j\right) \tag{5.69}$$

which is always pure. In particular it is pure whenever $\mu_i = \pm 1$, i.e. pure Gaussian states map to pure qubit states under the J-W transformation. However it is clear that Eq. (5.69) does not exhaust the set of all possible pure n qubit states. Therefore the set of all Gaussian states does not map into the whole set of pure qubit states under the J-W transformation.

Let us now write ν_j making use of the J-W transformation (cf. appendix F),

$$\nu_j = \mathrm{i}\,\mathrm{tr}\left(\rho c_{2j-1} c_{2j}\right) = -\,\mathrm{tr}\left(\rho Z_j\right). \tag{5.70}$$

Now note that for a Gaussian state ρ, $\{X_j\} = \{Y_j\} = 0$. To prove this we can make use of Wicks's theorem (cf. [49], Eq. (17)),

$$\mathrm{tr}\,\rho i^p c_{a_1} c_{a_2} \ldots c_{a_p} = \mathrm{pf} M|_{a_1, \ldots a_p} \tag{5.71}$$

with $1 \leq a_1 \leq a_p \leq 2n$ and $M|_{a_1, \ldots a_p}$ is the $p \times p$ submatrix of M obtained by keeping only the indicated rows and columns. Note that X_j and Y_j are always a product of an odd number of Majorana operators and according the Wick's theorem the average value of expressions involving an odd number of Majorana operators is the Pfaffian of an odd dimensional matrix, which is 0 [55].

Then, we have, for a Gaussian state ρ with reductions $\rho_i = \mathrm{tr}_{\setminus i}\,\rho$ and reduced spectra $\mathrm{spec}\rho_i = (\lambda_i^{\min}, \lambda_i^{\max})$

$$\nu_j = \lambda_j^{\max} - \lambda_j^{\min}. \tag{5.72}$$

Then, for pure Gaussian states, applying the J-W transformation to Eq. (5.67) we get an inner approximation for the allowed local spectra of n qubits,

$$\nu_n \geq \sum_{i=1}^{n-1} \nu_i - (n-2) \tag{5.73}$$

which actually agree with the marginal constraints for a system of n qubits (cf. Chapter 1) [6].

5.5 Conclusion

In this chapter we have characterized the particle Fock space marginal problem and showed that the 1-RDM in Fock space is not subject to any constraints, other than the Pauli's exclusion principle alone. This stands in sharp contrast to the fixed particle number case.

We have also realized that the local spectra for Gaussian states does not form a convex polytope, unlike one could have assumed *a priori*, and have pinpointed the reason to the fact that the set of Gaussian states is disconnected. We have as well fully characterized the correlation matrices of pure Gaussian states using the skew-symmetric Sing-Thomson theorem and showed that Gaussian states are enough to generate the spectral polytope for the qubit case, via the Jordan-Wigner transformation.

Chapter 6

Witnessing localizable entanglement from local information

It has recently been observed [10] that in some instances, strong statements about multi-particle entanglement can be deduced from single-site information alone. One of problems that can be formulated concerns the presence of *localizable entanglement*: the entanglement that can be localized (on average) between two separated qubits by performing local measurements on the other qubits. In this chapter we analyze the *computational complexity* of this task. We show that, while there are many efficiently solvable instances, the general problem is NP-complete. This leaves us with the situation that few, easily obtainable physical measurements may be sufficient to witness many-body entanglement, using localizable entanglement as a measure of entanglement, but that the classical post-processing is intractable. To the best of our knowledge, this is the first natural instance of a *pure state* entanglement problem that has been proven to be hard.

6.1 Multipartite entanglement

Entanglement is perhaps the most radical departure from classical mechanics in the quantum world. It is a purely quantum mechanical phenomenon and in entangled systems one can observe correlations that are stronger than what is classically allowed. Entanglement is of utmost importance in quantum information and computation since it is a necessary resource in many well known protocols [25]. For a pure state of a two particle system $|\psi\rangle \in \mathcal{H} = \mathcal{H}_1 \otimes \mathcal{H}_2$, a state is said to be *separable* if it can be written as

$$|\psi\rangle = |\psi_1\rangle \otimes |\psi_2\rangle\,,\ |\psi_i\rangle \in \mathcal{H}_i. \tag{6.1}$$

Otherwise the state is said to be *entangled*. For an N particle system, the situation is not as simple, for a pure state $|\psi\rangle \in \bigotimes_{i=1}^{N} \mathcal{H}_i$ can be separable, fully/genuinely entangled or partially entangled. In this case, a state is called genuinely entangled if it cannot be factorized with respect to any possible bipartition of the system and separable (or fully separable) if it can be written as a tensor product $|\psi\rangle = \otimes_{i=1}^{N} |\psi_i\rangle$, where each tensor factor $|\psi_i\rangle$ is supported only on the ith qubit.

Given that entanglement is concerned with the non local properties of physical states, (in fact, entanglement is necessary but not sufficient for non-locality, cf. Werner state [56]) a sensible theory of entanglement should provide us with entanglement (equivalence) classes that are invariant under local operations. These local operations can be simply local unitaries (LU), local operations and classical communications (LOCC) or their stochastic counterpart, stochastic local operations and classical communications (SLOCC) where local operations have a given probability of succeeding. For each of these local operations, our theory of entanglement should address the following questions [57]

- How many equivalence classes exist?
- How are these classes parametrized?
- How can we decide whether or not two states belong to the same class?

For bi-partitite qubit systems under LU operations, the Schmidt normal form

$$|\psi\rangle = \sin\theta\,|0,0\rangle + \cos\theta\,|1,1\rangle \tag{6.2}$$

gives us an answer to all the above questions. Our classes are parametrized by one parameter, the Schmidt angle $\theta \in [0, \pi/2]$. Two quantum states are LU equivalent if and only if their Schmidt normal form coincides. This means that we have an infinite and continuous number of equivalence classes. The situation for a multipartite system is much more complicated. If we consider a system of N qubits it can be shown [57] that one needs at least $2^{N+1} - 3N - 2$ continuous real parameters to parametrize the sets of inequivalent pure states under the action of $U_N(\mathbb{C}) = (U(\mathbb{C}))^{\otimes N}$, i.e. under LU. One must stress that this bound exhibits exponential growth. For a tri-partite system one needs at least 5 parameters to parametrize the set of inequivalent (pure) states. This means that a general pure tri-partite cannot be cast in the form,

$$|\psi\rangle = \sin\theta\,|0,0,0\rangle + \cos\theta\,|1,1,1\rangle \tag{6.3}$$

under the action of LU, unlike the bi-partite case.

Let us now turn our attention to SLOCC operations. Two states, $|\psi\rangle$ and $|\phi\rangle$ are SLOCC equivalents if $|\psi\rangle$ can be converted into $|\phi\rangle$ by invertible local operations (and vice versa),

$$|\psi\rangle = M_1 \otimes \ldots \otimes M_N\,|\phi\rangle\,. \tag{6.4}$$

with $M_i \in GL_2(\mathbb{C})$, i.e., if $|\psi\rangle$ and $|\phi\rangle$ lie in the same orbit of $GL_2(\mathbb{C}) \otimes \ldots \otimes GL_2(\mathbb{C})$. The probability that a given SLOCC operation succeeds is given by the "length" of $|\phi\rangle$ normalized by the length of $|\psi\rangle$. If one is not concerned about this length and the phase of the resulting state, but only about which states are equivalent, we can work with $M_i \in SL_2(\mathbb{C})$ instead. Again, it can be shown [57], simply by parameter counting, that we need $2^{N+1} - 6N - 2$ continuous real parameters to parametrize the set of inequivalent pure states under the action of $SL_2(\mathbb{C})$, i.e. under SLOCC. For the bipartite and tripartite case, $2^{N+1} - 6N - 2$ is negative. Therefore, we expect that instead of requiring a finite number of continuous parameters we only need a discrete number of parameters to parametrize the set of inequivalent classes under SLOCC. For the bipartite case, there are only two entanglement classes under SLOCC: separable and entangled. This is actually equivalent to classifying the states by their Schmidt rank which is 1 if and only if if the state is separable and 2 if and only if if the state is entangled. Let us check this. By definition, an arbitrary pure state $|\psi\rangle$ for a system of two qubits can be written as

$$|\psi\rangle = \sum_{i,j=0,1} c_{i,j} |i,j\rangle . \tag{6.5}$$

Then, under an SLOCC operation given by operators (M_1, M_2), the coefficient matrix, $[c_{i,j}] =: C$ transforms as $C' = M_1 C M_2^\dagger$ which in turn implies that the determinant of C is an invariant under SLOCC and in this case its rank as well. The rank of C then defines two equivalence classes: rank-1 states are separable while rank-2 states are entangled. For the case of three qubits it can be proved that there are six SLOCC classes [58]: separable, three biseparable classes with respect to all possible bipartitions, the GHZ class and the W class. For the case of four qubits, we need at least 6 continuous real parameters to parametrize the set of inequivalent classes and therefore the number of inequivalent classes under SLOCC is already infinite.

Some examples of entanglement measures for multi-partite systems are [59]:

- The Schmidt measure (invariant under SLOCC)
- The geometric measure of entanglement (invariant under LU)
- The tangle - based on the hyperdeterminant (invariant under SLOCC)
- The relative entropy of entanglement
- The localizable entanglement

However, not all of these measures are *entanglement monotones*, i.e. positive functions that vanish for separable states and that do not increase under LOCC. Namely the localizable entanglement and the geometric measure of entanglement fail to be so. One can, however, with minor modifications arrive at similar definitions that are indeed monotones [60–62].

6.2 Entanglement polytopes

Experimentally determining the entanglement class of a state under SLOCC is highly impractical since it requires measuring a number of parameters exponential in the particle number. Entanglement polytopes, originating on the work of Walter et al. [10] allows one to classify multi-particle entanglement based on a linear number of locally accessible parameters. Besides this property the method of entanglement polytopes is also robust against experimental noise.

Let us consider a pure state $\rho = |\psi\rangle\langle\psi|, |\psi\rangle \in \mathcal{H} = \left(\mathbb{C}^2\right)^{\otimes n}$ of n qubits. Its one body reduced density matrices (1-RDM) are given by $\rho_i^{(1)} = \mathrm{tr}_{\setminus i}\,\rho$ with spectra $(\lambda_{\min}^{(i)}, \lambda_{\max}^{(i)})$. As stated in Chapter 2, for each 1-RDM the spectrum must sum to one and one needs only one parameter to characterize the spectrum of each 1-RDM. We take this parameter to be $\lambda_i := \lambda_{\min}^{(i)} \in [0, 0.5]$. As mentioned in Chapter 9, it has been shown by Higuchi et al. [6] that for a pure state ρ its local spectra must satisfy the following compatibility inequalities

$$\lambda_i \leq \sum_{i \neq j} \lambda_j, \quad i = 1, \ldots, n. \tag{6.6}$$

which define a convex polytope (see Fig. 6.1a for a plot of this polytope for 3 qubits). For a non-increasingly ordered spectra, which is what we will consider from here onwards, one only needs to consider

$$\lambda_1 \leq \sum_{i \neq 1} \lambda_i. \tag{6.7}$$

We have seen that a pure state of n qubits ρ is called non-entangled or separable only if it can be written as a tensor product $\rho = \otimes_{i=1}^{n} \rho_i^{(1)}$. Consequently ρ is separable if and only if its 1-RDM are pure states. We call ρ bi-separable if it can be factorized into two pure states, such that $\rho = \rho_1 \otimes \rho_2$, with ρ_i supported in system S_i, such that $S_1 \sqcup S_2 = \{1, \ldots n\}$. In this case, each of these states should, independently, satisfy Higuchi's inequalities,

$$\begin{aligned} \lambda_1 &\leq \sum_{1 \neq i \in S_1} \lambda_i, \\ \lambda_k &\leq \sum_{k \neq i \in S_1^c} \lambda_i \end{aligned} \tag{6.8}$$

where we have taken, without loss of generality, the largest λ_i to be in the first set and $\lambda_k = \max_{i \in S_1^c} \lambda_i$.

What Walter et al. did was to associate to every entanglement class the collection of eigenvalues of the 1-RDM of the states in the closure of that class. This gives us, surprisingly, a convex polytope which is called *entanglement polytope*. In Fig. 6.1 we plot all the entanglement polytopes for 3 qubits. These polytopes provides us a local criterion for witnessing global multi-particle entanglement in the following way: if the spectra of the 1-RDM of a pure

state $|\psi\rangle$ does not lie in an entanglement polytope $\Delta_{\mathcal{C}}$, then that state does not belong to entanglement class $\mathcal{C}$,

$$(\lambda_1, \ldots \lambda_N) \notin \Delta_{\mathcal{C}} \Rightarrow |\psi\rangle \notin \mathcal{C}. \tag{6.9}$$

What is very important is that, unlike SLOCC classes of which there's an infinite number of them for systems consisting of more than three qubits, there are always only finitely different entanglement polytopes.

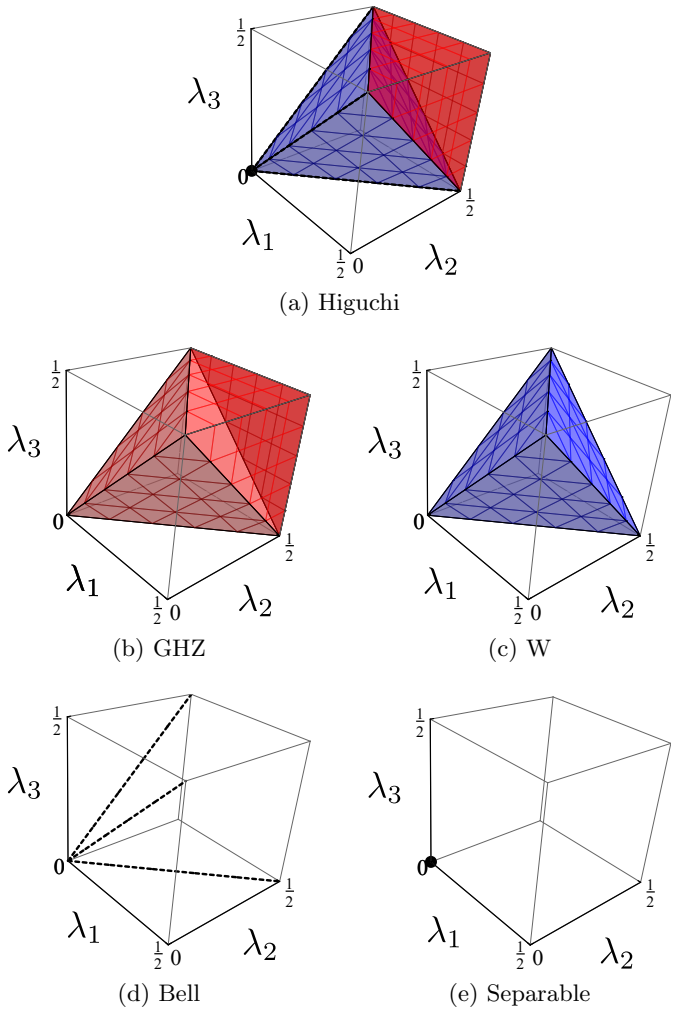

(a) Higuchi

(b) GHZ

(c) W

(d) Bell

(e) Separable

Figure 6.1: Higuchi polytope (a) and the entanglement polytopes for a tripartite system (b) - (e).

6.3 Witnessing localizable entanglement

The polytope method described in the previous section provides us a natural way of witnessing many-particle entanglement, as we shall see, namely localizable entanglement (LE) [63,64]. It can be shown, however, that the task of witnessing LE from local spectral information alone

is NP-complete. Before showing this, let us first review the concept of LE and prove some statements regarding it.

The LE of a state ρ is the maximal amount of entanglement that can be created, on average, between two particles at positions a and b by performing local measurements on the other particles. To make this more precise, consider a system of n qubits described by a pure state $\rho = |\psi\rangle\langle\psi|$ (in fact one does not need to work exclusively with qubits or pure states, but, for simplicity, we will restrict ourselves to this scenario). Consider a local measurement $\mathcal{M}$ on all qubits except the ath and the bth one. This local measurement consists of measurement operators M_s, $s = 1, \ldots, m$ such that,

$$\begin{aligned} \sum_s M_s^\dagger M_s &= \mathbb{1}, \\ p_s &= \operatorname{tr} M_s^\dagger \rho M_s \end{aligned} \tag{6.10}$$

where p_s give us the probability of obtaining outcome s. Moreover, since the measurement is local, these measurement operators are a tensor product of measurements on all qubits except the ath and the bth ones,

$$M_s = \otimes_{i\neq a,b}^n |\phi_i^s\rangle\langle\phi_i^s| \tag{6.11}$$

with $|\phi_i\rangle$ supported on the ith qubit. The two body reduced density matrix of the ath and bth qubits after obtaining the measurement outcome s is

$$\rho_s^{a,b} = \operatorname{tr}_{\setminus\{a,b\}} \left(\frac{1}{p_s} M_s^\dagger \rho M_s \right). \tag{6.12}$$

Given this, we define the average entanglement between qubits a and b under measurement $\mathcal{M}$ to be,

$$L_{a,b}^{\mathcal{M},E}(\rho) := \sum_s p_s E\left(\rho_s^{a,b}\right) \tag{6.13}$$

where E is a suitable two qubit entanglement measure. The localizable entanglement between qubits a and b is defined to be the largest average entanglement between these two qubits [64]

$$\mathcal{L}_{a,b}^E(\rho) = \sup_M L_{a,b}^{\mathcal{M},E}(\rho). \tag{6.14}$$

We wish now to prove that for a pure state $|\psi\rangle$, the LE between two qubits is positive if and only if these qubits belong to the same non-separable partition of $|\psi\rangle$.

In order to do so, let us consider a system of n qubits in a pure state $|\psi\rangle \in \mathcal{H} = \otimes_{i=1}^n \mathcal{H}^{(i)}$ with $\mathcal{H}^{(i)} \cong \mathbb{C}^2$. We aim to prove (without loss of generality) that whenever qubits 1 and n belong to a non factorizable partition of $|\psi\rangle$, $\mathcal{L}_{1,n}^E > 0$. Let us start by considering a bi-partition of the system, $I \subset \{1 \ldots n\}$, $\mathcal{H} = \mathcal{H}^{(I)} \otimes \mathcal{H}^{(I^c)}$ with $\dim \mathcal{H}^{(I^{(c)})} = 2^{|I^{(c)}|}$. Note that $|\psi\rangle$ may or may not factorize with respect to this partition. Given our partition, $|\psi\rangle$ can

be seen as a linear map from I to its complement in the following way: let $|\alpha\rangle \in \mathcal{H}^{(I)}$ and $\langle\psi|\alpha\rangle = \langle\beta| \in \mathcal{H}^{*(I^c)}$, then we define the following linear map

$$\tilde{\psi}_I |\alpha\rangle := \langle\psi|\alpha\rangle = \langle\beta| , \tag{6.15}$$

where $\tilde{\psi}_I \in L(\mathcal{H}^{(I)}, \mathcal{H}^{*(I^c)})$.

Lemma 39. *Let $|\psi\rangle$ be a pure n qubit state, $I \subset \{1, \ldots, n\}$ and $\tilde{\psi}_I \in L(\mathcal{H}^{(I)}, \mathcal{H}^{*(I^c)})$ a linear operator defined as in Eq.* (6.15)*. Then* $\operatorname{rank} \tilde{\psi}_I > 1$ *if and only if $|\psi\rangle$ does not factorize with respect to partition I.*

Proof. A rank r operator $X \in L\left(\mathcal{H}^A, \mathcal{H}^{*B}\right)$ has decomposition,

$$X = \sum_{i=1}^{r} \langle v_i| \langle w_i| \tag{6.16}$$

with $|w_i\rangle \in \mathcal{H}^A$, $\langle v_i| \in \mathcal{H}^{*B}$, as its smallest decomposition, where the size of the decomposition is measured in the number of terms involved. In our case, this implies that $|\psi\rangle = \sum_{i=1}^{r} |v_i\rangle \otimes |w_i\rangle$. Clearly $|\psi\rangle$ only factorizes with respect to partition I if and only if $\operatorname{rank} \tilde{\psi} = 1$ (note that $\operatorname{rank} \tilde{\psi} = 0 \Leftrightarrow \tilde{\psi} = 0$ and then one must have $|\psi\rangle = 0$). □

Consider now a local measurement on the ith qubit, $|\phi_i\rangle \in \mathcal{H}^{(i)}$. Then, we can see that,

Lemma 40. *For fixed i (i.e. fixing the qubit we are measuring),*

$$V_i = \left\{ \langle\psi|\phi_i\rangle \,|\, |\phi_i\rangle \in \mathcal{H}^{(i)} \right\} \subset \otimes_{j\neq i}^{n} \mathcal{H}^{*(j)} \tag{6.17}$$

V_i is a vector space with $\dim V \leq 2^{n-1}$.

Proof. Define,

$$\begin{aligned} \langle\chi| &=: \langle\psi|\phi_i\rangle , \\ \langle\chi'| &=: \langle\psi|\phi_i'\rangle . \end{aligned} \tag{6.18}$$

Then $\alpha \langle\chi| + \beta \langle\chi'| = \langle\psi| (\alpha |\phi_i\rangle + \beta |\phi_i'\rangle) \in V$ given that $\alpha |\phi_i\rangle + \beta |\phi_i'\rangle \in \mathcal{H}^{(i)}$. Also, take $|\phi_i\rangle = 0$. Then $\langle\psi|\phi_i\rangle = 0 \in V$. The dimension follows trivially from the embedding. □

Let us now define a bi-partition $I \subset \{1, \ldots n\} \setminus \{i\}$. For $\langle\chi| \in V_i = \left\{ \langle\psi|\phi_i\rangle \,|\, |\phi_i\rangle \in \mathcal{H}^{(i)} \right\} \subset \otimes_{j\neq i}^{n} \mathcal{H}^{*(j)}$, a post-measurement function, let $\tilde{\chi}_I : \mathcal{H}^I \to \mathcal{H}^{*I^c}$, defined as in (6.15) (which, given Lemma 40, is well defined). Let us define the set of "bad" vectors with respect to partition I to be

$$B_I = \{ \langle\chi| \in V | \operatorname{rank} \tilde{\chi}_I \leq 1 \} , \tag{6.19}$$

i.e. those functionals that, according to Lemma 39, factorize with respect to partition I. We wish now to show that B_I has a "low dimension" (this will be made precise down below) when compared to V, which would prove that we can always find "good" measurements $|\phi_i\rangle$ (in physical terms, a "good" measurement is one that, applied to a non bi-separable state, results in a non bi-separable state). First consider our measurement $|\phi_i\rangle$. It can be expanded in the computational basis. Neglecting normalization, we can characterize it by a single complex parameter $\lambda \in \mathbb{C}$,

$$|\phi_i\rangle = |0_i\rangle + \lambda\,|1_i\rangle\,. \tag{6.20}$$

Then for an arbitrary $\tilde{\chi}_I$, we have $\tilde{\chi}_I = \tilde{\chi}_I^0 + \lambda\tilde{\chi}_I^1$. Let $M_k^{(2)}(A)$ be a 2×2 minor of a finite dimensional operator A, indexed by k. Note that there are finitely many distinct minors. We then have the following,

$$M_k^{(2)}\left(\tilde{\chi}_0 + \lambda\tilde{\chi}_1\right) = 0, \quad \forall k \Leftrightarrow \text{rank}\,\left(\tilde{\chi}_0 + \lambda\tilde{\chi}_1\right) \leq 1. \tag{6.21}$$

$M_k^{(2)}\left(\tilde{\chi}_0 + \lambda\tilde{\chi}_1\right)$ is a polynomial in λ, therefore either it is identically zero, or it has a finite number of roots, $R_k = \left\{\lambda \in \mathbb{C} | M_k^{(2)}\left(\tilde{\chi}_0 + \lambda\tilde{\chi}_1\right) = 0\right\}$. From (6.19) we have,

$$|B_I| = |\cap_k R_k|. \tag{6.22}$$

We then have that B_I is finite unless all minors $M_k^{(2)}\left(\tilde{\chi}_0 + \lambda\tilde{\chi}_1\right)$ are identically zero. Let us assume for now that the set B_I is always finite, and relegate the possibility of B_I being infinite dimensional for latter. If we now consider all possible partitions of the finite dimensional set I, we can consider the global "bad" set $B = \cup_I B_I$. If all B_I are finite, we have that B, being the union of a finite number of finite sets, is also finite and the complement of B_I in V is an open and dense subset of V. What if one of the B_I is actually infinite? Then the following lemma applies:

Lemma 41. *Fix i and let $I \subset \{1,\ldots,n\}\setminus\{i\}$ and $I' \subset \{1,\ldots,n\}$ such that $I'\setminus\{i\} = I$ Let $\tilde{\chi}_I^j, j = 0,1 : \mathcal{H}^I \to \mathcal{H}^{*I^c}$, defined as above. If all $M_k^{(2)}\left(\tilde{\chi}_0 + \lambda\tilde{\chi}_1\right)$ are identically 0, then $|\psi\rangle$ factorizes with respect to partition I'.*

Proof. According to Eq. (6.21) if $M_k^{(2)}\left(\tilde{\chi}_0 + \lambda\tilde{\chi}_1\right) = 0, \forall k$ then $\text{rank}\,\tilde{\chi} \leq 1$ for an arbitrary $\tilde{\chi}$ (which by Lemma 39 implies that the post measurement state is separable). If $\text{rank}\,\tilde{\chi} = 0$, then $\tilde{\chi} = 0$ is the null operator and $|\psi\rangle = 0$. Let's then treat the case $\text{rank}\,\tilde{\chi} = 1$. In this case, we can write $\tilde{\chi} = \langle u_I|\,\langle v_{I^c}|$ for a $|u_I\rangle \in \mathcal{H}^{(I)}$ and $\langle v_{I^c}| \in \mathcal{H}^{*(I)}$. This in turn implies the decomposition, $\chi = \langle u_I|\,\langle v_{I^c}| = \left\langle\psi|\phi^{(i)}\right\rangle$. Note that fixing I, we have two possibilities for the set I'. Either $i \in I'$ or $i \in I'^c$. Let us consider that $i \in I'$. Then, expanding $\langle\psi| \in \mathcal{H}^{*(I')} \otimes \mathcal{H}^{*(I'^c)}$ we get,

$$\left\langle\psi|\phi^{(i)}\right\rangle = \sum_{kl} c_{kl} \left\langle\alpha_k|\phi^{(i)}\right\rangle \langle\beta_l| = \langle u_I|\,\langle v_{I^c}| \tag{6.23}$$

with $\langle\alpha_k| \in \mathcal{H}^{*(I')}$ and $\langle\beta_k| \mathcal{H}^{*(I'^c)}$. The only way we can satisfy this, for all $\left|\phi^{(i)}\right\rangle$ is if $\langle\psi|$ factorizes with respect to partition I'. The situation is identical when $i \in I'^c$. □

Note that we applied the above arguments for the case where we perform a measurement only on the ith qubit. However, if we perform successive measurements one qubit at a time, for all qubits except qubit 1 and n, we find the following

Lemma 42. *Let $|\psi\rangle$ be a pure state of n qubits not bi-separable with respect to any possible partition. Then the localizable entanglement between any two qubits is non zero.*

Proof. Let us assume, without loss of generality that we want to find the localizable entanglement between qubits 1 and n. Also, without loss of generality we assume we measure the remaining qubits in increasing order, $i = 2, \ldots n-1$. Then by our results above, there's always a dense "good" set of measurements such that the state after measurement is non-biseparable (note that lemma 41 asserts that in case the set of "bad" measurements is non-finite, $|\psi\rangle$ must be separable, which violates our assumption). We can repeat this procedure, until we have measured all but qubits 1 and n. The resulting two qubits state is then entangled, and by the definition of localizable entanglement Eq. (6.14), $\mathcal{L}^E_{1,n}(\rho) > 0$. □

We finally arrive at one of our main result of this section

Theorem 43. *Let $|\psi\rangle$ be a pure state of n qubits then the localizable entanglement between qubit a and b vanishes if and only if these qubits belong to the same non-separable partition (tensor factor) of $|\psi\rangle$.*

Proof. Let qubits a and b belong to different tensor factors of $|\psi\rangle$. The the localizable entanglement between these two qubits is obviously zero, since local measurements cannot create entanglement. Now let these two qubits belong to the same tensor factor of $|\psi\rangle$. If $|\psi\rangle$ is not bi-separable with respect to any bipartition, then by Lemma 42 the localizable entanglement between qubits and b is non zero. If, on the other hand $|\psi\rangle$ is bi-separable, it can be written as $|\psi\rangle = |\psi_I\rangle \otimes |\psi_{I^c}\rangle$, where we can take, without loss of generality, $a, b \in I$ and $|\psi_I\rangle$ not bi-separable. Then measurements in $|\psi_{I^c}\rangle$ do not affect qubits in I while for $|\psi_I\rangle$, since it is bi-separable then, according to Lemma 42, the localizable entanglement between qubits a and b is non zero. □

Consider then our pure n qubit state $|\psi\rangle$. With local spectra $\lambda = (\lambda_1, \ldots \lambda_n)$. Given one of the qubits, call it a, to Alice and the other, b, to Bob. We would like to answer the following question: looking at local spectral information alone, can we certify that a and b are part of one genuinely entangled subsystem?

For that, let us consider the following related computational problem,

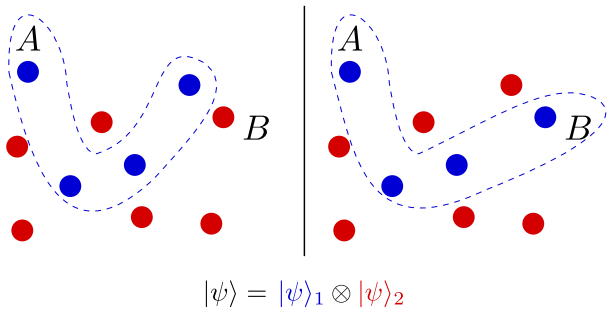

Figure 6.2: A pure bi-separable n qubits state $|\psi\rangle$. If Alice holds one qubit and Bob another one, they are either in the same tensor product of $|\psi\rangle$ or in two different ones.

BISEP-AB

INSTANCE: A set of $n+2$ numbers $\lambda_1, \ldots \lambda_n, a, b$ satisfying $\lambda_i \in [0, 0.5]$, $\lambda_i \geq \lambda_{i+1}$, $\lambda_1 \leq \sum_{i=2}^{n} \lambda_i$.

QUESTION: Is there $S_1 \subsetneq S = \{1, \cdots, n\}$, $1 \in S_1$ such that $\lambda_1 \leq \sum_{1 \neq i \in S_1} \lambda_i$ and $\lambda_k \leq \sum_{k \neq i \in S_1^c} \lambda_i$, $\lambda_k = \max_{i \in S_1^c} \lambda_i$ with $\lambda_a \in S_1$ and $\lambda_b \in S_1^c$?

If BISEP-AB is false, then we have that qubits a and b must belong to the same tensor factor of $|\psi\rangle$ and according to Theorem 43 are therefore entangled (using LE as our entanglement measure), i.e. BISEP-AP is a witness for LE.

We now proceed to show that deciding BISEP-AB is NP-complete. To do so, let us first state a well known problem, which will form the basis for our reduction.

PARTITION

INSTANCE: A set of m positive non-increasingly ordered integers , called weights, $\omega_1, \ldots \omega_m$.

QUESTION: Is there $A \subseteq B = \{1, \ldots, m\}$ such that $\sum_{i \in A} \omega_i = \sum_{i \in A^c} \omega_i$?

This is a very well known problem in Computational Complexity, shown by Karp to be NP-complete in his famous list of "21 NP-complete Problems" [65, 66]. We note that in the original problem the weights were not taken to be ordered. However, the ordering can obviously be achieved in polynomial time, and as such it does not affect our complexity results.

Let us now define a similar problem which we will use to prove the NP-hardness of BISEP-AB.

$\mathbb{Q}$-PARTITION

INSTANCE: A set of m positive non-increasingly ordered rationals, called weights , $\omega_1, \ldots \omega_m$.

QUESTION: Is there $A \subseteq B = \{1, \ldots, m\}$ such that $\sum_{i \in A} \omega_i = \sum_{i \in A^c} \omega_i$?

Lemma 44. *$\mathbb{Q}$-PARTITION is NP-complete*

Proof. (1) It is obvious that $\mathbb{Q}$-PARTITION $\in$ NP.
(2) Given that PARTITION, a well known NP-complete problem [65], is a particular instance of $\mathbb{Q}$-PARTITION, we have that $\mathbb{Q}$-PARTITION is NP-hard (PARTITION $\leq_P$ $\mathbb{Q}$-PARTITION).
Given (1) and (2), $\mathbb{Q}$-PARTITION is NP-complete. □

We are now in position to prove the following theorem

Theorem 45. *BISEP-AB is NP-complete*

Proof. (1) It is fairly obvious that BISEP-AB $\in$ NP.

(2) Consider a general instance of $\mathbb{Q}$-PARTITION, $\mathbb{Q}$-PARTITION$(\omega_1, \ldots, \omega_m)$. If $\omega_1 > \sum_{i=2}^{m} \omega_i$ then there is no way of satisfying $\mathbb{Q}$-PARTITION. This can obviously be checked in polynomial time. We now proceed to show that every instance of $\mathbb{Q}$-PARTITION, such that $\omega_1 \leq \sum_{i=2}^{m} \omega_i$ reduces, polynomially, to an instance of BISEP-AB. To do so, let us establish the following definitions,

$$\begin{aligned} \lambda_1 &:= \lambda_2 := \frac{1}{2\omega_1 m}\left(\sum_{i=1}^{m} \frac{\omega_i}{2}\right), \\ \lambda_i &:= \frac{\omega_{i-2}}{2\omega_1 m}, i = 3 \ldots, n, \\ n &:= m + 2, \\ a &:= 1, \\ b &:= 2. \end{aligned} \tag{6.24}$$

Using these definitions we have

$$\begin{aligned} \sum_{i=2}^{m} \omega_i &\geq \omega_1, \\ \sum_{i=1}^{m} \omega_i &\geq 2\omega_1, \\ \frac{1}{2\omega_1 m}\left(\sum_{i=1}^{m} \frac{\omega_i}{2}\right) &\geq \lambda_3, \\ \lambda_1 = \lambda_2 &\geq \lambda_3. \end{aligned} \tag{6.25}$$

Given this, which also implies $\lambda_1 \leq \sum_{i=2}^{n} \lambda_i$, and since $\lambda_i \in [0, 0.5], i = 1, \ldots, n$ and $\lambda_i \geq \lambda_{i+1}, i = 3, \ldots, n$ by construction, then the set $\{\lambda_1, \ldots, \lambda_n, a = 1, b = 2\}$ is a valid instance of BISEP-AB. Consider our original BISEP-AB problem, deciding whether there exists an $S_1 \subsetneq S = \{1, \ldots n\}$ with $1 \in S_1$ such that $\lambda_1 \leq \sum_{1 \neq i \in S_1} \lambda_i$ and $\lambda_k \leq \sum_{k \neq i \in S_1^c} \lambda_i$, $k = \text{argmax}_{i \in S_1^c} \lambda_i$ with $\lambda_a \in S_1$ and $\lambda_b \in S_1^c$. Note that given our choice of $a = 1$ and $b = 2$ we are effectively forcing $k = 2$.
Then we have

$$\begin{aligned} \lambda_1 &\leq \sum_{1 \neq i \in S_1} \lambda_i, \\ \lambda_2 &\leq \sum_{2 \neq i \in S_1^c} \lambda_i. \end{aligned} \tag{6.26}$$

Now, using Eq. (6.24) we can transform this into

$$\begin{aligned} \frac{1}{2\omega_1 m}\left(\sum_{j=1}^{m} \frac{\omega_j}{2}\right) &\leq \sum_{1 \neq i \in S_1} \frac{\omega_{i-2}}{2\omega_1 m}, \\ \frac{1}{2\omega_1 m}\left(\sum_{j=1}^{m} \frac{\omega_j}{2}\right) &\leq \sum_{2 \neq i \in S_1^c} \frac{\omega_{i-2}}{2\omega_1 m}. \end{aligned} \tag{6.27}$$

Taking $B = \{1, \ldots, n\}$ and $A = \{j \in B | j + 2 \in S_1\}$, then $A \subset B$ and its complement in B is $A^c = \{j \in B | j + 2 \in S_1^c\}$. Using this fact, we can write

$$\begin{aligned} \frac{1}{2\omega_1 m}\left(\sum_{j \in B} \frac{\omega_j}{2}\right) &\leq \sum_{j \in A} \frac{\omega_j}{2\omega_1 m}, \\ \frac{1}{2\omega_1 m}\left(\sum_{j \in B} \frac{\omega_j}{2}\right) &\leq \sum_{j \in A^c} \frac{\omega_j}{2\omega_1 m}. \end{aligned} \tag{6.28}$$

Now, using the fact that $\sum_{j\in B} \bullet = \sum_{j\in A} \bullet + \sum_{j\in A^c} \bullet$,

$$\begin{aligned} \sum_{j\in B} \frac{\omega_j}{2} &\leq \sum_{j\in A} \omega_j, \\ \sum_{j\in B} \frac{\omega_j}{2} &\geq \sum_{j\in A} \omega_j \end{aligned} \tag{6.29}$$

which means that

$$\sum_{j\in B} \frac{\omega_j}{2} \leq \sum_{j\in A} \omega_j \leq \sum_{j\in B} \frac{\omega_j}{2} \tag{6.30}$$

and consequently

$$\sum_{j\in A^c} \omega_j = \sum_{j\in A} \omega_j. \tag{6.31}$$

Which proves that any instance of $\mathbb{Q}$-PARTITION of such that $\omega_1 \leq \sum_{i=2}^{m} \omega_i$, reduces to a particular instance, BISEP-AB$(\lambda_1, \ldots, \lambda_n, a, b)$, of BISEP-AB. Given that all other instances of $\mathbb{Q}$-PARTITION can be decided in polynomial time, we have $\mathbb{Q}$-PARTITION $\leq_P$ BISEP-AB. Given (1) and (2), we have that BISEP-AB is NP-complete. □

We have then the tantalizing situation that even though we can, in principle, witness localizable entanglement from a small number of local measurements, the classical post processing of the data is, given current algorithms, intractable. In Appendix 12.1 we give an overview of several related physical problems and their computational complexity, including their relationship to BISEP-AB.

6.4 Comparing the computational complexity of classical and quantum marginals

This section is a bit disconnected from what has been discussed above. Here we show an instance of a natural problem that is solvable in the Quantum Mechanical setting but intractable (in a computational complexity sense) in the classical scenario.

6.4.1 Classical

Consider an alphabet $\chi = \{1, \ldots d\}$ and a string over this alphabet, $x \in \chi^{\otimes n}$. Consider now the joint probability mass function $P_{1,2}(x_1, x_2)$ where x_1 and x_2 are n and m length strings, respectively, with each character drawn at random from the alphabet χ, according to the

marginal probability mass function

$$\begin{aligned} P_1(x_1) &= \sum_{x_2 \in \chi^{\otimes n}} P_{1,2}(x_1, x_2) \\ P_2(x_2) &= \sum_{x_1 \in \chi^{\otimes m}} P_{1,2}(x_1, x_2) \end{aligned} \tag{6.32}$$

Now, imagine we forget about labels and simply order the values of the joint and the marginals probabilities mass function non-increasingly, denoting them by $P^{\downarrow}_{1,2}, P^{\downarrow}_1, P^{\downarrow}_2$ respectively.

We now ask the following question: When are $P^{\downarrow}_1$, $P^{\downarrow}_2$ compatible with a global (joint) $P^{\downarrow}_{1,2}$, in the sense that they come from marginalizing $P^{\downarrow}_{1,2}$? That is, we seek an answer to the following computational problem

C-MARG

INSTANCE: Three sets $P^{\downarrow}_{1,2}$, $P^{\downarrow}_1$, $P^{\downarrow}_2$, with $|P^{\downarrow}_1| = n$, $|P^{\downarrow}_2| = m$ and $|P^{\downarrow}_{1,2}| = nm$ such that the elements of any of these sets are in the interval $[0, 1]$ and the sum of the elements in any set sums to 1.

QUESTION: Is there a probability mass function $P_{1,2}(x_1, x_2)$ whose non-increasingly ordered version is given by $P^{\downarrow}_{12}$ such that its marginals $P_1(x_1)$ and $P_2(x_2)$ have as ordered versions $P^{\downarrow}_{(1)}$ and $P^{\downarrow}_{(2)}$ respectively?

We now proceed to show that deciding such problem is NP-hard.

Lemma 46. *C-MARG is NP-complete*

Proof. (1) It is obvious that C-MARG $\in$ NP.
(2) Consider the following particular case of our problem: Let $|P^{\downarrow}_1| = |P^{\downarrow}_2| = n, |P^{\downarrow}_{1,2}| = n^2$. Assume also that $P^{\downarrow}_1 = \left(\lambda^{(1)}_1, \lambda^{(2)}_2, 0, \dots 0\right)$ with $\lambda^{(1)}_1 = \lambda^{(2)}_2$. Hence one must have, $P^{\downarrow}_1 = \left(\lambda^{(1,2)}_1, \lambda^{(1,2)}_2, \dots, \lambda^{(1,2)}_{2n}, 0, \dots, 0\right)$. Let $B = \left\{\lambda^{(1,2)}_1, \lambda^{(1,2)}_2, \dots, \lambda^{(1,2)}_{2n}\right\}$. Then $P^{\downarrow}_1$ can only arise as a marginal from $P^{\downarrow}_{12}$ if there exists $B_1 \subset B$ such that $\lambda^{(1)}_1 = \sum_{b \in B_1} b = \sum_{b \in B^c_1} b = \lambda^{(2)}_2$, which is simply the PARTITION problem. Hence our compatibility problem is NP-hard.

Given (1) and (2), our problem is NP-complete. □

6.4.2 Quantum

We now consider the quantum analogue of the above classical problem.

Consider a bipartite quantum state $\rho_{AB} \in \left(\mathbb{C}^2\right)^{d_A} \otimes \left(\mathbb{C}^2\right)^{d_B}$, not necessarily pure. Then, by purification it can be converted into a pure tripartite state $\rho_{ABC} = |\psi\rangle\langle\psi|, \psi \in \mathbb{C}^{d_A} \otimes$

$\mathbb{C}^{d_B} \otimes \mathbb{C}^{d_C}$, such that $\mathrm{tr}_C\ \rho_{ABC} = \rho_{AB}$. Note that $|\operatorname{spec} \rho_i| = d_i$ and $|\operatorname{spec} \rho_{AB}| = d_A d_B$. In this case the following holds

Lemma 47 ([67]). *Let λ be the non-increasingly ordered spectrum of ρ_{AB} and $\tilde{\lambda}$ the non-increasingly ordered spectrum of its partial trace ρ_A. Then for every $k \in \{1, \ldots, d_A\}$ the inequality*

$$\sum_{i=1}^{k} \tilde{\lambda}_i \leq \sum_{i=1}^{d_B k} \lambda_i \tag{6.33}$$

must hold.

For a proof see [67]. Moreover, for $d_A = 2$ the equations in lemma 47 are sufficient to characterize the relationship between the spectrum of ρ_{AB} and that of ρ_A [67, Theorem 4.5]. In this case we only have the trivial inequalities

$$\begin{aligned} \tilde{\lambda}_1 &\leq \sum_{i=1}^{d_B} \lambda_i \\ \tilde{\lambda}_1 + \tilde{\lambda}_2 &\leq \sum_{i=1}^{d_B} \lambda_i \end{aligned} \tag{6.34}$$

And the problem of deciding if $(\operatorname{spec} \rho_{12}^{\downarrow}, \operatorname{spec} \rho_1^{\downarrow}, \operatorname{spec} \rho_2^{\downarrow})$ are compatible, is in P.

6.4.3 Conclusion

To the best of our knowledge, no natural instance of a *pure state* entanglement problem been shown before to be hard. Here we have shown that while it is easy to obtain the physical measurements for deciding whether two qubits are entangled or not in a localizable entanglement sense, processing the outcome in order to decide if this qubits are entangled is, in its generality, hard in a computational complexity sense. We have also given a curious example of a situation where deciding a given quantum problem is easy but not its classical analogue.

Chapter 7

Concluding remarks

The quantum marginal problem, despite its physical relevance and potential applications has remained in the dark for quite long. The solution obtained for Klyachko for the univariate quantum marginal problem has been a major breakthrough. We have provided here a simple proof that extremality of the eigenvalues of the 1-RDMs leads to structural simplifications of the possible wavefunctions associated with such 1-RDM. We have also provided the solution for the case when the 1-RDMs are degenerate, a case that, as far as we know, has not been treated previously and have computed the structural simplifications such case leads to. As we have discussed, such structural simplifications can prove to be useful for practical applications as for example the calculation of ground states. Therefore it is important to know if these structural simplifications are stable under small perturbation. To discuss the relevance of this extremality of eigenvalues of 1-RDMs we have undertaken a study of its relevance in the context of quantum chemistry: whether or not it could prove useful in the calculation of ground states of atomic and molecular systems. As we have seen answering this question is not a simple endeavor, for it is plagued by several problems: choosing the right method for the calculation of ground states, the high dimensionality necessary to achieve a good precision and ultimately the inability to examine a large number of systems and generalize our results.

We have also addressed the quantum marginal problem in Fock space and characterized the mode and particle reductions. We have shown that for the particle reduction there are no constraints in Fock space. We have also, in order to achieve our goal, characterized the reductions of free Fermions, and show that interestingly the spectra of free Fermions does *not* form a *convex polytope* as one could at first expect, based on the convexity properties of the moment polytope. We have pinpointed the problem to the fact that the set of free Fermions is *not* connected, a simple but still interesting fact. We have also considered the mode reductions for free Fermions and fully characterized it, resorting to the skew-symmetric Sing-Thompson problem. Resorting to the Jordan-Wigner transformation the obtained characterization corresponds exactly to the one known for a system of qubits.

At last we have examined the computational complexity of deciding from local spectral information whether many-body states are entangled or not, using a specific measure of entanglement: localizable entanglement. We have seen that while it is true that few easily obtainable physical measurements may be sufficient to witness many-body entanglement, the classical post processing of the obtained data is, in principle, intractable in the sense that the problem is NP-complete.

Part II

Electronic and conductance properties of geometrically frustrated systems

Acknowledgments

The work on this part has been done by the author with the support of Ricardo Guimarães Dias of the University of Aveiro, Portugal. The results displayed in section 9.3, 9.4 and 9.6, have appeared in the Master's thesis of the author and are here included for the sake of completeness. Everything else is new.

Organization

This part is organized as follows. In Chapter 8 we introduce preliminary background regarding tight-binding quantum rings. This background will prove useful for when we discuss the AB_2 chain in the following chapters. In Chapter 9 we present a detailed study of the the itinerant AB_2 chain, a prime example of the family of itinerant geometrically frustrated systems. We study not only the non-interacting AB_2 chain but also the AB_2 chain in the presence of nearest-neighbor interactions. In Chapter 10 we study the two-lead electronic conductance through non-interacting AB_2 chains and draw conclusions which should be applicable to identical flat-band frustrated systems. In Chapter 11 we introduce a new method for the calculation of the two-lead electronic conductance through interacting clusters. In Chapter 12 we study the two-lead electronic conductance through interacting spinless AB_2 chains using the method developed in the previous chapter and comparing our results against the non-interacting case and in Chapter 13 we conclude.

Chapter 8

Preliminary background

In this chapter we review some known results regarding discrete quantum rings. We are primarily interested in the energy dispersion of quantum rings and the modification introduced in the system by the presence of flux via the Aharonov-Bohm effect. These results will form a basis for studying the AB_2 chain further ahead, which is simply a chain of quantum rings.

8.1 Quantum rings

Even though one can consider continuous quantum rings, we are mainly interested in discrete ones, for discrete systems are what we will treat in the next chapters. Let us then consider a translational symmetric quantum ring consisting of N sites as depicted in Fig. 8.1. Using the tight binding approximation its Hamiltonian can be written as,

$$H = -t \sum_{j=1}^{N} c_{j+1}^{\dagger} c_j + c_j^{\dagger} c_{j+1}. \tag{8.1}$$

By transforming the operators into Fourier/momentum space,

$$c_k^{\dagger} = \sum_j \mathrm{e}^{\mathrm{i}kj} c_j^{\dagger}, \tag{8.2}$$

and using the orthogonality relation (valid for periodic boundary conditions),

$$\sum_j \mathrm{e}^{\mathrm{i}j(k-q)} = \delta_{k,q} N, \tag{8.3}$$

the Hamiltonian is diagonalized. Its eigenvalues are given by,

$$\epsilon_k = -2t\cos(k), \quad k = \frac{2\pi n}{N}, \tag{8.4}$$

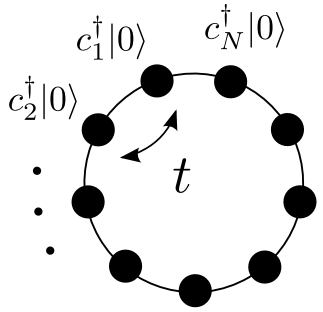

Figure 8.1: A tight-binding quantum ring.

where,

$$n = \begin{cases} -\frac{N}{2}, -\frac{N}{2}+1, \cdots, \frac{N}{2}-1 & , N \text{ even} \\ \\ -\frac{N-1}{2}, -\frac{N-1}{2}+1, \cdots, \frac{N-1}{2} & , N \text{ odd} \end{cases} \tag{8.5}$$

so that k belongs to the first Brillouin zone (FBZ).

Let us now introduce a magnetic flux through the ring and perpendicular to it, for example the one generated by an infinite solenoid. Let us also consider that the flux pierces a region where the amplitude of the wavefunction of the system tends to zero. Since the probability of an electron encountering the magnetic flux is basically zero, one could argue, on classical grounds, that since no force is exerted on the electrons nothing happens. One way of putting it is the following: Consider that the electrons are highly localized such that their wavefunction is only non-zero on the ring. Then, classicaly this would mean that the electrons are constrained to move along the ring, and as such, since the magnetic field outside the solenoid is non-existent, the Lorentz force on the electrons is zero as well.

However, as demonstrated by Ehrenberg and Siday and latter by Aharonov and Bohm, [68, 69] the requirement of gauge invariance implies that the phase of the wavefunction of an electron circulating through the ring is affected and therefore, although no magnetic field acts directly on the system, its properties are in fact affected by the magnetic flux. This is a simple consequence of the non locality of quantum mechanics.

Note that experimentally it is certainly impossible to have an infinite solenoid, and as such some magnetic field will "leak" out of the solenoid. Also one cannot guarantee with certainty that the electron's wavefunction is absolutely zero in the solenoid, but one can approximate these conditions to a very high degree [70].

Let us look at the Aharonov-Bohm effect in more detail. The wavefunction of the electron when the ring is threaded by the magnetic flux, $\psi_B(\theta)$, is related to its wavefunction in zero

field, $\psi_0(\theta)$, by,

$$\psi_B(\theta) = \exp\left[\mathrm{i}\frac{q}{\hbar}\int \vec{A}\cdot \mathrm{d}\,\vec{l}\right]\psi_0(\theta), \tag{8.6}$$

where θ is the angular position on the ring. Assuming that we have an infinite solenoid of area S inside our ring and perpendicular to its plane, with magnetic field $\vec{B} = B_0\hat{z}$ inside the solenoid, where B_0 is constant, and zero outside, means that one can choose the magnetic vector potential outside the solenoid to be

$$A = \frac{\phi}{2\pi r}\hat{\theta} \tag{8.7}$$

One can readily confirm that the curl of this vector potential vanishes,

$$\vec{B} = \vec{\nabla}\times\vec{A} = 0 \tag{8.8}$$

and that it satisfies Stoke's theorem

$$\oiint_S \vec{B}\cdot \mathrm{d}\,\vec{S} = \int_{\partial S}\vec{A}\cdot \mathrm{d}\,\vec{l}. \tag{8.9}$$

Then after a loop, the wavefunction of the electron is,

$$\psi_B(2\pi) = \psi_B(0)\mathrm{e}^{\mathrm{i}2\pi\phi/\phi_0}, \tag{8.10}$$

where $\phi_0 = h/q$ is the quantum of flux. From now on we will make $2\pi\phi/\phi_0 \to \phi$, where ϕ is now the reduced flux. Therefore, if the electron loops around the ring once, its wavefunction must acquire a phase given by the reduced flux. This can be inserted in our tight binding Hamiltonian by using the so called *twisted boundary conditions*,

$$H = -t\sum_{j=1}^{N-1}\left(c_{j+1}^\dagger c_j + c_j^\dagger c_{j+1}\right) - t\left(\mathrm{e}^{\mathrm{i}\phi}c_N^\dagger c_1 + \mathrm{e}^{-\mathrm{i}\phi}c_1^\dagger c_N\right). \tag{8.11}$$

Performing the gauge transformation,

$$c_j^\dagger \to \mathrm{e}^{-\mathrm{i}\phi/Nj}c_j^\dagger \tag{8.12}$$

our Hamiltonian can be written in the translational invariant form,

$$H = -t\sum_j \mathrm{e}^{\mathrm{i}\phi/N}c_{j+1}^\dagger c_j + \mathrm{e}^{-\mathrm{i}\phi/N}c_j^\dagger c_{j+1}, \tag{8.13}$$

where the flux has now been spread equally throughout all hops. As before, due to its translational invariance, the Hamiltonian is immediately diagonalized by transforming it into

Fourier space, its one particle eigenvectors being given by,

$$c_k^\dagger \left|0\right\rangle = \sum_j \mathrm{e}^{\mathrm{i}kj} c_j^\dagger \left|0\right\rangle , \tag{8.14}$$

and the associated eigenvalues being,

$$\epsilon_k = -2t \cos\left(k - \frac{\phi}{N}\right) . \tag{8.15}$$

Chapter 9

Study of the AB_2 chain

In this chapter we introduce the AB_2, an example of a geometrically frustrated system. The exact diagonalization of the spinless AB_2 chain is presented in the limiting cases of infinite or zero nearest-neighbor Coulomb interaction for any filling and in the presence of magnetic flux. Without interactions, the AB_2 chain has a flat band even in the presence of magnetic flux. A simple construction of the localized states that generate the flat bands both in the presence and absence of flux is presented and generalized to arrays of AB_n quantum rings. The flat band generates a plateau in the ground-state energy as a function of filling (for fillings between 1/3 and 2/3). A restricted Hartree-Fock study of the V/t versus filling phase diagram has been carried out. For finite V, the mean-field ground-state energy increases in relation to the independent Fermions ground-state energy, but remains negative for fillings lower than 2/3. For filling larger than 2/3, it becomes approximately linear reflecting the existence of nearest-neighbor occupied sites. In the mean-field phase diagram, a uniform density phase is found at low filling. For filling larger than 1/3, one of the mean-field solutions for the density difference between A sites and B and C pairs of sites disappears (due to Pauli's exclusion principle). The validity of the mean-field approach is discussed taking into account the exact results in the limiting cases.

We also discuss whether the strong coupling t-V AB_2 chain is a Luttinger liquid (LL). We argue that while for low filling, the low energy properties of t-V AB_2 chain can be described by the spinless Luttinger Hamiltonian, for filling near or larger than 2/9, the AB_2 set of eigenstates and eigenvalues becomes a complex mix of the sets of eigenstates and eigenvalues of LLs with different sizes, fillings, boundary conditions, and LL velocities.

9.1 Introduction

The field of itinerant geometrically frustrated electronic systems has attracted considerable interest in the last two decades [71–100]. A simple example of a geometrically frustrated lattice

is the AB_2 chain, also designated by diamond chain or bipartite lozenge chain [71–74,76]. This is a quasi-one-dimensional system consisting of an one-dimensional array of quantum rings. Such system can be used to model ML_2 (metal-ligand) chains [101] and azurite [72] and can be generalized to molecular systems displaying similar topology [102]. Also, given nowadays nanofabrication techniques, such as electron beam lithography, a diamond chain-like system can, in principle, be built from scratch [75]. A particular feature of the band structure of these frustrated systems is the presence of one or several flat bands in the one-particle energy dispersion, which reflect the existence of localized eigenstates of the geometrically frustrated tight-binding Hamiltonian [71–93].

The ground states of the Hubbard model for an AB_2 geometry are well studied [71–74,76] as well as for other frustrated lattices such as the sawtooth chain [89], the Kagome chain [89], etc. Some of these frustrated lattices fall onto the category of the cell construction lattices proposed by Tasaki [77–81] or the category of line graphs lattices proposed by Mielke [82–85]. The approach followed in some of these studies relies in the fact that the Hubbard interaction is a positive semidefinite operator and is limited to cases where the lowest band is a flat band or the chemical potential is fixed at the flat-band energy [71]. The frustrated systems have usually been studied in the absence of flux [74, 76, 91]. In the case of AB_2 Hubbard chain, the flux dependence of the ground-state energy has been studied but again only for chemical potential fixed at the flat band energy [71]. Many different ground states are possible in the AB_2 Hubbard chain, leading to a great variety of properties such as flat-band ferromagnetism or half-metallic conduction, depending on the values of filling, interaction or magnetic field [71].

The case of spinless Fermions in a AB_2 lattice, taking into account nearest-neighbor Coulomb interaction, is simpler than the Hubbard model due to the absence of spin degrees of freedom. We will designate the respective Hamiltonian for such system by t-V AB_2 Hamiltonian. The t-V model, in its strictly one-dimensional version (1D), can be mapped into the anisotropic Heisenberg model (more precisely, the XXZ or Heisenberg-Ising model) by the Jordan-Wigner transformation [103], whose Bethe ansatz solution has long been known [104, 104–106]. For quasi-1D models such as the one here discussed, a Bethe ansatz solution is not possible. However, a Jordan-Wigner transformation into the XXZ AB_2 chain should be possible using the extension of the Jordan-Wigner transformation to two dimensions which has been discussed by several authors [107–111]. In the case of a square lattice, this transformation requires the introduction of a gauge field which in contrast to the one-dimensional case affects the energy spectrum [108–110]. In particular, the strong-coupling limit of the repulsive t-V model under a Jordan-Wigner transformation is mapped into the strongly anisotropic antiferromagnetic Heisenberg model. During the last years, many studies of the antiferromagnetic Heisenberg model in geometrically frustrated lattices have been carried out [72,74,87,88,91,94–97,100,112]. Under high magnetic fields but below the saturation

field, the ground states of these frustrated magnetic systems consist of localized and independent magnons created in a ferromagnetic background. As a consequence of these localized magnons, quantized plateaus have been found in the respective magnetization curves [97].

9.2 The AB_2 chain

In Fig. 9.1(a), a diamond ring is shown with a magnetic flux ϕ threading each diamond plaquette and a magnetic flux ϕ_i threading the inner ring. The inner sites in Fig. 9.1(a) are denoted as C sites and the outer sites as B sites. Note that there are two ways to close the linear AB_2 chain shown in Fig. 9.1(b), either by leaving the B sites or the C sites in the interior of the ring. The two situations are physically equivalent and therefore we will assume that we have closed our ring so as to leave the C sites as inner sites. The system may be pictured as two rings, an outer one and an inner one, as shown in Fig. 9.1(a), so that an electron traveling through the outer ring sees an effective flux ϕ_o while and electron traveling through the inner ring sees a different effective flux ϕ_i. It will prove itself useful to introduce an auxiliary flux ϕ' such that

$$\begin{aligned} \phi_o &= \phi' + N_c\frac{\phi}{2}, \\ \phi_i &= \phi' - N_c\frac{\phi}{2}, \end{aligned} \tag{9.1}$$

where N_c is the number of cells of the diamond ring. In the case of zero ϕ', both effective fluxes still remain non-zero if ϕ is nonzero. In this case, the Peierls phase can be equally distributed in each plaquette, restoring the translational invariance in each ring as shown in Fig. 9.1(b). For $\phi = 0$ or π, the lattice is invariant in the "flip" of one plaquette (so that B and C sites exchange places), reflecting a local Z_2 symmetry [113].

Considering nearest-neighbor Coulomb interactions and particle hoppings, the t-V Hamiltonian for an AB_2 chain with N_c unit cells (or diamonds) is

$$H = H_0 + V\sum_j \left(n_j^A + n_{j+1}^A\right)\left(n_j^B + n_j^C\right), \tag{9.2}$$

where V is the value of the interaction and

$$\begin{aligned} H_0 = -t\sum_{j=1}^{N_c}\Big[&\mathrm{e}^{\mathrm{i}\phi_o/2N_c}(A_j^\dagger B_j + B_j^\dagger A_{j+1}) \\ &+ \mathrm{e}^{-\mathrm{i}\phi_i/2N_c}(C_j^\dagger A_j + A_{j+1}^\dagger C_j)\Big] + \text{H.c.} \end{aligned} \tag{9.3}$$

Here we have chosen a gauge such that the Peierls phases are equally distributed in the inner ring and in the outer ring.

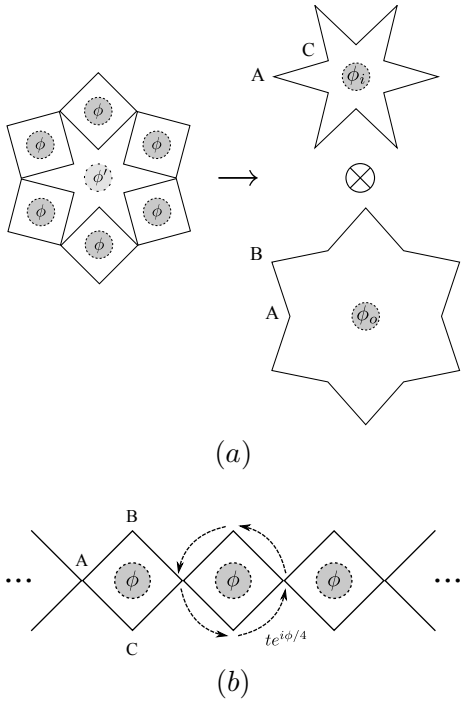

Figure 9.1: (a) The AB_2 chain consists of an one-dimensional array of diamond rings. Under magnetic field, each diamond ring is threaded by a magnetic flux ϕ and the inner star is threaded by a flux ϕ_i. This system can be pictured as an outer ring with flux ϕ_o and an inner ring with a flux ϕ_i. (b) The diamond chain when $\phi' = 0$.

9.3 Tight-binding limit

For simplicity, we will assume a flux configuration such that $\phi' = 0$ in this section. The general case is considered at the end of this section. The tight-binding Hamiltonian for AB_2 chain with N_c cells is

$$\begin{aligned} H = &- t \sum_{j}^{N_c} A_j^\dagger \left(\mathrm{e}^{\mathrm{i}\phi/4} B_j + \mathrm{e}^{-\mathrm{i}\phi/4} C_j \right) \\ &+ A_{j+1}^\dagger \left(\mathrm{e}^{-\mathrm{i}\phi/4} B_j + \mathrm{e}^{\mathrm{i}\phi/4} C_j \right) + \mathrm{H.c.} \end{aligned} \tag{9.4}$$

Employing the transformations

$$\begin{pmatrix} b_j^\dagger \\ c_j^\dagger \end{pmatrix} = \frac{1}{\sqrt{2}} \begin{pmatrix} \mathrm{e}^{-\mathrm{i}\phi/4} & \mathrm{e}^{\mathrm{i}\phi/4} \\ -\mathrm{i}\mathrm{e}^{-\mathrm{i}\phi/4} & \mathrm{i}\mathrm{e}^{\mathrm{i}\phi/4} \end{pmatrix} \begin{pmatrix} B_j^\dagger \\ C_j^\dagger \end{pmatrix}, \tag{9.5}$$

the system may be mapped into an Anderson-like model as depicted in Fig. 9.2. Its Hamiltonian is given by

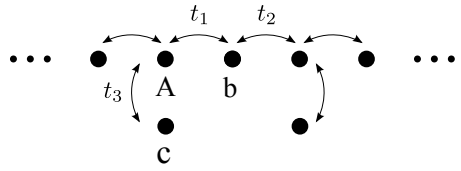

Figure 9.2: The Hamiltonian of the diamond chain threaded by an arbitrary flux can be mapped into a non-interacting periodic Anderson-like model with a basis of three sites per unit cell and with hopping amplitudes controlled by magnetic flux.

$$\begin{aligned} H = & - t_1 \sum_j b_j^\dagger A_j - t_2 \sum_j b_j^\dagger A_{j+1} \\ & - t_3 \sum_j c_j^\dagger A_{j+1} + \text{H.c.}, \end{aligned} \tag{9.6}$$

where

$$\begin{aligned} t_1 &= \sqrt{2}t, \\ t_2 &= \sqrt{2}\cos(\phi/2)t, \\ t_3 &= \sqrt{2}\sin(\phi/2)t. \end{aligned} \tag{9.7}$$

We note that the possibility of mapping a chain Hamiltonian into a periodic Anderson model has been already explored by Gulácsi *et al* by mapping the triangular-chain Hamiltonian into a periodic Anderson model [114]. In our case, when the flux is either zero or π, one has localized eigenstates, which lead to flat bands in the energy dispersion (see Fig. 9.4). For zero flux the system becomes a tight-binding ring of A and b sites with independent c sites (see Fig. 9.2), having plane-wave eigenstates in the ring and localized eigenstates at c sites, as depicted in Fig. 9.3(a). On the other hand, for $\phi = \pi$, the system behaves as a set of N_c independent systems with three sites and all the eigenstates are localized as depicted in Fig. 9.3(b) [114]. The eigenvalues for an arbitrary value of flux are given by

$$\begin{aligned} \epsilon_{\text{flat}} &= 0, \\ \epsilon_\pm &= \pm 2t\sqrt{1+\cos(\phi/2)\cos(k)}. \end{aligned} \tag{9.8}$$

In Fig. 9.4, the dispersion relation for several values of flux is shown. The flat band $\epsilon_k = 0$ is omitted since it is not modified by the presence of flux. We introduce here the Fermionic operators $f_k^\dagger$, $a_k^\dagger$ and $d_k^\dagger$, which create electrons in the single-electron bands, more precisely, $f_k^\dagger$ creates a particle with momentum k on the top band, $a_k^\dagger$ on the flat band, and $d_k^\dagger$ on the bottom band. The eigenstates creating operators are given by linear combinations of the creation operators on sites A, B and C, and for the flat band, the expression of the creation

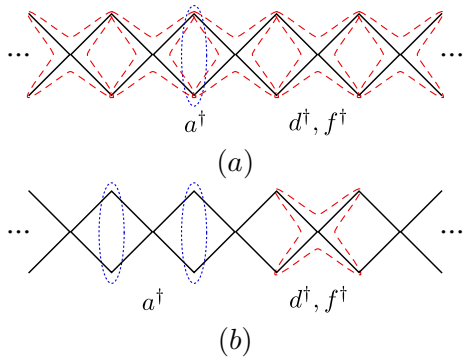

Figure 9.3: Eigenstates of the tight-binding AB_2 chain for (a) $\phi = 0$ and (b) $\phi = \pi$. For zero flux, itinerant (red dashed line) as well as localized eigenstates (blue dotted line) are present. For $\phi = \pi$, all states are localized [114].

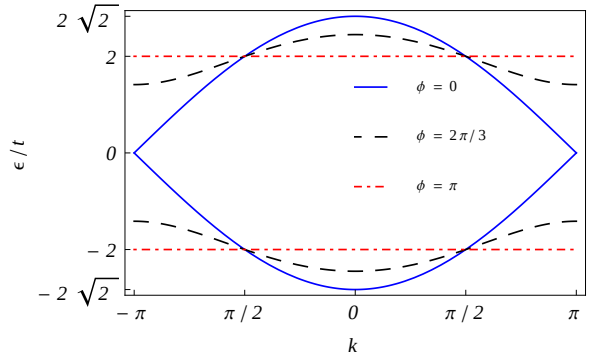

Figure 9.4: Dispersion relation of the diamond chain for different flux values (we have omitted the flat band $\epsilon_k = 0$ since it is not affected by the flux). For $\phi = \pi$, all bands are flat reflecting the local Z_2 symmetry of the Hamiltonian.

operator is rather simple,

$$a_k^\dagger = \frac{1}{\sqrt{1+\cos(\phi/2)\cos(k)}}\Big[\cos(\phi/4 - k/2)\, B_k^\dagger - \cos(\phi/4 + k/2)\, C_k^\dagger\Big]. \tag{9.9}$$

As can be concluded from the above results, the diamond chain presents always a flux independent dispersionless band and is gapless for zero flux. At finite flux a gap opens between the bottom and the top bands. This gap is given by $\Delta\epsilon = 4t\sqrt{1-\cos(\phi/2)}$, while the bandwidth of the system is $W = 4t\sqrt{1+\cos(\phi/2)}$.

In Fig. 9.4, it can be observed that for $k = \pi/2$, two flux independent eigenvalues appear. This condition is only fulfilled if the number of unit cells is a multiple of four, $N_c = 4n$ with n integer. We should also note that the system is 2π periodic on the flux when N_c is even and 4π periodic when N_c is odd. A flux of 2π interchanges the energies of the dispersive states

with $k = 0$ and $k = \pi$. These two values of momenta are allowed when N_c is even. The value $k = \pi$ is forbidden when N_c is even and the period of the system is 4π on the flux.

The eigenvalues for an arbitrary value of flux ϕ' are obtained following similar steps and the energy-dispersion relations become

$$\begin{aligned} \epsilon_{\text{flat}} &= 0, \\ \epsilon_{\pm} &= \pm 2t\sqrt{1+\cos(\phi/2)\cos(\phi'/N_c+k)}. \end{aligned} \tag{9.10}$$

The insertion of an extra flux ϕ' in the AB_2 chain only translates the energy-dispersion relation by ϕ'/N_c and therefore does nothing to the flat band. This result is expected since it is similar to what is observed in 1D quantum rings. One can use ϕ' to control the momentum for which the top/bottom band reach its maximum/minimum energy.

9.4 Density of states, filling and ground-state energy

Let us consider the thermodynamic limit (k continuous) and calculate the density of states (DOS) of the tight-binding AB_2 chain. The DOS of the flat band is a Dirac-delta function at $\epsilon = 0$. The dispersive bands are one-dimensional bands and the combined DOS of the two dispersive branches can be written as

$$D(\epsilon)_{\pm} = \frac{1}{\pi t}\left|\epsilon'\right| \frac{1}{\sqrt{\cos^2(\phi/2) - \left(\epsilon'^2 - 1\right)^2}}, \tag{9.11}$$

when ϵ belongs to the energy intervals associated with the dispersive bands and where $\epsilon' = \epsilon/2t$. The full DOS of the system is therefore, $D(\epsilon) = D_{\pm}(\epsilon) + \delta(\epsilon)$.

Filling is defined as the number of electrons N per site, $\rho = N/N_s = N/3N_c$, where N_s is the number of sites. Due to the symmetric nature of the energy spectrum and since each band can accommodate one electron per unit cell, we know that half filling occurs for $E_F = 0$. Since the flat band contains N_c states then when $\rho \in [1/3, 2/3]$ one has $E_F = 0$. If E_F lies on the bottom band we have

$$\rho = \frac{1}{3}\int_{\epsilon_{b,\min}}^{E_F} D_-(\epsilon)\,\mathrm{d}\,\epsilon, \tag{9.12}$$

where $\epsilon_{b,\min} = -2\sqrt{2}t\cos(\phi/4)$ is the bottom of the band and where the factor of $1/3$ is due to the fact that the integral of the DOS over a band is one and each band contributes equally

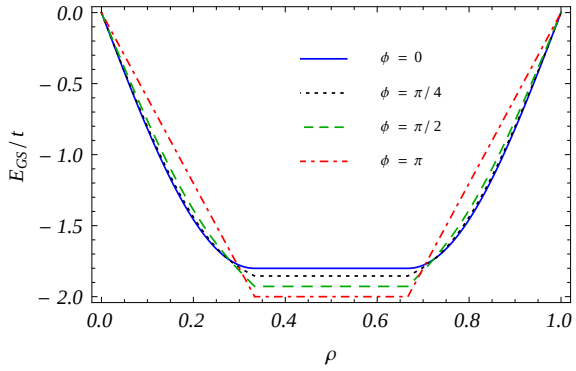

Figure 9.5: Ground state energy in the thermodynamic limit as a function of filling for several values of flux. E_{GS} remains constant when filling the flat band, $\rho \in [1/3, 2/3]$ achieving its minimum value in that interval for $\phi = \pi$. For $\phi = \pi$, E_{GS} has linear behavior in ρ, since all bands are flat.

to the DOS. Using Eq. (9.11) we have,

$$\rho = \frac{1}{6\pi}\left[\arctan\left(\frac{\epsilon'_{b,\min}}{\sqrt{\cos^2(\phi/2) - \epsilon'^2_{b,\min}}}\right) - \arctan\left(\frac{E'_F}{\sqrt{\cos^2(\phi/2) - E'^2_F}}\right)\right], \tag{9.13}$$

where

$$\begin{aligned} \epsilon'_{b,\min} &= \left(\frac{\epsilon_{b,\min}}{2t}\right)^2 - 1, \\ E'_F &= \left(\frac{E_F}{2t}\right)^2 - 1. \end{aligned} \tag{9.14}$$

If, on the other hand, E_F lies on the top band, one can use the symmetry of the density of states to write $\rho = 1 - \rho_h$, where

$$\rho_h = \frac{1}{3}\int_{\epsilon_{b,\min}}^{-E_F} D_-(\epsilon)\,\mathrm{d}\,\epsilon, \tag{9.15}$$

is given by Eq. (9.13).

Given the preceding results, we are able to calculate the ground-state energy of the system as a function of filling. The ground-state energy is given by

$$E_{\mathrm{GS}} = \int_{E_{\min}}^{E_F} D(\epsilon)\epsilon\,\mathrm{d}\,\epsilon, \tag{9.16}$$

while Eqs. (9.13) and (9.14) give us the relation between the Fermi energy and the filling. For a general value of ϕ there is no simple analytical expression and the ground-state energy should be calculated numerically. However, when $\phi = \pi$ it is very simple to derive an exact result, given that the system only has three energy levels, $\epsilon = 0, \pm 2t$ and that each can take N_c electrons. In this case, the ground-state energy per unit cell while the bottom band is not fully filled is given by $E_{\rm GS} = -2tN/N_c = -6t\rho$. At $\rho = 1/3$ the bottom band gets fully filled and from $\rho = 1/3$ to $\rho = 2/3$ we are filling the middle band whose energy is $\epsilon = 0$. Therefore, $E_{\rm GS} = -2t, \quad \rho \in [1/3, 2/3]$. For $\rho > 2/3$ we start filling the upper band, whose energy is $\epsilon = 2t$. In this situation the ground-state energy is given by $E_{\rm GS} = 6t(\rho - 2/3) - 2t$.

In Fig. 9.5 we plot the ground-state energy as a function of filling for several values of flux. As can be seen for $\rho \in [1/3, 2/3]$ the ground-state energy remains constant since we are filling the flat band $\epsilon_k = 0$. The ground-state energy is obviously even around $\epsilon_k = 0.5$ due to the symmetric nature of the dispersion relation. We also see that for $\rho \notin [1/3, 2/3]$ the dependence of the ground-state energy on the filling departs from its linear behavior when $\phi \neq \pi$.

9.5 Flat bands and localized states for arrays of quantum rings

It is well known that the single-particle flat band eigenstates of a geometrically frustrated lattice can be written as a set of localized eigenstates which are translated versions of the same state $|\psi_{\rm loc}\rangle$. This single-particle state is non-zero in a small lattice region and it is an eigenstate of the tight-binding Hamiltonian (a zero energy eigenstate in the case of the AB_2 chain). This means that if we write the eigenstate as $|\psi_{\rm loc}\rangle = \sum_i a_i c_i^\dagger |0\rangle$, where i runs over all lattice sites such that $a_i \neq 0$, then $\sum_i t_{ri} a_i = \epsilon a_r = 0$, where r can be any site in the lattice such that $a_r = 0$, t_{ri} is the hopping constant between sites r and i and ϵ is the kinetic energy of the state. In the particular case of AB_2 chains, $\epsilon = 0$ and the restrictions on sites i and r can be lifted, i.e., $\sum_i t_{ri} a_i = \epsilon a_r = 0$, where i runs over all lattice sites and r is any site of the lattice. We propose a particular perspective (but equivalent) for the case of any array of quantum rings similar to the AB_2 chain which easily allows us to identify the localized states in the absence or presence of flux. Let us also assume for now that the array is such that the shared sites between consecutive rings are directly opposite, and therefore the number of sites in each ring is even.

For zero flux, $\phi = \phi_o = \phi_i = 0$, all energy levels of the tight-binding ring are doubly degenerate with exception of the lowest and highest energy levels ($k = 0$ and $k = \pi$) and the respective eigenstates have opposite momenta, reflecting the time-reversal symmetry of the Hamiltonian. In the particular case of the AB_2 chain, the respective ring has four sites and there is only one degenerate level corresponding to zero energy. Subtracting the states of opposite momenta, one obtains a standing wave with nodes at $i = 0$ and $i = N_r/2$ (ring

sites are numbered clockwise from $i = 0$ to $i = N_r - 1$). For $N_r > 2n$ with $n > 2$ one has more than one flat band. More precisely, one has $N_{\rm ring}/2 - 1$ flat bands with energies $\epsilon_n = -2t\cos(2\pi n/N_r)$ with $n = 1, \ldots, N_r/2 - 1$. Since these nodes coincide with the sites shared by consecutive rings, one can say that for these standing wave states, the ring becomes uncoupled to the rest of the chain. Furthermore, if $N_r > 2n$ with $n > 2$ the standing waves may have more than two nodes and more complex lattices can have such localized states. Note however that the nodes position must be an integer. We conclude that in order to find flat band eigenstates of arrays of quantum rings, one may construct standing waves such that the nodes coincide with sites shared between different quantum rings. For instance, for $N_r = 8$, a square lattice is possible as shown in Fig. 9.8.

These arguments agree with the results obtained for the AB_2 chain. For $\phi = \phi_o = \phi_i = 0$, one has $a_k^\dagger = [B_k^\dagger - C_k^\dagger]/\sqrt{2}$, which can be Fourier transformed to obtain $a_i^\dagger = [B_i^\dagger - C_i^\dagger]/\sqrt{2}$. The single-particle state $a_i^\dagger|0\rangle$ is a localized eigenstate in cell i with zero energy.

Let us consider now $\phi = 0$ but $\phi_o = -\phi_i \neq 0$. Then the tight-binding constants in one ring become $t_{j,j+1} = e^{-i\phi_o/2N_c \cdot j}t$, for $j = 0, \ldots, N_r/2 - 1$ and $t_{j,j+1} = e^{i\phi_o/2N_c \cdot j}t$, for $j = N_r/2, \ldots, N_r - 1$ so that the total Peierls phase is zero reflecting the fact that $\phi = 0$. A simple gauge transformation

$$\begin{array}{rcll} c_j^\dagger & \rightarrow & e^{i\frac{\phi_o}{2N_c}\cdot j}c_j^\dagger, & j = 0, \ldots, \frac{N_r}{2} \\ c_j^\dagger & \rightarrow & e^{i\frac{\phi_o}{2N_c}\cdot (N_r - j)}c_j^\dagger, & j = \frac{N_r}{2} + 1, \ldots, N_r - 1 \end{array}$$

restores the translation invariance with a zero Peierls phase and the previous construction of localized states can be applied. Therefore, the same flat bands will be present. In the case of the AB_2 chain, the flat-band states will have the form $a_i^\dagger|0\rangle = e^{-i\frac{\phi_o}{2N_c}}[B_i^\dagger - C_i^\dagger]/\sqrt{2}|0\rangle$, but the phase term is obviously irrelevant.

Let us address now the case of $\phi \neq 0$ but $\phi' = 0$ (the case with $\phi' \neq 0$ is obtained following the same steps after a gauge transformation as explained for the $\phi = 0$ case). When $\phi \neq 0$, eigenstates of the tight-binding ring with opposite momenta k and $-k$ do not have the same energy (see Fig. 9.6) and therefore the standing wave obtained from the subtraction of these states is not an eigenstate of the tight-binding Hamiltonian of the ring. One can overcome this difficulty considering two consecutive rings and following a certain path in those rings such that the total Peierls phase in that path is zero as shown in Fig. 9.7. If one constructs standing waves for a ring of $2N_r$ sites with the additional condition of extra nodes at sites $N_r/2$ and $2N_r - N_r/2$ (sites A and B in Fig. 9.7), this state can be folded (making site A overlap with site B) to give an eigenstate of the two rings threaded by flux with nodes at the extremities. Note that the larger ring has non-zero Peierls phases associated with each hopping but the total phase is zero. So after a gauge transformation to eliminate these phases, the states of opposite momenta are degenerate and the standing wave is an eigenstate of the Hamiltonian of the two rings. Again, one or more flat bands are possible depending on the

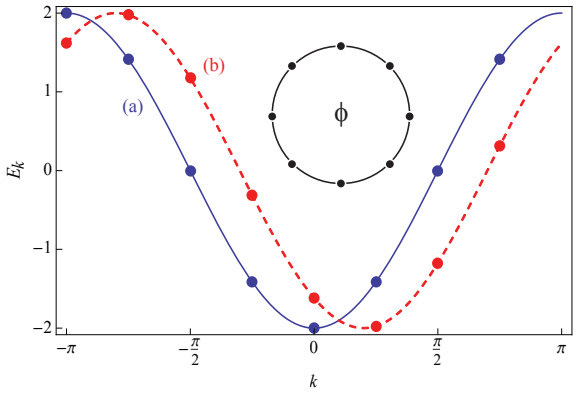

Figure 9.6: Dispersion relation of a tight-binding ring with eight sites: (a) without flux; (b) threaded by a magnetic flux $\phi = \pi/5$. For zero flux, states k and $-k$ are doubly degenerate (with the obvious exception of $k = 0$ and $k = \pi$). When $\phi \neq 0$, the eigenstates of the tight-binding ring with opposite momenta k and $-k$ do not have the same energy reflecting the loss of time-reversal symmetry.

size of the quantum ring.

The gauge transformation for the larger ring will be

$$\begin{aligned}
c_j^\dagger &\rightarrow e^{i\frac{\phi_o}{2N_c}\cdot j} c_j^\dagger, && j = 0, \ldots, \tfrac{N_r}{2} \\
c_j^\dagger &\rightarrow e^{i\frac{\phi_o}{2N_c}\cdot (N_r - j)} c_j^\dagger, && j = \tfrac{N_r}{2} + 1, \ldots, N_r \\
c_j^\dagger &\rightarrow e^{-i\frac{\phi_o}{2N_c}\cdot (j - N_r)} c_j^\dagger, && j = N_r + 1, \ldots, N_r + \tfrac{N_r}{2} \\
c_j^\dagger &\rightarrow e^{-i\frac{\phi_o}{2N_c}\cdot (2N_r - j)} c_j^\dagger, && j = N_r + \tfrac{N_r}{2} + 1, \ldots, 2N_r - 1
\end{aligned}$$

where the sites have been numbered clockwise in the larger ring. In the case of the AB_2 chain, after the gauge transformation the localized state (not normalized) will be $(c_1^\dagger - c_3^\dagger + c_5^\dagger - c_7^\dagger)|0\rangle$, which, inverting the gauge, transformation corresponds to the state $[e^{-i\frac{\phi_o}{2N_c}}(c_1^\dagger - c_3^\dagger) + e^{i\frac{\phi_o}{2N_c}}(c_5^\dagger - c_7^\dagger)]|0\rangle$. This state written in terms of the operators of the AB_2 chain becomes $[e^{-i\frac{\phi_o}{2N_c}}(B_j^\dagger - C_{j+1}^\dagger) + e^{i\frac{\phi_o}{2N_c}}(B_{j+1}^\dagger - C_j^\dagger)]|0\rangle$ or equivalently $[e^{-i\frac{\phi}{4}}(B_j^\dagger - C_{j+1}^\dagger) + e^{i\frac{\phi}{4}}(B_{j+1}^\dagger - C_j^\dagger)]|0\rangle$. These are exactly the localized eigenstates obtained Fourier transforming Eq. (9.9),

$$\begin{aligned}
&2e^{ik/2}\sqrt{1 + \cos(\phi/2)\cos(k)}\, a_k^\dagger = \\
&\qquad [e^{i\phi/4} + e^{-i(\phi/4 - k)}] B_k^\dagger - [e^{i(\phi/4 + k)} + e^{-i\phi/4}] C_k^\dagger.
\end{aligned} \tag{9.17}$$

Note that these localized states may overlap in real space, that is, they constitute a basis of the subspace of localized states but not an orthogonal basis. Such impossibility of constructing orthogonalized Wannier states for certain lattices with flat bands under a uniform magnetic field has been mentioned before [115].

As an example of application of the previous arguments, we show in Fig. 9.8 the localized states for the Lieb lattice. It is known that this lattice displays a flat band for zero and finite

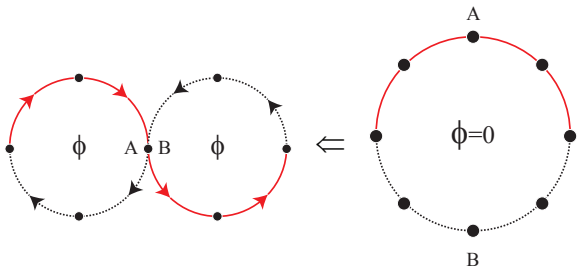

Figure 9.7: In the presence of flux, considering two consecutive rings and following first the continuous path (in red) and then the dotted path (in black) the total Peierls phase in that path is zero (the path is clockwise for the left ring and counter-clockwise for the right ring). If one constructs standing waves for a ring of $2N_r$ sites with the additional condition of extra nodes at sites A and B, this state can be folded to give an eigenstate of the two rings threaded by flux with nodes at the extremities and at site A.

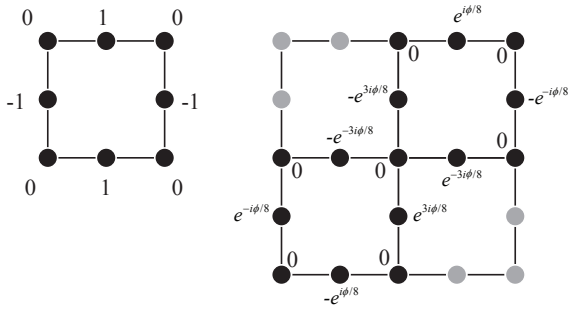

Figure 9.8: Localized states in the case of the Lieb lattice with or without magnetic flux. The introduction of magnetic flux extends the localized state to two plaquettes. These plaquettes are equivalent to the quantum rings discussed in the text and the localized state is a standing wave with nodes in the plaquettes vertices.

magnetic flux. Aoki *et al.* have found the respective localized state for zero flux as well as by inspection a localized "elongated ring state" for finite flux [115]. The zero flux localized state agrees with the one shown in Fig. 9.8, but our localized state for finite flux shown in Fig. 9.8 is considerably more compact than the "elongated ring state" of Ref. [115]. We expect that the previous arguments can be applied to other lattices that fall onto the Lieb lattice category, that is, bipartite lattices with different numbers, n_A and n_B, of A and B sublattice sites in a unit cell [116]. Another example of simple application is the B_c class superhoneycomb lattice [115]. Again our argument justifies the fact that the flat band in this system remains flat for finite magnetic field.

9.6 Mean-field results for general V

In this section, we present a mean-field study of the t-V AB_2 chain taking into account nearest-neighbor Coulomb interaction. The results obtained must be interpreted with caution, having

in mind the known drawbacks of this approach. One of these drawbacks is the fact that this approach neglects thermal fluctuations, which as stated by the Mermin-Wagner theorem prevent long range order at finite temperature. In this section, only the zero-temperature case is addressed, so one avoids this problem. Even at zero temperature, the mean-field approach overestimates the existence of an ordered phase, since quantum fluctuations oppose the emergence of an ordered phase and these quantum fluctuations are particularly strong in quasi-1D systems. Note however that the ground state of quasi-1D systems may in fact be ordered despite these quantum fluctuations.

When considering nearest-neighbor Coulomb interactions, we will be interested on the density of particles at A, B and C sites. We assume the particle density on site X to be the average number of particles per number of unit cell, $\rho_X = \overline{N}_X/N_c$. We also assume that the particle density at B and C sites is the same. Let ρ denote the total particle density,

$$\rho = \frac{\rho_A + 2\rho_B}{3}, \tag{9.18}$$

where ρ_A and ρ_B are the particle densities at A and B sites respectively. We then have

$$0 \leq \left\{ \begin{matrix} \rho \\ \rho_A \\ \rho_B \end{matrix} \right\} \leq 1. \tag{9.19}$$

In this situation, the interaction part of the mean-field Hamiltonian can be written as

$$H_{\text{int}} = 2V \sum_j \left[2\rho_B n_j^A + \rho_A n_j^B + \rho_A n_j^C \right] - 4N_c \rho_A \rho_B. \tag{9.20}$$

While there is no simple expression for the mean-field dispersion relation for general ϕ, a simple expression exists for zero flux,

$$\begin{aligned} \epsilon_{\text{flat}} &= 2V\rho_A, \\ \epsilon_{\pm} &= V\left(\rho_A + 2\rho_B\right) \pm \sqrt{8t^2 \cos^2(k/2) + \Delta_V^2}, \end{aligned} \tag{9.21}$$

where $\Delta_V = V\left(\rho_A - 2\rho_B\right)$. Again, a flat band is present, but its energy level depends on the density at sites A.

We define the order parameter as the excess of density at the A sites,

$$\Delta\rho = \frac{\rho_A - 2\rho_B}{\rho_A + 2\rho_B}. \tag{9.22}$$

Due to the equivalence of the B and C sites, we regard our system as being a dimerized system consisting of two alternating types of sites: A sites and BC pseudo-sites. Note however that this picture is to be interpreted with caution since BC pseudo-sites are not real sites and can

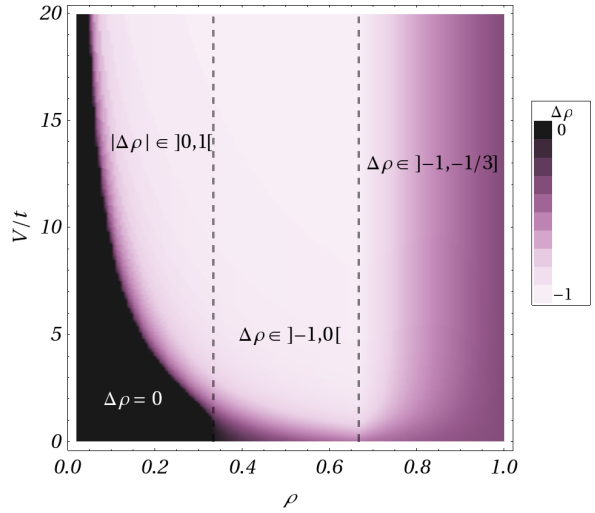

Figure 9.9: V/t versus filling mean-field phase diagram for the spinless diamond chain considering nearest-neighbor Coulomb interactions and $N_c = 128$. For $\rho < 1/3$ we can have a uniform density phase ($\Delta\rho = 0$) or a phase with excess of density at A or BC pseudo-sites ($\Delta\rho > 0$ or $\Delta\rho < 0$, respectively). For $\rho > 1/3$, Pauli's exclusion principle breaks the symmetry between A and BC pseudo-sites. A uniform density phase is not possible anymore and the density of particles can no longer be situated only at A sites. It can however, for $\rho < 2/3$, be situated only at BC pseudo-sites. For $\rho > 1/3$, due to Pauli's exclusion principle, the density of particles is required to be spread among A and BC sites and for $\rho = 1$ the order parameter is $\Delta\rho = -1/3$, which implies a uniform density of particles between the real A, B and C sites.

accommodate twice as many electrons as A sites. One must note that in a general situation we have $\Delta\rho \in [-1, 1]$. Since $0 < \rho_A, \rho_B < 1$, then for $\rho > 1/3$, $\Delta\rho$ is limited to the interval $[-1, \Delta\rho_{\max}]$, where $\Delta\rho_{\max}$ lies in $]-1, 0[$ and whose value decreases with increasing ρ. For the same reason, for $\rho > 2/3$, $\Delta\rho$ is limited to $]-1, -1/3]$, and not only the upper limit of $\Delta\rho$ decreases with increasing ρ, but also the lower limit of $\Delta\rho$ increases with increasing ρ. For $\rho = 1$ we have $\Delta\rho = -1/3$, corresponding to an equal density of particles on every site (the only possible state when the system is completely filled).

The phase diagram of the system is depicted in Fig. 9.9. a uniform density phase can exist only for a filling $\rho < 1/3$. For $\rho < 1/3$, starting in the uniform density phase, by increasing the interaction we are able to localize an excess of electron density at A sites or at BC pseudo-sites, both situations being symmetric. By further increasing the interaction we are able to localize all the Fermions at A sites or at BC pseudo-sites where both situations remain symmetric. As a consequence the order parameter $\Delta\rho$ can be double valued for these values of filling. In the region $1/3 < \rho < 2/3$ one no longer can localize the full electrons density at A sites while one can at BC sites and therefore although the Hamiltonian treats A and BC pseudo-sites equally, Pauli's exclusion breaks the symmetry between A and BC pseudo-sites, lowering the symmetry of the system. Consequently, for $\rho > 1/3$, the order parameter can

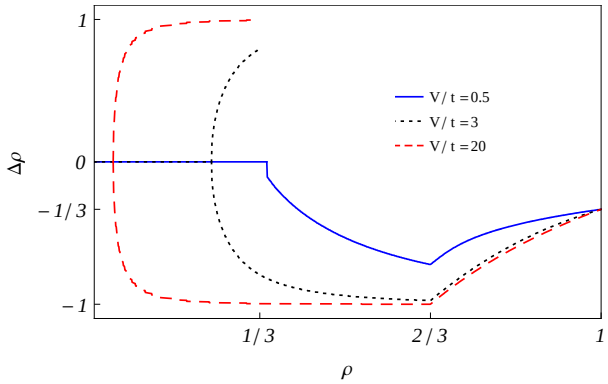

Figure 9.10: Order parameter as a function of filling for $V/t = 0.5$, 3 and 20 and $N_c = 200$. The changes of slope of the order parameter indicate the phase transitions. Note that the absence of a positive solution of $\Delta\rho$ for $\rho > 1/3$ reflects the fact that the A and BC pseudo-sites may be occupied by one and two Fermions, respectively. As a consequence, for $\rho < 1/3$ the order parameter can be double valued since we are able to localize all Fermions at A sites ($\Delta\rho > 0$) or at BC pseudo-sites ($\Delta\rho < 0$). Since for $\rho > 1/3$ we can no longer localize all Fermions at A sites, the order parameter can no longer be positive.

no longer be double valued. In the region $\rho > 2/3$, again due to Pauli's exclusion principle, one is not able to fully localize the density of electrons even at BC pseudo-sites and only one phase remains.

In Fig. 9.10, the order parameter as a function of filling is shown for $V/t = 0.5$, 3 and 20 and $N_c = 200$. The changes of slope of the order parameter indicate the phase transitions. The absence of a positive solution of $\Delta\rho$ for $\rho > 1/3$ reflects the fact that the A and BC pseudo-sites may be occupied by one and two Fermions, respectively.

In Fig. 9.11, we show the ground-state energy per site as a function of ρ for $V/t = 0$, 1, 3 and 20 and $N_c = 200$, obtained in the mean-field approach. For finite V, no flat region appears and the minimum energy is shifted to lower filling. Recalling Eq. (9.21), one concludes that a constant term $3V\rho^2$ is added to the non-interacting ground-state energy when $\Delta\rho = 0$, which shifts the minimum energy to lower ρ when V is small ($\Delta\rho = 0$ for low ρ). The ground-state energy remains negative for $\rho < 2/3$. For $\rho > 2/3$ and large V, the ground-state energy is almost linear in the filling with a large slope, since nearest-neighbor pairs are being created.

9.7 The AB_2 chain in the strong-coupling limit $V \to \infty$

Making t/V a small parameter, one drives the t-V AB_2 model into the so-called strong-coupling limit. There are two equivalent ways to reach this limit, either increasing V or reducing t. If $t = 0$, the Fermions are localized and all states with the same number of pairs of nearest-neighbor occupied sites, $\sum_i (n_j^A + n_{j+1}^A)(n_j^B + n_j^C)$, are degenerate. This degeneracy is much lower compared with the ground-state degeneracy of the $U/t \to \infty$ Hubbard AB_2

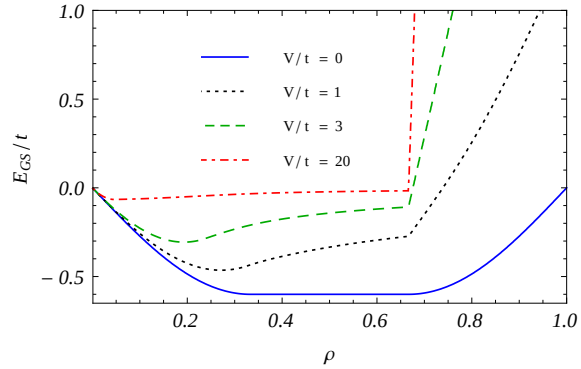

Figure 9.11: Ground state energy per site as a function of ρ for $V/t = 0$, 1, 3 and 20 and $N_c = 200$, obtained in the mean-field approach. For finite V, no flat region appears and the minimum energy is shifted to lower filling. The ground-state energy remains negative for $\rho < 2/3$. For $\rho > 2/3$, the ground-state energy is almost linear in the filling with a large slope, since nearest-neighbor pairs are being created.

model. This degeneracy is lifted if t/V is finite and up to first order in t, the eigenvalues are obtained diagonalizing the Hamiltonian within each of the degenerate subspaces. The Hamiltonian within each subspace is obtained using the Gutzwiller projection operators P_l, which project onto the subspace with l pairs of nearest-neighbor occupied sites. The set of eigenstates and eigenvalues of $l = 0$ subspace of this model can be determined as we will show below, relying at least for some of the eigenstates in the knowledge of the solution of the t-V chain [117].

In order to simplify the comparison between the t-V chain and the AB_2 chain, we number the sites in a different way, using odd numbers for A sites and even numbers for B and C sites.

Let us also define the operator $n_i^h = (1 - c_i^\dagger c_i)$ where c can be an operator A, B or C. In the strong-coupling limit $V/t \gg 1$, we obtain for the ground state subspace ($l = 0$) the projected Hamiltonian with $\phi = 0$ (but $\phi_i = \phi_o \neq 0$)

$$P_0 H P_0 = -t \sum_{j \text{ odd}} \mathrm{e}^{\mathrm{i}\phi_o/2N_c} \left[\prod_{i \,\epsilon\, \mathcal{P}_j} n_i^h \times A_j^\dagger (B_{j+1} + C_{j+1}) + \prod_{i \,\epsilon\, \mathcal{P}_{j+1}} n_i^h \times (B_{j+1}^\dagger + C_{j+1}^\dagger) A_{j+2} \right] + \text{H.c.}$$

where $\mathcal{P}_j$ is the set of sites nearest-neighbors of the pair of sites j and $j+1$ (excluding these sites) and the product of hole occupation numbers reflects the condition that a nearest-neighbor pair of occupied sites is not created when a particle hops.

Again, we emphasize that states belonging to subspaces with $l \neq 0$ pairs of nearest-neighbor occupied sites will be discarded since their energy is of the order of V.

Let us consider two consecutive sites and therefore, nearest neighbors of each other. Considering the subspace with $l = 0$, there are three possible configurations for this pair of sites,

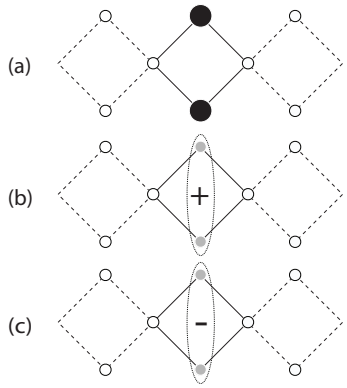

Figure 9.12: (a) Two-particle localized state and one-particle (b) itinerant and (c) localized state involving B and C sites. The filled and empty circles indicate occupied and unoccupied sites respectively. Gray circles indicate bonding (+) and anti-bonding (-) occupations. The particles in (a) are localized due to the interaction ($V/t = \infty$) and in (c) due to geometric frustration. In (b), the particle is free to hop to the neighboring A sites.

which we will call links and they are $(h\,p); (p\,h); (h\,h)$ where p stands for an occupied site and h for an empty one. The total number of these links in the AB_2 chain is given by

$$N_{hp} + N_{ph} + N_{hh} = 4N_c \tag{9.23}$$

and $N_{hp} = N_{ph}$. Note that unlike the case of the t-V chain, the number of links N_{hp} and N_{hh} in the strong coupling AB_2 chain is not a conserved quantity.

9.7.1 Basis

Let us consider a unit cell of the AB_2 chain (which has three sites, A, B and C). The set of states for this cell correspond to five possible configurations in what concerns the particles distribution : i) zero particles with all sites being unoccupied; ii) one particle which may be at site A,B or C. The states with just one particle either at site B or site C can be combined to give a bonding and an anti-bonding state [see Fig. 9.12(b) and Fig. 9.12(c)]. The anti-bonding state is a localized state as discussed in previous sections. The bonding state is a itinerant state; iii) two particles which must be at sites B and C in order to avoid a nearest neighbor occupied pair of sites [see Fig. 9.12(a)]. These particles are also localized particles because if they hopped, a state with a nearest neighbor occupied pair of sites would be created.

Let us consider now the case of N particles in a AB_2 chain with N_c unit cells. Let us define the operators $B^\dagger_{+,i} = (B^\dagger_i + C^\dagger_i)/\sqrt{2}$ and $B^\dagger_{-,i} = (B^\dagger_i - C^\dagger_i)/\sqrt{2}$. Note that the product of these two operators creates two particles, one at site B_i and the other at site C_i as expected.

Using this new basis, the Hamiltonian can be rewritten in a simpler form

$$P_0 H P_0 = -\sqrt{2}t \sum_{j=1}^{N_c} \quad \mathrm{e}^{\mathrm{i}\phi_o/2N_c} \left(\prod_{i\,\epsilon\,\mathcal{P}_j} n_i^h \times A_j^\dagger B_{+,j+1} + \prod_{i\,\epsilon\,\mathcal{P}_{j+1}} n_i^h \times B_{+,j+1}^\dagger A_{j+2} \right) + \text{H.c.} \tag{9.24}$$

One could be tempted to say that the localized states play no role in this simplified Hamiltonian since only the $B_{+,j}^\dagger$ operator appears, but that would be incorrect. A basis for the ground state subspace ($l = 0$) can be constructed from states of the form

$$|\Psi\rangle = \prod_{i=1}^{N_{BC}} B_{\alpha_i}^\dagger C_{\alpha_i}^\dagger \prod_{j=1}^{N_{B_-}} B_{-,\beta_j}^\dagger \prod_{n=1}^{N_{B_+}} B_{+,\gamma_n}^\dagger \prod_{m=1}^{N_A} A_{\mu_m}^\dagger |0\rangle \tag{9.25}$$

where the sets $\{\alpha\}$, $\{\beta\}$, $\{\gamma\}$, $\{\mu\}$, $\{\alpha \pm 1\}$, $\{\beta \pm 1\}$, $\{\gamma \pm 1\}$ and $\{\mu \pm 1\}$ have no common elements in order to satisfy the $l = 0$ condition and N_{BC}, N_{B_-}, N_{B_+} and N_A, are respectively the number of localized pairs of Fermions at sites B and C, of antibonding localized Fermions, of itinerant bonding Fermions and of itinerant Fermions at A sites, so that $2N_{BC} + N_{B_-} + N_{B_+} + N_A = N$. Due to the projection condition, the localized Fermions created by the $B_{-,j}^\dagger$ and $B_{+,j}^\dagger B_{-,j}^\dagger$ operators act creating open boundaries for the hoppings of Fermions. The Hamiltonian mixes states with different configuration for the $A_j^\dagger$ and $B_{+,j}^\dagger$ products but the part relative to the localized Fermions remains always the same. In Fig. 9.13, we illustrate this.

The diagonalization of the Hamiltonian given by Eq. (9.24) is achieved by first distributing the localized Fermions (if any) and then solving the remaining problem for the itinerant Fermions which move in regions confined by the localized particles, leading to a factorized form of the eigenstates, $|\text{itinerant Fermions}\rangle \otimes |\text{localized Fermions}\rangle$. The eigenvectors and eigenvalues of the 1D t-V model for twisted boundary conditions as well as open-boundary conditions can be obtained by use of the Bethe ansatz, but an equivalent but simpler algebraic solution is known in the strong-coupling limit. In the following, we shortly review the main results of the algebraic solution.

9.7.2 Itinerant states

Let us consider first the case when no particle is localized. In this case, the model becomes equivalent to the t-V chain apart from a renormalization of the hopping constant ($t \to \sqrt{2}t$). The solution of the t-V chain relies in recognizing that the condition $l = 0$ leads to a conservation of the number of links N_{hp} and N_{hh} so that the tight-binding term only exchanges the position of these links [117]. Interpreting the (hp) links as non-interacting particles hopping

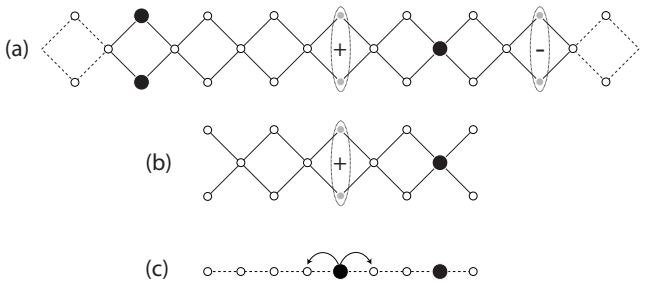

Figure 9.13: (a) State with localized as well as itinerant particles; (b) Open boundary region where the itinerant Fermions in the state given in (a) may move. Note that the open boundary regions terminate always at B and C sites. (c) Corresponding state of the linear lattice.

in a chain where the empty sites are the (hh) links, the solution is attained. Since the total number of (hh) and (hp) links is $\tilde{L} = L - N$, the effective chain is reduced in relation to the real t-V chain. Note that L is the number of sites in Fig. 9.13(c), after the mapping to a 1D chain. The fact that the tight-binding particles occupy two sites of the real t-V chain leads to a twisted boundary condition which is dependent on the momenta of the tight-binding particles and the eigenvalues are given by [117]

$$E(\{\tilde{k}\}, P) = -2\sqrt{2}t \sum_{i=1}^{N} \cos\left(\tilde{k}_i - \frac{P}{\tilde{L}} - \frac{\phi}{L}\right) \tag{9.26}$$

with $\tilde{k} = \tilde{n} \cdot 2\pi/\tilde{L}$, and $P = n \cdot 2\pi/L$, with $\tilde{n} = 0, \ldots, \tilde{L} - 1$ and $n = 0, \ldots, L - 1$. The set of pseudo-momenta $\{\tilde{k}\}$ and P must satisfy the following condition

$$P\frac{L}{\tilde{L}} = \sum_{i=1}^{N} \tilde{k} \pmod{2\pi}. \tag{9.27}$$

The mapping of this solution of the t-V chain (with even number of sites) into the AB_2 chain without localized particles is direct, with odd sites corresponding to A sites and even sites to sites B and C (which will be unoccupied or in a bonding configuration).

9.7.3 Localized states

Let us consider now a state where localized particles are present. Then one has one or more open boundary regions that terminate always in B and C sites as shown in Fig. 9.13, i.e., the number of sites is odd (the B_i and C_i sites count as one site). The solution for the itinerant particles in one open-boundary region is rather simple [118]. Again, a mapping to a system of free Fermions in a reduced linear lattice is possible in a similar way, thinking of (hp) links hopping in a background of (hh) links, but it is simpler to state as in [118, 119] that the positions $\tilde{i}$ of particles in the reduced chain are given by the relation $\tilde{i} = i - N_i$ where i is the

position of the particle in the t-V 1D lattice and N_i is the total number of particles between the initial site and site i. The number of sites of the reduced chain is $\tilde{L} = L - N + 1$. The energy contribution of these itinerant Fermions is $E_a = -2\sqrt{2}t \sum_{i=1}^{N_a} \cos(k_i)$ with $k = \pi n/(N_{\text{red}} + 1)$ and $n = 1, 2, \ldots, N_{\text{red}}$. Note that in the same state, and according to the distribution of the localized Fermions, several confined regions may be present.

9.7.4 Ground state

The contribution of localized Fermions to the energy of a given state is zero, but that does not necessarily imply that the ground state will always correspond to the minimum number of localized Fermions. As an example, let us consider $\rho = 1/3$. An eigenstate for this filling is $\prod_{m\ \text{odd}}^{2N_c-1} A_m^\dagger |0\rangle$. The respective energy is zero since this state corresponds to having the itinerant fermion band completely filled, so that the positive kinetic energies balance the negative kinetic energies. In this case, it is possible to construct lower energy eigenstates with localized fermion pairs (created by the operator $B_i^\dagger C_i^\dagger$), which allow room for the itinerant Fermions to move and therefore lower the total kinetic energy.

This competition between itinerant and localized states will in fact start to occur at lower filling, $\rho = 2/9$, since at this filling, the reduced chain is half-filled and therefore positive kinetic energy states will start to be filled when adding additional itinerant particles. In order to lower the energy, one wants to keep the number of itinerant Fermions just below half-filling and to have the maximum possible length for the reduced lattices where the itinerant particles move. Noting that a localized pair forbids the presence of particles in the two neighboring A sites, one concludes in order to maximize the number of sites available for the itinerant Fermions these localized pairs should gather in a single cluster.

The ground-state energy is obtained from Eq. (9.26) for fillings less than 2/9. If N is odd, all single-particle states with pseudo-momentum $\tilde{k}$ between $\pm 2\pi/\tilde{L} \cdot (N-1)/2$ are occupied and $\sum \tilde{k} = 0$. Therefore,

$$E_{\text{GS}}^{\text{odd}} = -2\sqrt{2}t \frac{\sin\left(\frac{\pi N}{2N_c - N}\right)}{\sin\left(\frac{\pi}{2N_c - N}\right)} \cos\left(\frac{\phi}{2N_c}\right) \tag{9.28}$$

If N is even, all states with $\tilde{k}$ between $-2\pi/\tilde{L} \cdot (N-2)/2$ and $2\pi/\tilde{L} \cdot N/2$ or between $-2\pi/\tilde{L} \cdot N/2$ and $2\pi/\tilde{L} \cdot (N-2)/2$ are occupied and $\sum \tilde{k} = \pm\pi/\tilde{L} \cdot N/L$. So,

$$E_{\text{GS}}^{\text{even}} = -2\sqrt{2}t \frac{\sin\left(\frac{\pi N}{2N_c - N}\right)}{\sin\left(\frac{\pi}{2N_c - N}\right)} \cos\left(\frac{\pi - \phi}{2N_c}\right) \tag{9.29}$$

In the thermodynamic limit, the difference in the last two expressions becomes irrelevant and

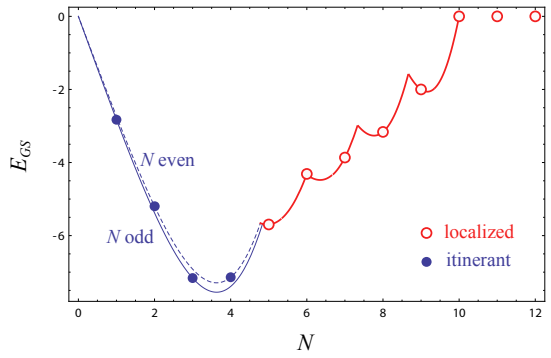

(a)

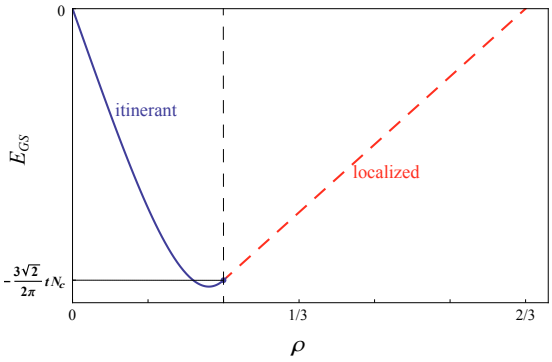

(b)

Figure 9.14: (a) Ground state energy as a function of filling of the AB_2 chain in the strong-coupling limit $V = \infty$ and with $N_c = 6$. The curves are the analytical results given by Eqs. (9.28), (9.29) and (9.31) and the dots are the energy levels obtained by numerical diagonalization of the $V = \infty$ AB_2 chain. (b) Ground state energy in the thermodynamic limit as a function of filling in the strong-coupling limit $V = \infty$. The transition between a metallic and an insulating ground state occurs exactly at $\rho = 2/9$ and the minimum energy is obtained when $\rho \approx 0.2$.

one can write

$$\frac{E_{\rm GS}^{\rm itin}}{N_c} = -\frac{2\sqrt{2}t}{\pi}(2-3\rho)\sin\left(\frac{\pi\rho}{\frac{2}{3}-\rho}\right) \tag{9.30}$$

For filling larger than 2/9, it is energetically favorable to have localized pairs of Fermions in consecutive unit cells so that only one region exists for itinerant Fermions, with $2N_c - 2N_{BC} - 1$ sites and the respective reduced lattice will have $\tilde{L} = 2N_c - N$ sites. The number of itinerant Fermions is $N_{\rm itin} = N - 2N_{BC}$. The number of BC localized pairs is such that the band for the itinerant Fermions in the respective reduced lattice is as near as possible from half-filling, so that $N_{BC} = {\rm Int}(3N/4 - N_c/2) + 1$ or $N_{BC} = {\rm Int}(3N/4 - N_c/2)$. In the thermodynamic limit, one can write $N_{\rm itin} = N_c - N/2$ and one has a closely packed localized cluster with length equal to $N_{BC}/2 = 3N/8 - N_c/4$.

The ground-state energy in this case is

$$E_{\mathrm{GS}}^{\mathrm{loc}} = -2\sqrt{2}t \cos\left[\frac{\pi}{2}\cdot\frac{N_{\mathrm{itin}}+1}{2N_c-N+1}\right]\frac{\sin\left[\frac{\pi}{2}\cdot\frac{N_{\mathrm{itin}}}{2N_c-N+1}\right]}{\sin\left[\frac{\pi}{2}\cdot\frac{1}{2N_c-N+1}\right]} \tag{9.31}$$

which for a large AB_2 chain simplifies to

$$\frac{E_{\mathrm{GS}}^{\mathrm{loc}}}{N_c} = -\frac{2\sqrt{2}t}{\pi}(2-3\rho), \tag{9.32}$$

where $\rho = N/3N_c$. Since this ground state is localized, no magnetic flux dependence is present. Note that for $N = 2N_c - 1$ the reduced lattice has only one site and the only possible energy is zero. Also for $N = 2N_c$, one has a Wigner crystal like state with $N_{BC} = N_c$ and zero energy. Also for $N = 2N_c - 2$, the reduced lattice has two sites and and the number of itinerant Fermions is zero or two, therefore the only possible energy is zero.

The density in the compact cluster of BC localized pairs present in the ground state for $\rho \geq 2/9$ has density equal to $2/3$, while the region available for the movement of the itinerant Fermions has constant density $N_{\mathrm{itin}}/(\frac{9}{2}N_{\mathrm{itin}}-1)$ which for large N_{itin} is approximately constant and equal to $2/9$. So as one increases the filling in the AB_2 chain, one is reducing the length of a phase with lower density and increasing the size of the higher density phase.

Phase separation has been observed in other 1D and 2D Hamiltonians [120, 121]. In the 1D t-J model, phase separation occurs for $J/t = 2.5 - 3.5$, with the system divided into an electron-rich region and a hole-rich region [121]. An open-boundary Heisenberg model rules the dynamic of spin degrees of freedom of the electron-rich phase. Particularly relevant to our study of the AB_2 chain is the phase separation of the anisotropic Heisenberg model or XXZ model, which can be mapped onto the 1D t-V model. In this case, phase separation corresponds to the appearance of the ferromagnetic phase in the XXZ model [122]. The anisotropy constant of the XXZ model, $\Delta = J_{\parallel}/J_{\perp}$ under the Jordan-Wigner transformation becomes $\Delta = -V/2|t|$ and for both models the phase separation occurs for $\Delta \geq 1$ [122, 123], that is, phase separation occurs for attractive nearest-neighbor interaction (ferromagnetic interaction). In the t-V AB_2 chain, we have shown that phase separation occurs for strong *repulsive* interaction. Note that a spinless fermion in the t-V model corresponds to an up-spin in XXZ model while a hole corresponds to a down-spin, and therefore the lower and higher density phases of the AB_2 chain correspond to different magnetization regions of the *antiferromagnetic* XXZ AB_2 model.

9.7.5 Luttinger liquid description

One of the most interesting points concerning the t-V AB_2 chain is the following: is the t-V AB_2 chain a Luttinger liquid? That is, can the low energy excitations of this model

be described as bosonic charge density fluctuations governed by the harmonic Hamiltonian [122, 124, 125]

$$H_{LL} = v_S \sum_q |q| b_q^\dagger b_q + \frac{\pi}{2L}[v_N (N - N_o)^2 + v_J J^2]? \tag{9.33}$$

In the LL Hamiltonian, N, J, L, v_N, v_J, and v_S are, respectively, the particle number, current number, system length, particle velocity, current velocity, and sound-wave velocity. One is easily tempted to calculate these Luttinger liquid parameters from the previous strong coupling results, obtaining for large L and for $\rho < 2/9$,

$$v_N = \frac{1}{\pi} \frac{\partial^2 (E_T/L)}{\partial (N/L)^2} = \frac{36\sqrt{2}t}{(2-3\rho)^3} \sin\left(\frac{3\pi\rho}{2-3\rho}\right) \tag{9.34}$$

$$v_J = \pi \frac{\partial^2 (E_T/L)}{\partial (\phi/L)^2} = \frac{9(2-3\rho)t}{2\sqrt{2}} \sin\left(\frac{3\pi\rho}{2-3\rho}\right) \tag{9.35}$$

$$v_S = \sqrt{v_N v_J} = \frac{9\sqrt{2}t}{2-3\rho} \sin\left(\frac{3\pi\rho}{2-3\rho}\right) \tag{9.36}$$

where $\rho = \frac{N}{L}$ and v_N, v_J, and v_S are respectively the particle, current, and sound velocities. Note that $N/L = 3\rho/2$ since $L = 2N_c$. These are results similar to those obtained for the strong coupling t-V ring [118, 119] in the thermodynamic limit. The Luttinger liquid parameter

$$\frac{1}{K_\rho} = e^{-2\psi} = v_N/v_S = \frac{4}{(2-3\rho)^2} \tag{9.37}$$

determines the anomalous correlation exponents and is filling dependent reflecting the reduction of the effective size of the chain with filling.

For filling larger than 2/9, the ground state has the localized pairs of Fermions in a compact cluster so that only one region exists for itinerant Fermions, with $2N_c - 2N_{BC} - 1$ sites and the respective reduced lattice will have $\tilde{L} = 2N_c - N$ sites. One again is tempted to describe the low energy behavior of this system of itinerant Fermions in this open-boundary lattice using as above a LL description. With open boundaries, one loses the translation invariance but it has been shown by several authors that an open-boundary bosonization can still be carried out [126–130]. Many of these studies of LLs with open boundaries were motivated by the fact that the introduction of a single local impurity in a Luttinger liquid breaks the 1D system in two parts, at least in what concerns the low energy properties of the system [131, 132]. There is a clear analogy between the role of these local impurities and the localized Fermions in the AB_2 chain. For very large L, one expects the solution of the system to become less dependent on the boundary conditions and therefore the LL velocities are the same as those of an equivalent system with periodic boundary conditions *at the same filling and with the same lattice size* (since the LL exponents are dependent on filling). But we have seen that the filling in this open-boundary region is constant and equal to 2/9, and since the

LL velocities depend only on filling, one obtains

$$v_N = \frac{243t}{8\sqrt{2}}, \quad v_J = 3\sqrt{2}t, \quad v_S = \frac{27t}{2\sqrt{2}}, \quad e^{-2\psi} = \frac{9}{4}. \tag{9.38}$$

Note that this ground state is N_c degenerate due to the translation invariance of the phase separation boundaries.

The missing point in the previous analysis is that the LL Hamiltonian does not describe the excitations of ground state that involve the creation of an additional localized anti-bonding fermion or an additional localized BC pair of Fermions. However this is only important if these excitations are low energy states. In a qualitative picture, the strong coupling AB_2 chain can be described as if there were a flat band at zero energy with N_c two-level sites. This is similar to the noninteracting case, but now the number of localized Fermions in such flat band is twice as many. For $\rho \ll 2/9$, the creation of a localized anti-bonding fermion or a localized BC pair of Fermions implies an excitation energy of the order of t and for energies and temperatures much less than this value, the LL description is valid. As the filling approaches $2/9$, these excitations become low lying (since the Fermi level goes to zero) and must clearly be taken into account in the low temperature description of the system. In this situation, even at very low temperature, the low energy AB_2 set of eigenvalues becomes a complex mix of the sets of eigenvalues of LLs with different sizes, fillings, boundary conditions, and LL velocities. Despite these remarks, one should note that the strong coupling LL velocities do indeed characterize the correlations that do not involve the creation of additional anti-bonding states or additional localized BC pairs of Fermions. For example, a two-point ground-state correlation involving only A sites such as the Green's function restricted to A sites.

For $\rho > 2/9$, the compressibility

$$\frac{1}{\kappa} = \frac{1}{L}\frac{\partial^2 E_0(\rho)}{\partial \rho^2} \tag{9.39}$$

is infinite due to the linear behavior of the ground-state energy. This is the expected behavior of a phase separated ground state and is known to occur also in the t-J model as well as in the XXZ model [123]. In these models, the compressibility diverges as $(\Delta_c - \Delta)^{-1}$ as one approaches the phase separation critical value (which is $\Delta_c = 1$ in the case of the attractive t-V chain) by increasing the interaction constant [123]. The compressibility can also be calculated from the LL relation

$$\kappa = \frac{2K_\rho}{\pi v_s}. \tag{9.40}$$

In the XXZ model (or in the equivalent attractive t-V model), the compressibility diverges since the sound velocity vanishes and the Luttinger parameter K_ρ diverges as $\Delta \to \Delta_c$. From the last two relations, one easily concludes that as the filling in the AB_2 approaches $2/9$, the compressibility does not diverge, since the curvature of the plot of $E(\rho)$ in Fig. 9.14(b) does

not vanish just below $\rho = 2/9$ or equivalently, neither the sound velocity vanishes nor the Luttinger parameter K_ρ diverges as $\rho \to 2/9$.

For $\rho < 2/9$, the current velocity gives the charge stiffness at zero temperature [133, 134]

$$D_c = \frac{1}{2}\frac{\partial^2(E_T/L)}{\partial(\phi/L)^2} \mid_{\phi_c=0} . \tag{9.41}$$

For $\rho \geq 2/9$, the charge stiffness is zero reflecting the open boundaries condition for the itinerant Fermions and consequent zero dependence of the energy levels on magnetic flux. This discontinuity of the Drude weight at the phase boundary is known to occur in other 1D models with phase separation [123]. In this case, the current velocity should correspond to a very small frequency peak in the optical conductivity since it is known that the open-boundary condition shifts the spectral weight associated to the Drude peak to a finite frequency peak [135].

9.8 Implications for the extended Hubbard AB_2 model

In this section, we discuss the relevance of the results obtained for the t-V AB_2 model for the spinful extended Hubbard model in the AB_2 geometry and in the strong-coupling limit $U \gg t$ and $U \gg V$.

First, let us recall the known facts about the strong coupling Hubbard model in a ring [136–140] and in a 1D chain with open-boundary conditions [141]. The extended Hubbard Hamiltonian for a ring with L sites is given by

$$\begin{aligned} H &= -t\sum_i (c^\dagger_{i\sigma}c_{i+1\sigma} + c^\dagger_{i+1\sigma}c_{i\sigma}) \\ &\quad +U\sum_i n_{i\uparrow}n_{i\downarrow} + V\sum_i n_i n_{i+1}, \end{aligned} \tag{9.42}$$

where the creation (annihilation) of an electron at site i with spin σ is denoted by $c^\dagger_{i\sigma}$ ($c_{i\sigma}$) with $n_{i\sigma}$ being the number operator $n_{i\sigma} = c^\dagger_{i\sigma}c_{i\sigma}$ and $n_i = n_{i\uparrow} + n_{i\downarrow}$. When $t = 0$, all states with the same number N_d of doubly occupied sites and the same number $\sum_{\sigma\sigma'} N_{\sigma\sigma'}$ of nearest-neighbor occupied sites are degenerate, where $N_{\sigma\sigma'}$ is the total number of nearest-neighbor pairs with spin configuration $\sigma\sigma'$. The eigenvalues of the extended Hubbard model in the atomic limit are given by $E(N_d, \{N_{\sigma\sigma'}\}) = N_d \cdot U + \sum_{\sigma\sigma'} N_{\sigma\sigma'} \cdot V$. Here we will only address the low energy subspace of the strong-coupling limit where $N_d = 0$ to make this discussion simpler.

If we consider the Hubbard ring with $t \ll U$, but $V = 0$, one has the so-called Harris-Lange model [142] and the model eigenfunctions can be written as a tensorial product of the eigenfunctions of a tight-binding model of independent spinless Fermions in the ring (where the spinless Fermions are the electrons deprived of spin) and the eigenfunctions of

an Heisenberg model (with exchange constant $J = t^2/U$) for the spins of the electrons in a reduced chain [136–140]. The spinless Fermions ring is threaded by a fictitious magnetic flux $\phi = q_s$ generated by the spin configurations in the reduced Heisenberg chain (where q_s is the total spin momentum) and the eigenvalues to order t are given by

$$E(k_1, \ldots, k_{N_h+N_d}) = 2t \sum_{i=1}^{N_h} \cos\left(k_i - \frac{q_s}{L}\right), \tag{9.43}$$

where $k_i = (2\pi/L)n_i$, $n_i = 0, \ldots, L-1$ are the momenta of the holes in the spinless ring.

The nearest-neighbor interaction is obviously independent of spin of the electrons that occupy nearest-neighbor sites and it is easily introduced in the previous picture so that for $U \gg t$ and $U \gg V$, the $N_d = 0$ spectrum of the Hubbard model to the order of t is that of interacting spinless Fermions in a ring threaded by a fictitious magnetic flux $\phi = q_s$ (since the nearest-neighbor repulsion between electrons leads to an nearest-neighbor repulsion between spinless Fermions), that is, the extended Hubbard model in a ring in the limit $U \to \infty$ has the energy dispersion of the spinless t-V chain. The only effect of spin in this limit is the generation of a fictitious flux and the increase of degeneracy.

If now we consider the strong coupling Hubbard chain with open-boundary conditions, the solution is even simpler. As stated in Ref. [141], for $\rho < 1$, the physics of the model is the same as that of a spinless tight-binding model. In fact, the electrons hop along the chain but the spin configuration of the electrons remains always the same and becomes irrelevant for the determination of the eigenvalues of the model. The different spin configurations only contribute to the degeneracy of the energy levels. The same reasoning as above can be followed and one concludes that the extended Hubbard chain with open-boundary conditions and in the limit $U \gg t$ and $U \gg V$ has the same energy spectrum as the t-V chain with open-boundary conditions.

Let us now consider the extended Hubbard model in the AB_2 geometry,

$$\begin{aligned} H &= H_0 + V \sum_j \left(n_j^A + n_{j+1}^A\right)\left(n_j^B + n_j^C\right) \\ &+ U \sum_i (n_{i\uparrow}^A n_{i\downarrow}^A + n_{i\uparrow}^B n_{i\downarrow}^B + n_{i\uparrow}^C n_{i\downarrow}^C), \end{aligned} \tag{9.44}$$

where

$$\begin{aligned} H_0 = -t \sum_\sigma \sum_{j=1}^{N_c} & \Big[\mathrm{e}^{\mathrm{i}\phi_o/2N_c}(A_{j\sigma}^\dagger B_{j\sigma} + B_{j\sigma}^\dagger A_{j+1\sigma}) \\ &+ \mathrm{e}^{-\mathrm{i}\phi_i/2N_c}(C_{j\sigma}^\dagger A_{j\sigma} + A_{j+1\sigma}^\dagger C_{j\sigma})\Big] + \mathrm{H.c.} \end{aligned} \tag{9.45}$$

We consider the limit $U \to \infty$ where no doubly occupied sites are possible.

In the AB_2 geometry, we can not state as we did for the Hubbard chain that for $V = 0$ the model can be mapped into a system of spinless Fermions in a tight-binding AB_2 chain threaded by fictitious magnetic flux generated by the spin configuration momentum. The reason is that in the case of the Hubbard chain, only hoppings at the boundaries generate a different spin configuration and all the different configurations generated can be obtained from one of them applying a circular permutation operator [136–140]. However, in the AB_2 geometry, besides the circular permutation of the spin configuration due the hoppings at the boundaries, additional spin mixing can also be generated by electrons hopping along one plaquette (which circularly permute a subset of two or three spins). However, this additional exchange process requires the existence of an occupied nearest-neighbor pair of sites in that plaquette as an intermediate step. Therefore, as V is increased, this exchange process is inhibited.

Let us therefore address the extended Hubbard AB_2 model in the limit $t \ll V \ll U$. In this case the additional plaquette exchange does not occur. We show below that the low energy spectrum of this model, that is, the set of eigenvalues corresponding to eigenstates with no doubly occupied sites and no occupied nearest-neighbor pair of sites will be the same as that of the t-V AB_2 model in the limit $t \ll V$, but with enlarged degeneracy just like for the extended Hubbard ring in the strong-coupling limit. The picture behind this result will be a mix of the pictures presented for the Hubbard ring and for the Hubbard chain with open-boundary conditions.

First we show that the itinerant and localized states of the extended Hubbard AB_2 model remain the same as those of the strong coupling t-V AB_2 model in what concerns the charge distribution, but now one has a considerable larger set of states due the spin degrees of freedom. We adopt the same basis as that of the previous section, but now spin must be considered, that is, the bonding and anti-bonding states have a spin degree of freedom. In the previous section we have shown that two type of localized Fermions could occur: i) one-particle localized states corresponding to a single particle in one plaquette in a standing wave state, which obviously remains localized if the particle has spin; ii) two-particle BC localized states induced by the large nearest-neighbor repulsion. The spinless localized pair maps into four localized BC pairs with different spin configurations which again remain localized due to the large nearest-neighbor repulsion. Concerning the itinerant particles, the Hamiltonian does not alter the spin of the bonding states as the particles hop along the AB_2 chain.

Therefore, we can construct the eigenstates of the extended Hubbard AB_2 model in the limit case $t \ll V \ll U$ in an equivalent way to that followed in the previous section. If no localized particles are present, the extended Hubbard AB_2 model in the limit case $t \ll V \ll U$ can be mapped into the extended Hubbard ring in the same limit and the energy levels are

given by

$$E(\{\tilde{k}\},P) = -2\sqrt{2}t\sum_{i=1}^{N}\cos\left(\tilde{k}_i - \frac{P}{\tilde{L}} - \frac{q_s+\phi}{L}\right) \tag{9.46}$$

where $\tilde{k}_i$ and $\tilde{L}$ have the same definition as for the t-V ring in the strong-coupling limit, q_s has the same definition as for the Hubbard chain and ϕ is a external magnetic flux (but keeping a zero flux in each plaquette). In the thermodynamic limit, the effect of the fictitious and external fluxes becomes irrelevant.

If localized particles are present, they create open boundary regions where itinerant electrons (in bonding states when at sites B and C) will move according to the extended Hubbard AB_2 model in the strong-coupling limit. Each of these open boundary systems has a fixed number of particles and can be mapped as above into the extended Hubbard chain in the same limit, but now with open-boundary conditions. In this case, as stated before, the spin configuration is irrelevant and contributes only to the degeneracy of the energy levels which are exactly those described in the previous section for the spinless t-V AB_2 model with open-boundary conditions. Since the energy levels in the thermodynamic limit are the same as those of the t-V AB_2 model in the strong-coupling limit, phase separation will also occur in the extended Hubbard AB_2 ring and precisely at the same filling. This exact correspondence required the strong-coupling limit and was obtained only for the low energy subspace. Higher energy subspaces involve the presence of occupied nearest-neighbor pairs of sites or of double occupancies, but a similar approach can in principle be followed again with a mapping to higher energy subspaces of the extended Hubbard chain.

For intermediate values of the nearest-neighbor interaction V, the mapping is no longer exact, but qualitatively the features described for the t-V AB_2 chain should be expected in the extended Hubbard AB_2 chain (with $U \gg t$ and $U \gg V$). For example we expect a similar evolution for the ground-state energy with decreasing V, but with different evolution of filling. Note that the ground-state energy for non-interacting electrons (with spin) as a function of filling has the same form of Fig. 9.5, but the spin degeneracy of the single-particle eigenvalues implies that the filling values as well as the ground-state energy must be multiplied by two. This is equivalent to distributing spinless particles among two independent AB_2 chains.

9.9 Conclusions

As mentioned in the introduction, the 1D anisotropic Heisenberg model (the XXZ model) can be mapped using the Jordan-Wigner transformation into the 1D spinless t-V model (with an additional "chemical potential" term, which can also be interpreted as an on-site energy). The ground state filling of the t-V model is related to the ground state magnetization of the XXZ model, which can be controlled by the application of an external magnetic field to the XXZ model. This external field does not change the eigenstates of the XXZ model, but creates

an additional chemical potential term in the t-V model which allows to control the filling of the ground state. A ferromagnetic Heisenberg interaction means that the spinless Fermions attract each other while an antiferromagnetic exchange implies a repulsive interaction between nearest-neighbor spinless Fermions. A Jordan-Wigner transformation is also possible in quasi-1D or 2D lattices (see Ref. [143] for a review), and in particular, the XXZ AB_2 model in the strongly anisotropic limit can be mapped into the strong coupling t-V AB_2 model with additional phase factors which are nonlocal (and therefore usually treated in a mean-field approach) [143]. We have not gone into the details of the transformation of the XXZ AB_2 model into the t-V AB_2 model (which would require the determination of the phase factors and the introduction of the on-site energy terms), but some conclusions can be drawn on general arguments. First, one-magnon localized states in the strongly anisotropic XXZ AB_n model corresponding to standing waves in a t-V AB_n array will exist since no additional phase factors appear when only one spinless fermion is present (only one spin flip). Also, states with several spin flips corresponding to localized magnons in different plaquettes are also eigenstates since the XX term of the XXZ model gives a zero contribution in the regions between the localized magnons (since all spins are aligned). So the one-particle localized states in the t-V AB_2 model correspond to localized and independent magnons created in a ferromagnetic background, which have been observed in frustrated magnetic systems under high magnetic fields but below the saturation field [97]. Second, independently of the phase factors, the two-particle localized BC particles will remain the same because the nearest-neighbor interaction obtained in the Jordan-Wigner transformation retains the same form as in the 1D case, and since these two particles are completely localized, the phase factors are irrelevant. Furthermore, these localized particles create open boundary regions for the itinerant Fermions independently of the phase factors. So, we expect a similar behavior of the XXZ AB_2 model in the strongly anisotropic limit to the one here described for the strong coupling t-V AB_2 model. Such two-particle localized states in the strong coupling t-V AB_2 model correspond to localized pairs of magnons in the the XXZ AB_2 model in the strongly anisotropic limit.

The results presented in Sec. IV for single-particle states in AB_n lattices may also be relevant to Josephson junction arrays (with the same geometry) both in the quantum limit and in the high capacitance (classical) limit. It is known that a Josephson junction AB_2 chain with half a flux quantum per plaquette exhibits a highly degenerate classical ground state reflecting the completely flat energy bands of the AB_2 tight-binding model for this value of flux [113]. The tunneling of Cooper pairs between the different superconducting islands in an AB_2 geometry can also be described using a bosonic tight-binding AB_2 model. Furthermore, in the high-capacitance limit, the charging energy due to the electrostatic interaction within each (large) superconducting island can be neglected and the Hamiltonian becomes a classical XY model, $H = -J\sum_{\langle ij\rangle}\cos(\phi_i - \phi_j - A_{ij})$, where ϕ_i is the superconducting phase of the

island i, J is the Josephson coupling and A_{ij} is the phase shift due to the presence of an external magnetic field, obtained from the integral of the vector potential along the path from i to j. This Hamiltonian can be mapped into a one-particle tight-binding model with the same geometry and under the same magnetic flux [144]. In most geometries, the minimum energy phase configuration of the Josephson junction array will be obtained from the state of minimum energy of the tight-binding model (if this state is homogeneous). In the most general case, the Hamiltonian can be interpreted as the mean energy of a phase vector and the stable phase configuration of the Josephson junctions array is obtained minimizing this energy and this minimization may imply mixing tight-binding states of different bands.

Let us now compare the exact results of the strong coupling AB_2 chain with the mean-field results. Comparing Figs. 9.11 and 9.14 (b), one concludes that the mean-field results overestimate the interaction energy contribution for $\rho < 2/3$. Basically, within the mean-field approach the low energy band increases its energy with increasing V, missing the fact that itinerant states are possible, which avoids the positive energy contribution of the nearest-neighbor interaction as found in the strong-coupling limit. The mean-field results are qualitatively correct in what concerns the energy interval for the ground-state energy for $\rho < 2/3$. In Fig. 9.11, one can see that the ground-state energy remains negative even for large V in the density range $0 < \rho < 2/3$. The minimum of the ground-state energy as a function of filling shifts continuously to lower filling in contrast with the $V = \infty$ result where such minimum occurs at $\rho \approx 0.2$. Also the large slope for $\rho > 2/3$ agrees with the fact that for such fillings nearest-neighbor pairs are present and such states have infinite energy when $V = \infty$.

To conclude, in this chapter the spinless AB_2 chain with nearest-neighbor Coulomb interactions has been studied for any filling and taking into account magnetic flux. In the case of independent Fermions, a simple construction of the localized states that generate the flat bands both in the presence and absence of flux has been found and generalized for 1D or 2D arrays of quantum rings. The V/t versus filling phase diagram of the AB_2 chain was obtained using a mean-field approach. The dependence on filling of the mean-field ground-state energy agrees qualitatively with the exact ground-state energy for infinite V. The ground-state energy for infinite nearest-neighbor repulsion has a quantum critical point at filling 2/9 where a metal-insulator transition occurs. This transition reflects the phase separation between a high density phase ($\rho = 2/3$) and a low-density phase ($\rho = 2/9$) that occurs at fillings larger than 2/9. Such phase separation occurs because the infinite nearest-neighbor repulsion leads to the appearance of two-particle localized states (besides the one-particle localized states due to the topology of the AB_2 chain). These localized states create open boundary regions for itinerant carriers and in order for these itinerant Fermions to have only negative kinetic energy, phase separation becomes favorable. At low filling, the low energy properties of t-V AB_2 chain can be described by the spinless Luttinger Hamiltonian, but for filling near or larger than 2/9, the AB_2 set of eigenvalues becomes a complex mix of the sets of eigenvalues

of LLs with different fillings, boundary conditions, and LL velocities. If the itinerant Fermions have spin, but a very strong on-site repulsion is present (that is, in the case of the extended Hubbard model in the strong-coupling limit $U \gg V \gg t$), the energy-dispersion relation to the order of the hopping integral remains the same as that of the spinless AB_2 model in the presence of a flux and phase separation occurs at the same filling.

Chapter 10

Conductance through a non interacting AB_2 chain

In this chapter we consider the electronic conductance through a non-interacting AB_2 chain in a two terminal scenario. We consider different placements of the conducting leads and different values of the threading flux. We show the presence of a zero frequency dipped peak in the conductance which is a fingerprint of the localized states of the AB_2 chain and which should be present in systems exhibiting identical geometry. The work here contained has been published in [145].

10.1 Introduction

The conductance through molecular devices, nanowires and other nano systems has been extensively studied both theoretically and experimentally. Nano transport phenomena such as Coulomb blockade [146], conductance quantization [147], resonant tunneling [148], quantum interference, Aharonov-Bohm oscillations in the conductance [69, 149] are now well understood.

The conductance fingerprints of localized states, however, induced by the topology of a nanocluster [71–76, 78, 82, 87, 89–100] has never been addressed as far as we know. Do these localized states inhibit the electronic transport through the cluster or is the conductance indifferent to their existence? The answer is rather complex and unexpected. Here we show that in the case of the AB_2 ring (which is an example of the family of itinerant geometrically frustrated electronic systems [71–76, 78, 82, 87, 89–100]), these localized states act as zero frequency conductance absorbers for zero magnetic flux, but surprisingly generate a dipped zero frequency conductance peak when magnetic flux is applied. Similar features should be observed in the conductance through other elements of the family of the itinerant geometrically frustrated electronic systems of the Lieb lattice kind, that is, systems which display localized

states with nodes in their probability density as was addressed in 9.

10.2 Exact diagonalization of the AB_2 chain and localized states

In order to address the phenomena of coherent transport through an AB_2 ring, we consider a two terminal set up of one-dimensional (1D) tight-binding leads coupled to the AB_2 ring, as depicted in Fig. 12.1. Our results are easily generalized to the case of 3D leads as long as only one site of each lead contacts the cluster. We shall often focus on the case where the number of cells of the AB_2 ring, N_c, is equal to 4, and assume that each plaquette is threaded by an identical magnetic flux, ϕ.

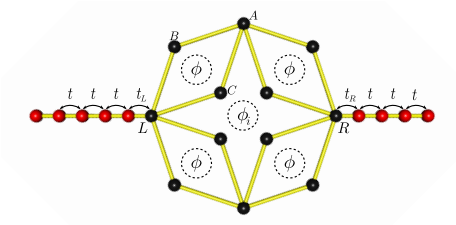

Figure 10.1: The AB_2 ring is connected at sites L and R, to semi-infinite tight binding leads via a hopping amplitude t'. Except where otherwise stated, the hopping amplitude of the leads is taken to be the same to that of the star, t. Here it is shown the situation for $N_c = 4$, a particular case we will study in detail. The magnetic fluxes threading the plaquettes and the inner ring are respectively ϕ and ϕ_i.

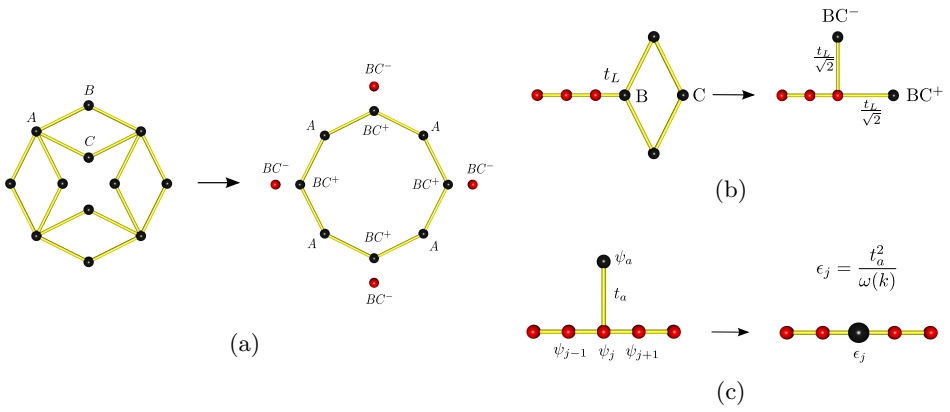

Figure 10.2: (a) In the absence of magnetic flux, rewriting the Hamiltonian in the basis of antibonding BC^-, bonding BC^+ and A states, one obtains a tight-binding ring of sites A and bonding BC sites (with hopping constant $\sqrt{2}t$) and a ring of decoupled anti-bonding BC states. (b) The hopping term from the left lead to a B site of the AB_2 ring, in the basis of antibonding BC, bonding BC and A states, becomes $t_L/\sqrt{2}$. (c) For a incident particle with energy $\omega = -2t\cos(k)$, an extra transverse hopping t_a to a dangling site effectively modifies the on-site energy of site j to $\epsilon_j = t_a^2/\omega$.

The Hamiltonian of the full system is given by

$$H_{\text{ring}} + H_{\text{leads}} + H_{\text{LR}}, \tag{10.1}$$

where H_{leads} is the Hamiltonian of the isolated leads, assumed to be semi-infinite,

$$\begin{aligned} H_{\text{leads}} = -t \sum_{j=1}^{\infty} \sum_{\sigma=\uparrow,\downarrow} & |a_{j,\sigma}\rangle \langle a_{j+1,\sigma}| \\ & + |a_{-j-1,\sigma}\rangle \langle a_{-j,\sigma}| + \text{H.c.}, \end{aligned} \tag{10.2}$$

where $|a_j, \sigma\rangle$ is a lead Wannier state at site j and with spin σ. $j \in (-\infty, -1]$ correspond to left lead states while $j \in [1, \infty)$ correspond to right lead states. H_{star} is the Hamiltonian for an AB_2 chain with N_c unit cells (cf. Eq. 9.3),

$$\begin{aligned} H_{\text{ring}} = -t \sum_{j=1}^{N_c} \sum_{\sigma=\uparrow,\downarrow} & \mathrm{e}^{\mathrm{i}\phi_o/2N_c} (|A_{j,\sigma}\rangle \langle B_{j,\sigma}| + |B_{j,\sigma}\rangle \langle A_{j+1,\sigma}|) \\ & + \mathrm{e}^{-\mathrm{i}\phi_i/2N_c} (|C_{j,\sigma}\rangle \langle A_{j,\sigma}| + |A_{j+1,\sigma}\rangle \langle C_{j,\sigma}|) + \text{H.c.}, \end{aligned} \tag{10.3}$$

where $|A_{j,\sigma}\rangle$, $|B_{j,\sigma}\rangle$, $|C_{j,\sigma}\rangle$ correspond to states on A, B and C sites, respectively, of the jth cell/plaquette, with spin σ. Here we have chosen a gauge such that the Peierls phases are equally distributed in the inner ring and in the outer ring. In Fig. 10.1, an AB_2 ring is shown with a magnetic flux ϕ threading each plaquette and a magnetic flux ϕ_i threading the inner ring. The magnetic flux enclosed by the outer ring is $\phi_o = \phi_i + 4N_c\phi/4$ and we introduce an auxiliary flux ϕ' such that $\phi_o = \phi' + 2N_c\phi/4$, $\phi_i = \phi' - 2N_c\phi/4$. The inner sites in the AB_2 ring of Fig. 10.1 are denoted as C sites and the outer sites as B sites. Spinal sites are denoted as A sites. The hybridization between the AB_2 ring and the leads is given by

$$H_{\text{LR}} = -\sum_{\sigma=\uparrow,\downarrow} t_L |a_{-1,\sigma}\rangle \langle X_{L,\sigma}| + t_R |a_{1,\sigma}\rangle \langle X_{R,\sigma}| + \text{H.c.}, \tag{10.4}$$

where $t_{L,R}$ are the hopping amplitudes coupling the leads and the star and X stands for an A, B or C site depending on where the left (L) and right (R) contacts are. Since we don't consider spin-spin interactions, each spin channel is independent and we disregard spin in the rest of our discussion, without any loss of generality.

As seen in chapter 9, without interactions the tight-binding AB_2 chain has a flat band even in the presence of magnetic flux (Fig. 10.3 displays the dispersion relation of the nearest neighbor AB_2 chain for several values of the plaquette threading flux). The eigenvalues for

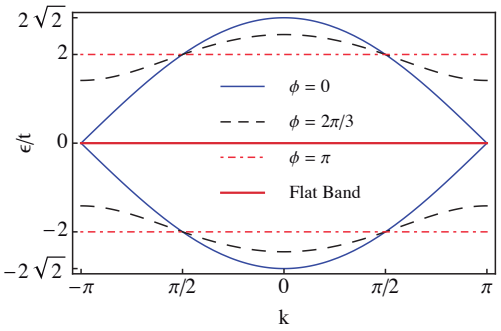

Figure 10.3: Dispersion relation of the AB_2 ring for $\phi' = 0$ and several values of ϕ. Note that a gap opens between the localized band and the itinerant bands when there is a finite flux. Also, for $\phi = \pi$ all bands are flat, and therefore, all states are localized.

an arbitrary value of flux were found to be

$$\begin{aligned} \epsilon_{\text{flat}} &= 0, \\ \epsilon_{\pm} &= \pm 2t\sqrt{1+\cos(\phi/2)\cos(\phi'/N_c+k)}, \end{aligned} \tag{10.5}$$

where k is the momentum.

Localized states associated with the flat band can be written in the most compact form as standing waves in one (in the absence of magnetic flux) or two consecutive plaquettes (in the presence of magnetic flux). In the particular case of zero flux, localized states are simply the anti-bonding combination of the B and C states, $\text{BC}_j^- = (|B_j\rangle - |C_j\rangle)/\sqrt{2}$, and itinerant states in the AB_2 ring are linear combinations of A and bonding BC^+ states, $\text{BC}_j^+ = (|B_j\rangle + |C_j\rangle)/\sqrt{2}$. Rewriting the Hamiltonian in the basis of antibonding BC^-, bonding BC^+ and A states, one obtains a tight-binding ring of sites A and bonding BC sites (with hopping constant $\sqrt{2}t$) and a ring of decoupled anti-bonding BC states, as shown in Fig. 10.2a.

The number of localized states is equal to the number of rhombi and in the presence of flux, if written in the most compact form (each localized state taking place in two consecutive plaquettes) they form a non-orthogonal set of states. Orthogonalization of these set of states implies that the extension of the localized states ranges from two consecutive plaquettes to the complete ring (see Fig. 10.4e), except for $\phi = 0$ and for $\phi = \pi$ (in this case, the orthogonal localized states occupy only two consecutive plaquettes). This will imply a clear difference in the conductance when compared with the zero flux case. Note that a gap opens between the localized band and the itinerant bands when flux is present.

Assuming $\phi' = 0$ to simplify, the non-orthogonal localized states are of the form $(|B_j\rangle - e^{i\frac{\phi}{2}}|C_j\rangle) + (e^{i\frac{\phi}{2}}|B_{j+1}\rangle - |C_{j+1}\rangle)$ where the sites have been numbered clockwise in the AB_2 ring, that is, j indexes the plaquettes in the AB_2 ring.

Since the localized states have nodes at the A sites, we can write these localized states indicating only the one-particle state amplitudes at the pairs of B and C sites of the AB_2 ring,

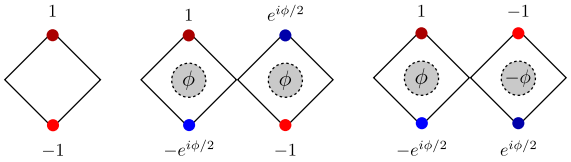

(a) $\phi = 0$ (b) Ferromagnetic (c) Antiferromagnetic

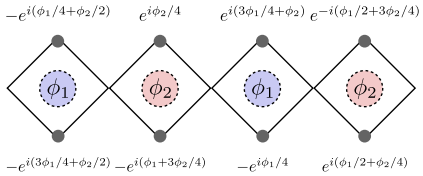

(d) Two cells periodic flux

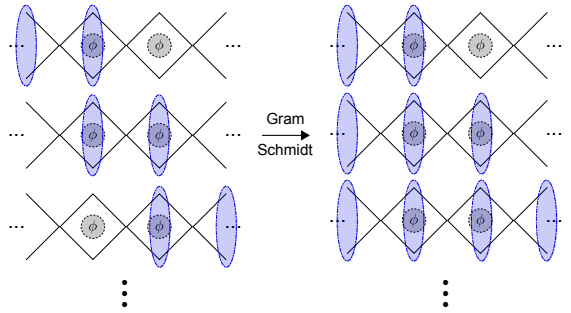

(e) Localized states orthonormalization

Figure 10.4: (a), (b) and (c): Localized states for AB_2 chains without flux and threaded by ferromagnetic or anti-ferromagnetic flux, respectively. For simplicity the states are not normalized and we only draw the cells where the wavefunction is non-zero. (d) Localized states for $N = 2$, where N is the periodicity in the flux (in terms of number of cells). (e) Our non-orthonormal basis of localized states, occupying two cells, can be transformed into an orthonormal basis where they occupy, $1, 2, \ldots N_c$ cells, via the Gram-Schmidt procedure.

that is, we can write the localized state as a list with $2N_c$ entries $(b_1, c_1 \ldots, b_n, c_n)$, where b_j and c_j are, respectively, the value of the wavefunction on site B_j and C_j. Then our localized states are,

$$|\psi_j\rangle = \frac{1}{\sqrt{4}}\left(0, \ldots, 0, \underbrace{1}_{b_j}, \underbrace{-\mathrm{e}^{-\mathrm{i}\phi/2}}_{c_j}, \underbrace{\mathrm{e}^{-\mathrm{i}\phi/2}}_{b_{j+1}}, \underbrace{-1}_{c_{j+1}}, 0, \ldots, 0\right) \tag{10.6}$$

Note that for $\phi = 0$, we have for $|\psi_j\rangle$ that $b_j = b_{j+1}$ and $c_j = c_{j+1}$, and and for $\phi = \pi$, $\langle\psi_j|\psi_{j+1}\rangle = 0$. There are many possible ways of constructing an orthogonal basis for the subspace of localized states. Our results for the conductance are obviously independent of

this choice. We simply use the Gram-Schmidt orthogonalization, starting with the basis

$$\begin{aligned}
|\psi_1\rangle &= \frac{1}{\sqrt{4}}\left(1, -\mathrm{e}^{-\mathrm{i}\phi/2}, \mathrm{e}^{-\mathrm{i}\phi/2}, -1, 0, \ldots, 0\right), \\
|\psi_2\rangle &= \frac{1}{\sqrt{4}}\left(0, 1, -\mathrm{e}^{-\mathrm{i}\phi/2}, \mathrm{e}^{-\mathrm{i}\phi/2}, -1, 0, \ldots, 0\right), \\
&\vdots \\
|\psi_{N_c}\rangle &= \frac{1}{\sqrt{4}}\left(\mathrm{e}^{-\mathrm{i}\phi/2}, -1, 0, \ldots, 0, 1, -\mathrm{e}^{-\mathrm{i}\phi/2}\right).
\end{aligned} \tag{10.7}$$

For such a basis we have

$$\langle\psi_i|\psi_j\rangle = \delta_{i,j} + \frac{\cos\phi/2}{2}\left(\delta_{i-1,j} + \delta_{i+1,j}\right). \tag{10.8}$$

For simplicity, let us define the support of a wavefunction, denoted by supp, to be those site where the wavefunction is non-zero. Then we have $\operatorname{supp}|\psi_j\rangle = \{B_j, C_j, B_{j+1}, C_{j+1}\}$.

Let $\{|\phi_j\rangle\}_{j=1}^{N_c}$ denote the orthonormalized basis after the G-S procedure, defined by the recursive expression,

$$\begin{aligned}
\left|\phi_j'\right\rangle &= |\psi_j\rangle - \sum_{i=1}^{j-1}\langle\phi_i|\psi_j\rangle\,|\phi_i\rangle\,, \\
|\phi_j\rangle &= \frac{\left|\phi_j'\right\rangle}{\sqrt{\left\langle\phi_j'|\phi_j'\right\rangle}}.
\end{aligned} \tag{10.9}$$

We focus on $\phi \neq \pi$ (for in that case, the basis is already orthonormalized) and begin by making $|\phi_1\rangle = |\psi_1\rangle$, which implies $\operatorname{supp}\phi_1 = \{B_1, C_1, B_2, C_2\}$. Then $|\phi_2'\rangle = |\psi_2\rangle - \langle\phi_1|\psi_2\rangle\,|\phi_1\rangle$. In this case, since $\langle\phi_1|\psi_2\rangle \neq 0$, $\operatorname{supp}\phi_2 = \{B_1, C_1, B_2, C_2, B_3, C_3\}$. We then have $|\phi_3'\rangle = |\psi_3\rangle - \langle\phi_2|\psi_3\rangle\,|\phi_2\rangle - \langle\phi_1|\psi_3\rangle\,|\phi_1\rangle$. Note that $|\phi_1\rangle$ and $|\psi_3\rangle$ have disjoint support, hence $\langle\phi_1|\psi_3\rangle = 0$. Also, $\langle\phi_2|\psi_3\rangle \propto \langle\psi_2|\psi_3\rangle \neq 0$. Since $\operatorname{supp}|\psi_3\rangle = \{B_3, C_3, B_4, C_4\}$ and $\operatorname{supp}\phi_2 = \{B_1, C_1, \ldots B_3, C_3\}$, and since, there is no destructive interference on sites B_3 and C_3 (it is a simple exercise to show this), $\operatorname{supp}\phi_3 = \{B_1, C_1, \ldots B_4, C_4\}$. Continuing the above procedure we finally arrive at

$$\operatorname{supp}|\phi_j\rangle = \{B_1, C_1, \ldots B_{j+1}, C_{j+1}\}. \tag{10.10}$$

and therefore the extension of the orthogonalized localized states (constructed this way) ranges between two consecutive plaquettes and the full AB_2 ring. This is illustrated schematically in Fig. 10.4e.

However, as we have already mentioned, one has two exceptions:

i) for $\phi = 0$, the states $|\alpha_j\rangle = (0, \cdots, 0, \underbrace{1}_{b_j}, \underbrace{-1}_{c_j}, 0, \cdots, 0)$ already constitute an orthogonal set of localized states for $\phi = 0$ as stated in the previous paragraph;

ii) for $\phi = \pi$, $\langle\psi_j|\psi_{j+1}\rangle = 0$ are orthogonal and in this case the range of the localized states in their most compact form is just two plaquettes.

There are many possible ways of constructing an orthogonal basis for the subspace of localized states. It must be stressed that our results for the conductance are obviously independent of this choice.

Using the construction for localized states presented in chapter 9, it is easy to extend some of the results here presented to geometries other than the AB_2 geometry. To make this more concrete let us give some examples. Let us start by considering an AB_2 chain with an arbitrary number of cells. Assume, for now, that the flux through each cell has the same value, a situation we call *ferromagnetic* (shown in Fig. 10.4b). Then, localized states occupying only two cells can be found for an arbitrary value of flux (albeit non orthogonal, except when $\phi = \pi$), while for zero flux one can find localized states occupying only one cell as shown in Fig. 10.4a. Now consider a situation where the magnetic flux through each plaquette is symmetric to the one threading its neighboring cells, a situation we call *anti-ferromagnetic*. Then a similar state to the situation above can be found as is shown in Fig. 10.4c. For this particular case, using this construction, we can find localized states that occupy two cells. However, these states form an orthonormal basis only for $\phi = \pi$ and for the ferromagnetic flux situation, as can be readily seen calculating the overlap between neighboring states. Let $|\psi_j\rangle$ be the state localized in the jth and $(j+1)$th cells. For the ferromagnetic situation the overlap between neighboring states is $\langle\psi_{j+1}|\psi_j\rangle = \dfrac{\cos(\phi/2)}{2}$ while for the anti-ferromagnetic situation one has $\langle\psi_{j+1}|\psi_j\rangle = -\dfrac{1}{2}$. Note that this flux threading each cell is not necessarily an external flux, since it may be generated by the spin of an atom/molecule, embedded into the chain as is the case of some coper oxide systems, namely CuO_4 chains [150, 151].

If the flux through each plaquette is distinct, but repeats every N cells (Fig. 10.4d shows the situation for $N = 2$), one can also use the same construction to find localized states. In this case however, one must consider $2N$ adjacent cells instead of 2, as before, and we will find a localized states that extend through $2N$ cells. As before, these are not necessarily orthonormal, but can be made so by using Gram-Schmidt orthonormalization. In the extreme case, where there is no periodicity, translational invariance is obviously broken and our procedure will give us an extended state instead. A particular case of the $N = 2$ situation, with $\phi_1 = 2\phi_2$ has been studied in [152].

10.3 Conductance through a non interacting AB_2 ring

In this section we discuss the conductance through the AB_2 ring. We will begin by addressing the case without magnetic flux. Since we do not consider two-particle interactions in this chapter, the transmission probability $|t(\omega)|^2$ for an incident particle with momentum k and energy $\omega = -2\cos(k)$ can be calculated using quantum scattering theory [153], and is given by the following expression [154],

$$\begin{aligned} |t(\omega)|^2 &= 4t_L^2 t_R^2 \sin^2 k |\langle R|[\epsilon_k \hat{I}_s - H_s \\ &+ e^{ik}\left(t_L^2|L\rangle\langle L| + t_R^2|R\rangle\langle R|\right)]^{-1}|L\rangle|^2, \end{aligned} \tag{10.11}$$

where the inverse is to be found within the subspace of the cluster sites (in our case, the AB_2 ring) positions and $\hat{I}_s$ is the identity operator in that subspace. This equation includes the effect of the coupling of the ring to the leads as modifications of the on-site energies of sites L and R. If the conductance is normalized by the conductance of an ideal one dimensional system, $G_0 = e^2/\pi\hbar$, then the conductance is given by the transmission probability at the chemical potential. [155]. In what follows, we will always deal with this normalized conductance, i.e., transmission probability.

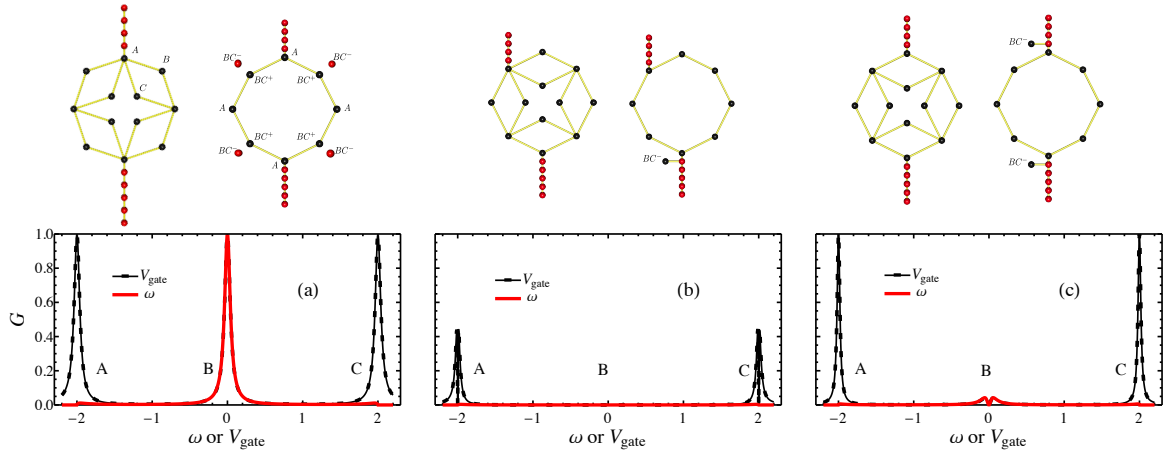

Figure 10.5: Normalized conductance through the AB_2 ring as function of the energy of the incident electron (or chemical potential of the leads) and as function of V_{gate} for several positions of the leads. The positions of the leads are shown on the top figures. We show beside the AB_2 circuits, figures of equivalent systems which have exactly the same conductance profiles. Parameters: $t_L = t_R = 0.3t$.

In Fig. 10.5, we show several profiles of the conductance through the AB_2 ring with four unit cells as function of the energy of the incident electron (or chemical potential of the leads) or as function of a potential V_{gate} applied to the AB_2 ring. These profiles correspond to certain positions of the leads which are shown at the top of the Fig. 10.5a, Fig. 10.5b and

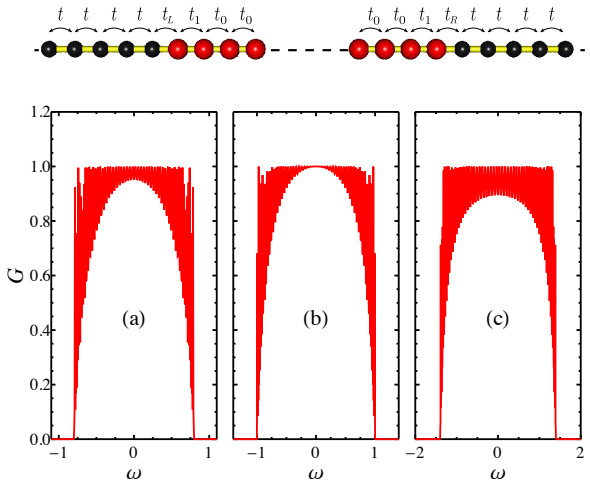

Figure 10.6: The conductance through the AB_2 ring (or a linear ring) in the absence of flux and with opposite contacts at sites A is the same as for a linear chain (shown in the top figure, where the larger, red sites replace the AB_2 ring). In (b), one has the conductance for the particular case of $2t_1/\sqrt{2} = 2t_0 = t_L = t_R = 1$ in units of t and one sees that the central cluster (corresponding to the AB_2 ring) becomes transparent to an incoming particle for energies around zero, i.e., the bond with hopping constant t_1 acts as a monoatomic anti-reflection coating between the regions with hoppings t and t_0. Deviations of the hopping constants from the previous values introduce oscillations in the conductance for energies around zero, as shown in (a) and (c) (where $t_1/\sqrt{2} = t_0 = .4$ and $t_1/\sqrt{2} = t_0 = .7$, respectively).

Fig. 10.5c. In these figures we also include diagrams of equivalent systems, that is, systems that exhibit exactly the same conductance profiles as the AB_2 ring.

In the case of Fig. 10.5a, the leads are connected to sites A, therefore the anti-bonding BC "sites" can be ignored since they are completely decoupled from the leads. The remaining "ring" of sites A and bonding BC sites form a tight binding ring. Therefore, if the contacts are sites A, the conductance is exactly the same as that of the equivalent tight-binding ring (with hopping constant $\sqrt{2}t$). [156] For small coupling between the leads and the AB_2 ring, the conductance has peaks when the chemical potential coincides with any of the system eigenvalues of the AB_2 ring, due to resonant tunnelling. These peaks have the Breit-Wigner shape. In Fig. 10.5a, three peaks A, B and C are observed in $G(V_{\text{gate}})$ in a potential interval corresponding to the bandwidth of the leads (the chemical potential of the leads is equal to zero). The same peaks should also be observed in the $G(\omega)$-plot of Fig. 10.5a where $V_{\text{gate}} = 0$ and the chemical potential (or equivalently the energy ω of the incident particle) is varied from the bottom of the leads band to the top. However peaks A and B are absent because they correspond to the bottom and top energies of the leads bands and the particle velocity is zero for these energies.

If the left contact is a site B or C (let us assume it is a site B) and the right contact is a site A, as in the case of Fig. 10.5(b), the conductance profile is the same as that of a tight-binding

ring but with the $\omega = 0$ peak absent. This absence reflects the fact that the hopping term from the left lead to a B site of the AB_2 ring, in the basis of antibonding BC^-, bonding BC^+ and A states, becomes a hopping between the left lead and a bonding state bonding BC^+ and a hopping to a localized state BC^-, both with a smaller hopping constant $t_L/\sqrt{2}$. Since this localized state is decoupled from all other states of the ring, it only leads to a reflected wave back into the left lead. For $\omega = 0$, this reflected wave interferes destructively with the incident wave and one can say the localized state BC^- acts as a conductance absorber for frequencies close to $\omega = 0$ (in close analogy with $\lambda/4$ sound absorbers). The absence of the $\omega = 0$ peak can also be explained in the following way. The hopping to the BC^- "site" is a "dangling bond". If one considers a linear chain with a dangling site as shown in Fig. 10.2c (with hopping constant t_a to the dangling site), then the equation for the wavefunction amplitude ψ_a at the dangling site of a particle with energy $\omega = -2t\cos(k)$ is $\omega\psi_a = -t_a\psi_j$. Substituting ψ_a in the the equation for the wavefunction amplitude at site j, ψ_j, one has $\omega\psi_j = -t\psi_{j-1} - t\psi_{j+1} + (t_a^2/\omega)\psi_j$, therefore the dangling site effectively modifies the on-site energy of site j to $\epsilon_j(\omega) = (t_a^2/\omega)$. When $\omega = 0$, the on-site energy becomes infinite and one has zero conductance at $\omega = 0$. The peaks A and C in Fig. 10.5(b) have a reduced amplitude compared to those in Fig. 10.5a due to the difference in paths in the upper and lower arms of the ring.

If both the left and right contacts are sites B (or C) as shown in Fig. 10.5(c), an analogous reasoning applies and the system is equivalent to a linear ring connected to leads but with two dangling sites, one at the end of each lead. Again, localized states act as a filter of the $\omega = 0$ peak.

In the case of Fig. 10.5a, the remaining "ring" of sites A and bonding BC sites can be mapped onto a linear chain since the leads are coupled to opposite A sites. In this case, the leads define an axis of symmetry of the diamond ring and the anti-bonding combinations of an A (or bonding BC) site with the one obtained by reflection in this axis of symmetry are decoupled from the contact sites, or equivalently, the tight-binding hoppings from the contact sites generate a bonding combination of the nearest-neighbor bonding BC "sites" and this bonding combination couples only to the bonding combination of A sites. So, for the purpose of calculating the conductance across the AB_2 ring, it is enough to consider the linear sequence of these bonding states (see the top diagram in Fig. 10.6 where the cluster of larger, red sites replaces the AB_2 ring). In Fig. 10.6b, one has the conductance for the particular case of $2t_1/\sqrt{2} = 2t_0 = t_L = t_R = 1$ in units of t, that is, we have three regions with different hopping constants t, t_0 and t, separated by single hoppings of constant t_1. The central cluster (and therefore also the AB_2 ring) becomes transparent to the incoming particle for energies around zero. Deviations of the hopping constants from the previous values introduce oscillations in the conductance for energies around zero, as shown in Fig. 10.6a and Fig. 10.6c, where the dome of minima of the conductance oscillations is below one.

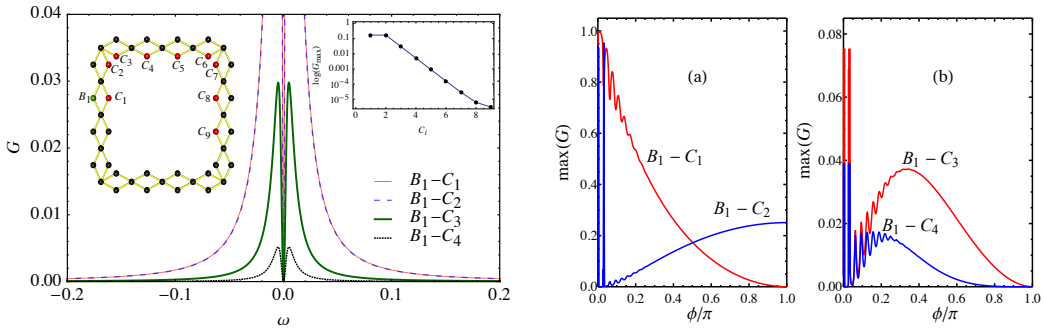

Figure 10.7: (a) Conductance as a function of the frequency of the incident particle for an AB_2 ring of 16 plaquettes, $\phi = \pi/2$, and several positions of the leads contacts. For this flux value, only localized states contribute significantly to the $\omega = 0$ conductance peak. (b) Maximum of the conductance as a function of the flux for 16 plaquettes. For leads contacts at B_1-C_2 and $\phi = \pi$, the peak value of the conductance is 0.25, since in this case the AB_2 is mapped onto the cluster of Fig. 10.9a with equal values of the hopping constants. For leads at B_1-C_1 it is zero for $\phi = \pi$, since the left and right leads couple to orthogonal states which do not overlap. The oscillations at low flux reflect dependence of the inner magnetic flux ϕ_i and disappear as the gap between the itinerant bands and the localized states grows with increasing flux.

This result can be explained with an analogy with a quarter wavelength anti-reflection coating [157], that is, the bond with hopping constant t_1 acts as a monoatomic anti-reflection coating between the regions with hopping constant t and t_0. A anti-reflection coating generates an additional reflected wave which is out of phase with the first reflected wave and therefore partially cancels the reflection. If the refraction index of the coating is the geometric mean of the refraction indices of the materials to the left and right of the coating, $n_c = \sqrt{n_{\text{left}} n_{\text{right}}}$, the transmittance becomes one when the wavelength of incident wave, λ, is such that the thickness of the coating is an odd multiple of the $\lambda/4$. This can be translated into our problem in the following way. The relation $n_c = \sqrt{n_{\text{left}} n_{\text{right}}}$ can be written as $n_c/n_{\text{right}} = \sqrt{n_{\text{left}}/n_{\text{right}}}$ which is equivalent to a relation between velocities $v_{\text{right}}/v_c = \sqrt{v_{\text{right}}/v_{\text{left}}}$. The ratio between velocities in our system for energies close to zero is approximately the ratio of hopping constants and the previous relation becomes $t_1/t_0 = \sqrt{t/t_0}$. So perfect transmission occurs when $2t_1/\sqrt{2} = 2t_0 = t$ (as in the case of Fig. 10.6b) and when $\lambda/4$ is equal to one interatomic distance (which we have assumed to be one), that is, for $k = \pi/2$ or equivalently, energy $\omega = -2t\cos(k)$ equal to zero.

When magnetic flux is present, a gap opens between the flat band and the itinerant bands of the AB_2 ring. The conductance peaks corresponding to energies of itinerant states follow the behavior of the conductance peaks of a linear ring and we do not address them here (see [156]). The behavior of the conductance for energies close to $\omega = 0$ (which is determined

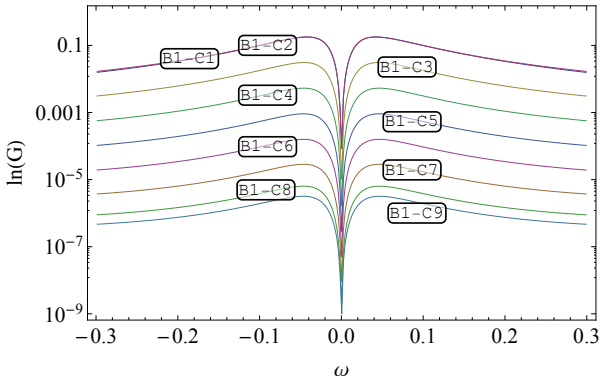

Figure 10.8: Logarithm of the conductance for 16 cells and $\phi = \pi/2$ around $\omega = 0$, for all the inequivalent lead positions such that one of the leads is on a B site and the other on a C site.

only by the localized states of the AB_2 ring when flux is finite and the coupling between the leads and the cluster is small) is rather unusual. A zero frequency dipped conductance peak is observed despite the fact that the energies of the itinerant states of the ring are far from this zero frequency peak. This is shown in Fig. 10.7a for the case of an AB_2 ring with 16 unit cells and for $\phi = \pi/2$. This dipped peak only occurs if the contact sites are sites B or C (otherwise the peak is absent) and shows distinct behavior as function of the positions of the contact sites and as function of the magnetic flux. As shown in the inset of Fig. 10.7a, the peak maximum decays quasi-exponentially as a function of the contact sites distance, except for the first two distances, where the conductance peak maximum remains the same. Such behavior is also visible in Fig. 10.8 where the logarithm of the conductance for small frequencies of an incident particle is plotted for several inequivalent positions of the leads. The dependence with flux of the maximum of the conductance peak shows rather peculiar behavior depending on the position of the contacts. In Fig. 10.7b, we show the maximum of the $\omega = 0$ conductance peak as a function of the flux threading each plaquette, ϕ, for several choices of contacts positions. When the contacts are the sites B_1 and C_1 (see the labeling of the sites in the inset of Fig. 10.7a), the maximum starts at one, oscillates for small ϕ and goes smoothly to zero as ϕ approaches π. The oscillations near $\phi = 0$ reflect the contribution to the conductance of the itinerant states which oscillates as a consequence of the Aharonov-Bohm effect due to the varying flux threading the inner region of the AB_2 ring (an uniform field was applied to the AB_2 cluster). These oscillations disappear as ϕ grows due to the larger gap between the itinerant bands and the $\omega = 0$ energy. Note that localized states do not "feel" this inner flux, that is, their energy is independent of this field and therefore do not contribute to an Aharonov-Bohm effect. When the contacts are the sites B_1 and C_2, contrasting behavior occurs and the maximum approaches zero when ϕ is small and tends to 0.25 when ϕ goes to π. For larger distance between contacts, the graphs of the maximum of the $\omega = 0$ conductance peak exhibit dome-like profiles (see Fig. 10.7b(b)), with the peak

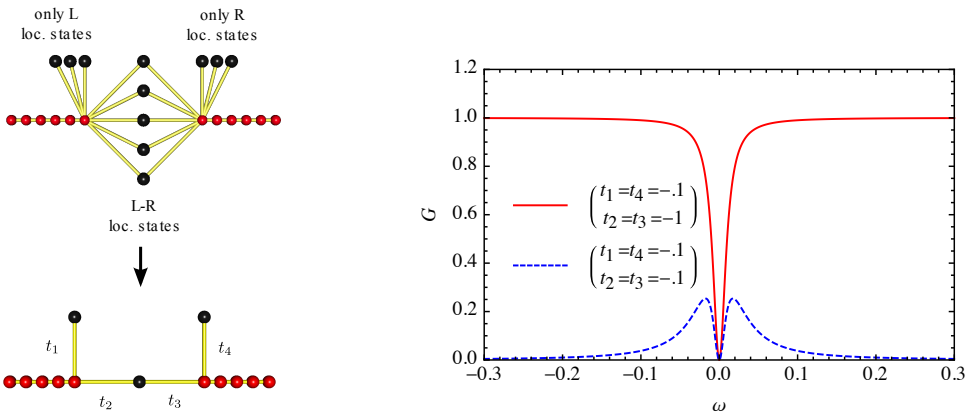

(a) (b)

Figure 10.9: (a) The coupling of the leads to the localized states of the AB_2 ring in the presence of flux is described by the top diagram where one has dangling sites connected to the left (right) lead representing the localized states which have finite wavefunction amplitude at site L (R), but zero amplitude at site R (L). The system on top is equivalent to the bottom system consisting of only one L, R and LR localized states. (b) Whenever all hopping constants in the bottom system are equal, the maximum of the conductance is 0.25 regardless of their value. Due to the dangling sites, the conductance always goes to zero at zero frequency.

maximum growing from near zero when ϕ is small, reaching a maximum value and decreasing to zero when ϕ approaches π.

These results can explained recalling our previous discussion of the extension of localized states when the flux is finite. Since this extension ranges from two unit cells to the full ring, and ignoring the itinerant states of the ring which are energetically far from the $\omega = 0$ energy region, the conductance is only finite if one has localized states that extend from the left contact to the right contact in the AB_2 ring. More precisely, we can divide the localized states in the following way: states I that extend from the left contact to the right contact, that is, that have finite wavefunction amplitudes at the sites L and R of the AB_2 ring; states II that have finite wavefunction amplitudes at the site L but not at the site R of the AB_2 ring; states III that have finite wavefunction amplitudes at the site R but not at the site L of the AB_2 ring; states IV that have zero wavefunction amplitudes at both the sites L and R of the AB_2 ring. Note that the choice of basis for the subspace of localized states influences the number of states in each of these groups, but the explanation for the conductance results remains the same. The larger the extension of the localized states, the smaller the wavefunction amplitude at the contact sites, and consequently the smaller the effective hopping between the extremities of the leads and the localized state. So, our system is equivalent to that displayed in the top diagram of Fig. 10.9a. The hopping constants between the leads (smaller, red spheres) and the localized states (larger, black spheres) are in general different but all these hopping can be simplified and the system can be reduced to that shown in the bottom diagram of Fig. 10.9a.

In fact, several dangling sites (states II) contribute to the on-site energy of the site at the end of the left lead and t_1 is the hopping constant that generates an on-site energy equal to the sum of the on-site energies generated by the dangling sites at the left lead. The same goes for t_4. The effect of the localized states of the type I can also be reproduced with a single site but with different hopping constants to the left lead and to the right lead. In Fig. 10.9b, we show the conductance through this simplified system. If $t_2 = t_4 = t$, without the dangling sites, we would have perfect transmittance for any energy of the incident electron. The effect of the dangling sites is the creation of the dip at $\omega = 0$ as one can see in Fig. 10.9b (red solid curve). If t_2 and t_3 are rather smaller than t and no dangling site is present ($t_1 = t_4 = 0$), a peak appears at $\omega = 0$ of width proportional to t_2 (assuming $t_2 = t_3$). The effect of the dangling sites in this case is again the introduction of the dip at the center of this peak. If the width of the dip becomes larger than that of the peak, the dipped peak maximum becomes small.

One can now explain the behavior displayed in Fig. 10.7b. One should recall that the non-orthogonal localized states are of the form

$(|B_j\rangle - e^{i\frac{\phi}{2}}|C_j\rangle) + (e^{i\frac{\phi}{2}}|B_{j+1}\rangle - |C_{j+1}\rangle)$. The overlap between consecutive localized states is equal to $\cos(\phi/2)/2$, so it is zero whenever $\phi = \pi$, and $1/2$ when $\phi = 0$ (the latter value implies that shorter and orthogonal localized states can be found of the form $\mathrm{BC}_j^- = 1/\sqrt{2}(|B_j\rangle - |C_j\rangle)$). We consider only the mean evolution of the conductance, that is, the dependence of the conductance remaining if the oscillations due to the Aharonov-Bohm effect are removed. This behavior consists of the following: if the contacts are the sites B_1 and C_1, the maximum of the conductance is one for zero flux and with increasing magnetic flux, the conductance decreases and becomes zero for flux equal to π. Note that for $\phi = \pi$, the localized states, $|\psi_j\rangle = 1/2\,|(B_j\rangle - i\,|C_j\rangle) + (i\,|B_{j+1}\rangle - |C_{j+1}\rangle$, are orthogonal and both leads couple to only two of these states, $|\psi_1\rangle$ and $|\psi_{N_c}\rangle$. That is, we have only two states of type I and all other localized states are of type IV. The transport through the cluster is given by the transfer terms to these localized states of the form $\langle\psi_1|\,H\,|0\rangle$ which collected (omitting the hopping terms in the leads) give rise to $(-t_L/2)\,|0\rangle\,[\langle\psi_1| + i\,\langle\psi_{N_c}|] + (-t_R/2)\,|N+1\rangle\,[-i\,\langle\psi_1| - \langle\psi_{N_c}|] + \mathrm{H.c.}$ But $[\langle\psi_1| + i\,\langle\psi_{N_c}|]$ and $[-i\,\langle\psi_1| - \langle\psi_{N_c}|]$ are orthogonal bras, therefore the left and right leads are effectively decoupled and the transmittance is zero. A similar reasoning can be followed when ϕ approaches zero. In this case the leads couple to only one localized state, $\mathrm{BC}_1^- = 1/\sqrt{2}(|B_1\rangle - |C_1\rangle)$, that is, we have one state of type I and no dangling sites, so the transmittance approaches one.

If the contacts are the sites B_1 and C_2, the maximum of the conductance is zero for zero flux and, with increasing magnetic flux, the conductance increases and becomes $1/4$ for flux equal to π. The fact that the conductance maximum approaches zero as ϕ goes to zero is common to all other contact possibilities with exception of the previous one and reflects a similar argument, that is, the left lead couples to only one localized state, $\mathrm{BC}_1^- = 1/\sqrt{2}(|B_1\rangle - |C_1\rangle)$

and the right lead couples only to one other localized state which is orthogonal to the former, and consequently the transmittance is zero. The fact the conductance goes to 1/4 when the flux goes to π can also be justified as before, collecting the transfer integrals and one has $(-t_L/2)\,|0\rangle\,[\langle\psi_1| + i\,\langle\psi_{N_c}|] + (-t_R/2)\,|N+1\rangle\,[-\langle\psi_1| - i\,\langle\psi_2|] + \text{H.c.}$, and this corresponds to the bottom diagram displayed in Fig. 10.9b with $t_1 = it_L/2$, $t_4 = -it_L/2$, $t_2 = t_L/2$, and $t_3 = t_R/2$. Since we considered $t_L = t_R$, all these hopping constants are equal in absolute value and therefore the conductance is equal to 1/4 in agreement with what is shown in Fig. 10.9b. Note that the phase terms are irrelevant at the dangling sites.

If one of the contacts is the site B_1 and the other is a C_j site with $j \neq N_c, 1, 2$, the maximum of the conductance goes to zero as the flux goes to zero and with increasing magnetic flux, the conductance increases, reaches a maximum (this maximum becomes smaller as the distance between contacts increases) and goes again to zero when the flux approaches π, reflecting the fact that the orthogonal localized states are all two unit cells long.

10.4 Conclusions

We have shown that localized states in itinerant geometrically frustrated electronic systems generate rather striking behavior in the two terminal electronic conductance. In the absence of magnetic flux, the localized states act as a filter of the zero frequency conductance peak (we suggested an analogy with $\lambda/4$ sound absorbers), if there is a finite hopping probability between the leads contact sites and the localized states. In contrast, when magnetic flux is present, some localized states contribute to the appearance of a zero frequency conductance peak while other localized states act as a conductance absorber, and as a consequence, the conductance exhibits a zero frequency peak with a dip.

We have shown that such different roles of the localized states are due to the fact that the presence of magnetic flux implies that any orthogonal basis of the subspace of localized states is composed of localized states with variable extensions (ranging from two unit cells to the complete ring, in the case of the AB_2 ring). Such peculiar dipped peak fixed at the localized states energy, even when magnetic flux is varied, is a distinct fingerprint of the existence of localized states in itinerant geometrically frustrated electronic systems. Furthermore, depending on the distance between contact sites, different profiles for the maximum of the dipped conductance peak as function of the magnetic flux have been obtained, and this implies that the two terminal conductance can be used as a probe of the localized states spatial dependence.

Chapter 11

Derivation of a conductance formula for an interacting cluster

In this chapter we derive a conductance formula, akin to the Jagla-Balseiro approach [158], for the conductance through interacting clusters. The work here contained has been published in [159].

11.1 Introduction

The signatures of electronic interactions in the conductance through nanosystems has drawn a great deal of attention in the past few years. Many conductance studies have addressed the interaction effects using the method of non-equilibrium Keldysh Green functions. [160,161] In this approach, one assumes non-interacting leads and the non-equilibrium current is obtained as a function of the exact propagators of the interacting cluster (including the contribution of the leads).

When the coupling between the non-interacting leads and the interacting cluster is small, a simpler approach by Jagla and Balseiro [158] which requires only the determination of the Green's functions of the decoupled interacting cluster can be used. This approach maps the scattering through the interacting cluster into a Landauer-type formula which relates the electrical resistance to the one-particle scattering properties of an effective impurity. Note however that this approach does not capture the correlation effects that lead to the Kondo phenomena.

In this chapter, a new method (that reproduces the results in Jagla's and Balseiro's approach) for the two-terminal conductance through interacting clusters is proposed. This method relies in the approximation that despite interacting with other particles in the scattering region, the incident particles remain independent in the leads. This assumption allows us to work in a reduced Hilbert space and the conductance is obtained from the solution of a

system of $M+2$ coupled linear equations (avoiding the need to calculate Green's functions), where M is the number of cluster states with one particle more or less relatively to the ground state of the cluster.

11.2 Notation

Let us begin by fixing our notation. We let $c_i^\dagger |0_{L,R}\rangle$ denote the one-particle Wannier state of the leads corresponding to a particle at site i (with $|0_{L,R}\rangle$ being the vacuum state of the left or right lead) and $|\mathrm{GS}(N)\rangle$ denote the ground state of the cluster with N particles. Whenever we consider the tensorial product of three states, $|\cdot\rangle \otimes |\cdot\rangle \otimes |\cdot\rangle$, the first state is a left lead state, the second one is right lead state and the last one a cluster state.

11.3 Description of our method

We consider a cluster with sites L and R connected to left and right leads respectively. We consider these leads to be described by a one-dimensional tight binding model and to be weakly coupled to our cluster as depicted in Fig. 11.1. The Hamiltonian of the full system is given by

$$H = H_C + H_{\text{leads}} + H_{LR} \tag{11.1}$$

where H_C is the Hamiltonian of the isolated cluster (an AB_2 ring, in the case of Fig. 10.1), H_{leads} is the Hamiltonian of the isolated leads, assumed to be semi-infinite,

$$H_{\text{leads}} = -t \sum_{j=1}^{\infty} (a_j^\dagger a_{j+1} + a_{-j-1}^\dagger a_{-j}) + \text{H.c.}, \tag{11.2}$$

and the hybridization term is

$$H_{LR} = -t_L a_{-1}^\dagger X_L - t_R a_1^\dagger X_R + \text{H.c.} \tag{11.3}$$

where t_L and t_R are the hopping amplitudes coupling the leads and the cluster and $X_L^\dagger$ and $X_R^\dagger$ create an electron on site L and R, respectively, of the cluster. For simplicity, we have assumed spinless Fermions, but our approach can be generalized to the spinful case as well as to a multi-terminal configuration.

Let us discuss first the non-interacting case. In this case, each energy value in the band continuum of the semi-infinite leads is twice degenerate. If $t_L = t_R = 0$, and assuming incoming particles only from one lead, this corresponds to states where an incoming particle is totally reflected in the left lead or in the right lead. When $t_L, t_R \neq 0$, the presence of the cluster leads to a certain mix of these states (again assuming incoming particles only from one lead). In fact, apart from the cluster, this particle wave function with energy in the

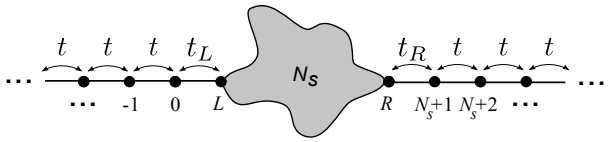

Figure 11.1: An interacting cluster with N_s sites connected to two semi-infinite tight-binding leads at sites L and R ($L, R \in \{1, \dots N_s\}$).

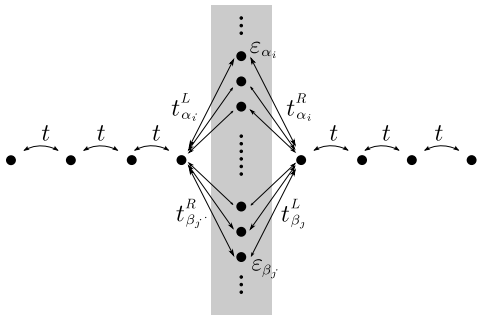

Figure 11.2: Non-interacting cluster obtained in our method. The onsite energies ε_{α_i} (ε_{β_j}) are determined from the one-particle (one-hole) excitations of the interacting cluster and the hopping terms $t^{L/R}_{\alpha_i}$ ($t^{L/R}_{\beta_j}$) are given by the overlap between the interacting N particle ground state and the one-particle (one-hole) excitations of the interacting cluster with $N+1$ ($N-1$) particles. See the next section for the exact expressions of these parameters.

band continuum of the semi-infinite leads remains a combination of incident, reflected and transmitted plane waves. Eigenstates with energies outside the band continuum are localized states in the cluster. Note that this is valid for any value of t_L and t_R if the cluster is finite and the leads are semi-infinite, and this can be understood noting that any finite localized term in the Hamiltonian is an infinitesimal perturbation in the plane wave basis, if the leads are infinite.

When interactions are present in the cluster, we assume that the same occurs, that is, that the presence of the interacting cluster will merely mix the non-interacting one-particle states of the left and right leads with same energy state and that particles in the leads remain independent despite interacting with other particles in the scattering region (this is also implicit in Balseiro's approach) and therefore we can study the transmission of a single incoming particle following a Landauer-like procedure. Furthermore, the cluster state remains the same as in the decoupled situation when the incoming particle is far from the cluster since the number of particles in the cluster is fixed by the chemical potential in the leads (we consider an infinitesimal chemical potential difference between the leads). Therefore the incoming particle will arrive at the contact site, with the cluster at its interacting ground state, and in order for transmission to occur the system must be able to have a transition into the state where a particle is at the right contact site and the cluster is again in the ground state.

There are two possible paths for such transition, one path involving an intermediate state with $N+1$ particles in the cluster and zero particles in the leads and another path involving an intermediate state $N-1$ particles in the cluster and one particle at site 0 and one particle at site N_s+1, where N_s is the number of sites of the cluster (see Fig. 11.1). This reasoning allows us to work in a reduced Hilbert space and the conductance is obtained from the solution of a system of $M+2$ coupled linear equations, where M is the number of cluster states with one extra particle or one less relatively to the ground state of the cluster. So, we reduce the determination of the conductance through an interacting cluster to a one-particle transmission problem through a non-interacting cluster but with hopping constants and local energies determined taking into account the interacting cluster. The analytical details of this approach can be found in the next section. The relation between the transmission probability and the conductance is given by the usual Landauer formula [162].

In Fig. 11.2, we show the non-interacting cluster obtained using our method, with M decoupled sites, with different onsite energy and connected to the leads with renormalized hoppings constants. The onsite energies are determined from the one-particle (one-hole) excitations of the interacting cluster and the hopping terms are given by the overlap between the interacting N particle ground state and the one-particle (one-hole) excitations of the interacting cluster with $N-1$ ($N+1$) particles. Note that these onsite energies and renormalized hoppings do not depend on the energy of the incident particles (as in Jagla's and Balseiro's approach [158], but only on the number of particles in the ground state of the cluster. Note also the exchange of the indices L and R in the case of hoppings to β sites, reflecting the fact that transmission of an incoming particle through these states involves first a particle hop from the cluster to the right lead and second, the hopping of the incoming particle from the left lead to the cluster.

One can ask what happens when the ground state of the interacting cluster is degenerate. Some authors have avoided this problem assuming the existence of a small perturbation that lifts the ground state degeneracy [163]. Depending on this perturbation, some conductance peaks may however disappear from the conductance profile. Here we use a different approach. Since we are addressing the differential conductance at zero temperature, the chemical potential of the cluster is well defined, and the distribution of cluster states at finite temperature will be given by the density operator for the grand canonical ensemble,

$$\rho = \frac{\mathrm{e}^{-\beta(H-\mu)}}{\mathrm{tr}\,\mathrm{e}^{-\beta(H-\mu)}} \tag{11.4}$$

and the average current will, consequently, be given by

$$\langle I \rangle := \mathrm{tr}\,\rho I. \tag{11.5}$$

At zero temperature, the sum will be over only ground states

$$\langle I \rangle = \frac{\sum_i \left\langle E^{(i)}_{\text{G.S.}} \middle| I \middle| E^{(i)}_{\text{G.S.}} \right\rangle}{\sum_i \left\langle E^{(i)}_{\text{G.S.}} | E^{(i)}_{\text{G.S.}} \right\rangle} \tag{11.6}$$

such that the average conductance is simply the arithmetic mean of the conductances for each ground state. This way, all conductance peaks associated with the several ground states will be present in the conductance profile. However, note these peaks may have the height reduced due to the averaging, if their are associated with only one ground state. Even if every ground state generates a certain conductance peak, the peak may have a different width for each cluster ground state (due to different values of the effective hopping to these states, see Fig. 11.2) and the averaging will generate a peculiar non-Lorentzian peak with a sharper maximum.

11.4 Derivation of our conductance formula

As explained before we study the transmission of a single incoming particle through the interacting cluster following a Landauer-like procedure assuming that the particles in the leads remain independent despite interacting with particles in the cluster. Furthermore, the number of particles in the cluster is fixed by the chemical potential in the leads and the electrons in the lower energy states of the cluster do no tunnel to the leads due to the Pauli's exclusion principle. Let us assume that the chemical potential is adjusted so that the ground state of the cluster has exactly N electrons. Considering this simpler problem of a single particle in the leads and N particles in the cluster, one is lead to the conclusion that when the particle in the leads is far from the cluster, the ground state of the cluster is the same as that of the decoupled system. Also, the incoming particle will be in a plane wave state (since these are eigenstates of the leads Hamiltonian and we take the hybridization to be small). So, when the incoming particle is far in the left lead ($j \ll 0$), the particle+cluster eigenfunction for a certain energy $\omega_k + E_{GS(N)}$ will be a combination of a incident plane wave with a reflected plane wave due to the cluster

$$\left(\mathrm{e}^{\mathrm{i}kj} + \psi_r \mathrm{e}^{-\mathrm{i}kj}\right) c_j^\dagger \left|0_L\right\rangle \otimes \left|0_R\right\rangle \otimes \left|\mathrm{GS(N)}\right\rangle, \tag{11.7}$$

while when the particle is far in the right lead ($j \gg N+1$) one has a transmitted component

$$\left|0_L\right\rangle \otimes \psi_t \mathrm{e}^{\mathrm{i}kj} c_j^\dagger \left|0_R\right\rangle \otimes \left|\mathrm{GS(N)}\right\rangle. \tag{11.8}$$

The previous expressions of the eigenstate with energy $\omega_k + E_{GS(N)}$ can be extended to $j \leq 0$ and $j \geq N+1$, respectively, applying the induction method starting from these far away

components [as for the non-interacting case (Appendix 10), cf. Eq. (H.8)] using,

$$\omega_k \psi_j = -\psi_{j+1} - \psi_{j-1}, \tag{11.9}$$

That is, solving successively the previous matrix equation, we can get closer to the cluster, starting from the $j \to -\infty$ and $j \to \infty$ cases.

There are two possibilities for the transmission of the incoming particle through the cluster, one involving an intermediate state with $N+1$ particles in the cluster and zero particles in the leads and another involving an intermediate state $N-1$ particles in the cluster and one particle at site 0 and one particle at site N_s+1. Taking into account the above discussion, we restrick our analysis to the following subspace of states

$$\begin{aligned} c_j^\dagger \left|0_L\right\rangle \otimes \left|0_R\right\rangle \otimes \left|\mathrm{GS}(N)\right\rangle, \quad & j \leq 0 \\ \left|0_L\right\rangle \otimes c_j^\dagger \left|0_R\right\rangle \otimes \left|\mathrm{GS}(N)\right\rangle, \quad & j \geq N+1 \\ \left|0_L\right\rangle \otimes \left|0_R\right\rangle \otimes \left|N+1_{(n)}\right\rangle & \\ c_0^\dagger \left|0_L\right\rangle \otimes c_{N+1}^\dagger \left|0_R\right\rangle \otimes \left|N-1_{(m)}\right\rangle & \end{aligned} \tag{11.10}$$

where $\left|N+1_{(n)}\right\rangle$ represents all cluster states with $N+1$ particles and $\left|N-1_{(m)}\right\rangle$ represents cluster states with $N-1$ particles. The reduced Hilbert space implies that when the particle in the leads is far from the cluster, the ground state of the cluster is the same as that of the decoupled system, which is a valid approximation given that we assumed that the hybridization between the leads and the cluster is small.

Let us now write the full form of the eigenstate with energy $\omega_k + E_{GS,N}$, not forgetting that we are working in a restricted subspace (we are in fact, simply expanding this state in terms of the basis for our subspace, using the knowledge we have of how the eigenstate on the leads must look like)

$$\begin{aligned} \left|\psi_k\right\rangle = \sum_{j\leq 0} \left(e^{\mathrm{i}kj} + \psi_r \mathrm{e}^{-\mathrm{i}jk}\right) c_j^\dagger \left|0_L\right\rangle \otimes \left|0_R\right\rangle \otimes \left|\mathrm{GS(N)}\right\rangle + \sum_{j\geq N+1} \psi_t \mathrm{e}^{\mathrm{i}kj} \left|0_L\right\rangle \otimes c_j^\dagger \left|0_R\right\rangle \otimes \left|\mathrm{GS(N)}\right\rangle \\ + \sum_n \alpha_n \left|0_L\right\rangle \otimes \left|0_R\right\rangle \otimes \left|N+1_{(n)}\right\rangle + \sum_m c_0^\dagger \left|0_L\right\rangle \otimes c_{N+1}^\dagger, \left|0_R\right\rangle \otimes \beta_m \left|N-1_{(m)}\right\rangle \end{aligned} \tag{11.11}$$

where $\left|N+1_{(n)}\right\rangle$ denotes the nth eigenvector of the cluster Hamiltonian when it has $N+1$ particles and identically for $\left|N-1_{(m)}\right\rangle$. Let us now look at the Hamiltonian matrix equations

which involve V_{LR}. For $c_0^\dagger |0_L\rangle \otimes |0_R\rangle \otimes |\mathrm{GS(N)}\rangle$ we have

$$\begin{aligned}\left(\omega_k + E_{\mathrm{GS(N)}}\right)\psi_0 c_0^\dagger |0_L\rangle \otimes |0_R\rangle \otimes |\mathrm{GS(N)}\rangle = &-\psi_{-1} c_0^\dagger |0_L\rangle \otimes |0_R\rangle \otimes |\mathrm{GS(N)}\rangle \\ &- t_L c_0^\dagger |0_L\rangle \otimes |0_R\rangle \otimes \sum_i \left(\alpha_i c_L \left|N + 1_{(i)}\right\rangle\right) \\ &- t_R c_0^\dagger |0_L\rangle \otimes |0_R\rangle \otimes \sum_j \left(\beta_j c_R^\dagger \left|N - 1_{(j)}\right\rangle\right) \\ &+ E_{\mathrm{GS(N)}}\psi_0 c_0^\dagger |0_L\rangle \otimes |0_R\rangle \otimes |\mathrm{GS(N)}\rangle\,.\end{aligned} \tag{11.12}$$

We emphasize that we work in a restricted subspace where only one state with N particles in the cluster is available, the ground state, so a projector is implicit in the previous equation. The degenerate ground state case can be treated by using the Gibbs state as described in section 11.3. Given this, and through some straightforward calculations we can arrive at

$$\begin{aligned}\omega_k\psi_0 + \psi_{-1} &= -t_L \sum_n \alpha_n \langle \mathrm{GS}(N)| c_L \left|N + 1_{(n)}\right\rangle - t_R \sum_m \beta_m \langle \mathrm{GS}(N)| c_R^\dagger \left|N - 1_{(m)}\right\rangle \\ &= -\sum_n \left(t^L_{\alpha_n(N)}\right)^* \alpha_n - \sum_m \left(t^R_{\beta_m(N)}\right)^* \beta_m\end{aligned} \tag{11.13}$$

Now, for $|0_L\rangle \otimes \otimes |0_R\rangle\, \alpha_n \left|N + 1_{(n)}\right\rangle$ after some calculations we get

$$\begin{aligned}\left(\omega_k + E_{\mathrm{GS}}(N) - E_{\alpha_n}\right)\alpha_n &= -t_L\psi_0 \left\langle N + 1_{(n)}\right| c_L^\dagger |\mathrm{GS}(N)\rangle - t_R\psi_{N+1} \left\langle N + 1_{(n)}\right| c_R^\dagger |\mathrm{GS}(N)\rangle \\ &= -\left(t^L_{\alpha_n(N)}\right)\psi_0 - \left(t^R_{\alpha_n(N)}\right)^* \psi_{N+1}\end{aligned} \tag{11.14}$$

For $c_0^\dagger |0_L\rangle \otimes c_{N+1}^\dagger |0\rangle \otimes \beta_m \left|N - 1_{(m)}\right\rangle$ we get

$$\begin{aligned}\left(\omega_k + E_{\mathrm{GS}}(N) - E_{\beta_m}\right)\beta_m &= +t_L\psi_{N+1} \left\langle N - 1_{(m)}\right| c_L |\mathrm{GS}(N)\rangle - t_R\psi_0 \left\langle N - 1_{(m)}\right| c_R |\mathrm{GS}(N)\rangle \\ &= -\left(t^L_{\beta_m(N)}\right)^* \psi_{N+1} - \left(t^R_{\beta_m(N)}\right)\psi_0\end{aligned} \tag{11.15}$$

Finally for $|0_L\rangle \otimes c_{N+1}^\dagger |0\rangle \otimes |\mathrm{GS}(N)\rangle$ we have

$$\begin{aligned}\omega_k\psi_{N+1}+\psi_{N+2} &= -t_R\sum_n \alpha_n \langle \mathrm{GS}(N)|\, c_R \left|N+1_{(n)}\right\rangle + t_L\sum_m \beta_m \langle \mathrm{GS}(N)|\, c_L^\dagger \left|N-1_{(m)}\right\rangle \\ &= -\sum_n \left(t^R_{\alpha_n(N)}\right)\alpha_n - \sum_m \left(t^L_{\beta_m(N)}\right)\beta_m\end{aligned} \tag{11.16}$$

Note we have introduced the parameters

$$t^L_{\alpha_n(N)} = t_L \left\langle N+1_{(n)}\right| c_L^\dagger \left|\mathrm{GS}(N)\right\rangle, \tag{11.17}$$

$$t^R_{\alpha_n(N)} = t_R \langle \mathrm{GS}(N)|\, c_R \left|N+1_{(n)}\right\rangle, \tag{11.18}$$

$$t^R_{\beta_m(N)} = t_R \left\langle N-1_{(m)}\right| c_R \left|\mathrm{GS}(N)\right\rangle, \tag{11.19}$$

$$t^L_{\beta_m(N)} = -t_L \langle \mathrm{GS}(N)|\, c_L^\dagger \left|N-1_{(m)}\right\rangle. \tag{11.20}$$

Defining

$$\varepsilon_{\alpha_n(N)} = E_{\alpha_n} - E_{\mathrm{GS}}(N), \tag{11.21}$$

$$\varepsilon_{\beta_m(N)} = E_{\beta_m} - E_{\mathrm{GS}}(N), \tag{11.22}$$

one concludes that Eqs. 11.13, 11.14, 11.15 and 11.16 correspond to the Hamiltonian matrix equations of the effective system shown in Fig. 11.2.

The solution of this set of $M+2$ equations (that is, Eqs. 11.13, 11.14, 11.15 and 11.16) allows us to determine ψ_t and ψ_r. Note that ψ_0, ψ_{-1}, ψ_{N+1} and ψ_{N+2} are given by expressions $\psi_j = \left(\mathrm{e}^{\mathrm{i}kj} + \psi_r \mathrm{e}^{-\mathrm{i}kj}\right)$ for $j \leq 0$ and $\psi_j = \psi_t \mathrm{e}^{\mathrm{i}kj}$ for $j \geq N+1$ and are functions of ψ_r and ψ_t, therefore we have $M+2$ variables. The transmission probability is then given by the square of the absolute value of the ratio between the amplitude of the outgoing wave ψ_t and the amplitude of the incident wave (which we have assumed to be 1).

11.5 Application of our method for a simple scenario

In this section we consider the simple situation, depicted in Fig. 11.3, of a single site connected to semi-infinite leads with Hamiltonain given by

$$H = H_C + H_{\mathrm{leads}} + H_{LR} \tag{11.23}$$

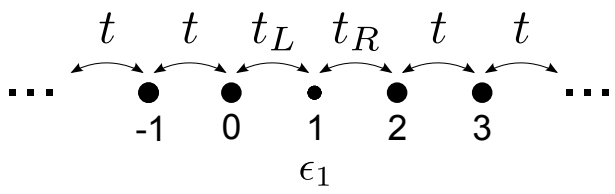

Figure 11.3: A single site connected to two infinite leads by different hopping constants to those of the leads.

with

$$\begin{aligned} H_C &= \epsilon_1 c_1^\dagger c_1 \\ H_{\text{leads}} &= -t\left(\sum_{j=-\infty}^{-1} c_{j+1}^\dagger c_j + \text{H.c}\right) - t\left(\sum_{j=2}^{\infty} c_{j+1}^\dagger c_j + \text{H.c}\right) \\ H_{LR} &= -t_L\left(c_1^\dagger c_0 + \text{H.c}\right) - t_R\left(c_2^\dagger c_1 + \text{H.c}\right) \end{aligned} \tag{11.24}$$

Let us now calculate the transmittance through this system using the method we have developed in the previous section. For that we simply need to make use of Eqs. (11.13-11.16) In this simple case we have the following

$$\begin{aligned} \alpha_1 &= \psi_1 \\ \beta_1 &= 0 \\ E_{\alpha_1} &= \epsilon_1 \end{aligned} \tag{11.25}$$

and our equations reduce to

$$\begin{aligned} \omega_k\psi_0 + \psi_{-1} &= -t_L\psi_1 \\ (\omega_k - \epsilon_1)\,\psi_1 &= -t_L\psi_0 \\ \omega_k\psi_2 + t\psi_3 &= -t_R\psi_1 \\ (\omega_k - \epsilon_1)\,\psi_1 &= -t_R\psi_2 \end{aligned} \tag{11.26}$$

These correspond directly to Eqs. (H.11-H.14) in Appendix H whenever there is only one site in the quantum ring. For the simpler situation $\epsilon_1 = 0, t_L = t_R = t_1$, we can easily calculate an analytical expression for the transmittance, which is given by

$$T = |\psi_2|^2 = \left| \frac{\mathrm{i}\dfrac{\partial\omega_k}{\partial k}}{\left(\dfrac{t^2}{t_1^2} - 1\right)\omega_k + \mathrm{i}\dfrac{\partial\omega_k}{\partial k}} \right|^2 \tag{11.27}$$

for $\omega_k = -2t\cos(k)$. For more complex scenarios, without interaction, a direct comparison

between the conductance equations of this chapter and the ones of 10 is not possible as in the first case we make use of eigenvectors of the cluster, while in the latter we make use of localized cluster states (which coincides for a single cluster site). Our method is, however, exact in the limit of no interactions, and the two methods will always produce the same results. We have also performed numerical studies for the case of interacting rings and the AB_2 chain, which have shown that our method produces results identical to the one in [163], the difference between the two methods being negligible.

11.6 Conclusions

In this paper, a new method for the determination of the two-terminal differential conductance through an interacting cluster has been presented and applied to the case of the conductance of spinless Fermions through an AB_2 ring considering nearest neighbors interactions. This method is exact in two limits: (i) vanishing interactions; (ii) vanishing coupling between leads and cluster, and its main approximation is the assumption that particles in the leads remain independent and therefore the system can be reduced to a simpler problem of one incoming particle which interacts with N particles in the cluster. This simpler problem can studied in a truncated Hilbert space and in this space, it can mapped exactly into the problem of the transmission of an incoming particle through a non-interacting cluster of M independent sites (where M is the number of cluster states with one particle more or less than the ground state of the cluster).

The simplicity of our method allows simple generalizations to more complex situations (which are apparently not trivial in Jagla and Balseiro's method) such as: i) the multi-terminal case, where an incoming particle from a lead can be transmitted into several leads connected to the cluster. This situation is described adding several equations of the type of Eq. (11.16) to the system of equations; ii) the transmission of entangled pairs. In this case, a similar truncation of the Hilbert space can be followed, considering a single incoming pair in the left lead and allowing for interactions only in the cluster. This problem will be addressed in a future work. Eqs. (11.13-11.16); iii) the transmittance of magnons through magnetic nanoclusters coupled to ferromagnetic spin chains. A Jordan-Wigner transformation or a Matsubara-Matsuda transformation allows one to map the transport of magnons into the problem of the transport of one spinless particle through a nearest-neighbor interacting nanocluster (assuming Heisenberg interactions in the cluster). The work here contained has been published in [159].

Chapter 12

Conductance through interacting spinless AB_2 chains

In this chapter we study the conductance through the AB_2 for a two terminal set-up in the presence of interactions. We show that for the conductance thorough an interacting AB_2 chain one has that the non-interacting conductance profiles persist for small values of the interaction, with a small shift of the peaks and a small splitting of the peaks (when degeneracy is present in the non-interacting limit). We also see that some conductance peaks are not present due to a particle number jump (observed for any value of the interaction) that occurs as the gate potential is varied and that can be associated with the flat band of the AB_2 ring when interactions are absent.

12.1 Conductance in the AB_2 chain

In this section, we apply the method described in section II (and detailed in appendix A) to the study of the conductance through an AB_2 ring (see Fig. 12.1). Recently, we have shown that due to the existence of one-particle localized states in this ring (consequence of the geometrical frustration), the conductance through the non-interacting AB_2 ring displays a peculiar dipped conductance peak at zero frequency. Here, we discuss the effect of the nearest-neighbor interactions on the presence of this peak as well as effects due to a particle number jump [due to the existence of a flat band when no interactions are present (see appendix B), but that persists when interaction is taken into account] which occurs as a gate voltage V_g is varied.

In Fig. 12.1, an AB_2 ring is shown with a magnetic flux ϕ threading each plaquette and a magnetic flux ϕ_i threading the inner ring. The inner sites in the AB_2 ring of Fig. 12.1 are denoted as C sites and the outer sites as B sites. Spinal sites are denoted as A sites. The number of unit cells (or plaquettes) is denoted N_c. Therefore, the magnetic flux enclosed

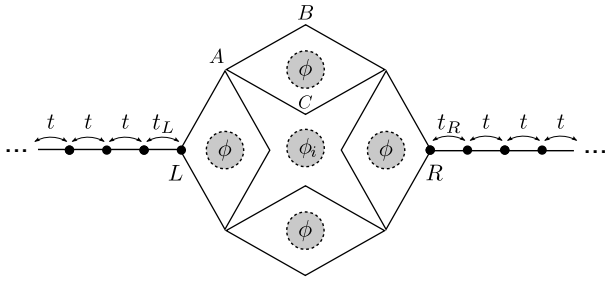

Figure 12.1: The diamond star is connected at sites L and R, to one-dimensional semi-infinite tight binding leads via hopping amplitudes t_L and t_R. Each plaquette is threaded by a magnetic flux ϕ while the inside ring is threaded by a magnetic flux ϕ_i.

by the outer ring is $\phi_o = \phi_i + 4N_c\phi/4$ and we introduce an auxiliary flux ϕ' such that $\phi_o = \phi' + 2N_c\phi/4$, $\phi_i = \phi' - 2N_c\phi/4$.

The Hamiltonian for an AB_2 chain with N_c unit cell is

$$H_C = H_0 + V \sum_j \left(n_j^A + n_{j+1}^A\right)\left(n_j^B + n_j^C\right), \tag{12.1}$$

where V is the value of the interaction and

$$\begin{aligned} H_0 = -t \sum_{j=1}^{N_c} \Big[& \mathrm{e}^{\mathrm{i}\phi_o/2N_c}(A_j^\dagger B_j + B_j^\dagger A_{j+1}) \\ & + \mathrm{e}^{-\mathrm{i}\phi_i/2N_c}(C_j^\dagger A_j + A_{j+1}^\dagger C_j)\Big] + \text{H.c.} \end{aligned} \tag{12.2}$$

where $A_j^\dagger$ creates a particle at the spinal site of the unit cell j of the AB_2 ring, and $B_j^\dagger$ and $C_j^\dagger$ creates a particle at the edge sites (see Fig. 12.1). Here we have chosen a gauge such that the Peierls phases are equally distributed in the inner ring and in the outer ring of the AB_2 ring. By introducing a gate voltage in our cluster one needs to modify the cluster Hamiltonian, $H_C \to H_C - eV_gN$.

In the case of a transport experiment, the AB_2 ring is connected to particle reservoirs and one needs to know the ground state of the AB_2 ring as function of the chemical potential. The phase diagram of an AB_2 ring with four unit cells (as in Fig. 12.1) as a function of the chemical potential and of the interaction is displayed in Fig. 12.2a for zero flux and in Fig. 12.2b for flux per plaquette equal to $\pi/2$.

For zero flux, the phase diagram Fig. 12.2a shows a particle number jump to a high density state, from 3 particles to 8 particles (or better, from N_c-1 to $2N_c$). It is interesting to note that the cluster is never at half-filling or close to it. As that is the situation corresponding to the largest Hilbert subspace, the fact that one can neglect these states means that our computational effort is reduced. This particle jump can be associated with the existence of zero energy localized states (due to the geometric frustration of the AB_2 chain) when V/t

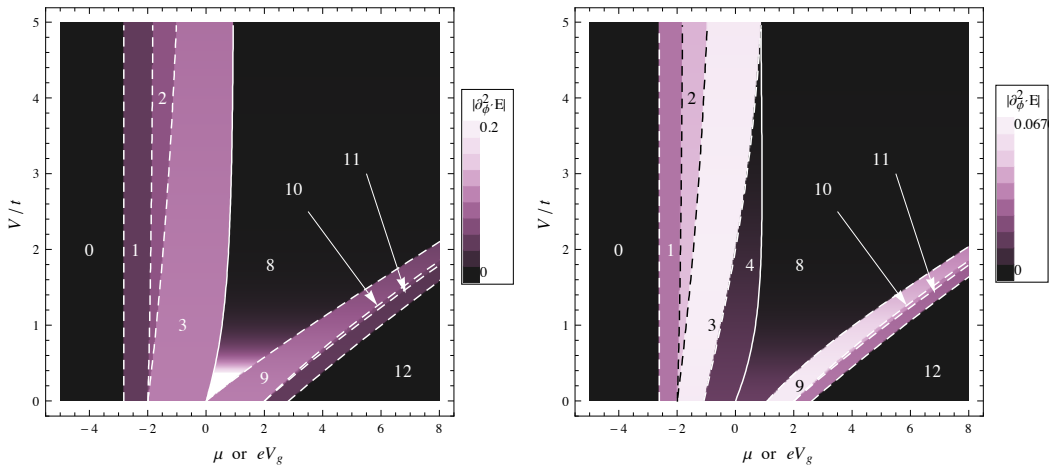

(a) $\phi = 0$ (b) $\phi = \pi/2$

Figure 12.2: Phase diagram of the AB_2 ring connected to a particle reservoir as a function of the chemical potential and the interaction for the particular case $N_c = 4$ and (a) zero flux or (b) flux per plaquette $\phi = \pi/2$. The white and black lines delimit areas of different number of particles on the ground state while the density plot gives us the magnitude of the second derivative of the ground state energy with respect to the flux ϕ' at $\phi' = 0$ (proportional to the the charge stiffness). The numbers indicate the number of particles in the ground state. The results were obtained using forward differences and a step size of $d\phi = \pi \times 10^{-4}$.

is zero (see appendix B), so that a small chemical potential shift around $\mu = 0$ implies the immediate fill of the respective flat band (which separates two bands of itinerant states). Curiously this particle jump survives for any value of V/t. This is not obvious since we do not expect the states of the flat band to remain localized when V is finite, if the lower itinerant band is full.

In Fig. 12.2 we also show as a density plot the charge stiffness at zero temperature (or better, the curvature of the ground state energy) as a function of the chemical potential and of the interaction. As first stated by Kohn, [133, 164] in 1D systems the charge stiffness at zero temperature can be obtained from the ground state energy dependence on the magnetic flux and this allows one to distinguish an ideal insulating state from a ideal metallic one. In the case of the AB_2 ring, the change of boundary conditions is related to the variation of flux ϕ' and the charge stiffness is given by

$$D_c = N_c \left. \frac{\partial^2 E(\mu, V)}{\partial \phi'^2} \right|_{\phi'=0} \tag{12.3}$$

where $E(\mu, V)$ is the many body ground state energy of the AB_2 ring with chemical potential μ and interaction V and ϕ' is equivalent to the flux threading a normal quantum ring. At zero temperature one expects $D_c = 0$ for an insulating state and $D > 0$ for a metallic one. Note that for fixed ϕ, a derivative in order to ϕ' is the same as a derivative in order to ϕ_i or

ϕ_o.

In Fig. 12.2a one can see that while an increase in V has a small impact on the charge stiffness for most values of μ, for 8 particles, a small increase in the interaction immediately turns the system into an insulator. This reflects the fact that for 8 particles in the cluster and strong interaction, the ground state corresponds to a Wigner crystal configuration, with all B and C sites occupied (all particles are localized due to the interaction).

When the magnetic flux threading the AB_2 plaquettes is $\pi/2$, the phase diagram (Fig. 12.2b) displays an additional region corresponding to 4 particles in the AB_2 ring, and the particle number jump occurs between from 4 to 8 particles. This region becomes narrower as the interaction grows and disappears for $V/5 \sim 1$. The existence of this region is justified by the fact that a finite flux ϕ through each plaquette induces a gap between the itinerant bands and the localized band when $V/t = 0$. Therefore one has a finite chemical potential interval (corresponding to this gap), where the lower itinerant band is completely full. This behavior remains for finite values of the interaction as long as the interaction is small compared with the gap. This doesn't happen for $\phi = 0$ since in that case the energy of highest level of the lower itinerant band is zero and coincides with the flat band.

As expected, the conductance profiles obtained using the method of section II reflect closely these phase diagrams, with some peculiarities that we describe below. Fig. 12.3 shows conductance peaks for a fluxless AB_2 chain with conducting leads contacting sites B and C of the same unit cell, as a function of the gate potential. In Fig. 12.3 as well as in Figs. 12.4 and 12.5, we show the conductance profiles with fixed number N of particles in the cluster (top curves) as well as the observable conductance profile (bottom red curve) which takes into account the transitions in cluster particle number given by the thick blue curve. The conductance profiles with fixed N are shifted in order to show clearly the observable regions in each of them. Whenever the ground state is degenerate we use the averaging procedure described in section 11.3. The chemical potential of the leads is assumed to be 0.

For $V/t = 0.1$ (see Fig. 12.3a), the conductance profiles are very similar independently of the particle number in the cluster. This reflects the fact that without interaction, the conductance profiles are the same independently of the number of particles in the cluster and the effect of the small interaction is to shift slightly the peaks and partially lift the degeneracy of the cluster Hamiltonian, therefore splitting some peaks. We observe that the zero frequency dipped peak (discussed in detail in chapter 10) survives for small V/t, but slightly shifted in frequency. For $V/t = 1$ (see Fig. 12.3b), this dipped peak is absent, but a trace of this peak is still observed at point A of the bottom profile of Fig. 12.3b. This trace appears to be a very asymmetric peak since it is the union of two tails due to the particle number jump. In the case of Fig. 12.3c, we show the conductances profiles for $V/t = 100$ and we see that a conductance peak is not necessarily associated with the energy of the particle number jump. This just means that the jump occurs before the ground state with 3 particles becomes degenerate with

the ground state with 4 particles.

In Fig. 12.4, we show the conductance profiles in the case of a flux per plaquette $\phi = \pi/2$ (created by an uniform magnetic field). All other parameters are the same as in Fig. 12.3. These conductance profiles reflect the existence of the $N = 4$ region in the phase diagram of Fig. 12.2b by showing an additional conductance peak when V/t is less than 5.

A peculiar feature of the conductance profiles with fixed N shown in Figs. 12.3 and 12.4 is presence of peaks of height 0.5. This is a consequence of the degeneracy of the ground state with N particles and of the existence of a conductance peak for only one of the degenerate ground states. Since we average the conductance over the possible ground states, this leads to a lower height conductance peak associated with transition $N \to N + 1$. Note that this average does not occur when the transition occurs in the direction $N + 1 \to N$ and this leads to a non-Lorentzian peak as observed in the bottom curve of Fig. 12.3b (peak B).

The strong coupling limit solution given in chapter 9 also indicates that for small particle number the AB_2 ring should behave as a renormalized ring with hopping $\sqrt{2}t$ and reduced length equal to $2N_c/3$. Fig. 12.5 shows a comparison of the conductance peaks for an incident particle with $k = \pi/2$ as a function of the gate voltage for an AB_2 ring and for the corresponding renormalized linear ring with leads at opposite A sites for an interaction $V = 100t$. As expected, the conductance profiles of the two are almost identical. However the linear ring does not have jumps in particle number as the gate potential is varied. Note that the jump from 3 to 8 particles in the AB_2 ring can be considered similar to the transition from 3 to 4 particles in the linear ring (every other site occupied in the ring and every pair of B and C sites occupied in the AB_2 ring), but the latter leads to a conductance peak while the former may not, as explained above. Also, the transition from 3 to 8 in the AB_2 ring occurs much earlier.

12.2 Conclusion

The main results obtained in our study of the conductance features due to interactions in the AB_2 ring are: (i) the non-interacting conductance profiles persist for small values of the interaction, with a small shift of the peaks and a small splitting of the peaks (when degeneracy is present in the non-interacting limit); (ii) some conductance peaks are not present due to a particle number jump (observed for any value of the interaction) that occurs as the gate potential is varied and that can be associated with the flat band of the AB_2 ring when interactions are absent.

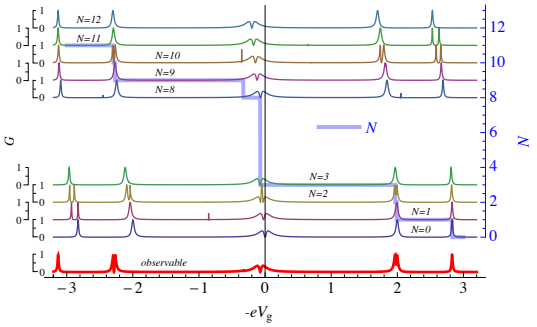

(a) $V/t = 0.1$

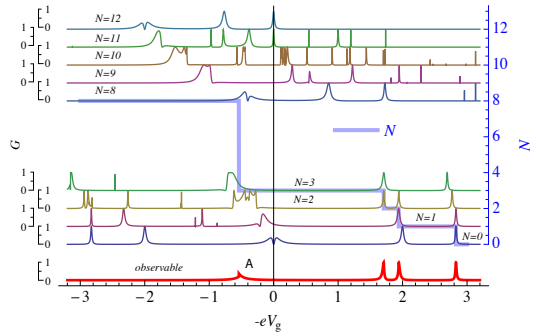

(b) $V/t = 1$

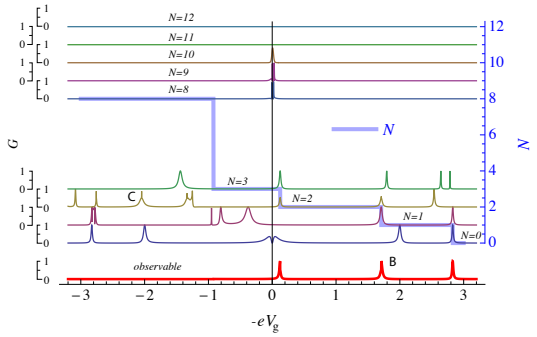

(c) $V/t = 100$

Figure 12.3: Conductance as function of $-eV_g$ for several values of the interaction constant, (a) $V/t = 0.1$, (b) $V/t = 1$ and (c) $V/t = 100$, with contacts at sites B and C of the same unit cell and for zero flux. The conductance profiles for fixed particle number in the cluster are shown as well as the observable conductance (bottom red line) obtained taking into account the particle number transitions (blue thick line, right axis).

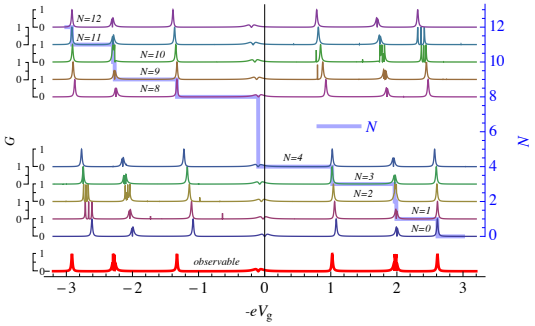

(a) $V/t = 0.1$

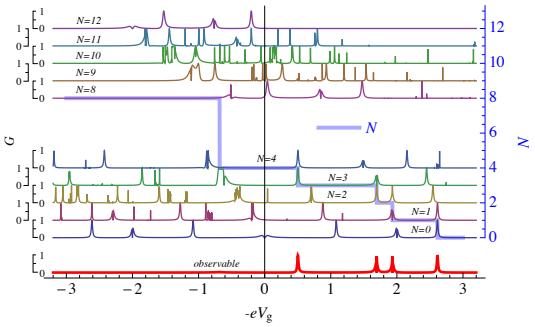

(b) $V/t = 1$

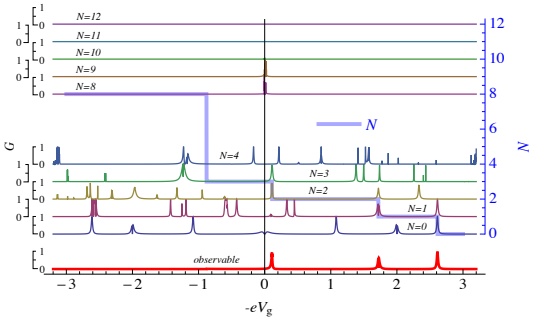

(c) $V/t = 100$

Figure 12.4: Conductance profiles in the case of a flux per plaquette $\phi = \pi/2$ (created by an uniform magnetic field). All other parameters are the same as in Fig. 12.3. An additional peak corresponding to the transition between 3 and 4 particles is present for small and intermediate V/t, but absent for large V/t.

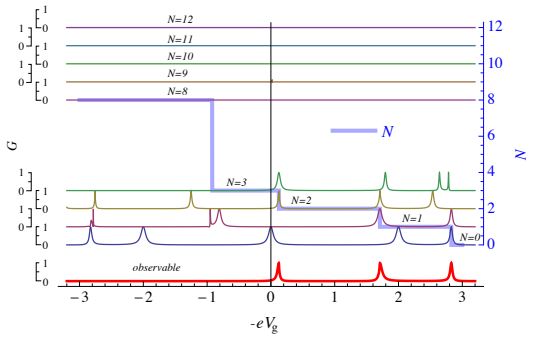

(a) AB_2 ring

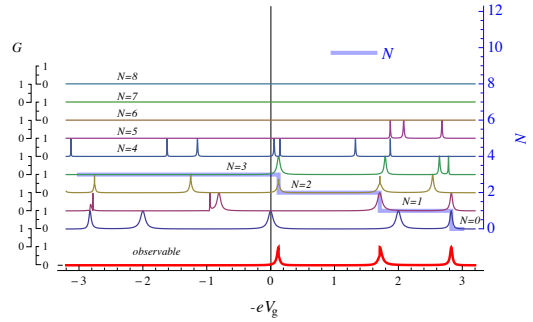

(b) linear ring

Figure 12.5: Conductance profile as a function of the gate voltage for: (a) an AB_2 ring with $N_c = 4, V = 100, \omega = 0$ and $t_L = t_R = 0.3t$ with contacts at opposite sites A; (b) the equivalent linear ring, with the same parameters but ring hoppings renormalized as $t \to \sqrt{2}t$ and leads contacts at opposite sites.

Chapter 13

Concluding remarks

The electronic properties of mesoscopic systems and the conductance through such systems are of utmost for future nano-technological applications. In particular due to the miniaturization of current electronics. Geometrically frustrated systems in particular exhibit very interesting and fundamental phenomena. The AB_2 chain as a prime example of such systems exhibits very interesting properties: a flat band independently of the magnetic flux threading each plaquette, a gap that opens up when flux is applied, among others. The quasi-unidimensional characteristic of the AB_2 chain allows behavior which would be non-existent in 1D systems while still rendering it amenable to exact solutions even in the presence of interactions, as for example in the strong coupling limit of the t-V model. In this case, as we have seen, it can be mapped into a 1D system, and can be solved using a variety of techniques such as Dias method [117] or Bethe Ansatz. Via a Jordan-Wigner transformation, the t-V AB_2 system can in be mapped onto a XXZ AB_2 system and so our itinerant spinless results for the AB_2 chain are also relevant for non-itinerant spinful AB_2 chains. In particular the strong coupling limit of the t-V AB_2 chain can be mapped into an XXZ AB_2 chain in the strong anisotropic limit. We have also performed a restricted Hartree-Fock study of the AB_2 chain and shown that for a strong interaction the results obtained agree qualitatively with the exact results obtained in the strong coupling limit.

Our study of the AB_2 chain has led us to propose a method for constructing localized states in non-interacting geometrically frustrated systems which leads to states which are highly localized. We believe that this intuitive and simple method can be of use in studying the effects of localized impurities (since a highly localized basis is, in this case, a "better" basis than a not so localized one).

We have also shown that the localized states in geometrically frustrated systems lead to rather interesting behavior in the two terminal electronic conductance through such systems. Without magnetic flux, these localized states act as filters of the zero frequency conductance peak (where we refer to the frequency of an incident electron). The addition of magnetic

flux changes the behavior of the localized stats in the conductance: some still filter the zero frequency peak while others contribute to the appearance of a zero frequency peak, and as such the conductance profile exhibits a zero frequency peak with a dip. This dip is a distinct fingerprint of localized states and as we have shown its height varies as a function of the distance between contacts. We thus expect that conductance dips can be used as an experimental probe of the spatial dependence of localized states.

We have proposed a new method for calculating the conductance through interacting clusters, and shown that it is in agreement with already well known methods. Our method is exact in two limits: whenever the interactions in the cluster vanish or whenever the coupling between leads and cluster vanish. We have finally used this method for the calculation of the conductance through AB_2 chains. We have shown that the non-interaction conductance profiles persist for small values of the interaction and that some expected conductance peaks are actually experimentally non-accessible due to the flat band of the AB_2 chain.

Appendices

Appendix A

A digression on symplectic geometry and the moment map

In this chapter we discuss preliminary background useful to the understanding of quantum marginals. Particularly important is the moment map, which we will briefly introduce. For this, notions of differential geometry and symplectic geometry are necessary. Given that many physicists are not acquainted with these mathematical tools (including the author himself before starting to work on this subject), we thought it would make sense to start from the very beginning.

In what follows we will always deal exclusively with finite dimensional spaces, except if otherwise stated. This makes the discussion much easier, preventing the need to delve into functional analysis and without greatly diminish the applicability of our results. Our main references for this section are [165] and [22]. We provide other references where appropriate. The material here contained is not in any sense complete, and we therefore refer the reader to the above mentioned references for extra material and for proofs.

A.1 Symplectic vector spaces

Consider a vector space V over a field K of characteristic different from 2. Consider now a bilinear form on V, $\omega : V \times V \to K$. If this bilinear form is skew-symmetric, i.e.

$$\omega(v_1, v_2) = -\omega(v_2, v_1), \quad v_1, v_2 \in V \tag{A.1}$$

and non-degenerate,

$$\omega(v_1, v_2) = 0, \quad \forall v_1 \in V \Rightarrow v_2 = 0 \tag{A.2}$$

then this bilinear form is called a *symplectic form*. Note that these conditions immediately imply that the quadratic form $\omega(v, v)$ is 0. The tuple (V, ω) is called a *symplectic vector space*.

Canonical vector space	$\mathbb{R}^n$	$\mathbb{R}^{2n}$
Bilinear form	Symmetric Non-degenerate	Skew-symmetric Non-degenerate
Canonical matrix form	$\begin{pmatrix} \mathbb{1}_p & \\ & -\mathbb{1}_k \end{pmatrix}$	$\begin{pmatrix} 0_n & \mathbb{1}_n \\ \mathbb{1}_n & 0_n \end{pmatrix}$

Table A.1: Comparison between inner product and symplectic spaces. We always assume non-degeneracy.

In a given basis, the symplectic form can be represented as a matrix Ω and the above equations can be written as

$$\begin{aligned} &v_1^T \Omega v_2 = -v_2^T \Omega v_1 \\ &v_1^T \Omega v_2 = 0, \quad \forall v_1 \in V \Rightarrow v_2 = 0 \end{aligned} \tag{A.3}$$

That is the same as to say that such matrix must be skew-symmetric and invertible (non-singular).

It is a simple result that a necessary condition for an $n \times n$ skew-symmetric matrix to be invertible is for n be even. Hence symplectic vector spaces are always even dimensional. The canonical symplectic space is taken to be $\mathbb{R}^{2n}$. Using the canonical basis the symplectic form takes the form,

$$\Omega = \begin{pmatrix} 0_n & \mathbb{1}_n \\ \mathbb{1}_n & 0_n \end{pmatrix} \tag{A.4}$$

which is that of a symplectic matrix, i.e. a transformation which leaves the symplectic for unchanged, $\omega(\Omega v_1, \Omega v_2) = \omega(v_1, v_2)$. Refer to table A.1 for a simple comparison between inner product an symplectic spaces. These give rise, respectively, to Riemannian and symplectic manifolds.

A.2 Symplectic manifolds

In order to talk about symplectic manifolds we need some notions of manifolds and differential geometry which we will now introduce.

A.2.1 Smooth manifolds

In what follows we deal exclusively with *smooth* manifolds. Informally a (smooth) manifold M is a set of points connected to each other smoothly and that locally looks like Euclidean space. An hyperplane, an n-sphere and an n-torus are all examples of manifolds. A double cone, a plane with a line intersecting it and anything with kinks is not a manifold (see Fig. A.1).

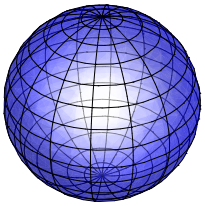

(a) Sphere

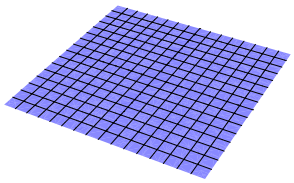

(b) Plane

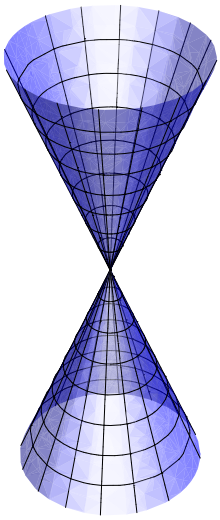

(c) Double cone

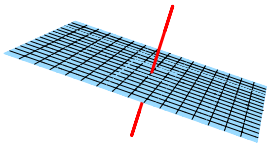

(d) Plane and line

Figure A.1: Example of manifolds (sphere, plane) and not manifolds (double cone, line intersecting a plane)

More formally consider a point m $\in M$ and a neighborhood U_m of this point. For M to be an l dimensional manifold, there must exist a bijective continuous function $\phi : U_m \to \mathbb{R}^l$ which maps U_m to to a neighborhood of $\phi(m) \in \mathbb{R}^l$. The tuple (U_m, ϕ) is called a *coordinate chart*.

Consider now another chart $\psi : V_{m'} \to \mathbb{R}^l$ and consider the composite function, called a *transition map*, $\psi \circ \phi^{-1} : \phi(U_m \cap V_{m'}) \to \psi(U_m \cap V_m)$. We assume that either $U_m \cap V_{m'}, = \varnothing$, in which case we call the charts *non-overlapping* or that $\psi \circ \phi^{-1}$ possesses derivatives of all orders (hence we call our manifold *smooth*). A collection of charts that covers the entire manifold and that are smooth between themselves is called a *smooth atlas*, $A = \{(U_i, \phi_i) : M = \cup_i U_i\}$. It then makes sense to define a manifold to be a set M with an atlas A, (M, A). We are now in position to define precisely a smooth manifold

Definition 48 (Smooth manifold)**.** *A smooth manifold M is a manifold for which all tran-*

sition maps are smooth, i.e., class C^∞.

A.2.2 Maps between manifolds, curves and tangent vectors

Consider two manifolds M and N. Consider a map between these two manifolds $\psi : M \to N$. Such map is smooth if for every chart (U_M, ϕ_M) in M and every chart (U_N, ϕ_N) the map $\phi_N \circ \psi \circ \phi_M^{-1}$ is smooth wherever it is defined. Such map is called a *coordinate expression* of ψ. If the map ψ is smooth and a bijection with smooth inverse, then it is called a *diffeomorphism*. Two manifolds for which there exist a diffeomorphism between them are called *diffeomorphic*.

If $N = \mathbb{R}$ then ψ is called a *function* on M and we will denote it by f. The space of smooth functions on M will be denoted by $\mathcal{F}(M)$. If instead one takes $M = \mathbb{R}$, ψ is called a *curve* on N and will be denoted by γ.

Let $\gamma : [-t, t] \to M$ be a curve on M with $m = \gamma(0)$. Then we can define the action of this curve on a function $f \in \mathcal{F}(M)$ by $\gamma(f) := \nabla_t|_{t=0} f(\gamma(t)) : \mathbb{R} \to \mathbb{R}$. Two curves γ_1 and γ_2 are called equivalent if $\forall f \in F(M)$, $\gamma_1(f) = \gamma_2(f)$. We then define the equivalence class of curves through p, $[\gamma_p] = \{\gamma' : \gamma(f) = \gamma'(f) \forall f \in \mathcal{F}, \gamma'(0) = p\}$.

A tangent vector at m is defined to be an equivalence class of curves through p. We define then the tangent space $T_m M$ at m to be the set of all tangent vectors at p. The tangent space is a vector space with the same dimension as that of the manifold. If we embed the manifold into $\mathbb{R}^{l+1}$ then the situation is very similar as that from extrinsic calculus. A basis for the tangent space at a point m is given by

$$\{\partial_i|_m\}_{i=1}^l . \tag{A.5}$$

In the same way one defines a tangent space of M at m, T_m, M one can define its dual, the *cotangent space* T_m^*. The elements of the cotangent space are called *one-forms*. In vector space terms, a one-form is merely a linear functional over a vector space. A basis for the cotangent space at a point m is given by

$$\left\{d^i|_m\right\}_{i=1}^l \tag{A.6}$$

And we have

$$d^i|_m \partial_j|_m = \delta^i_j. \tag{A.7}$$

A.2.3 Tangent and cotangent bundle, vectors fields

The tangent and cotangent spaces are defined locally on M. By collecting all the tangent spaces of M, this gives rise to the tangent bundle of M, TM

$$TM = \cup_{m \in M} T_m M \tag{A.8}$$

Likewise the union of all cotangent space of M gives rise to the cotangent bundle of M,

$$T^*M = \cup_{m\in M} T^*_m M \tag{A.9}$$

The space T^*M is the dual of TM and it can be shown that these have dimension $2l$ where l is the dimension of M.

With the definition of tangent and cotangent bundles we can define the notion of vector field

Definition 49 (Vector Field)**.** *A vector field on a manifold M is an assignment of a tangent space to every point $m \in M$. More formally a vector field is a map $X : M \to TM$ such that $X(m) = X|_m in T_m M$. The collection of all vector fields on M is denoted by $\mathfrak{X}(M)$.*

The notion of one-form fields is analogous except one needs to swap TM for T^*M. From there we can easily define the notion of a tensor field of any degree.

A vector x at a point $m \in M$ can act on a function $f \in \mathcal{F}(m)$, $x : f \in \mathcal{F}(m) \to \mathbb{R}$. Extending this definition pointwise, one can define the action of a vector field on an arbitrary function on M, $(X(f))(m) := X_m(f) = x(f), f \in \mathcal{F}$. Vector fields are linear mappings that satisfy Leibniz rule

$$\begin{aligned} \text{linearity} &: X(\alpha f + \beta g) = \alpha X(f) + \beta X(g) \\ \text{Leibniz} &: X(fg) = (X(f))\, g + (X(g))\, f \end{aligned} \tag{A.10}$$

One can also prove the following important relationship (see next section for the definition of the differential d)

$$X(f) = \mathrm{d}\, f(X). \tag{A.11}$$

A.2.4 Differential and pullback of a map

Let $\psi : M \to N$ be a smooth map between manifolds. Then there is an induced map $\psi_* = \mathrm{d}\,\psi : TM \to TN$ called the differential or the pushforward of ψ, since it pushes vectors from TM to TN. There is yet another induced map $\psi^* : T^*N \to T^*M$ called the pullback of ψ, given that it pulls one-forms from T^*N to T^*M. See Fig. A.2 and A.3 for a graphical depiction of these maps

Since tensors are built from products of the tangent and cotangent space, the pullback and the pushforward (of a diffeomorphism) can be used to transform tensor fields from M to N or vice-versa.

Obviously the question is, why go through all this when everything was so easy on $\mathbb{R}^n$? One reason is physical. If the manifold is something like the universe, we cannot expect it to be embedded into something else, as it is per definition *everything*. The other is mathematical,

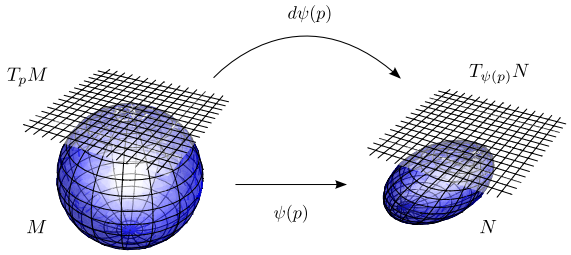

Figure A.2: Pushforward of a smooth map.

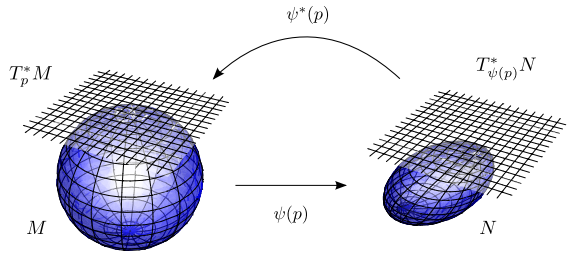

Figure A.3: Pullback of a smooth map.

since some quantities of interest are independent of the embedding, such as the Gauss intrinsic curvature defined in the *Theorema Egregium* of Gauss [166, Chapter 3].

A.2.5 Exterior calculus and differential forms

Let us begin by defining the concept of differential form

Definition 50 (Differential form)**.** *Let M be a manifold and $m \in M$ with $\Lambda^p_m(M)$ the space of antisymmetric tensors of rank p on the cotangent space of M at m, T^*_mM, $\Lambda^p_m(M) \subset (T^*_mM)^{\otimes}p$. Then a differential p-form ω is a mapping $\omega : M \to \Lambda^pM$ such that $\omega(m) \in \Lambda^p_mM$.*

The direct sum of the space of antisymmetric tensors of rank $p = 0, \dots \dim M$

$$\Lambda(M) = \bigoplus_{p=0}^{\dim M} \Lambda^pM \tag{A.12}$$

is called the *exterior algebra* over M.

Having defined differential forms we are now in position to define the exterior derivative

Definition 51 (Exterior derivative)**.** *Consider a p-form $\omega \in \Lambda^p(M)$ and a q-form $\nu \in \Lambda^q(M)$. Let $\mathrm{d} : \Lambda^p(M) \to \Lambda^{p+1}(M)$ be a map satisfying*

1. *(linearity)* $\mathrm{d}(\omega + \nu) = \mathrm{d}\,\omega + \mathrm{d}\,\nu$ *whenever* $p = q$

2. *(nilpotency)* $(\mathrm{d})^2 = 0$

3. *(uniqueness)* d *agrees with the differential of smooth functions,* $\mathrm{d}\, f = \psi_* f, \quad f \in \mathcal{F}(M)$

4. *(antiderivation)* $\mathrm{d}(\omega + \nu) = \mathrm{d}\,\omega \wedge \nu + (-1)^p \omega \wedge (\mathrm{d}\,\nu)$

The exterior derivative is also known in the literature as *Cartan derivative*. It is important to note that it can be proved that exterior derivative as defined above, exists and is unique.

Note that from the definitions above, a function $f \in \mathcal{F}(M)$ is a 0-form and we have $\Lambda^0 M = \mathcal{F}$.

A form ω such that $\mathrm{d}\,\omega = 0$ is called *closed* while a form ω such that $\omega = \mathrm{d}\,\nu$ with ν a differential form, is called *exact*. Given the nilpotency of the differential operator, it follows trivially that an exact form is closed.

A.3 Flow, Lie derivative and the interior derivative

The flow on a given set X is a group action $\Phi : X \times I \to X$, $I \subset \mathbb{R}$ such that for $x \in X$ and $t, t' \in \mathbb{R}$ and defining $\Phi^t(x) := \Phi(x, t)$ one has

$$\begin{aligned} \Phi^0(x) &= \mathrm{Id} \\ \Phi^t(x)\Phi^{t'}(x) &= \Phi^{t+t'}(x) \end{aligned} \tag{A.13}$$

forming a one-parameter group of transformations. We call a flow *complete* if the map above is defined for any t, $I = \mathbb{R}$. In the case $X = M$, with M a manifold we talk of a flow on a manifold.

Note that a flow defines a vector field and likewise a vector field defines a flow. As such we use the notation Φ^t_X to denote the flow associated with the vector field X such that

$$\frac{\mathrm{d}\,\Phi^t_X(m)}{\mathrm{d}\,t} = X(\Phi^t_X(m)) \tag{A.14}$$

Having defined the flow we can now define the important Lie derivative of a tensor field T in the direction of a vector field X.

$$\mathcal{L}_X T_m = \frac{\mathrm{d}}{\mathrm{d}\,t}|_{t=0} (\Phi^t_X)^* T_{\Phi^t_X(p)} \tag{A.15}$$

In the particular case of the Lie derivative of a vector field Y in the direction of the vector field X one has

$$\mathcal{L}_X Y = [X, Y], \tag{A.16}$$

where $[\cdot, \cdot]$ is a Lie bracket.

Note that the exterior derivative gives us a (p+1)-form from a p-form while the Lie derivative gives us a p-form from a p-form. In contrast with the exterior derivative we define

the interior derivative, also know as interior product, as a map that gives us a (p-1)-form from a p-form

Definition 52. *Let X be a vector field and let ω be a p-form on a manifold M. Then the map* interior derivative *or* interior product *of the vector field X, $\iota_X : \Lambda^p(M) \to \Lambda^{p-1}(M)$ given by*

$$\iota_X \omega\left(X_1, \ldots X_{p-1}\right) = \omega\left(X, X_1, \ldots X_{p-1}\right) \tag{A.17}$$

and $\iota_X \omega = 0$ whenever $\omega \in \Lambda^0(T^*M)$.

We now state several relationships between the three derivatives we have introduced: the exterior, Lie and interior derivatives. Let $\omega \in \Lambda^p(M)$ be a differential p-form, $f \in \Lambda^0(M)$ a function and $X \in \mathcal{X}(M)$ a vector field. Then one has the following relationships between the three derivatives defined above

1. (Cartan's identity) $L_X \omega = \iota_X \,\mathrm{d}\,\omega + \mathrm{d}\,\iota_X \omega$
2. $\iota_X \,\mathrm{d}\, f = \mathcal{L}_X f$
3. $\mathcal{L}_{f(X)} \omega = f(\mathcal{L}_X \omega) + \mathrm{d}\, f \wedge \iota_X \omega$

Cartan's identity, in particular, is of utmost importance in symplectic geometry

A.3.1 Symplectic manifold

As we have defined above, the tangent spaces of a manifold M are vector space. As such we can equip them with a symplectic form as defined in section A.1 to turn them into symplectic vector spaces. Demanding this form to be closed, we arrive at the notion of a symplectic manifold. Symplectic manifolds are crucial for classical mechanics as the classical phase space is a sympelctic manifold. Also in quantum mechanics a symplectic structure is present.

Definition 53. *A symplectic manifold is a manifold M with a 2-form $\omega_m : T_m M \times T_m M \to \mathbb{R}$ such that*

1. *ω_m is a symplectic form $\forall m \in M$*
2. *ω is a closed form, $\mathrm{d}\,\omega = 0$*

For the canonical situation $M = \mathbb{R}^{2n}$, the 2 form

$$\omega_c = \sum_i^n \mathrm{d}\, p^i \wedge \mathrm{d}\, q^i \tag{A.18}$$

is symplectic. According to the very important Darboux's theorem, any symplectic form ω on a manifold M of dimension m is locally isomorphic to the canonical one ω_c for $\mathbb{R}^{2n}$.

Consider an Hilbert space H with Hermitian inner product $(\cdot\,,\,\cdot) : H \times H \to \mathbb{C}$. Now consider $v_1, v_2 \in H$. Then we can decompose $(v_1,\, v_2) = (v_1,\, v_2)_{\mathrm{Re}} + \mathrm{i}(v_1,\, v_2)_{\mathrm{Im}}$ with $(v_1,\, v_2)_{\mathrm{Re}}$, $(v_1,\, v_2)_{\mathrm{Im}} \in \mathbb{R}$. Then, given the skew-symmetry of the Hermitian inner product, $(v_1,\, v_2) = \overline{(v_2,\, v_1)}$, and that $(v_2,\, v_1) = \overline{(v_1,\, v_2)} = (v_1,\, v_2)_{\mathrm{Re}} - \mathrm{i}(v_1,\, v_2)_{\mathrm{Im}}$, the real part of the Hermitian inner product gives us a symmetric form while the imaginary part gives us a skew-symmetric form. It follows trivially that this skew-symmetric form is actually a symplectic form (i.e. non degenerate). Hence the Hilbert space of quantum mechanics gives rise naturally to a *symplectic manifold* [1] [167].

We need only one extra piece of information. Consider a manifold M, a non-degenerate bilinear form on M, $\omega : TM \times TM \to \mathbb{R}$ and a vector field $X \in \mathfrak{X}(M)$ on M. We then define the flat map $\flat : TM \to T^*M$ as,

$$X^\flat := \omega(X,\, \cdot) \tag{A.19}$$

Identically we define the sharp map $\sharp : T^*M \to TM$ to be the inverse of the flat map $\sharp = \flat^{-1}$, an operation that is well-defined since we imposed the need for our form to be non-degenerate. These maps are called *musical isomorphisms*.

Whenever the bilinear form ω is symmetric we have a Riemannian manifold and these are simply the operations of lowering ($\flat$) and raising ($\sharp$) indices used in Ricci's calculus. In our symplectic manifolds, these are analogue operations

In canonical coordinates the musical isomorphisms take the form

$$\begin{aligned} (\partial_{p_i})^\flat &= \mathrm{d}\, q^i \\ (\partial_{q_i})^\flat &= -\,\mathrm{d}\, p^i \end{aligned} \tag{A.20}$$

A.4 coadjoint orbits and the moment map

Having briefly sketched the idea of symplectic manifolds we are now almost in position to introduce the moment map. We just need to talk a bit about coadjoint orbits.

A.5 coadjoint orbits

Consider a Lie group G and an element of the corresponding Lie algebra $\xi \in \mathfrak{g} \cong T_eG$. Let M be a manifold and consider the action $\Phi(\exp t\xi, m) : G \times M \to M$ (for a simple introduction to group action, see Appendix B). Then the vector at m

$$\xi_M(m) = \frac{\mathrm{d}}{\mathrm{d}\, t}|_{t=0} \Phi(\exp t\xi, m) \tag{A.21}$$

is called the *infinitesimal generator* of the action Φ.

[1] It gives rise to even more than that. It has the structure of a Kähler manifold but this is not important for our discussion.

Consider a group G and another group H. The adjoint action of G on H is a map $\mathrm{Ad} : g \times h \to ghg^{-1}$, $g \in G, h \in H$. In particular, the action of a Lie group G on its Lie algebra is quite important, $\mathrm{Ad} : g \times \xi \to g\xi g^{-1}$, $g \in G, \xi \in \mathfrak{g}$. It is a simple exercise to show that the infinitesimal generator of the adjoint action $\mathrm{Ad}_g(\xi)$ is $\xi_M = \mathrm{ad}_\xi$, i.e. $\mathrm{ad}_\xi(x) := [\xi, x]$.

The coadjoint action of a Lie group on the dual of its Lie algebra, $\mathrm{Ad}^* : G \times \mathfrak{g}^*$, is defined in terms of the adjoint action via, $\mathrm{Ad}^*_g = \mathrm{Ad}_{g^{-1}}$. The orbits of this action are called *coadjoint orbits*. It can be proved that the coadjoint orbits are symplectic manifolds with a natural 2-form inherited from $\mathfrak{g}$. The sympelctic form on the coadjoint orbits of $\mathfrak{g}^*$ is given by,

$$\omega_\xi(\mathrm{ad}_\xi\ x, \mathrm{ad}_\xi\ y) = \mathrm{tr}\ \xi\, \mathrm{ad}_x\, y \tag{A.22}$$

known as the Kirillov-Kostant-Souriau symplectic form [168], which is a symplectic form on $\mathrm{ad}_\xi\ x$ and $\mathrm{ad}_\xi\ y$.

A.5.1 Hamiltonian actions and moment maps

Let (M, ω) be a symplectic manifold and $H : M \to \mathbb{R}$ a function on M. The vector field given by $X_H = (\mathrm{d}\, H)$ is called *Hamiltonian vector field* with *Hamiltonian* H. The tuple (M, ω, X_H) is known as *Hamiltonian system*.

Let M be a symplectic manifold on which a Lie group G acts. Then the action of G on M is called *symplectic* if $g^*\omega = \omega$, $\forall g \in G$. The action of G on M, Ψ, is called *Hamiltonian* if there exists a map $\mu : M \to \mathfrak{g}^*$ that satisfies the following conditions

1. For $X \in \mathfrak{g}$, $\mathrm{d}\, \mu^X = \iota_{X'\omega}$ where $\mu^X(m) = \langle \mu(m), X \rangle$ is the component of μ along X and X' is the vector field on M generated by the flow $\Phi = \exp tX$.

2. $\mu \circ \Psi = \mathrm{Ad}^*_g \circ \mu$, where Ψ is the action of G on M.

The map μ is called *moment map* and the tuple (M, ω, G, μ) a *Hamiltonian G-space*.

For pedagogical reasons let us look at an example. Let us consider a system of 3 particles in 1D with spacial coordinates q_i and momentum p_i, $i = 1, 2, 3$. In this case the phase space is $M = \mathbb{R}^6$ and given by $(q_1, p_1, q_2, p_2, q_3, p_3)$. As would follow from Hamiltonian mechanics [169], phase space is equipped with the canonical symplectic form $\omega_c = \sum_i \mathrm{d}\, q_i \wedge \mathrm{d}\, p_i$. We let now $G = \mathbb{R}^3$ act on M by translations with action ψ

$$\psi(\vec{q}, \vec{p}) = \left(\vec{q} + \vec{d}, \vec{p}\right),\ \vec{d} \in \mathbb{R}^3 \tag{A.23}$$

Then the vector field X' in M generated by the flow $\Phi = \exp t\vec{d}$ is given by $X' = d_i \dfrac{\partial}{\partial q_i}$ and we have

$$\mathrm{d}\, \mu^X(\vec{p}) = \iota_{X'}\omega(\vec{p}) = \vec{a} \cdot \mathrm{d}\, \vec{p} \tag{A.24}$$

where we have used the fact that $\frac{\partial}{\partial q_i}\,\mathrm{d}\,q_j = \delta_i^j$. Given that $\mu^X = \langle \mu, \vec{a} \rangle$, one then has $\mu(\vec{x}, \vec{p}) = \vec{p}$, which justifies the name *moment map*.

A.5.2 Abelian Moment polytope

We now state, without proof, the following important theorem,

Theorem 54 (Abelian convexity theorem (Atiyah [170],Guillemin-Sternberg [171]))**.** *Let (M, ω) be a compact connected symplectic manifold and G be a compact connected Abelian Lie group. Consider an Hamiltonian action $\Psi : G \times M \to M$ of G on M and let M^G be the fixed points of this action. Denote the moment map associated with this action by $\mu : M \to \mathfrak{g}^*$. Then we have the following:*

- *$\mu(M^G)$ is finite*
- *$\mu(M) = \mathrm{conv}\,\mu(M^G)$*

Hence it follows that $\Delta_\mu = \mu(M)$ is a convex polytope, which is called the moment polytope *of M.*

Let us see a simple example of the moment map and the Abelian convexity theorem. Consider the unit sphere $M = S^2$ equipped with the canonical symplectic form $\omega_c = \mathrm{d}\,x \wedge \mathrm{d}\,y = \mathrm{d}\,\theta \wedge \mathrm{d}\,z$, where we have used cylindrical coordinates. This gives rise to the symplectic manifold (S^2, ω_c). In quantum mechanics one can think about the Bloch sphere instead. Consider then the group action of the circle group $G = T$ by rotations on our manifold. This action has associated vector field $X = \frac{\partial}{\partial \theta}$ (see Fig. A.4). This vector field is Hamiltonian

$$\iota_X \omega_c = \mathrm{d}\,z = \mathrm{d}\,H \tag{A.25}$$

with Hamiltonian function $H = z$. Note that the two poles are the fixed points of the action $M^G = \{|0\rangle, |1\rangle\}$. The image of the fixed points is $\mu(M^G) = \{0, 1\}$, while the image of the manifold under the moment map is $\mu(M) = [-1, 1]$. Hence $\mu(M) = \mathrm{conv}\,\mu(M^G)$, in accordance with theorem 54 (see Fig A.5).

One good example on the usage of theorem 54 is in proving, in a straightforward way, Schur-Horn's theorem, which characterizes the diagonal elements of Hermitian matrices with respect to their spectra [172].

A.5.3 Non-Abelian moment map

For the non-Abelian case, the image of the moment map, unlike before, is not necessarily convex. However, the intersection of the image of the moment map with the positive Weyl chamber does give us a convex polytope called the *moment polytope* or *Kirwan polytope*

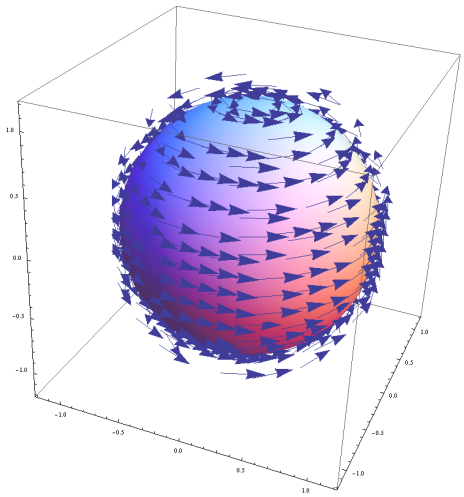

Figure A.4: Vector field $X = \dfrac{\partial}{\partial\theta}$ on the sphere S^2.

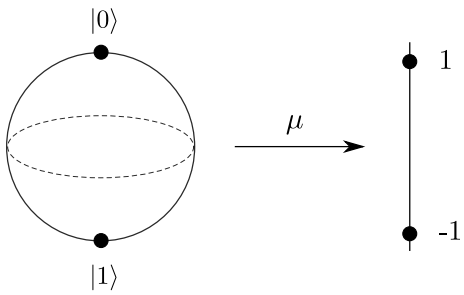

Figure A.5: Moment map induced by the action of the circle group T by rotations on the sphere S^2.

Theorem 55 (Non abelian convexity theorem (Kirwan [16]))**.** *Let G be a compact connected group that has an Hamiltonian action on a compact connected symplectic manifold M. Let the moment map associated with this action be given by $\mu : M \to \mathfrak{g}^*$. Let t_+^* denote the positive Weyl chamber of the dual of the Lie algebra of the maximal torus T of G. Then,*

$$\Delta(M)_\mu = \mu(M) \cap t_+^* \tag{A.26}$$

is a convex polytope.

Where we have used the definition of *maximal torus*.

Definition 56. *The maximal torus T of a group G is the maximal Abelian subgroup of G.*

For the particular case of $U(n)$ the maximal torus are the unitary diagonal matrices

$$T = \{\mathrm{diag}\left(\mathrm{e}^{\mathrm{i}\alpha_1} \dots \mathrm{e}^{\mathrm{i}\alpha_n}\right) | \alpha_1, \dots \alpha_n \in \mathbb{R}\} \tag{A.27}$$

There is some freedom in choosing the positive Weyl chamber. In our case and in the case of $U(n)$, we take the positive Weyl chamber of the dual of the Lie algebra of T to be those diagonal matrices whose entries are ordered non-increasingly.

This theorem can be used, for example, to prove Horn's theorem which characterizes the spectrum of the sum of two Hermitian matrices A, B with respect to the spectra of A and B [172].

A.6 Convexity of the spectra of 1-RDMs

Let us now connect the previous results with the quantum univariate marginal problem. This discussion is based on [9].

Let $\mathcal{H}$ be a Hilbert space of dimension d and consider an observable $O = \mathrm{i}A$ on this Hilbert space. The operator A is anti-Hermitian and traceless, hence $A \in \mathfrak{su}(d)$. From this Hilbert space we can consider the projective space $\mathcal{P}(H) = \{\rho = |\psi\rangle\langle\psi| \mid |\psi\rangle \in \mathcal{H}\}$, which is simply the set of pure states on $\mathcal{H}$ and a smooth manifold. Consider now the functional $-\mathrm{i}\,\mathrm{tr}(\cdot\rho) \in \mathfrak{g}^* \cong \mathfrak{su}^*(d)$. One can clearly establish an isomorphism between this functional and ρ. Moreover, using $\langle \cdot, \square \rangle := \mathrm{tr}(\cdot, \square)$ as the natural pairing between $\mathfrak{g}$ and $\mathfrak{g}^*$ the map $\mu(\rho) : \mathbb{P}(\mathcal{H}) \to \mathfrak{su}^*(d)$ defined by

$$\langle \mu(\rho), A \rangle := -\mathrm{i}\,\mathrm{tr}(A\rho) \quad A \in \mathfrak{g} \tag{A.28}$$

is a moment map (cf. Section A.5.1). Note that $-\mathrm{i}\,\mathrm{tr}(A\rho) = \mathrm{tr}(O\rho)$, the average value of O.

Let us now introduce subsystems. We start by considering the case of N distinguishable particles. In this case the Hilbert space is given by the tensor product $\mathcal{H} = \bigotimes_{i=1}^N \mathcal{H}_i$ where

Setting	Hilbert space $\mathcal{H}$	Group G
N distinguishable particles	$\mathbb{C}^{d_1} \otimes \ldots \otimes \mathbb{C}^{d_N}$	$\mathrm{SU}(d_1) \times \ldots \times \mathrm{SU}(d_N)$
N bosons	$\mathrm{Sym}^N\left(\mathbb{C}^d\right)$	$\mathrm{SU}(d)$
N Fermions	$\Lambda^N\left(\mathbb{C}^d\right)$	$\mathrm{SU}(d)$
n-mode Fermionic Fock space	$\mathcal{F}_n = \oplus_{i=1}^n \Lambda^i\left(\mathbb{C}^d\right)$	$\oplus_{i=1}^n \mathrm{SU}(d)$

Table A.2: The quantum marginal problem is modeled by the action of G on $\mathcal{H}$. (adapted from [9])

$\mathcal{H}_i$ is the Hilbert space of the ith particle. In this case the ith 1-RDM is defined by

$$\mathrm{tr}(O_j \rho_j) := \mathrm{tr}(\mathbb{1}_{\mathcal{H}_1 \otimes \ldots \otimes \mathcal{H}_{j-1}} \otimes O_j \otimes \mathbb{1}_{\mathcal{H}_{j+1} \otimes \ldots \otimes \mathcal{H}_N}), \quad \forall O_j,\, j = 1, \ldots N \tag{A.29}$$

where O_j is an observable on $\mathcal{H}_j$. We embed $SU(\mathcal{H}_j)$ into $SU(\mathcal{H})$ through the map $U_j \mapsto \mathbb{1}_{\mathcal{H} \otimes \ldots \otimes \mathcal{H}} \otimes U_j \otimes \mathbb{1}_{\mathcal{H} \otimes \ldots \otimes \mathcal{H}}$. This in turn induces a restriction the Lie algebra level and on the level of its dual as well. Via Eq. (A.28), this gives rise to the map $\rho \mapsto \rho_j$. By considering $j = 1, \ldots N$, one can send ρ to all corresponding 1-RDMs, which by our previous discussion is the same as computing the moment polytope $\Delta_\mu(\mathbb{P}(\mathcal{H}))$ associated with the Hamiltonian action of $G = SU(\mathcal{H}_1) \otimes \ldots \otimes SU(\mathcal{H}_N)$ with moment map given by Eq. A.28 and hence the solution to the pure univariate quantum marginal problem, for distinguishable particles, is a convex polytope.

For indistinguishable particles the discussion is similar and can be found in [9], so we refrain from discussing it here. The case of Fermionic Fock space is treated in Chapter 5. For all these cases, the difference is in the Hilbert space $\mathcal{H}$ and the group G acting on our coadjoint orbit. On Table A.2 we summarize these differences.

Appendix B

Group action

This chapter serves as a very elementary introduction to group actions, which play a very important role in mathematics and physics by serving the purpose of characterizing symmetries of objects using the language of group theory.

B.1 Action on sets

Let G be a group and X a set. Then a left group action of G on X is a map $\Phi : G \times X \to X$ such that

- $\Phi\left(g, \Phi(h, x)\right) = \Phi\left(gh, x\right), \quad \forall g, h \in G, \forall x \in X$
- $\Phi(e, x) = x$

For simplicity one often writes $\Phi(g, x) := g.x$. One can identically define a right group action $\Phi : X \times G \to X$

- $\Phi\left(\Phi(x, h), g\right) = \Phi\left(x, hg\right), \quad \forall g, h \in G, \forall x \in X$
- $\Phi(x, e) = x$

written as $\Phi(x, g) := x.g$ One can identify left and right group actions by considering the map $x.g^{-1} := g.x$. Hence there's no loss of generality in considering left actions alone and this is what we shall do onwards. The action of a group G on a set X is commonly referred to as *G-action*.

An example of a very important group action is *action by conjugation* defined as $g.x = gxg^{-1}$. That this is indeed a group action is trivial to check:

$$\begin{aligned} g_1.(g_2.x) &= g_1.(g_2 x g_2^{-1}) \\ &= g_1(g_2 x g_2^{-1})g_1^{-1} \\ &= g_1 g_2 x (g_1 g_2)^{-1} \\ &= (g_1 g_2).x \end{aligned} \tag{B.1}$$

Also, trivially $exe^{-1} = x$. Hence action by conjugation is a group action.

An important thing to remark is that the action of a group G on a set X is isomorphic to the group homomorphisms $G \to \mathrm{Sym}X$,

Proof. Let us write define the endomorphism $\pi_g : X \to X$ by $\pi_g(x) := g.x$ Then $g_1.(g_2.x) = (g_1 g_2).x$ for all x implies that $\pi_{g_1} \circ \pi_{g_2} = \pi_{g_1 g_2}$. Also, $e.x = x$ implies that π_e is the identity on X. From here it follows that $\pi_g \circ \pi_{g^{-1}} = \pi_e$. Hence one has $\pi_g \in \mathrm{Sym}(X)$ and the map $G \to \mathrm{Sym}$ given by $g \mapsto \pi_g$ is a group homomorphism. Conversely consider the homomorphism $f : G \to \mathrm{Sym}(X)$. Hence $f(g) =: \pi_g$ gives us a permutation of the set X and since f is an homomorphism we have $\pi_{g_2 g_1} = \pi_{g_1} \circ \pi_{g_2}$. Performing the identification $g.x =: \pi_g(x)$ we identify the action of a permutation as a group action. That this is a valid group action follows trivially from the fact that f is a homomorphism. □

If a set X admits a group action Ψ of G, the tuple (X, G, Φ) is called a *G-set*.

B.2 Action on manifolds

The action of a Lie group on a manifold is $\Phi : G \times M \to M$ is a map similar to the group action described above except that we now require this map to be smooth.

The analogue of the above homomorphism in this case is $\Phi : G \to \mathrm{Diff}(M)$, where Diff denote the group of diffeomorphisms on M. So in this case, instead of the group of permutations on M we have the group of diffeomorphisms on M, the continuous analogue.

If a manifold M admits a group action of G, the tuple (M, G, Φ) is called a *G-manifold* (in topology it is known as *G-space*).

B.3 Orbits and stabilizers

Let us begin by defining the orbit of a group. Consider the action of a group G on a set X, given by $G.X$. The *orbit* of $x \in X$ under the action of G is

$$G.x = \{g.x | g \in G\} \tag{B.2}$$

i.e. the elements of X to which x is mapped under G.

We note here, without proof, that the orbits of G on X define a partition of X and so define equivalence classes: $x, y \in X$ are equivalent if and only if their orbit under G are the same.

The *fixed points of the action*, denoted by X^G, is the set of points $x \in X$ that are invariant under the action of G

$$X^G = \{x \in X | G.x = x\}. \tag{B.3}$$

The *stabilizer subgroup* of $x \in X$ is the subgroup of G that fixes x, i.e.,

$$G_x = \{g \in G | g.x = x\}. \tag{B.4}$$

As a simple example of these concepts, let us consider the action of $SO(2)$, the group of rotations on the plane, on $\mathbb{R}^2$ (see Fig B.1). Note that the orbit of every point are circles centered at the origin. The point (0,0) is the only fixed point of the action and the stabilizer subgroup is trivial, i.e. $G_x = \{e\}$ for all points except the origin, for which it is the entire group.

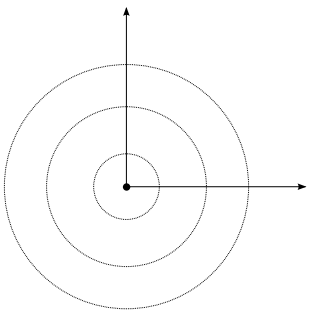

Figure B.1: Action of SO(2) on $\mathbb{R}^2$. The doted circles are the orbits while the dot at the center is the only fixed point of the action.

Appendix C

Bogoliubov transformation and BCS

In condensed matter physics, namely in BCS theory one is interested in *electron pairing*. As such, the BCS ground state is a linear combination of states living in Fock layers containing an *even* number of particles. This means that in BCS theory one consider only $O \in SO(2n)$ and ignores all entirely transformations such that $\det O = -1$. In fact in condensed matter one usually assumes [173, p. 211], [51, p. 177], [174, p. 4],

$$\begin{aligned} U &= U^* \\ V &= -V^* \end{aligned} \tag{C.1}$$

for two modes, labeled by k and $-k$, this reduces to,

$$\begin{aligned} U &= \begin{pmatrix} u_k & 0 \\ 0 & u_{-k} \end{pmatrix} \\ V &= \begin{pmatrix} 0 & v_k \\ v_{-k} & 0 \end{pmatrix} \end{aligned} \tag{C.2}$$

The multi-mode scenario follows trivially.

Appendix D

Results on the spectra of the 1-RDM for some atoms

1	0.99241576
2	0.99241576
3	0.00416068
4	0.00416068
5	0.00114119
6	0.00114119
7	0.00114119
8	0.00114119
9	0.00114119
10	0.00114119

Table D.1: Natural occupation numbers for the ground state of Helium calculated using full-CI and a 6-31++G** basis set.

1	9.99956850e-01
2	9.99899091e-01
3	9.99874121e-01
4	3.24402153e-05
5	3.22779332e-05
6	3.22779332e-05
7	3.22779332e-05
8	3.18761352e-05
9	2.99844510e-05
10	2.99844510e-05
11	2.99844510e-05
12	3.61887485e-06
13	3.61887485e-06
14	3.61887485e-06
15	7.22910383e-07
16	7.22910383e-07
17	7.22910383e-07
18	7.22910383e-07
19	7.22910383e-07
20	7.22891553e-07
21	7.22891553e-07
22	7.22891553e-07
23	7.22891553e-07
24	7.22891553e-07
25	3.63566017e-07
26	3.13443923e-07
27	2.22870198e-08
28	2.22870198e-08
29	2.22870198e-08
30	4.38298977e-09

Table D.2: Natural occupation numbers for the ground state of Lithium calculated using full-CI and a 6-31++G** basis set.

1	9.99758047e-01
2	9.99758047e-01
3	9.03090382e-01
4	9.03090382e-01
5	3.18868732e-02
6	3.18868732e-02
7	3.18868732e-02
8	3.18868732e-02
9	3.18868732e-02
10	3.18868732e-02
11	1.12956124e-03
12	1.12956124e-03
13	1.29508096e-04
14	1.29508096e-04
15	3.24524902e-05
16	3.24524902e-05
17	3.24524902e-05
18	3.24524902e-05
19	3.24524902e-05
20	3.24524902e-05
21	3.24524902e-05
22	3.24524902e-05
23	3.24524902e-05
24	3.24524902e-05
25	2.32064181e-05
26	2.32064181e-05
27	2.32064181e-05
28	2.32064181e-05
29	2.32064181e-05
30	2.32064181e-05

Table D.3: Natural occupation numbers for the ground state of Beryllium calculated using full-CI and a 6-31++G** basis set.

Appendix E

Jordan Wigner transformation

Let us consider a k modes Fock space, $\mathcal{F}_k$. Consider a Fermionic state, with a well defined number of Fermions, in occupation number representation given by (different sources may use a different ordering of the creation operators),

$$|n_1, \ldots, n_k\rangle := (a_1^\dagger)^{n_1} \ldots (a_k^\dagger)^{n_k} |0\rangle \tag{E.1}$$

with $n_i = 0, 1$, the ith mode occupation number. For the sake of completeness, note that an arbitrary Fock state is the linear combination of all such states.

Consider now a system of k qubits, $\mathcal{H} = \left(\mathbb{C}^2\right)^{\otimes k}$ and consider the Pauli operators on the jth qubit, $\{Z_j, Y_j, X_j\}$. These can be written in the computational basis (we omit the subscript indicating the qubit whenever there is no loss of generality),

$$\begin{aligned} Z &= |0\rangle\langle 0| - |1\rangle\langle 1|, \\ Y &= \mathrm{i}\left(\sigma^\dagger - \sigma\right), \\ X &= \sigma + \sigma^\dagger \end{aligned} \tag{E.2}$$

where we have defined the lowering operator $\sigma = |0\rangle\langle 1|$ and the raising operator (its Hermitian conjugate), $\sigma^\dagger$.

Then we can set up an isomorphism between the Fermionic operators and the Pauli operators. It is given by the Jordan-Wigner (J-W) transformation [175]

$$a_j = \otimes_{k=1}^{j-1} Z_k \otimes \sigma_j. \tag{E.3}$$

Using,

$$\begin{aligned} aa^\dagger &= |0\rangle\langle 0|, \\ a^\dagger a &= |1\rangle\langle 1| \end{aligned} \tag{E.4}$$

we can invert the J-W transformation

$$Z_j = a_j a_j^\dagger - a_j^\dagger a_j. \tag{E.5}$$

One also has,

$$\begin{aligned} X_j &= \otimes_{k+1}^{j-1} Z_k \left(a_j + a_j^\dagger\right), \\ Y_j &= -\mathrm{i} \otimes_{k+1}^{j-1} Z_k \left(a_j - a_j^\dagger\right). \end{aligned} \tag{E.6}$$

Consider now the Majorana representation

$$\begin{aligned} c_{2j-1} &:= a_j^\dagger + a_j, \\ c_{2j} &:= -\mathrm{i}\left(a_j^\dagger - a_j\right). \end{aligned} \tag{E.7}$$

Using Majorana operators, and the J-W transformation, we can write.

$$\begin{aligned} X_j &= \otimes_{k+1}^{j-1} Z_k \left(c_{2j-1}\right), \\ Y_j &= -\otimes_{k+1}^{j-1} Z_k \left(c_{2j}\right), \\ Z_j &= -\mathrm{i} X_j Y_j = \mathrm{i} c_{2j-1} c_{2j} \end{aligned} \tag{E.8}$$

where in the last equation we used the fact that $Z^2 = \mathbb{1}$.

Appendix F

Basis expansion of a qubit density matrix

Consider the density matrix for a single qubit $\rho \in L(\mathbb{C}^2, \mathbb{C}^2) \cong \mathbb{C}^4$. Let $b = \left\{\sigma_0 = \mathbb{1}, \sigma_1 = X, \sigma_2 = Y, \sigma_3 = Z\right\}, \sigma_i \in L(\mathbb{C}^2, \mathbb{C}^2)$. Then since these operators are linearly independent and the cardinality of b equals the cardinality of $\mathbb{C}^4$, these operators constitute a basis for our space. We can then write,

$$\rho = \frac{1}{2}\sum_{i=0}^{3} = c_i\sigma_i, c_i \in \mathbb{C}. \tag{F.1}$$

Introducing the Hilbert Schmidt inner product between two operators, $(A, B) := \operatorname{tr} A^\dagger B$, it is easy to see that our basis b is actually orthogonal. In fact $(\sigma_i, \sigma_j) = 2\delta_{i,j}$. Then we can write,

$$\rho = \sum_{i=0}^{3} \frac{1}{2}\left(\sigma_i, \rho\right)\sigma_i. \tag{F.2}$$

Since our basis operators are Hermitian, $(\sigma_i, \rho) = \langle\sigma_i\rangle$. Therefore, if $\langle X\rangle = \langle Y\rangle = 0$ we have that ρ is diagonal in the spin basis $\{|0\rangle, |1\rangle\}$ of $\mathbb{C}^2$. Furthermore, let $\operatorname{spec}\rho = (\lambda_{\max}, \lambda_{\min})$. Then for a diagonal ρ, we have $\langle Z\rangle = \lambda_{\max} - \lambda_{\min}$.

This result is easily extended to an n qubit system by expanding,

$$\rho = \frac{1}{2^n}\sum_{i_1,\ldots i_n=0}^{3} c_{i_1,\ldots i_n}\sigma_{i_1} \otimes \ldots \otimes \sigma_{i_n} \tag{F.3}$$

and we conclude that rho is diagonal if $\langle X_j\rangle = \langle Y_j\rangle$. Moreover if ρ is diagonal and its reduced spectra are $\operatorname{spec}\operatorname{tr}_{\setminus i}\rho = (\lambda_i^{\min}, \lambda_i^{\max})$, then $\langle Z_i\rangle = \lambda_i^{\max} - \lambda_i^{\min}$.

Appendix G

Zoo of decision problems: physical interpretation and reductions

This section strives to be as self contained as possible. As such we will repeat some of the notions and derivations already in the main text.

Consider the following scenario: A system of n qubits in a pure state $|\psi\rangle$. Consider now the local reductions obtained by tracing out all qubits except the ith ones. By the necessity of Higuchi's conditions [6], since our state is pure we must have,

$$\lambda_i^{\min} \leq \sum_{j \neq i} \lambda_j^{\min}, \ \forall i. \tag{G.1}$$

Now, considering our spectra to be ordered simply as a matter of convenience (and without any loss of generality), we reduce our problem to the following inequality

$$\lambda_1 \leq \sum_{i=1}^{n} \lambda_i. \tag{G.2}$$

We can now ask the very natural question: Imagine you perform only local measurements and obtain the local spectra of the system. Is this local spectra compatible with a bi-separable state? This can be cast formally into the following decision problem

BISEPARABILITY

INSTANCE: A set of n numbers $\lambda_1, \ldots \lambda_n$ satisfying $\lambda_i \in [0, 0.5]$, $\lambda_i \leq \lambda_{i+1}$, $\lambda_1 \leq \sum_{i=2}^{n} \lambda_i$.

QUESTION: Is there $S_1 \subsetneq S = \{1, \cdots, n\}$, $1 \in S_1$, such that $\lambda_1 \leq \sum_{1 \neq i \in S_1} \lambda_i$ and $\lambda_k \leq \sum_{i \in S_1^C} \lambda_i$, where $\lambda_k = \max_{k \neq i \in S_1^C} \lambda_i$?

One can now ask what the computational complexity of this problem is. While we have no concise answer, we strongly suspect the problem to be NP-hard.

We can, however formulate a series of related problems for which we can decide their computational complexity.

Let us imagine the following scenario: Consider again a set of n qubits and a globally pure state. Without loss of generality assume that the local spectra is ordered non increasingly. By this definition qubit one has the largest minimal local eigenvalue. For simplicity, let's say that we give this first qubit to Alice. Now choose one of the other qubits, say b, and give it to Bob. We can now ask, is this local spectra compatible with a bi-separable state such that Alice's and Bob's qubits belong to different tensor factors of our global state ψ and such that Bob's qubit has the largest minimal local eigenvalue in its tensor factor? This can be formally stated as the following decision problem.

BISEP-LARGEST-B

INSTANCE: A set of $n+1$ numbers $\lambda_1, \dots \lambda_n, b$ satisfying $\lambda_i \in [0, 0.5]$, $\lambda_i \leq \lambda_{i+1}$, $\lambda_1 \leq \sum_{i=2}^{n} \lambda_i$.

QUESTION: Is there $S_1 \subsetneq S = \{1, \cdots, n\}$, $1 \in S_1$ such that $\lambda_1 \leq \sum_{1 \neq i \in S_1} \lambda_i$ and $\lambda_b \leq \sum_{i \in S \setminus S_1} \lambda_i$

Although not a very natural problem, we will, in an instant connect it to more relevant ones.

Consider again a set of n qubits and a globally pure state $|\psi\rangle$. Again we will consider only the minimal eigenvalues of the local reductions, which are taken to be non increasingly ordered. Now choose two qubits. Give one, call it a, to Alice and give another one, call it b, to Bob. We now ask the following question: looking at local spectral information alone, can we certify that a and b are part of one genuinely entangled subsystem? We have discussed this setting in the previous chapter where we have said that it can can be formally stated as the following decision problem.

BISEP-AB

INSTANCE: A set of $n+2$ numbers $\lambda_1, \dots \lambda_n, a, b$ satisfying $\lambda_i \in [0, 0.5]$, $\lambda_i \geq \lambda_{i+1}$, $\lambda_1 \leq \sum_{i=2}^{n} \lambda_i$.

QUESTION: Is there $S_1 \subsetneq S = \{1, \cdots, n\}$, $1 \in S_1$ such that $\lambda_1 \leq \sum_{1 \neq i \in S_1} \lambda_i$ and $\lambda_k \leq \sum_{k \neq i \in S_1^c} \lambda_i$, $\lambda_k = \max_{i \in S_1^c} \lambda_i$ with $\lambda_a \in S_1$ and $\lambda_b \in S_1^c$?

We now proceed to connect all the above mentioned problems. We begin by connecting

BISEPARABILITY and BISEP-LARGEST-B through the following lemma.

Lemma 57. *BISEPARABILITY* $\leq_P$ *BISEP-LARGEST-B*

Proof. Consider a general instance of BISEP-LARGEST-B, BISEP-LARGEST-B$(\lambda_1, \ldots, \lambda_n, b)$. Let us now assume that we posses an oracle which can decide BISEP-LARGEST-B in a single operation. Then, by querying the oracle for all possible values of $b = 2, \ldots n$, it can decide BISEPARABILITY in a polynomial number of operations.

Hence we have that BISEPARABILITY $\leq_P$ BISEP-LARGEST-B. □

We are now in position to prove the following lemma concerning the computational complexity of BISEP-LARGEST-B.

Lemma 58. *PARTITION* $\leq_P$ *BISEP-LARGEST-B*

Proof. Consider a general instance of $\mathbb{Q}$-PARTITION, $\mathbb{Q}$-PARTITION$(\omega_1, \ldots, \omega_m)$. If $\omega_1 > \sum_{i=2}^{m} \omega_i$ then there is no way of satisfying $\mathbb{Q}$-PARTITION. This can obviously be checked in polynomial time. We now proceed to show that every instance of $\mathbb{Q}$-PARTITION, such that $\omega_1 \leq \sum_{i=2}^{m} \omega_i$ reduces, polynomially, to an instance of BISEP-LARGEST-B. To do so, let us establish the following definitions,

$$\begin{aligned} \lambda_1 := \lambda_2 &:= \frac{1}{2\omega_1 m}\left(\sum_{i=1}^{m} \frac{\omega_i}{2}\right), \\ \lambda_i &:= \frac{\omega_{i-2}}{2\omega_1 m}, i = 3 \ldots, n, \\ n &:= m + 2, \\ b &:= 2. \end{aligned} \tag{G.3}$$

Using these definitions we have

$$\begin{aligned} \sum_{i=2}^{m} \omega_i &\geq \omega_1 \\ \sum_{i=1}^{m} \omega_i &\geq 2\omega_1 \\ \frac{1}{2\omega_1 m}\left(\sum_{i=1}^{m} \frac{\omega_i}{2}\right) &\geq \lambda_3 \\ \lambda_1 = \lambda_2 &\geq \lambda_3. \end{aligned} \tag{G.4}$$

Given this, which also implies $\lambda_1 \leq \sum_{i=2}^{n} \lambda_i$, and since $\lambda_i \in [0, 0.5], i = 1, \ldots, n$ and $\lambda_i \geq \lambda_{i+1}, i = 3, \ldots, n$ by construction, then the set $\{\lambda_1, \ldots, \lambda_n, b = 2\}$ is a valid instance of BISEP-LARGEST-B. Consider our original BISEP-LARGEST-B problem, deciding whether there

exists an $S_1 \subsetneq S = \{1, \dots n\}$ with $1 \in S_1$ such that $\lambda_1 \leq \sum_{1 \neq i \in S_1} \lambda_i$ and $\lambda_b \leq \sum_{b \neq i \in S_1^c} \lambda_i$, with $\lambda_b \in S_1^c$. Then we have

$$\begin{aligned} \lambda_1 &\leq \sum_{1 \neq i \in S_1} \lambda_i, \\ \lambda_2 &\leq \sum_{2 \neq i \in S_1^c} \lambda_i. \end{aligned} \tag{G.5}$$

Now, using Eq. (G.3) we can transform this into

$$\begin{aligned} \frac{1}{2\omega_1 m} \left(\sum_{j=1}^{m} \frac{\omega_j}{2} \right) &\leq \sum_{1 \neq i \in S_1} \frac{\omega_{i-2}}{2\omega_1 m}, \\ \frac{1}{2\omega_1 m} \left(\sum_{j=1}^{m} \frac{\omega_j}{2} \right) &\leq \sum_{2 \neq i \in S_1^c} \frac{\omega_{i-2}}{2\omega_1 m}. \end{aligned} \tag{G.6}$$

Taking $B = \{1, \dots, n\}$ and $A = \{j \in B | j + 2 \in S_1\}$, then $A \subset B$ and its complement in B is $A^c = \{j \in B | j + 2 \in S_1^c\}$. Using this fact, we can write

$$\begin{aligned} \frac{1}{2\omega_1 m} \left(\sum_{j \in B} \frac{\omega_j}{2} \right) &\leq \sum_{j \in A} \frac{\omega_j}{2\omega_1 m}, \\ \frac{1}{2\omega_1 m} \left(\sum_{j \in B} \frac{\omega_j}{2} \right) &\leq \sum_{j \in A^c} \frac{\omega_j}{2\omega_1 m}. \end{aligned} \tag{G.7}$$

Now, using the fact that $\sum_{j \in B} \cdot = \sum_{j \in A} \cdot + \sum_{j \in A^c} \cdot$,

$$\begin{aligned} \sum_{j \in B} \frac{\omega_j}{2} &\leq \sum_{j \in A} \omega_j \\ \sum_{j \in B} \frac{\omega_j}{2} &\geq \sum_{j \in A} \omega_j \end{aligned} \tag{G.8}$$

which means that

$$\sum_{j \in B} \frac{\omega_j}{2} \leq \sum_{j \in A} \omega_j \leq \sum_{j \in B} \frac{\omega_j}{2} \tag{G.9}$$

and consequently

$$\sum_{j \in A^c} \omega_j = \sum_{j \in A} \omega_j. \tag{G.10}$$

Which proves that any instance of $\mathbb{Q}$-PARTITION such that $\omega_1 \leq \sum_{i=2}^{m} \omega_i$, reduces to a particular instance, BISEP-AB$(\lambda_1, \dots, \lambda_n, a, b)$, of BISEP-LARGEST-B. Given that all other instances of $\mathbb{Q}$-PARTITION can be decided in polynomial time, we have $\mathbb{Q}$-PARTITION $\leq_P$

BISEP-LARGEST-B. Since PARTITION $\leq_P$ $\mathbb{Q}$-PARTITION it follows that PARTITION $\leq_P$ BISEP-LARGEST-B. □

In fact since one can easily see that BISEP-LARGEST-B $\in$ NP, which, given the lemma above, implies the stronger statement that BISEP-LARGEST-B $\in$ NP-complete.

We now finally prove the following lemma relating BISEPARABILITY and BISEP-AB,

Lemma 59. *BISEPARABILITY* $\leq_P$ *BISEP-AB*

Proof. Consider a general instance of BISEP-AB, BISEP-AB$(\lambda_1, \ldots, \lambda_n, a, b)$ Let us assume that we posses an oracle which can decide BISEP-AB in a single operation. Then querying the oracle for $a = 1$ and all possible values of $b = 2, \ldots, n$ it can decide BISEPARABILITY in a polynomial number of operations

Hence we have that BISEPARABILITY $\leq_P$ BISEP-AB. □

Hence we arrive at a series of reductions relating our problems, as shown in Fig. G.1.

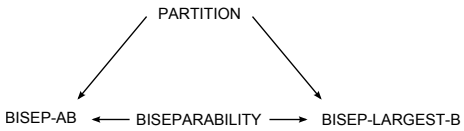

Figure G.1: Reduction tree for our decision problems.

Appendix H

Conductance equations through a non interacting quantum ring

In this chapter we present a simple method for calculating the conductance through a non interacting quantum ring connected to two semi-infinite leads and threaded by a magnetic flux ϕ. The work presented here has been done in collaboration with Bruno Zeferino António and Ricardo Guimarães Dias and has been published in [176].

Our system is composed by a tight-binding cluster with N sites connected to 2 semi-infinite 1D leads modeled as 1D tight-binding semi-chains. The system Hamiltonian is the sum of the leads and cluster Hamiltonians, H_0, and the coupling between each lead and the cluster, V_{LR},

$$H = H_0 + V_{LR}, \tag{H.1}$$

with

$$H_0 = \underbrace{-\sum_{j=-\infty}^{0}(|j-1\rangle\langle j| + \text{H.c.})}_{\text{left lead}} \underbrace{-\sum_{j=N+1}^{\infty}(|j\rangle\langle j+1| + \text{H.c.})}_{\text{right lead}} + \underbrace{H_S}_{\text{cluster}} \tag{H.2}$$

where H_s is the single-particle Hamiltonian in the scattering region (the cluster) and $|j\rangle$ is the Wannier state localized on the atomic site j. The leads connected to the cluster are considered ideal with nearest-neighbor hopping $t = 1$. The coupling V_{LR} between the leads and the cluster is given by

$$V_{LR} = -t_L|0\rangle\langle L| - t_R|R\rangle\langle N+1| + \text{H.c.}, \tag{H.3}$$

where the hopping matrix elements t_L and t_R connect the left and right leads, respectively, to the cluster sites L and R. The Hamiltonian of the cluster is

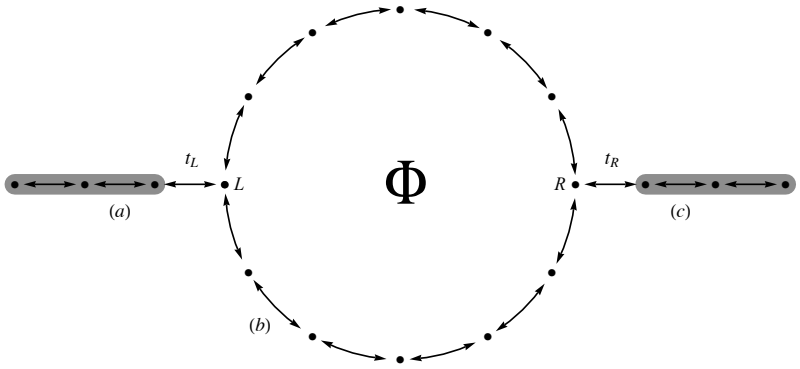

Figure H.1: Schematic representation of the studied systems. In (a) and (c) one has the left and right semi-infinite 1D leads, respectively. These leads are considered to be perfect conductors. In (b), we show the cluster described by a tight-binding model. The hopping factors which couple the left and right leads to the cluster are, respectively, t_L and t_R.

$$H_S = \sum_j \epsilon_j |j\rangle\langle j| - \sum_{ij, i\neq j} \left(t_{ij} e^{i\phi_{ij}} |i\rangle\langle j| + \text{H.c.} \right) \tag{H.4}$$

where the indices i and j run over all cluster sites. For a general gauge and an arbitrary geometry of the cluster, the phase shifts ϕ_{ij} in the hopping factors between sites $\mathbf{r}_i = \mathbf{a}$ and $\mathbf{r}_j = \mathbf{b}$ are determined from $\phi_{ij} = -\frac{e}{\hbar} \int_{\mathbf{a}}^{\mathbf{b}} \mathbf{A}.d\mathbf{r}$ where the integral is a standard line integral of the vector potential $\mathbf{A}$ along the line segment which links sites a and b. The tight-binding Hamiltonian of a ring of N sites enclosing an external magnetic flux can be expressed as

$$H_S = \sum_{j=1}^{N} \epsilon_j |j\rangle\langle j| - \sum_{j=1}^{N} t \left(e^{i\phi'/N} |j\rangle\langle j+1| + e^{-i\phi'/N} |j+1\rangle\langle j| \right) \tag{H.5}$$

where $\phi' = 2\pi\Phi/\Phi_0$ is the reduced flux, ϵ_j is the on-site energy, t is the hopping integral between two nearest neighbor sites, and $\Phi_0 = h/e$ is the flux quantum

The hoppings t_L and t_R generate finite transmission probability across the cluster. Since no two-particle interactions are considered in our case, the transmission probability $|t(\epsilon_k)|^2$ for an incident particle with momentum k and energy $\epsilon_k = -2\cos(k)$ can be calculated solving directly the respective eigenvector equation for the tight-binding Hamiltonian, $\hat{H}|\Psi_k\rangle = \epsilon_k|\Psi_k\rangle$. This method is similar to that followed in the determination of the band structure of a tight-binding model, which is usually taught in a undergraduate Solid State course. Since $|\Psi_k\rangle = \sum_{n=\infty}^{\infty} \psi_n |n\rangle$ where ψ_n is the eigenfunction amplitude at site n, the eigenvector equation can be written as a matrix equation $[H](\psi) = \epsilon_k(\psi)$, where (ψ) is the column vector of the eigenfunction amplitudes ψ_n and $[H]$ is the matrix representation of the Hamiltonian in the Wannier function basis $\{|n\rangle\}$. This matrix equation is equivalent to an infinite system of linear equations (the number of equations is equal to the number of sites which is infinite in

our system) of the form

$$\epsilon_k \psi_n = \sum_{m=-\infty}^{\infty} H_{nm} \psi_m \tag{H.6}$$

where $H_{nm} = \langle n|\hat{H}|m\rangle$. The matrix element H_{nm} is zero except if the site m is a nearest-neighbor of site n. One should now recall that our system is constituted by the left lead, the cluster and the right lead. If $t_L = t_R = 0$, the system of equations decouples into three independent sets of equations and the particle can be restricted to one of the three regions. For instance, the eigenvectors and eigenvalues when the particle is confined to the cluster are obtained from $[H_S](\psi_S) = \omega(\psi_S)$ where (ψ_S) is the column vector of the eigenfunction amplitudes at the cluster sites and the corresponding equations in the case of the tight-binding ring are of the form

$$\omega\psi_j = \epsilon_j \psi_j - te^{i\phi'/N}\psi_{j+1} - te^{-i\phi'/N}\psi_{j-1} \tag{H.7}$$

where $j = 1, \cdots, N$ and with periodic boundary conditions, $\psi_{N+1} = \psi_1$.

Let us now assume finite t_L and t_R. Since we are interested in the transmission probability of a right-moving particle, we can limit our study to states with energy $\omega_k = -2\cos(k)$ which can be written as an incident wave plus the respective reflected wave on the left lead and a transmitted wave on the right lead. This implies that the equations for the wavefunction amplitude at any site j of the leads (with $j < 0$ or $j > N + 1$),

$$\omega_k \psi_j = -\psi_{j+1} - \psi_{j-1}, \tag{H.8}$$

are automatically satisfied if the wavefunction in the leads is of the form

$$\psi_j = e^{ikj} + \psi_r e^{-ikj}, \qquad j \leq 0, \tag{H.9}$$

$$\psi_j = \psi_t e^{ikj}, \qquad j \geq N + 1, \tag{H.10}$$

where ψ_r and ψ_t are the amplitudes of the reflected and transmitted waves, respectively. So these equations can be dropped from the the global system of equations. We are left with the equations for the amplitudes at sites 0 and $N+1$ which involve the hopping constants t_L and t_R and depend on the amplitudes ψ_L and ψ_R at the sites L and R of the ring,

$$\omega_k \psi_0 = -t_L \psi_L - \psi_{-1}, \tag{H.11}$$

$$\omega_k \psi_{N+1} = -\psi_{N+2} - t_R \psi_R. \tag{H.12}$$

The amplitude equations for the cluster sites remain the same when t_L and t_R are finite, that is, $[H_S](\psi_S) = \omega_k(\psi_S)$, except for the equations corresponding to sites L and R which have

an additional term $-t_L\psi_0$ and $-t_R\psi_{N+1}$ and are given by

$$\omega_k\psi_L = -t_L\psi_0 + \epsilon_L\psi_L - te^{i\phi'/N}\psi_{L+1} - te^{-i\phi'/N}\psi_{L-1}, \tag{H.13}$$

$$\omega_k\psi_R = -t_R\psi_{N+1} + \epsilon_R\psi_R - te^{i\phi'/N}\psi_{R+1} - te^{-i\phi'/N}\psi_{R-1}. \tag{H.14}$$

The solution of this set of $N+2$ equations (that is, Eqs. H.7, H.11, H.12, H.13, and H.14) allows us to determine ψ_t and ψ_r. Note that ψ_0, ψ_{-1}, ψ_{N+1} and ψ_{N+2} are given by Eqs. H.9 and H.10 and are functions of ψ_r and ψ_t, therefore we have $N+2$ variables. The transmission probability is then given by the square of the absolute value of the ratio between the amplitude of the outgoing wave ψ_t and the amplitude of the incident wave (which we have assumed to be 1).

Bibliography

[1] Alexander Klyachko. Quantum marginal problem and representations of the symmetric group. *arXiv:quant-ph/0409113*, September 2004.

[2] A. J. Coleman and V. I. Yukalov. *Reduced Density Matrices: Coulson's Challenge*. Springer, 2000 edition, May 2000.

[3] A. Yu Kitaev, A. H. Shen, and M. N. Vyalyi. *Classical and Quantum Computation*. Amer Mathematical Society, May 2002.

[4] Julia Kempe, Alexei Kitaev, and Oded Regev. The complexity of the local hamiltonian problem. In Kamal Lodaya and Meena Mahajan, editors, *FSTTCS 2004: Foundations of Software Technology and Theoretical Computer Science*, number 3328 in Lecture Notes in Computer Science, pages 372–383. Springer Berlin Heidelberg, January 2005.

[5] Yi-Kai Liu, Matthias Christandl, and F. Verstraete. Quantum computational complexity of the n-representability problem: QMA complete. *Phys. Rev. Lett.*, 98(11):110503, March 2007.

[6] A. Higuchi, A. Sudbery, and J. Szulc. One-qubit reduced states of a pure many-qubit state: Polygon inequalities. *Phys. Rev. Lett.*, 90(10):107902, March 2003.

[7] Sergey Bravyi. Requirements for compatibility between local and multipartite quantum states. *Quantum Info. Comput.*, 4(1):12–26, January 2004.

[8] Matthias Christandl, Aram W. Harrow, and Graeme Mitchison. Nonzero kronecker coefficients and what they tell us about spectra. *Commun. Math. Phys.*, 270(3):575–585, March 2007.

[9] Matthias Christandl, Brent Doran, Stavros Kousidis, and Michael Walter. Eigenvalue distributions of reduced density matrices. *Commun. Math. Phys.*, 332(1):1–52, November 2014.

[10] Michael Walter, Brent Doran, David Gross, and Matthias Christandl. Entanglement polytopes: Multiparticle entanglement from single-particle information. *Science*, 340(6137):1205–1208, June 2013.

[11] Alexander A. Klyachko. The pauli exclusion principle and beyond. *arXiv:0904.2009*, April 2009.

[12] Christian Schilling, David Gross, and Matthias Christandl. Pinning of fermionic occupation numbers. *Phys. Rev. Lett.*, 110(4):040404, January 2013.

[13] Adam Sawicki, Michał Oszmaniec, and Marek Kuś. Critical sets of the total variance can detect all stochastic local operations and classical communication classes of multiparticle entanglement. *Phys. Rev. A*, 86(4):040304, October 2012.

[14] Matthias Franz. Moment polytopes of projective **g**-varieties and tensor products of symmetric group representations. *J. Lie Theory*, 12(2):539 – 549, 2002.

[15] Alexander A. Klyachko. Quantum marginal problem and n-representability. *J. Phys.: Conf. Ser.*, 36(1):72, April 2006.

[16] Frances Kirwan. Convexity properties of the moment mapping, III. *Invent Math*, 77(3):547–552, October 1984.

[17] H. Witała, W. Glöckle, D. Hüber, J. Golak, and H. Kamada. Cross section minima in elastic nd scattering: Possible evidence for three-nucleon force effects. *Phys. Rev. Lett.*, 81(6):1183–1186, August 1998.

[18] David Mazziotti. Significant conditions for the two-electron reduced density matrix from the constructive solution of n representability. *Phys. Rev. A*, 85(6):062507, June 2012.

[19] David Mazziotti. Structure of fermionic density matrices: Complete n-representability conditions. *Phys. Rev. Lett.*, 108(26):263002, June 2012.

[20] Maho Nakata, Hiroshi Nakatsuji, Masahiro Ehara, Mitsuhiro Fukuda, Kazuhide Nakata, and Katsuki Fujisawa. Variational calculations of fermion second-order reduced density matrices by semidefinite programming algorithm. *The Journal of Chemical Physics*, 114(19):8282–8292, May 2001.

[21] Barry Simon. *Representations of Finite and Compact Groups*. American Mathematical Society, Providence, R.I, December 1995.

[22] Sadri Hassani. *Mathematical physics: a modern introduction to its foundations*. Springer, New York, 1999.

[23] Attila Szabo and Neil S. Ostlund. *Modern Quantum Chemistry: Introduction to Advanced Electronic Structure Theory*. Dover Publications, Mineola, N.Y, new edition edition edition, July 1996.

[24] Alexander L. Fetter. *Quantum Theory of Many-Particle Systems*. Dover Publications, Mineola, N.Y, June 2003.

[25] Michael A Nielsen and Isaac L Chuang. *Quantum computation and quantum information*. Cambridge Univ. Press, Cambridge, 2010.

[26] John Schliemann, J. Ignacio Cirac, Marek Kuś, Maciej Lewenstein, and Daniel Loss. Quantum correlations in two-fermion systems. *Phys. Rev. A*, 64(2):022303, July 2001.

[27] Murat Altunbulak and Alexander Klyachko. The pauli principle revisited. *Commun. Math. Phys.*, 282(2):287–322, September 2008.

[28] R. E. Borland and K. Dennis. The conditions on the one-matrix for three-body fermion wavefunctions with one-rank equal to six. *J. Phys. B: At. Mol. Phys.*, 5(1):7, January 1972.

[29] Murat Altunbulak. *The Pauli principle, representation theory, and geometry of flag varieties*. PhD thesis, Bilkent University, July 2008.

[30] R. Cirelli, M. Gatti, and A. Manià. The pure state space of quantum mechanics as Hermitian symmetric space. *Journal of Geometry and Physics*, 45(3–4):267–284, March 2003.

[31] Brian Hall. *Lie Groups, Lie Algebras, and Representations: An Elementary Introduction*. Springer, New York, August 2004.

[32] John B. Conway. *A Course in Functional Analysis*. Springer New York, New York, 2nd edition, February 2010.

[33] Tosio Kato. *Perturbation Theory for Linear Operators*. Springer, Berlin, 2nd edition, October 2013.

[34] Christian Schilling. *Quantum Marginal Problem and its Physical Relevance*. PhD thesis, ETH Zürich, 2014.

[35] Christian Schilling. Quasipinning and its relevance for n-fermion quantum states. *arXiv:1409.0019 [math-ph, physics:quant-ph]*, August 2014.

[36] Josef Stoer and R. Bulirsch. *Introduction to Numerical Analysis*. Springer, New York, 3rd edition, August 2002.

[37] Laimutis Bytautas, Joseph Ivanic, and Klaus Ruedenberg. Split-localized orbitals can yield stronger configuration interaction convergence than natural orbitals. *The Journal of Chemical Physics*, 119(16):8217–8224, October 2003.

[38] Karen L. Schuchardt, Brett T. Didier, Todd Elsethagen, Lisong Sun, Vidhya Gurumoorthi, Jared Chase, Jun Li, and Theresa L. Windus. Basis set exchange: A community database for computational sciences. *J. Chem. Inf. Model.*, 47(3):1045–1052, May 2007.

[39] Rick Muller. PyQuante, 2014.

[40] Gilbert Strang. *Linear Algebra and Its Applications, 4th Edition*. Cengage Learning, Belmont, CA, 4th edition edition, July 2005.

[41] James S. Sims and Stanley A. Hagstrom. High-precision hy–CI variational calculations for the ground state of neutral helium and helium-like ions. *Int. J. Quantum Chem.*, 90(6):1600–1609, January 2002.

[42] Mariusz Puchalski, Dariusz Kedziera, and Krzysztof Pachucki. Ground state of Li and Be+ using explicitly correlated functions. *Phys. Rev. A*, 80(3):032521, September 2009.

[43] James S. Sims and Stanley A. Hagstrom. Hylleraas-configuration-interaction nonrelativistic energies for the 1s ground states of the beryllium isoelectronic sequence. *J Chem Phys*, 140(22):224312, June 2014.

[44] María Belén Ruiz. Hylleraas method for many-electron atoms. i. the hamiltonian. *Int. J. Quantum Chem.*, 101(3):246–260, January 2005.

[45] María Belén Ruiz. Hylleraas method for many-electron atoms. II. integrals over wave functions with one interelectronic coordinate. *Int. J. Quantum Chem.*, 101(3):261–273, January 2005.

[46] Carlos Benavides-Riveros, José Gracia-Bondía, and Michael Springborg. Quasipinning and entanglement in the lithium isoelectronic series. *Phys. Rev. A*, 88(2):022508, August 2013.

[47] Volker Bach. Error bound for the hartree-fock energy of atoms and molecules. *Commun.Math. Phys.*, 147(3):527–548, July 1992.

[48] Jens Eisert, Tomáš Tyc, Terry Rudolph, and Barry C. Sanders. Gaussian quantum marginal problem. *Commun. Math. Phys.*, 280(1):263–280, May 2008.

[49] Sergey Bravyi. Lagrangian representation for fermionic linear optics. *Quantum Info. Comput.*, 5(3):216–238, May 2005.

[50] Jean-Paul Blaizot and Georges Ripka. *Quantum Theory of Finite Systems*. The MIT Press, December 1985.

[51] Charles P Poole. *Superconductivity*. Academic Press, Amsterdam ;London, 2007.

[52] John R. Silvester. Determinants of block matrices. *Math Gaz*, 84(501):460–467, November 2000.

[53] Leite R.S., Richa T.R.W., and Tomei C. Geometric proofs of some theorems of schur-horn type. *Linear Algebra and its Applications*, 286(1):149–173, 1999.

[54] Tin-Yau Tam. Partial superdiagonal elements and singular values of a complex skew-symmetric matrix. *SIAM J. Matrix Anal. Appl.*, 19(3):737–754, July 1998.

[55] Peter D Lax. *Linear algebra and its applications*. Wiley-Interscience, Hoboken, N.J., 2007.

[56] Reinhard F. Werner. Quantum states with einstein-podolsky-rosen correlations admitting a hidden-variable model. *Phys. Rev. A*, 40(8):4277–4281, October 1989.

[57] Jens Eisert and David Gross. Multiparticle entanglement. In Dagmar Bruß and G. Leuchs, editors, *Lectures on Quantum Information*, pages 237–252. Wiley-VCH Verlag GmbH, 2008.

[58] W. Dür, G. Vidal, and J. I. Cirac. Three qubits can be entangled in two inequivalent ways. *Phys. Rev. A*, 62(6):062314, November 2000.

[59] Martin B. Plenio and Shashank Virmani. An introduction to entanglement measures. *Quant. Inf. Comput.*, 7(1,2):001–051, January 2007.

[60] Gilad Gour and Robert W. Spekkens. Entanglement of assistance is not a bipartite measure nor a tripartite monotone. *Phys. Rev. A*, 73(6):062331, June 2006.

[61] Ya Cao and An Min Wang. Revised geometric measure of entanglement. *J. Phys. A: Math. Theor.*, 40(13):3507, March 2007.

[62] K. Uyanık and S. Turgut. Geometric measures of entanglement. *Phys. Rev. A*, 81(3):032306, March 2010.

[63] F. Verstraete, M. Popp, and J. I. Cirac. Entanglement versus correlations in spin systems. *Phys. Rev. Lett.*, 92(2):027901, January 2004.

[64] M. Popp, F. Verstraete, M. A. Martín-Delgado, and J. I. Cirac. Localizable entanglement. *Phys. Rev. A*, 71(4):042306, April 2005.

[65] Richard M. Karp. Reducibility among combinatorial problems. In Raymond E. Miller, James W. Thatcher, and Jean D. Bohlinger, editors, *Complexity of Computer Computations*, The IBM Research Symposia Series, pages 85–103. Springer US, January 1972.

[66] Silvano Martello. *Knapsack problems: algorithms and computer implementations*. Wiley & Sons, New York, 1990.

[67] Sumit Daftuar and Patrick Hayden. Quantum state transformations and the schubert calculus. *Annals of Physics*, 315(1):80–122, January 2005.

[68] W. Ehrenberg and R. E. Siday. The refractive index in electron optics and the principles of dynamics. *Proc. Phys. Soc. B*, 62(1):8, January 1949.

[69] Y. Aharonov and D. Bohm. Significance of electromagnetic potentials in the quantum theory. *Phys. Rev.*, 115(3):485–491, August 1959.

[70] Nobuyuki Osakabe, Tsuyoshi Matsuda, Takeshi Kawasaki, Junji Endo, Akira Tonomura, Shinichiro Yano, and Hiroji Yamada. Experimental confirmation of aharonov-bohm effect using a toroidal magnetic field confined by a superconductor. *Phys. Rev. A*, 34(2):815–822, August 1986.

[71] Zsolt Gulácsi, Arno Kampf, and Dieter Vollhardt. Exact many-electron ground states on the diamond Hubbard chain. *Phys. Rev. Lett.*, 99(2):026404, July 2007.

[72] H. Kikuchi, Y. Fujii, M. Chiba, S. Mitsudo, T. Idehara, T. Tonegawa, K. Okamoto, T. Sakai, T. Kuwai, and H. Ohta. Experimental observation of the 1/3 magnetization plateau in the diamond-chain compound $Cu_3(CO_3)_2(OH)_2$. *Phys. Rev. Lett.*, 94(22):227201, June 2005.

[73] Julien Vidal, Remy Mosseri, and Benoit Doucot. Aharonov-Bohm cages in two-dimensional structures. *Phys. Rev. Lett.*, 81(26):5888–5891, December 1998.

[74] A. M. S. Macedo, M. C. dos Santos, M. D. Coutinho-Filho, and C. A. Macedo. Magnetism and phase separation in polymeric Hubbard chains. *Phys. Rev. Lett.*, 74(10):1851–1854, March 1995.

[75] Hiroyuki Tamura, Kenji Shiraishi, Takashi Kimura, and Hideaki Takayanagi. Flat-band ferromagnetism in quantum dot superlattices. *Phys. Rev. B*, 65(8):085324, February 2002.

[76] R. R. Montenegro-Filho and M. D. Coutinho-Filho. Doped AB_2 Hubbard chain: Spiral, Nagaoka and resonating-valence-bond states, phase separation, and Luttinger-liquid behavior. *Phys. Rev. B*, 74(12):125117, September 2006.

[77] Hal Tasaki. The Hubbard model - an introduction and selected rigorous results. *J. Phys.: Condens. Matter*, 10(20):4353, May 1998.

[78] Hal Tasaki. From nagaoka's ferromagnetism to flat-band ferromagnetism and beyond an introduction to ferromagnetism in the Hubbard model. *Prog. Theor. Phys.*, 99(4):489–548, April 1998.

[79] Hal Tasaki. Ferromagnetism in Hubbard models. *Phys. Rev. Lett.*, 75(25):4678–4681, December 1995.

[80] Hal Tasaki. Stability of ferromagnetism in the Hubbard model. *Phys. Rev. Lett.*, 73(8):1158–1161, August 1994.

[81] Hal Tasaki. Ferromagnetism in the Hubbard models with degenerate single-electron ground states. *Phys. Rev. Lett.*, 69(10):1608–1611, September 1992.

[82] Andreas Mielke. Ferromagnetism in single-band Hubbard models with a partially flat band. *Phys. Rev. Lett.*, 82(21):4312–4315, May 1999.

[83] A. Mielke. Exact ground states for the Hubbard model on the kagome lattice. *J. Phys. A: Math. Gen.*, 25(16):4335, August 1992.

[84] A. Mielke. Ferromagnetism in the Hubbard model on line graphs and further considerations. *J. Phys. A: Math. Gen.*, 24(14):3311, July 1991.

[85] A. Mielke. Ferromagnetic ground states for the Hubbard model on line graphs. *J. Phys. A: Math. Gen.*, 24(2):L73, January 1991.

[86] Andreas Mielke and Hal Tasaki. Ferromagnetism in the Hubbard model. *Commun.Math. Phys.*, 158(2):341–371, November 1993.

[87] Oleg Derzhko and Johannes Richter. Structural instability of two- and three-dimensional pyrochlore spin lattices in high magnetic fields. *Phys. Rev. B*, 72(9):094437, September 2005.

[88] Oleg Derzhko and Johannes Richter. Finite low-temperature entropy of some strongly frustrated quantum spin lattices in the vicinity of the saturation field. *Phys. Rev. B*, 70(10):104415, September 2004.

[89] O. Derzhko, J. Richter, A. Honecker, M. Maksymenko, and R. Moessner. Low-temperature properties of the Hubbard model on highly frustrated one-dimensional lattices. *Phys. Rev. B*, 81(1):014421, January 2010.

[90] Akinori Tanaka and Hal Tasaki. Metallic ferromagnetism in the Hubbard model: A rigorous example. *Phys. Rev. Lett.*, 98(11):116402, March 2007.

[91] Y. F. Duan and K. L. Yao. Theoretical model of an organic ferrimagnetic state for a bipartite lozenge chain. *Phys. Rev. B*, 63(13):134434, March 2001.

[92] Zsolt Gulacsi and Dieter Vollhardt. Exact ground states of the periodic anderson model in d=3 dimensions. *Phys. Rev. B*, 72(7):075130, August 2005.

[93] Zsolt Gulacsi and Dieter Vollhardt. Exact insulating and conducting ground states of a periodic anderson model in three dimensions. *Phys. Rev. Lett.*, 91(18):186401, October 2003.

[94] Johannes Richter, Oleg Derzhko, and Jorg Schulenburg. Magnetic-field induced spin-Peierls instability in strongly frustrated quantum spin lattices. *Phys. Rev. Lett.*, 93(10):107206, September 2004.

[95] J. Richter, J. Schulenburg, A. Honecker, J. Schnack, and H.-J. Schmidt. Exact eigenstates and macroscopic magnetization jumps in strongly frustrated spin lattices. *J. Phys.: Condens. Matter*, 16(11):S779, March 2004.

[96] K. C. Rule, A. U. B. Wolter, S. Sullow, D. A. Tennant, A. Bruhl, S. Kohler, B. Wolf, M. Lang, and J. Schreuer. Nature of the spin dynamics and 1/3 magnetization plateau in azurite. *Phys. Rev. Lett.*, 100(11):117202, March 2008.

[97] J. Schulenburg, A. Honecker, J. Schnack, J. Richter, and H.-J. Schmidt. Macroscopic magnetization jumps due to independent magnons in frustrated quantum spin lattices. *Phys. Rev. Lett.*, 88(16):167207, April 2002.

[98] Congjun Wu, Doron Bergman, Leon Balents, and S. Das Sarma. Flat bands and wigner crystallization in the honeycomb optical lattice. *Phys. Rev. Lett.*, 99(7):070401, August 2007.

[99] Congjun Wu and S. Das Sarma. $p_{x,y}$-orbital counterpart of graphene: Cold atoms in the honeycomb optical lattice. *Phys. Rev. B*, 77(23):235107, June 2008.

[100] M. E. Zhitomirsky and Hirokazu Tsunetsugu. Lattice gas description of pyrochlore and checkerboard antiferromagnets in a strong magnetic field. *Phys. Rev. B*, 75(22):224416, June 2007.

[101] Jerome Silvestre and Roald Hoffmann. Tetrahedral and square-planar one-dimensional chains: the interplay of crystal field and band width in MS2 compounds. *Inorg. Chem.*, 24(24):4108–4119, November 1985.

[102] Yan-Zhen Zheng, Ming-Liang Tong, Wei Xue, Wei-Xiong Zhang, Xiao-Ming Chen, Fernande Grandjean, and Gary J. Long. A "star" antiferromagnet: A polymeric iron(III) acetate that exhibits both spin frustration and long-range magnetic ordering. *Angew. Chem. Int. Ed.*, 46(32):6076–6080, 2007.

[103] P. Jordan and E. Wigner. Über das paulische Äquivalenzverbot. *Z. Physik*, 47(9-10):631–651, September 1928.

[104] Rodney Baxter. Eight-vertex model in lattice statistics and one-dimensional anisotropic Heisenberg chain. III. eigenvectors of the transfer matrix and hamiltonian. *Ann. Phys.*, 76(1):48 – 71, 1973.

[105] Rodney Baxter. Eight-vertex model in lattice statistics and one-dimensional anisotropic Heisenberg chain. II. equivalence to a generalized ice-type lattice model. *Ann. Phys.*, 76(1):25 – 47, 1973.

[106] H. Bethe. Zur theorie der metalle. *Z. Phys.*, 71(3):205–226, 1931.

[107] Eduardo Fradkin. Jordan-wigner transformation for quantum-spin systems in two dimensions and fractional statistics. *Phys. Rev. Lett.*, 63(3):322–325, July 1989.

[108] Y. R. Wang. Spin-liquid state of Wigner-Jordan fermions of the quantum antiferromagnetic Heisenberg model on a triangular lattice. *Phys. Rev. B*, 45(21):12604–12607, June 1992.

[109] Y. R. Wang. Low-dimensional quantum antiferromagnetic Heisenberg model studied using Wigner-Jordan transformations. *Phys. Rev. B*, 46(1):151–161, July 1992.

[110] Y. R. Wang. Ground state of the two-dimensional antiferromagnetic Heisenberg model studied using an extended Wigner-Jordon transformation. *Phys. Rev. B*, 43(4):3786–3789, February 1991.

[111] J. Ambjørn and G.W. Semenoff. Fermionized spin systems and the boson-fermion mapping in (2+1)-dimensional gauge theory. *Physics Letters B*, 226(1–2):107–112, August 1989.

[112] Roderich Moessner and Arthur P. Ramirez. Geometrical frustration. *Physics Today*, 59(2):24–29, 2006.

[113] Benoit Douçot and Julien Vidal. Pairing of cooper pairs in a fully frustrated josephson-junction chain. *Phys. Rev. Lett.*, 88(22):227005, May 2002.

[114] Zsolt Gulácsi, Arno Kampf, and Dieter Vollhardt. Exact many-electron ground states on diamond and triangle Hubbard chains. *Prog. Theor. Phys. Supp.*, 176:1–21, 2008.

[115] Hideo Aoki, Masato Ando, and Hajime Matsumura. Hofstadter butterflies for flat bands. *Phys. Rev. B*, 54(24):R17296–R17299, December 1996.

[116] Elliott H. Lieb. Two theorems on the Hubbard model. *Phys. Rev. Lett.*, 62(10):1201–1204, March 1989.

[117] R. G. Dias. Exact solution of the strong coupling $t - v$ model with twisted boundary conditions. *Phys. Rev. B*, 62(12):7791–7801, September 2000.

[118] G. Gómez-Santos. Generalized hard-core fermions in one dimension: An exactly solvable Luttinger liquid. *Phys. Rev. Lett.*, 70(24):3780–3783, June 1993.

[119] G. Gómez-Santos. Current-carrying states and Luttinger-liquid behavior in the spin-1/2 XXZ linear chain. *Phys. Rev. B*, 46(21):14217–14218, December 1992.

[120] V. J. Emery, S. A. Kivelson, and H. Q. Lin. Phase separation in the t-J model. *Phys. Rev. Lett.*, 64(4):475–478, January 1990.

[121] Masao Ogata, M. U. Luchini, S. Sorella, and F. F. Assaad. Phase diagram of the one-dimensional t-J model. *Phys. Rev. Lett.*, 66(18):2388–2391, May 1991.

[122] F. D. M. Haldane. General relation of correlation exponents and spectral properties of one-dimensional fermi systems: Application to the anisotropic S=1/2 Heisenberg chain. *Phys. Rev. Lett.*, 45(16):1358–1362, October 1980.

[123] Masaaki Nakamura and Kiyohide Nomura. Phase separation as an instability of the Tomonaga-Luttinger liquid. *Phys. Rev. B*, 56(20):12840–12846, November 1997.

[124] F. D. M. Haldane. Effective harmonic-fluid approach to low-energy properties of one-dimensional quantum fluids. *Phys. Rev. Lett.*, 47(25):1840–1843, December 1981.

[125] F. D. M. Haldane. 'Luttinger liquid theory' of one-dimensional quantum fluids. i. properties of the Luttinger model and their extension to the general 1d interacting spinless fermi gas. *J. Phys. C: Solid State*, 14(19):2585, 1981.

[126] M. Fabrizio and Alexander O. Gogolin. Interacting one-dimensional electron gas with open boundaries. *Phys. Rev. B*, 51(24):17827–17841, June 1995.

[127] Sebastian Eggert, Henrik Johannesson, and Ann Mattsson. Boundary effects on spectral properties of interacting electrons in one dimension. *Phys. Rev. Lett.*, 76(9):1505–1508, February 1996.

[128] Y. Wang, J. Voit, and Fu-Cho Pu. Exact boundary critical exponents and tunneling effects in integrable models for quantum wires. *Phys. Rev. B*, 54(12):8491–8500, September 1996.

[129] Johannes Voit, Yupeng Wang, and Marco Grioni. Bounded Luttinger liquids as a universality class of quantum critical behavior. *Phys. Rev. B*, 61(12):7930–7940, March 2000.

[130] V. Meden, W. Metzner, U. Schollwöck, O. Schneider, T. Stauber, and K. Schönhammer. Luttinger liquids with boundaries: Power-laws and energy scales. *Europ. Phys. J. B*, 16(4):631–646, 2000.

[131] C. L. Kane and Matthew P. A. Fisher. Transport in a one-channel Luttinger liquid. *Phys. Rev. Lett.*, 68(8):1220–1223, February 1992.

[132] C. L. Kane and Matthew P. A. Fisher. Transmission through barriers and resonant tunneling in an interacting one-dimensional electron gas. *Phys. Rev. B*, 46(23):15233–15262, December 1992.

[133] Walter Kohn. Theory of the insulating state. *Phys. Rev.*, 133(1A):A171–A181, January 1964.

[134] B. Sriram Shastry and Bill Sutherland. Twisted boundary conditions and effective mass in Heisenberg-Ising and Hubbard rings. *Phys. Rev. Lett.*, 65(2):243–246, July 1990.

[135] R. M. Fye, M. J. Martins, D. J. Scalapino, J. Wagner, and W. Hanke. Drude weight, optical conductivity, and flux properties of one-dimensional Hubbard rings. *Phys. Rev. B*, 44(13):6909–6915, October 1991.

[136] Masao Ogata and Hiroyuki Shiba. Bethe-ansatz wave function, momentum distribution, and spin correlation in the one-dimensional strongly correlated Hubbard model. *Phys. Rev. B*, 41(4):2326–2338, February 1990.

[137] Andreas Schadschneider. Superconductivity in an exactly solvable Hubbard model with bond-charge interaction. *Phys. Rev. B*, 51(16):10386–10391, April 1995.

[138] F. Gebhard, K. Born, M. Scheidler, P. Thomas, and S. W. Koch. Exact results for the optical absorption of strongly correlated electrons in a half-filled peierls-distorted chain. *Phil. Mag. B*, 75(1):13–46, 1997.

[139] Ricardo G. Dias and J. M. B. Lopes dos Santos. Simple representation of the eigenstates of the $u \to \infty$ one dimensional Hubbard model. *J. Phys. I France*, 2(10):1889–1897, 1992.

[140] N. M. R. Peres, R. G. Dias, P. D. Sacramento, and J. M. P. Carmelo. Finite-temperature transport in finite-size Hubbard rings in the strong-coupling limit. *Phys. Rev. B*, 61(8):5169–5183, February 2000.

[141] Liliana Arrachea and A. A. Aligia. Exact solution of a Hubbard chain with bond-charge interaction. *Phys. Rev. Lett.*, 73(16):2240–2243, October 1994.

[142] A. Brooks Harris and Robert V. Lange. Single-particle excitations in narrow energy bands. *Phys. Rev.*, 157(2):295–314, May 1967.

[143] O. Derzhko. Jordan-wigner fermionization for spin-1/2 systems in two dimensions: A brief review. *J. Phys. Stud. (L'viv)*, 5:49, 2001.

[144] M. Y. Choi and S. Doniach. Phase transitions in uniformly frustrated XY models. *Phys. Rev. B*, 31(7):4516–4526, April 1985.

[145] A. A. Lopes, B. A. Z. António, and R. G. Dias. Conductance through geometrically frustrated itinerant electronic systems. *Phys. Rev. B*, 89(23):235418, June 2014.

[146] C.J Gorter. A possible explanation of the increase of the electrical resistance of thin metal films at low temperatures and small field strengths. *Physica*, 17(8):777–780, August 1951.

[147] B. J. van Wees, H. van Houten, C. W. J. Beenakker, J. G. Williamson, L. P. Kouwenhoven, D. van der Marel, and C. T. Foxon. Quantized conductance of point contacts in a two-dimensional electron gas. *Phys. Rev. Lett.*, 60(9):848–850, February 1988.

[148] A. Douglas Stone and P. A. Lee. Effect of inelastic processes on resonant tunneling in one dimension. *Phys. Rev. Lett.*, 54(11):1196–1199, March 1985.

[149] R. A. Webb, S. Washburn, C. P. Umbach, and R. B. Laibowitz. Observation of h/e Aharonov-Bohm oscillations in normal-metal rings. *Phys. Rev. Lett.*, 54(25):2696–2699, June 1985.

[150] M. Matsuda, K. M. Kojima, Y. J. Uemura, J. L. Zarestky, K. Nakajima, K. Kakurai, T. Yokoo, S. M. Shapiro, and G. Shirane. Ordering of oxygen moments in ferromagnetic edge-sharing CuO_4 chains in $La_{14-x}Ca_xCu_{24}O_{41}$. *Phys. Rev. B*, 57(18):11467–11471, May 1998.

[151] J. Schlappa, K. Wohlfeld, K. J. Zhou, M. Mourigal, M. W. Haverkort, V. N. Strocov, L. Hozoi, C. Monney, S. Nishimoto, S. Singh, A. Revcolevschi, J.-S. Caux, L. Patthey, H. M. Rønnow, J. van den Brink, and T. Schmitt. Spin-orbital separation in the quasi-one-dimensional Mott insulator Sr_2CuO_3. *Nature*, 485(7396):82–85, May 2012.

[152] J. L. Movilla and J. Planelles. Quantum level engineering for Aharonov-Bohm caging in the presence of electron-electron interactions. *Phys. Rev. B*, 84(19):195110, November 2011.

[153] John R Taylor. *Scattering theory: the quantum theory of nonrelativistic collisions*. Dover Publications, Mineola, NY, 2006.

[154] T. Enss, V. Meden, S. Andergassen, X. Barnabé-Thériault, W. Metzner, and K. Schönhammer. Impurity and correlation effects on transport in one-dimensional quantum wires. *Phys. Rev. B*, 71(15):155401, April 2005.

[155] Yoseph Imry and Rolf Landauer. Conductance viewed as transmission. *Rev. Mod. Phys.*, 71(2):S306–S312, March 1999.

[156] D. Kowal, U. Sivan, O. Entin-Wohlman, and Y. Imry. Transmission through multiply-connected wire systems. *Phys. Rev. B*, 42(14):9009–9018, November 1990.

[157] Eugene Hecht. *Optics*. Addison-Wesley, Reading, Mass., 4th edition, 2002.

[158] E. A. Jagla and C. A. Balseiro. Electron-electron correlations and the Aharonov-Bohm effect in mesoscopic rings. *Phys. Rev. Lett.*, 70(5):639–642, February 1993.

[159] A. A. Lopes and R. G. Dias. Simple approach for the two-terminal conductance through interacting clusters. *arXiv:1407.5922 [cond-mat]*, July 2014.

[160] P. N. Keldysh. Diagram technique for nonequilibrium processes. 20(4):1018–1026, April 1965.

[161] Yigal Meir and Ned S. Wingreen. Landauer formula for the current through an interacting electron region. *Phys. Rev. Lett.*, 68(16):2512–2515, April 1992.

[162] Rolf Landauer. Electrical resistance of disordered one-dimensional lattices. *Philosophical Magazine*, 21(172):863–867, 1970.

[163] Julián Rincón, A. A. Aligia, and K. Hallberg. Features of spin-charge separation in the equilibrium conductance through finite rings. *Phys. Rev. B*, 79(3):035112, January 2009.

[164] X. Zotos and P. Prelovšek. Evidence for ideal insulating or conducting state in a one-dimensional integrable system. *Phys. Rev. B*, 53(3):983–986, January 1996.

[165] Ana Cannas da Silva. *Lectures on symplectic geometry*. Springer, Berlin; New York, 2001.

[166] Mikhail G. Katz and Jake P. Solomon. *Systolic Geometry and Topology*. American Mathematical Society, Providence, R.I, April 2007.

[167] José M. Isidro. *The Geometry of Quantum Mechanics*.

[168] Jean-Paul Dufour and Nguyen Tien Zung. *Poisson Structures and Their Normal Forms*. Birkhäuser, Basel ; Boston, auflage: 2005 edition, September 2005.

[169] Charles P. Poole Jr. *Classical Mechanics*. Addison-Wesley, San Francisco, 3rd edition, June 2001.

[170] M. F. Atiyah. Convexity and commuting Hamiltonians. *Bull. London Math. Soc.*, 14(1):1–15, January 1982.

[171] V. Guillemin and S. Sternberg. Convexity properties of the moment mapping. *Invent Math*, 67(3):491–513, October 1982.

[172] Allen Knutson. The symplectic and algebraic geometry of Horn's problem. *arXiv:math/9911088*, November 1999.

[173] John Boyd Ketterson. *Superconductivity*. Cambridge Univ. Press, Cambridge, 1999.

[174] Sergei Kruchinin, Hidemi Nagao, and Shigeyuki Aono. *Modern aspects of superconductivity theory of superconductivity*. World Scientific, Singapore; Hackensack, 2011.

[175] Gerald D Mahan. *Many-particle physics*. Kluwer Academic/Plenum Publishers, New York, 2000.

[176] B. A. Z. António, A. A. Lopes, and R. G. Dias. Transport through quantum rings. *Eur. J. Phys.*, 34(4):831, July 2013.